STUDY OF THE PERFORMANCE OF A LARGE, MECHANICALLY-AGITATED EXTRACTION COLUMN

by

ABDUL MAJID ABDUL RAZZAK AL-OBAID

A thesis submitted to

The University of Aston in Birmingham

for the degree of

Doctor of Philosophy

November 1985

Department of Chemical Engineering

The University of Aston in Birmingham

THE UNIVERSITY OF ASTON IN BIRMINGHAM

A Study of the Performance of a Large Mechanically-Agitated Extraction Column

Abdul Majid Abdul Razzaq Al-Obaid

PhD November 1985

SUMMARY

The literature relating to mechanically-agitated extraction columns and relevant phenomena eg. droplet break-up and coalescence, axial mixing, single drop mass transfer mechanisms and flooding/phase-inversion, and related mathematical models have been reviewed.

An experimental study was performed of the hydrodynamic and mass transfer characteristics of a 0.45m diameter, 4.3m high Rotating Disc Contactor. The system used was Clairsol-350 (dispersed)-acetone-de-ionised water. Hydrodynamics were studied with mutually-saturated phases and in the presence of mass transfer.

Drop size distributions under all conditions were best described by the Mugele-Evans Upper-Limit function. However with mass transfer from the dispersed to continuous phase d_{32} was, on average, approximately 22.8% greater and hold-up was 57% less than for non-mass transfer conditions. Therefore data obtained under non-mass transfer conditions should be applied with caution in extractor design. The phenomenon of flooding, rather than phase inversion, was the best criteria for limiting capacity.

Operation at 80% of flooding, resulted in increased hold-ups and higher volumetric overall mass transfer coefficients $(Ka)_{exp}$. Increasing rotor speed, up to a maximum at which a haze was generated, resulted in an increase in overall mass transfer coefficient (Ka).

To calculate the overall mass transfer coefficient (K_{exp}), the mean driving force was calculated from the experimentally-determined concentration profile along the column using Simpson's Rule. Theoretical overall mass transfer coefficients were calculated using the drop size distribution diagram to determine the volume or area fraction of stagnant, circulating and oscillating drops in the sample population in conjunction with single drop mass transfer correlations. Both approaches predicted considerably lower mass transfer rates than were obtained experimentally. This was attributed to the drop swarm, in reality, oscillating due to drop interaction and because local drop velocities were much higher than the slip velocity used to calculate K_{cal}. Assuming that all the drops were oscillating, with mass transfer from the dispersed to continuous phase, the Rose and Kintner correlation gave the best approximation to the overall experimental mass transfer coefficient.

A novel method is proposed for calculation of axial mixing coefficients based on the experimentally-determined concentration profile in the continuous phase.

Key words : Liquid-Liquid Extraction, Rotating Disc Contactor, Overall Mass Transfer Coefficient, Axial Mixing

ACKNOWLEDGEMENTS

The author wishes to express his gratitude to Professor G V Jeffreys, the Head of the Department of Chemical Engineering for providing the facilities for this research, for his invaluable supervision, for his encouragement and for his continued advice and constructive criticism.

Sincere appreciation is felt for:

Dr C J Mumford for his supervision, for his interest in the subject of this study and for his encouragement throughout this study.

The laboratory and technical staff of the Department of Chemical Engineering for their willingness to help, and finally to Miss Ferry for her diligence in typing this thesis.

CONTENTS

LIST OF FIGURES

APPENDICES

LIST OF TABLES

APPENDICES

1. INTRODUCTION

Liquid-liquid extraction is a chemical engineering unit operation used to separate the components of a liquid mixture by treatment with a solvent in which one or more of them is preferentially soluble. The process has been used increasingly for separation due to the rapid world-wide development of the chemical industry and the increasing importance of oil, petrochemical, synthetic fibre, and nuclear industries.

Extraction is a potentially useful method for separating components of solutions which are particularly difficult, or expensive, to separate by other conventional methods, ie. distillation, absorption, evaporation or chemical precipitation. Extraction can be used when the substance, or substances, to be recovered are relatively non-volatile, close boiling, heat sensitive, or present in relatively small amounts.

Following extraction it is necessary to recover the solute and solvent, often by evaporation or distillation. Any extraction process therefore involves:

i) Bringing the solvent and solution into intimate contact.
ii) Separation of the two phases, eg. in a settler involving flocculation and coalescence and,
iii) Removal and recovery of solute and solvent.

A wide variety of equipment can be used to carry out steps (i) and (ii) in either a continuous or stage-wise manner. The equipment, their applications and advantages are discussed in Chapter 2.

In order to provide intimate contact between the phases in all practical extractors one phase is dispersed as droplets. The rate of solute transfer N, can then be

expressed as the product of an overall mass transfer coefficient K, the interfacial area A, and the concentration driving force ΔC_m,

$$N = K A \Delta C_m \tag{1.1}$$

The overall coefficient is dependent on the series resistance to diffusion inside the drop, outside the drop and at the interface. Interfacial resistance is generally neglected and the overall coefficient expressed as,

$$\frac{1}{K_d} = \frac{1}{k_d} + \frac{m}{k_c} \tag{1.2}$$

or

$$\frac{1}{K_c} = \frac{1}{k_c} + \frac{1}{mk_d} \tag{1.3}$$

where m is the distribution coefficient of the solute. The choice of the use of K_d or K_c depends on the driving force chosen in equation (1.1), ie. referred to the continuous or dispersed phase. To maximise the rate of mass transfer (equation 1.1) an attempt is generaly made to maximise A, which depends on the drop size and dispersed phase hold-up x, in the contactor. Assuming that the drops are spherical and their diameter can be represented by a mean value d_{vs} (22),

$$A = \frac{6x}{d_{vs}} \tag{1.4}$$

where x is the dispersed phase hold-up.

The resistance to mass transfer inside the drop depends on the hydrodynamics of the drop. The fluid inside the drop may be stagnant or circulating, or the drop may oscillate between an oblate and prolate profile. The different coefficients for each mode of transfer are reviewed in Chapter 4. However, a wide distribution of droplet size exists in practical contactors, dependent upon the degree of turbulence which results in break-up and recoalescence effects.

In recent years mechanically-agitated extractors involving internal pulsing or rotary agitation, giving rise to increased turbulence, have found wide application. Generally, they offer the advantage of flexibility in operation and good mass transfer performance.

The present work forms part of a continuing study of hydrodynamics and mass transfer efficiencies of mechanically-agitated columns on a laboratory and large scale since,

a) Many RDC columns are in use commercially under conditions for which phases cannot be observed and with uncertainty as to their mode of operation.
b) RDC columns are increasingly attractive in flexibility, high efficiency and reasonable volumetric capacity compared to other extraction types and are widely used in industry.

The rotating disc contactor (RDC) invented in 1951, is traditionally designed from data obtained on small scale columns, with the efficiency and capacity measured in terms of heights of transfer unit and flooding flowrates respectively. However, the efficiency of a column generally decreases with the increase in column diameter due to increased axial mixing. Wall effects may also be significant in small columns, because

droplet break-up, coalescence and flow in an unrestricted continuous phase differ from those in the vicinity of the wall. The literature on the RDC and its performance is reviewed in Chapter 5.

Axial mixing is generally an important feature limiting the efficiency of large extraction columns. Therefore the literature and mathematical models relating to axial mixing are reviewed in Chapter 6.

The majority of work to characterise RDC performance in terms of droplet fundamental behaviour, ie. drop size distribution, dispersed phase hold-up and discrete drop mass transfer coefficients has been for specific systems in laboratory columns. In such columns drop size distribution and back mixing effects are quite unrelated to those on an industrial scale (1, 2).

Therefore in the present study hydrodynamics and mass transfer have been studied using a 0.45m diameter and 4.3m high, large scale RDC. The objective was to further knowledge of hydrodynamics and mass transfer characteristics of large mechanically-agitated extractors of industrial design and to improve the design procedure for specific applications.

2. LIQUID-LIQUID EXTRACTION

In liquid-liquid extraction, separation of miscible liquids is achieved by the use of a solvent, which preferentially dissolves one of them.

The basic requirement of extraction equipment is to provide intimate contact between the phases by creating a reasonably-uniform dispersion of one in the other, so that a large interfacial area can be attained resulting in a high separation efficiency. The main objectives are to obtain the highest volumetric throughputs and mass transfer rates. In addition, for particular applications, it may be important to minimize inventory (eg. in radioactive chemicals processing), or to cope with solids (eg. in metal extraction). The physical properties of the system (eg. interfacial tension, density difference and phase viscosities) also influence equipment selection, since they affect dispersion, coalescence gravity-flow and resistances to mass transfer.

In recent years liquid-liquid extraction has found wide application in the chemical, petroleum and related industries as an important separation tool. Commercially, the petroleum industry is the largest user (3) of liquid-liquid extraction.

The reduced energy consumption is one factor which makes liquid extraction attractive (4). Among many other advantages, extraction is chosen due to the comparative simplicity of the equipment, its ease of operation and control, and the generally wide choice of solvents available as extractive agents. The process does, of course, involve the consumption of energy since an extraction plant is generally accompanied by stripping columns to recover the solvent from the extract and raffinate streams. This generally involves distillation or evaporation which introduces additional operating costs. A major factor determining the success or otherwise of a liquid extraction process is the correct choice of solvent in terms of selectivity, cost, resistance to degradation and recoverability.

2.1 EQUIPMENT CLASSIFICATION

The equipment used in industrial processes comprises either,

I) Stagewise contactors in which the liquids are mixed, the solute extracted and the phases separated in discrete stages. The mixer-settler range of equipment is included in this class.

II) Differential contactors in which continuous counter-current contact is established between the immiscible phases to give the equivalent of any desired number of stages. These may be categorised as follows.

1. Gravity-operated extractors, which include:
    - A) No mechanically operated moving parts:
        - a) Perforated plate (sieve-plate) columns.
        - b) Baffle columns (eg. disc and doughnut).
        - c) Spray columns.
        - d) Packed columns.
    - B) Mechanically -agitated extractors:
        - a) Pulsed columns (with plates or packings).
        - b) Rotary agitated columns:
            - i) Rotary Disc Contactors RDC.
            - ii) The Oldshue-Rushton Column.
            - iii) The Scheibel Column.
            - iv) The Assymetric RDC
            - v) Other rotary extractors (eg. the Wirz Column).
2. Centrifugal extractors

The major classification is determined by whether or not gravity or centrifugal force is used to separate the phases. Most commercial extractors employ gravity. Continuous columns without mechanical agitation are generally unsuitable for use with systems of high interfacial tension, since adequate dispersion cannot be achieved throughout the continuous phase.

Figure 2.1 provides guidelines for the selection of commercial contactors (5).

Figure 2.2 shows an equipment classification on the basis of energy input (6). There is also a range of energy input for mechanically-agitated columns,the lowest being the RDC. A comparison between different extractors is difficult but a crude comparison can be made through the limiting capacity (7) Table 2.1. A summary of the agitated column designs is given in Table 2.2.

2.2 CHOICE OF EQUIPMENT

The choice of an extractor involves many factors including the reliability of scale-up, the number of actual stages required, flow-rates, floor space availability, maintenance, 'turn-down' flexibility, permissible liquid residence times and emulsification tendencies. Treybal (8) and Mumford (9) have presented reviews of this subject.

Continuous contactors are generally preferable to mixer-settlers when large throughputs are to be handled since they offer economies in agitation and power equipment costs, floor space and solvent inventory. They operate with a relatively small amount of hold-up of raffinate and extract. This is important when processing radioactive, flammable, expensive or low-stability materials.

In extraction processes it is necessary as a final step, or in multi-contact stagewise equipment, at intermediate steps, to separate the two phases. Rapid coalescence is desirable since otherwise either an excessive residence time is required or some of the continuous phase will be removed with 'bulk' dispersed phase, resulting in reduced efficiency, reduced capacity and loss of solvent. The contactor which gives the most rapid solute transfer is not necessarily therefore the most economic.

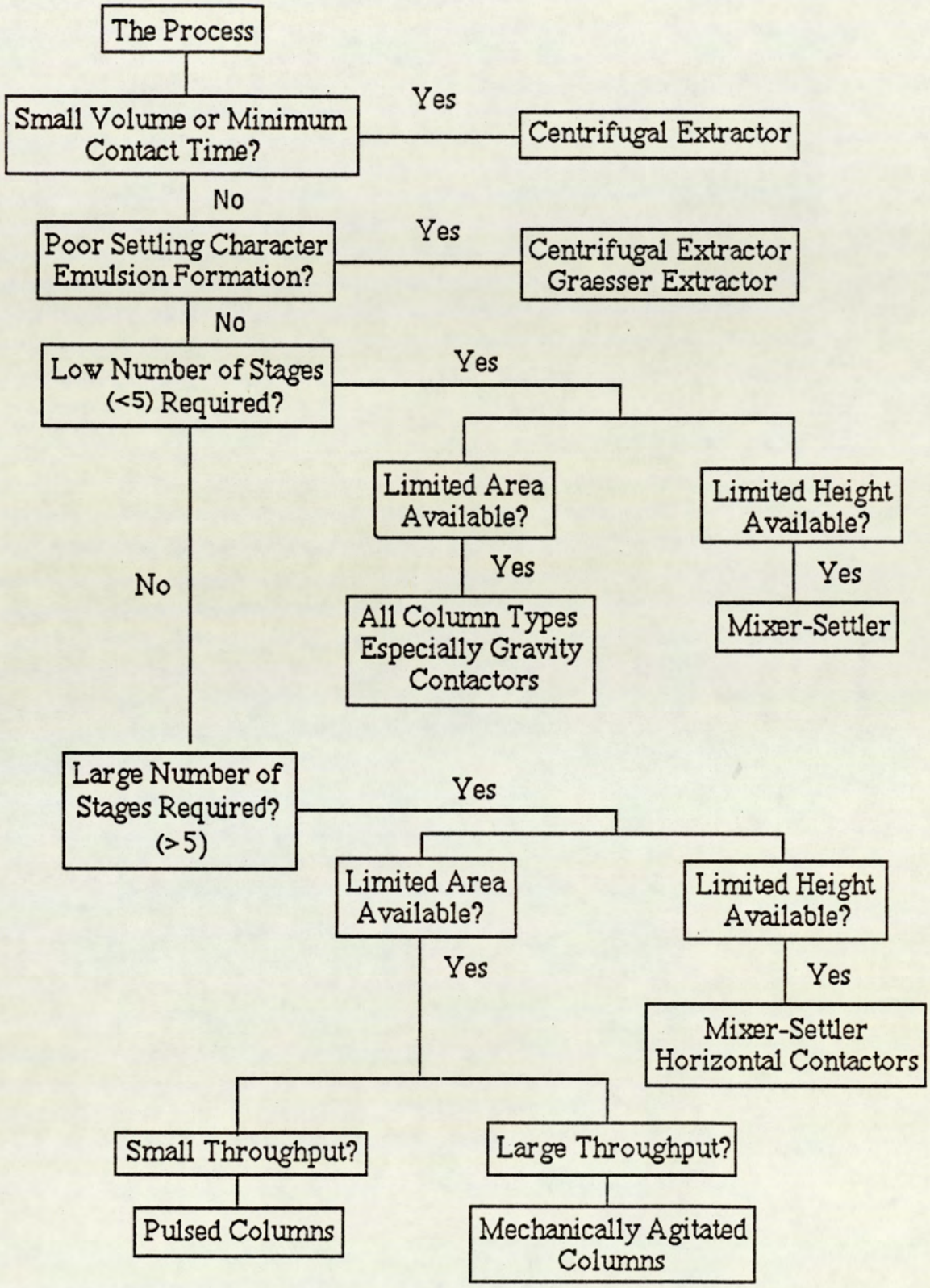

Figure 2.1 Selection Guide for Extractors

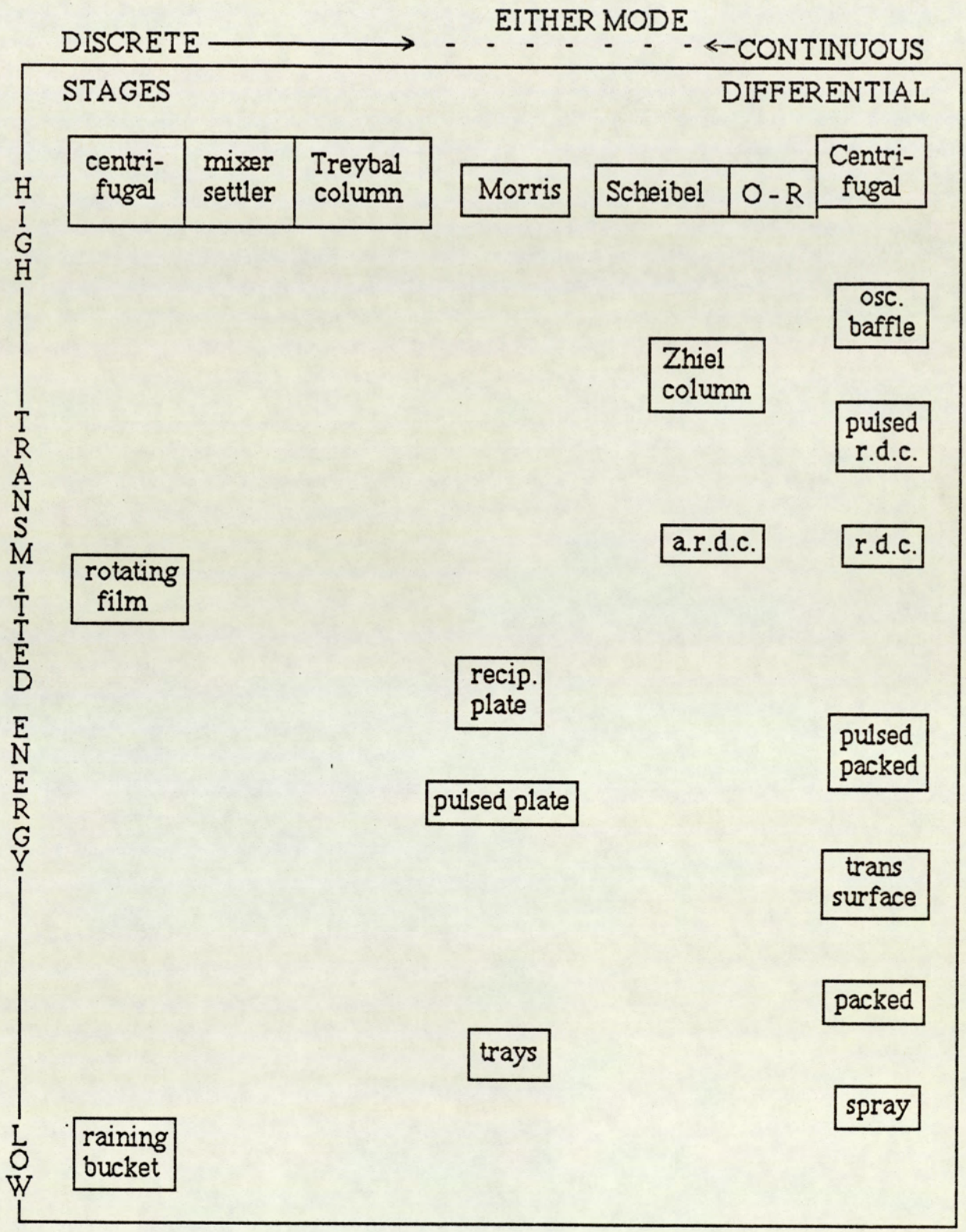

Figure 2.2 Industrial Contactors Classification on Energy Input Basis

Table 2.1 Capacity Comparison for Different Extractors (7)

Extractor Type	Limiting Capacity m^3/m^2h	Max. Column Diameter m	Maximum Flow m^3/h
Graesser Contactor	10	1.8	25
Scheibel Column	20	1.0	16
ARD	20	4.0	250
Lurgi-TE	30	8.0	1500
PFK (10) (Pulsed-Packed)	40	2.0	120
RDC	40	8.0	2000
Kuhni Column	50	3.0	350
PSE	60	3.0	420
Karr Column (11) (Pulsed Plates)	80-100	1.5	180

These values were determined for:

- high suface tension 30-40 dyne/cm
- phase ratio 1:1
- density difference ~ 0.6 g/cm^3

Table 2.2 Continuous Differential Contactors

CONTACTOR	TYPE	COMMENT
1. RDC (6)	Centrally-located discs driven by a central shaft in compartments separated by stator rings.	Operation reasonably flexible; efficfency not much affected by phase flow ratio; HETS about 20% of that for a simple packed tower. Hydrodynamics and mass transfer characteristics are partially known.
2. A.R.D.C. (12, 13)	Similar to the RDC but the rotor is off-set from the column axis; separation of phases take place in a shielded transfer section.	Mixing and separation zones claimed to reduce backmixing but phase entrainment in settling zone reduces overall efficiency (14). No special advantages over RDC.
3. Oldshue Rushton (15)	Vertical column divided into compartments by horizontal stator rings with vertical baffles in each compartment. Turbine in each compartment driven by a central shaft.	Coalescence-redispersion predominates. Stage efficiencies varied from 40% to 90%. HETS nearly half that of a simple packed tower of same diameter (15).
4. Zhiel Extractor (16)	Vertical column terminating at top and bottom in large vessel to assist settling. Contains a shaft fitted with a number of star-shaped impellers. Vertical-reciprocal, as well as rotary, motion is imposed on the impellers for effective mixing.	Theoretical efficiencies claimed to have been attained in the manufacture of phenol formaldehyde resin (16). No mass transfer data is available.
5. Scheibel Column (17)	Consists of alternate fully-baffled mixing sections and packing sections. Agitation is provided by centrally-located impellers.	Coalescence-redispersion predominates. Mass transfer coefficient is related by $Ka = c\left(\frac{\Delta\rho}{\gamma}\right)^{1.5}$ Capacity is limited by permissible flow rate through the packing.
6. Kuhni Extractor (18)	Incorporates the principles of RDC Oldshue-Rushton and sieve plate columns. Divided into compartments by plates perforated only at the centre so that flow from one compartment to the next is directed towards the agitator. Each compartment has four vertical baffles. Impeller agitator is provided. End sections are large for effective settling.	Published mass transfer data are limited. Capacity and scale-up are expressed by $\frac{d}{D} = C.Re^{0.61}.We^{0.6}\,Fr^{0.05}$ The design allows only relatively low throughputs. Modified designs have found limited application (18).
7. Pulsed Columns (8)	Phases are interdispersed by inducing a pulsating motion either by means of diaphragm pump or a valveless piston. A variety of internal packing or baffles may be used. In one design the plates are pulsed.	Commercial application limited. Employed in the extraction of metals from radio-active solutions. Power requirements are high. No published information is available for scale-up. Mass transfer data have been reported by various authors (19, 20).

Continuous columns without mechanical agitation perform poorly with systems of high interfacial tension since adequate dispersion cannot be achieved throughout the continuous phase (9). Centrifugal extractors have relatively high capital and operating costs and the number of stages which can be accommodated in a single unit is limited. Nevertheless, they are superior to all other contactors for processes requiring a low hold-up, or low contact time, or if there is a low density difference between the phases.

Mixer settlers are commonly used where only a few (eg. < 7) contact stages are required. They can handle mixtures of liquids containing suspended solids better than most other contactors, with the exception of certain rotary agitated types (9).

Table 2.3 is a useful "rule of thumb" method for a preliminary narrowing of the choice between the various types of extractor (21). Not all the features in the Table can be equated and, as will be discussed, special process factors often govern extractor selection. Equipment installation and operating costs are of primary importance. On this basis, and dependent on the number of stages for a given application, and the ease of phase dispersion/separation, an extractor selection chart can be drawn for any given feed rate range.

Logsdail (22) has described the various design considerations and process parameters to be considered in arriving at a decision on solvent extraction equipment; the various factors and choice of extractors are outlined in Table 2.4.

The choice of equipment for a given separation process should be based on the minimum annual cost for the complete plant, ie. extractor and associated equipment, as well as on operating and solvent-loss costs. The simplest operation, while it may not be the least costly, is sometimes desired because it will be trouble-free. For a given feed rate range, Todd (21) has developed an extractor selection chart, as shown in Figure 2.3.

Table 2.3 Advantages and Disadvantages of Various Contactors (21)

Type	Capital cost	Operating and maintenance costs	Efficiency	Total capacity	Flexibility	Volumetric Efficiency	Space		Ability to handle systems that emulsify
							Vertical	Floor	
Spray Tower	5	5	1	2	2	1	0	5	3
Baffle Plate	4	5	2	4	2	3	1	5	3
Packed Tower	4	5	2	2	2	2	1	5	3
RDC	3	4	4	3	5	4	3	5	3
Pulsed Plate Column	3	3	4	3	4	4	3	5	1
Mixer Settler	2	2	3	4	3	3	5	1	0
Centrifugal	1	2	5	3	5	5	5	5	5

O = Unsuitable, 1 = Poor, 2 = Fair, 3 = Adequate, 4 = Good, 5 = Outstanding (Preferred).

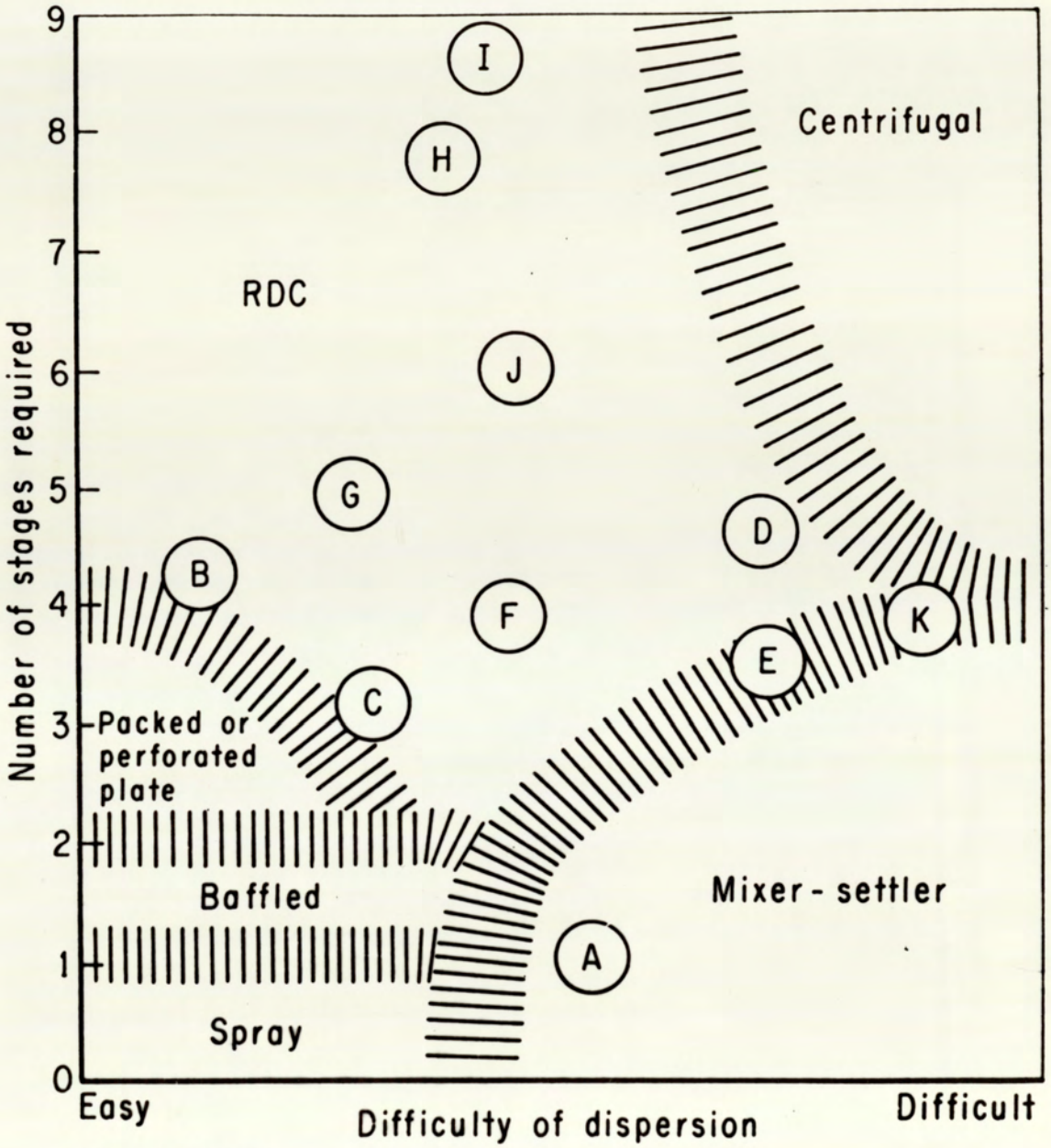

Key Letters:

A	Disulfide wash	G	Lube oil-furfural
B	SO_2 - Kerosene	H	Phenol recovery
C	Propane deasphating	I	Rare earths
D	Heavy naptha solutiser	J	Chlorohydriextraction
E	Gasoline solutiser	K	CAA butadiene extraction
F	Gas oil extraction		

Figure 2.3 Range of Applicability of Various Extractors.

The governing consideration in the chart is the cost of installation and operation. Many of the extractors will operate outside their allocated regions but at higher cost. The abscissa of the chart and the border lines within it are necessarily approximate. Figure 2.3 also illustrates theoretical stage-dispersibility requirements for several commercially-important systems. In general systems become difficult to disperse as interfacial tension and density difference increase. Hence, from Figure 2.3, for intermediate dispersible systems, mechanically-aided extractors, such as the RDC, are appropriate for any process requiring more than two stages.

2.3 THE ROTATING DISC CONTACTOR-APPLICATIONS AND ADVANTAGES

The RDC has achieved application in almost all petroleum extraction processes, food, metal separation, the processing of nuclear fuels, and in the organic chemical industries. As in other agitated columns, eg. the Oldshue-Rushton and Scheibel columns, mechanical energy is applied to achieve a high mass transfer efficiency. As indicated by Tables 2.3 and 2.4 the RDC possesses several inherent advantages over other extractors. These advantages and its applications are outlined in the following section.

2.3.1 Advantages of the RDC over other extraction devices

The main advantages of an RDC may be summarised as (6, 23, 24, 25):

i) High efficiency, measured as low HTU or HETS. The high rate of mass transfer in an RDC is due primarily to the maintenance of large interfacial area.

ii) The ability to maintain this efficiency over a large capacity range. This is practicable because, by variation of rotor speed, the flow conditions

in the contactor can be maintained at the optimum for any particular feed conditions.

iii) It is relatively cheap, simple to build and operate and easy to maintain (26).

iv) The power consumption of an RDC, is low.

v) The column is reasonably resistant to 'plugging'.

vi) It can be operated in the presence of surface active agents and of other impurities eg. by appropriate adjustments of rotor speed.

Reman (23) compared the performance of an RDC with a packed column, for purification of synthetic detergent and found that a single RDC of 145cm diameter and a total height of 5.18 metres could replace two packed columns, each 122cm in diameter, and 21.34 metres high in the purification of 75 ton/day crude detergent solution. The erected cost of the contactor was 45% that of the two packed towers.

Misek (27) compared the RDC against a sieve-plate extractor and found that for dephenolisation of 68 m^3/hr of aqueous ammoniacal solution with benzene, use of an R.D.C. saved 74% (81 tons) of material of construction and reduced operating cost by 72%. The information provided in Tables 2.3 and 2.4 provides guidelines for equipment selection.

2.3.2. Applications of the RDC

There are many examples of the use of the RDC in industry. In petroleum refineries these include gas oil extractions, propane deasphalting, sulfur dioxide extraction of kerosene fractions, solutizer treating, recovery of phenol from effluents, and extraction of catalytic reformates. It has also been used for the separation of oxy-compounds from Fisher-Tropsch synthesis oils (28). Use of the RDC as a continuous reactor has also been reported (23).

Table 2.4 Factors Determining the Choice of an Extractor (22)

FACTOR	CONTACTOR
1. Number of stages required:	
(i) few (2-3) stages,	All types.
(ii) (10-20) stages.	Agitated Columns.
2. Volumetric Capacity:	
(i) intermediate to high,	Spray or Packed Columns
(ii) low.	RDC, Oldshue-Rushton Column.
3. Residence time:	
(i) short,	Centrifugal types.
(ii) long.	Mixer-Settler, Differential Contactors
4. Phase ratio:	
(i) large,	Mixer-Settler
(ii) moderate to low.	Other types.
5. Physical Properties:	
(i) small $\frac{\sigma}{\Delta\rho}$,	Non-agitated Contactors.
(ii) large $\frac{\sigma}{\Delta\rho}$,	Mechanically-Agitated Contactors.
(iii) high viscosities.	Mechanically-Agitated Contactors.
6. Direction of mass transfer:	
(i) from dispersed to continuous phase,	Mechanically Agitated Contactors.
(ii) from continuous to dispersed phase.	Little information is available.
7. Phase dispersion and hold-up:	
(i) If the phase of the highest throughput is to be dispersed	Difficulties may be encountered in column contractors due to flooding and phase inversion.
(ii) If the low hold-up of one is required.	Centrifugal Contactors.
8. Presence of solid in one or both feeds.	Mixed Columns eg.Oldshue-Rushton Contactor.

Brief details of the main applications are:

· Lubricating Oils Extraction With Furfural.

This is the earliest RDC extraction process, with the furfural as selective solvent, and has been very successful for the past 30 years (26, 29, 30, 31). The contactor was found to be ideally-suited for it, where high efficiencies at high specific loads can be obtained.

· Extraction of Mercaptans From a Gasoline Fraction.

This is a well-established refining operation in the oil industry for quality improvement; either caustic solution or Solutizer Solution can be used as solvent (31), depending on the boiling range or the fraction to be treated. Economical and satisfactory removal of the mercaptans can be achieved by RDCs.

· Extraction of Oxygen-Containing Compounds From Fruit Juices With Alcohol.

Although this is a difficult extraction to carry out in a mixer-settler cascade, due to a tendency to emulsify, it can be satisfactorily performed in an RDC using low rotor speeds (31).

. Propane Desphalting.

The use of an RDC improves the yield of propane, and gives better quality asphalt, than the earlier mixer settler process (25, 32, 33).

· Purification of Synthetic Detergent Solution.

It is often necessary to remove unreacted and polymerized hydrocarbons and higher alcohols from the reaction mixture by extracting with a low boiling gasoline fraction. The use of an RDC proved more economical than packed columns (23).

· Phenol Recovery.

Benzene is used as a solvent for the dephenolization of waste water effluents.Classical equipment, such as tray or packed columns, is unsuitable for this operation, since because of the relatively low efficiency, the cost of equipment and of operation are rather high. The RDC exhibited a high efficiency and high throughput (27).

· Extraction of Caprolactam.

In caprolactam production an RDC proved less costly in operation and had lower power requirements. It is claimed that the RDC is more economical than centrifugal extractors and superior in flexibility of operation and insensitivity to solid phase impurities. Use of the RDC enhanced efficiency (24).

3. DROPLET PHENOMENA

In a continuous counter-current extractor the light phase is generally introduced into the the continuous phase via a distributor to obtain a uniform initial drop size distribution. However, despite careful design of the distributor, a wide range of drop sizes may be observed in agitated counter-current extractors. This distribution results from the redispersion, and possibly re-coalescence, mechanism arising from the application of external energy.

In studies with a variety of organic liquids dispersed in water in a pilot-scale RDC, it was found that in the absence of mass transfer, interdrop coalescence was negligible until flow rates approached flooding (34). However, both the drop break-up and formation mechanisms, and interdroplet coalescence phenomena merit consideration since they provide a fundamental basis for understanding column operation.

3.1. DROP FORMATION

Except in very large agitated columns, where the dispersed phase tends to be introduced via tangential pipe inlets, drops are formed at a distributor, and care must be taken in the distributor design - providing a number of nozzles to obtain a reasonably uniform drop size. The drop size is, of course, of primary importance because it determines the surface area over which mass transfer occurs. Simply drilling holes in a flat plate will result in the drops tending to spread out, giving a large distribution of drop size and consequently a wide range of residence times in the column. Therefore it is preferable to simulate discrete nozzles by drilling holes in the size range 1 to 3mm and then punching to provide small projections.

The distribution plates must be designed with the following features:

1. The material of construction of the distributor should not be wetted by the dispersed phase (35).
2. The orifice should have a sharp chamfered end (8).
3. The nozzle velocity should not exceed 10cm/s (36).

A number of modified forms of distribution plate design are described by Morello and Poffenberger (37).

At low velocities through the nozzles, the drops form slowly at the opening, then break away and rise uniformly. At increased velocity jets of dispersed phase form and drops are produced subsequently by jet-rupture. Up to a nozzle velocity of 10cm/s the drops are of uniform size and therefore they should pass through the column at the same rate. If the nozzle velocity is increased the drops produced by jet-rupture have a wide size distribution. Under these conditions there is a possibility that the smaller drops will be entrained in the continuous phase, take little part in the mass transfer process, and introduce a complex phase separation problem.

Recent work (38) has shown that the rate of mass transfer of solute during drop formation in a spray extractor is large, such that 10% of the extraction occurs in the formation period. However, the majority of mass transfer occurs during drop travel through the continuous phase and this depends more on the fluid dynamics inside, and outside, the drops than on their distance of travel.

The rate of mass transfer in any liquid-liquid system is affected by the different stages in drop life, namely the rate of formation of the droplet, its rate of passage through the continuous phase and finally its rate of coalescence.

The volume, V of a drop released from a nozzle may be represented as a function of the time of formation, t_f in the form shown in Figure 3.1 (39). In region I

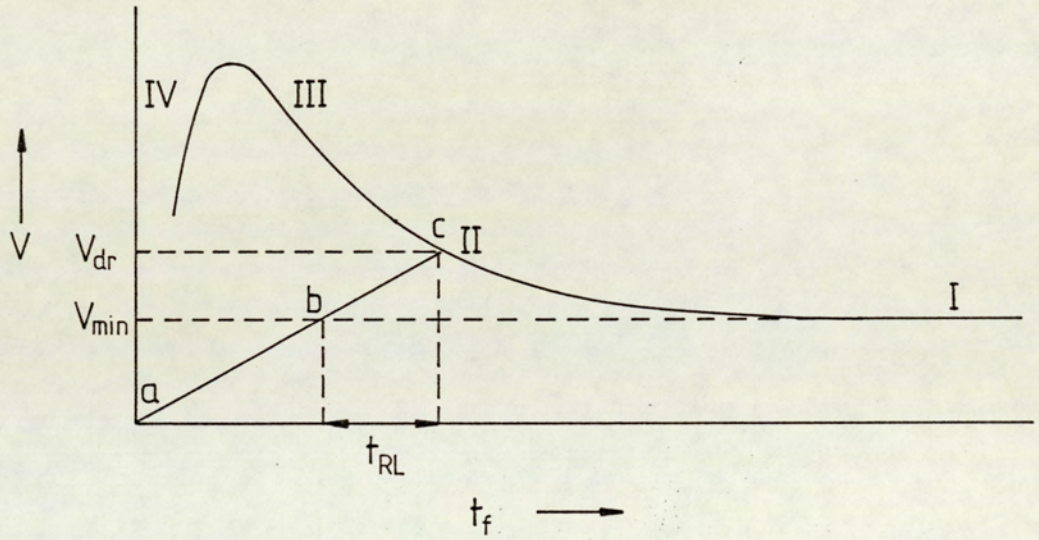

Figure 3·1 The relation between drop volume and time of formation. (39)

the drop volume, V_{min}, is independent of the time of formation, and can be estimated with fair accuracy by a method of Harkins and Brown (40). Region II has been the subject of extensive studies and many correlations have been proposed, eg. those from Hayworth and Treybal (41) and from Null and Johnson (42). However, both correlations have been found to be unsatisfactory over a wide range of liquid properties and nozzle geometries, errors of 350% being observed (43).

Probably the most widely-used correlation for drop volume calculation is that proposed by Meister and Scheele (44) for non-jetting, which can be correlated by the expression:

$$V_F = F\left[\frac{\pi \sigma D_N}{g\Delta\rho} + \frac{20\,\mu_c Q D_N}{d_F^2 g\Delta\rho} - \frac{4\,\rho_d Q U_N}{3\,g\Delta\rho} + 4.5\left\{\frac{Q^2 D_N^2 \rho\sigma}{(g\Delta\rho)^2}\right\}^{1/3}\right] \qquad (3.1)$$

Where F is the Harkins-Brown (44) correlation factor, which an be estimated from a plot of F vs. $D_N/(F\,V_F)^{1/3}$ given in the literature (36, 44). Little work has been published regarding region III in which jetting from the nozzle becomes apparent (44). In region IV jetting is fully developed and drop formation takes place at the end of the Rayleigh jet (39).

In region IV, large contributions to mass transfer are caused by strong circulation in the drop. Thus Groothuis and Kramers (45) observed a jet action in the drop at Re > 40 to 50; the characteristic diameter here was based on the inside diameter of the capillary. This is in agreement with the results of Dixon and Russell (46). In this region jetting is fully-developed and drop formation takes place at the end of the Rayleigh jet (39).

In an RDC under conditions of normal operation, the drops from the distributor will exist at most for the first 3 or 4 compartments following injection. Therefore it will be preferable to produce drops from the distributor slightly larger than the size ultimately required, rather than risk jetting with the generation of small drops with the consequences already described.

For optimum performance, column internals should preferentially be wetted by the continuous phase to prevent reduction in interfacial area due to coalescence of dispersed phase into globules, or in the extreme channelling of the dispersed phase as jets which is undesirable. The effect of plate wettability on drop formation is discussed later in Chapter 5.

3.2. DROP BREAK-UP MECHANISMS

The size of drops has a pronounced influence on volumetric capacity as well as efficiency of agitated extractors. In an agitated column, two parallel processes with opposing tendencies occur, viz break-up of drops as a result of agitation and coalescence of drops resulting from their collision. The break-up of a drop occurs when it undergoes sufficient deformation, and the local flow pattern persists for a sufficient length of time.

Break-up of droplets in an RDC occurs when:

a) the size of the dynamic pressure acting upon a drop surpasses the size of the cohesive surface forces,

and

b) the droplet stays in the high shear zone for a sufficient period of time.

Kolmogoroff (47) first studied turbulent flow in a stirred tank and developed a theory of local isotropy. This postulated that in a turbulent flow instability of the main flow

amplifies existing disturbances and produces primary eddies, which have a wave length, or scale, similar to that of the main flow. The large primary eddies are also unstable and disintegrate into smaller and smaller eddies until all their energy is dissipated by viscous flow.

Many authors have used the theory of local isotropy to derive expressions for the stable drop size in a turbulent field and supported it with experimental results. Hinze (48) considered the fundamentals of the break-up process and characterised them by two dimensionless groups,

$$N_{vi} = \frac{\mu_d/d}{(\rho_d\, \sigma/d)^{1/2}} \qquad \text{viscosity group}$$

$$N_{we} = \frac{P}{\sigma/d} \qquad \text{Weber number}$$

Deformation increases with increasing N_{We} until, at a critical N_{We}, break-up occurs. For break-up to result from viscous stresses, the drop must be small compared to the region of local viscous flow (48), a condition not likely to be attained in agitated columns.

Break-up due to dynamic pressure fluctuations has been considered by Hinze (48). Changes in velocity over a distance equal to the drop diameter, cause dynamic pressure to develop; this pressure determines the size of the largest drops present. Hinze (48) extended Kolmogoroff's (47) energy distribution law to predict the size of the maximum stable drop in a turbulent field as:

$$d_{max} = C_1 \left(\frac{g.\sigma}{\sigma_c} \right)^{3/5} . E^{-2/5} \qquad (3.2)$$

Where C_1 = 0.72 based on analysis of the data of Clay (49) for rotating cylinders and

$$E = \frac{4}{\pi} C_2 . \left(\frac{N^3 R^5}{H D^2} \right)$$

From the work of Kolmogoroff (47) and later Levich (50), Jeffreys and Mumford (51) suggested that the stable drop radius can be represented by

$$r_{s.d} = \sqrt{2} \left(\frac{\sigma}{K_f \rho_c} \right)^{3/5} \left(\frac{L^{2/5}}{V^{6/5}} \right) \qquad (3.3)$$

Where K_f is the Kolmogoroff constant $\cong$ 0.5 and V is the velocity component in the vicinity of the rotor disc. It was proposed that equation 3.3 could be applied to an RDC provided the discs were non-wetted by the dispersed phase.

3.3. DROP SIZE IN AGITATED COLUMNS

In all liquid extraction devices, a knowledge of the drop sizes is required as a basis for design calculations. To analyse performance the assumption is made that these drops are spherical and of uniform size. An interfacial area a, contact time t, and transfer coefficient K, can then be defined, based on an average drop. From this the characteristic number of transfer units can be obtained

$$T = K.a.t \qquad (3.4)$$

at a certain plane in the column and for the drop population as a whole.

The above assumption simplifies the application of single drop models of mass transfer to assess the equipment performance. Olney (52) studied the variation of drop size distribution with rotor speed, hold-up and system properties. He pointed out that such an assumption would lead to serious error, since a distribution of drop size, always exists in each compartment or column section, in all extractors. In many mechanically-agitated extractors the drop size distribution is the result of competing effects, viz generation of new drops through break-up by shear or local turbulence in the bulk flow and coalescence due to drop interaction.

In practice, drop break-up and coalescence occur simultaneously and the extreme complexity of this situation makes it very difficult to obtain a theoretical model from which drop sizes can be predicted. All the available drop size correlations in agitated systems are of a semi-empirical nature, combining the most important parameters of each of the individual coalescence and break-up models.

In any real dispersion a wide range of drop diameters exists. In calculating an average drop diameter to characterise a dispersion, attention must be given to the ultimate use of this average. Since the final objective is to calculate the total interfacial area, more weight should be given to the small drops. This follows from the fact that specific surface (ie. the surface per unit weight) increases as the particle size decreases.

The following method has been suggested by Dallavalle (53) to correct for this phenomenon.

Consider the particles to be spheres then,

$$\text{Specific surface} = S_w = \frac{\text{Area}}{\text{Weight}} = \frac{6}{\rho d} \tag{3.5}$$

$$\text{Area of a sphere} = \pi d^2 \tag{3.6}$$

$$\text{Weight of a sphere} = \frac{\rho \pi d^3}{6} \tag{3.7}$$

Where ρ is the density of the particle. Let y_i = weight fraction of particles with diameter d_i, and specific surface S_{wi}. Then,

$$y_i = \frac{n_i d_i^3}{\Sigma_i n_i d_i^3} \tag{3.8}$$

Where n is the number of drops.

The average specific surface $\bar{S}_w$ is given by a weighted arithmetic mean,

$$\bar{S}_w = \frac{\text{Total Area}}{\text{Total Weight}} = \Sigma_i y_i S_{wi} = \frac{\Sigma_i n_i d_i^3}{\Sigma_i n_i d_i^3} . S_{wi} \tag{3.9}$$

Let d_{vs} be the diameter of a fictitious sphere having a specific surface equal to $\bar{S}_w$.

Then,

$$d_{vs} = \frac{6}{\rho S_w} = \frac{6}{\rho \Sigma_i y_i S_{wi}} = \frac{6}{\rho} \left[\frac{1}{\frac{\Sigma_i n_i d_i^3 S_{wi}}{\Sigma_i n_i d_i^3}} \right] \tag{3.10}$$

Therefore,

$$d_{vs} = \frac{6}{\rho} \frac{\Sigma_i n_i d_i^3}{\Sigma_i n_i d_i^3 \cdot \left(\frac{6}{\rho d_i}\right)} = \frac{\Sigma_i n_i d_i^3}{\Sigma_i n_i d_i^2} \qquad (3.11)$$

Thus, to estimate the total surface area of a particulate material the average volume surface diameter, d_{vs}, should be used. This diameter is termed the Sauter mean diameter d_{32}, and has been presumed (52, 54) to be the appropriate mean drop diameter to represent dispersion behaviour in the RDC. From a knowledge of d_{32} an idealised approach enables the rate of mass transfer according to equation 1.1 to be calculated. Misek (56, 57) considered that a higher order of mean size

$$d_{43} = \frac{\Sigma n_i d_i^4}{\Sigma n_i d_i^3} \qquad (3.12)$$

represented the hydrodynamic and mass transfer processes better. Various workers (52, 55, 56, 57) have concluded that it is not sufficient to evaluate a mean size, but the distribution of drop sizes must be considered in predicting column performance.

3.3.1. Drop Size Distribution

Mass transfer efficiency in any RDC is dependent on the drop size, which in turn is controlled by the use of an appropriate rotor speed. In extractors the drop size distribution under operating conditions influences both the hydro-dynamics and mass transfer performance. To achieve a useful analysis of extraction data, as mentioned earlier, the assumption is commonly made that the drops are spherical and of uniform size.

In most studies, there has been considerable disagreement over the shape of the drop size distribution curve in the agitated system. Some investigators reported a normal distribution (58, 59, 60, 61) while others found the distribution to be log normal (52, 62, 63, 64, 65). For a fixed volumetric throughput, a comparison of the two types of dispersion is illustrated in Table 3.1.

Table 3.1. Comparison Between Normal and Log-Normal Distribution Dispersion

PROPERTY OF DISPERSION	NORMAL	LOG NORMAL
Proportion of smaller droplets.	Lower.	Higher.
Mean mass transfer coefficients.	Higher, because more drops are circulating.	Lower, more stagnant drops.
Interfacial area.	Lower.	Higher.
Settling rate.	Higher.	Lower.
Tendency to flood the column.	Higher.	Lower.

Chartes and Korchinsky (63) measured drop size distribution in a 23cm diameter, 135cm high RDC column. Inlet drop size was found to have a strong influence on measured column drop size and measured extraction efficiency. With a large inlet droplet size, the column drop size was influenced by the break-up rate of drops which was dependent on the presence of solute and on the direction of mass transfer.

From limited experimental work, Misek (66) identified three regions of break-up in an RDC; as turbulent, transitional and laminar. For the turbulent region where, $Re > 5.74 \times 10^4$ the hydraulic mean drop diameter is given by:

$$\frac{d_o N^2 R^2 \rho_c}{\sigma \exp(0.0\,887\,\Delta D)} = 16.3\left(\frac{H}{D}\right)^{0.46} \qquad (3.13)$$

where σ is the interfacial tension and $\Delta D = (D - R)/2$ is the distance between column wall and agitator and d_o = mean drop size.

For the transitional region, $Re < 5.74 \times 10^4$, and

$$\frac{d_o N^2 R^2 \rho_c}{\sigma \exp(0.0887\,\Delta D)} = 1.345 \times 10^{-6}\left(\frac{R^2 N}{\mu_c}\right)^{1.42} \qquad (3.14)$$

In the laminar region, $Re < 10^4$

$$d_o = 0.38\left(\frac{\sigma}{\Delta \rho g}\right)^{0.5} \qquad (3.15)$$

Mumford (67) found that in the region of $Re \sim 10^4$, mean drop sizes were independent of hold-up and in agreement with the correlation proposed by Misek in Equation 3.15. At increased speeds, the overall tendency was for drop sizes to increase, over the whole spectrum, with hold-up.

Jeffreys et al (51) have shown that droplet break-up by impact on stators or discs was not the predominant mechanism influencing drop sizes. However, drops may rupture by impact on the edge of the discs or stators as shown by Thornton (68).

Mumford and Al-Hemeri (54) derived an equation for the Sauter diameter in terms of system properties and column height, where d_{32}, decreased with column height and the results were correlated by:

$$\frac{d_{32}}{R} = 4.7 \times 10^{17} \left[\left(\frac{NR^2\rho_c}{\mu_c} \right)^{-3.33} \left(\frac{\mu_d}{\mu_c} \right)^{0.23} \left(\frac{NR\mu_c}{\sigma} \right)^{2} (x)^{0.255} \left(\exp 0.4 \left(\frac{N}{Z} \right) \right) \right] \tag{3.16}$$

Recently Blazej et al (69) have proposed a correlation for drop size under mass transfer conditions for the water-acetone-toluene system in a 65mm diameter extractor as:

$$\frac{d_{32}}{D} = 1.43 \left(\frac{V_d (1 - x)}{V_c} \right)^{0.45} \left(\frac{D.N (1 - x)}{V_c} \right)^{-0.56} \left(\frac{\rho_c . H_E . V_c}{\mu_c (1 - x)} \right)^{-0.12} \tag{3.17}$$

The above equation was extended by Al-Aswad (99) to include column dimensions as:

$$\frac{d_{32}}{R} = 1.48 \left(\frac{V_d . H . \rho_c}{\mu_c . x} \right)^{-0.23} \left(\frac{N^2 R^3 \rho_c}{\sigma} \right)^{-0.04} \left(\frac{V_d}{g_c D x^2} \right)^{0.44} \left(\frac{\Delta\rho}{\rho_c} \right)^{-0.57} \left(\frac{H}{D - S} \right)^{-0.24} \left(\frac{n}{Nc} \right)^{-0.07} \tag{3.18}$$

In all the above studies there has been considerable disagreement over the shape of the drop size distribution curve for the agitated system.

Chartes and Korchinsky (63) have confirmed Olney's (52) conclusion that the use of a single average drop size d_{32} may not be a proper mean drop size to represent the transfer rate for the drop population as a whole, and that the drop size distribution in an RDC fits the upper limit distribution proposed by Mugele and Evans (70) to give an accurate representation for drop size distribution in an RDC, ie:

$$\frac{d\upsilon}{dr} = \frac{\delta}{\sqrt{\pi}} \exp\left(-\delta^2 r^2\right) ; \tag{3.19}$$

where

$$r = \ln\left[\frac{a' d}{d_m - d}\right] \tag{3.20}$$

or

$$\Delta V_i = \frac{\delta}{\sqrt{\pi}} \exp\left(-\delta^2 r^2\right) \Delta r_i \tag{3.21}$$

To define the function requires the specification of three parameters: a',δ and d_m (or d_{32})

$$a' = \frac{d_m - d_{50}}{d_{50}} \tag{3.22}$$

$$\delta = \frac{0.907}{\ln\left[\frac{d_{90}}{d_m - d_{90}} - \frac{d_m - d_{50}}{d_{50}}\right]} \tag{3.23}$$

The upper limit distribution is a modified log-normal distribution which may be compared with the standard form of the log-normal distribution.

$$\frac{d\upsilon}{dr} = \frac{\delta}{\sqrt{\pi}} \exp(-\delta^2 r^2) \qquad (3.26)$$

where $$r = \ln \frac{d}{d_{vg}} \qquad (3.27)$$

where d_{vg} is the geometric mean drop diameter.

Another function proposed by Gal-or and Hoelscher (71) and used by Rod (72) is given by the following one parameter function:

$$\frac{d\upsilon}{dr} = 4\left(\frac{\delta^3}{\pi}\right)^{0.5} r^2 (\exp - \delta r^2) \qquad (3.31)$$

where $r = d$.

The Gal-or distribution function (71) was found less suitable by Olney and the log normal distribution quite inadequate. Jeffreys et al (65) confirm the adequacy of the upper-limit distribution law.

Examples of particle size distribution functions, some of which have been proposed for drop sizes in different types of extractor, are summarised in Table 3.2.

Table 3.2. Drop Size Distribution Equations

Distribution	dυ/dr	Mean Diameter d_{32}
Mugele-Evans (Upper Limit) (70)	$\frac{\delta}{\sqrt{\pi}} \exp(-\delta^2 r^2)$ (3.19)	

where:

$$r = \ln \frac{a'd}{d_m - d} \quad (3.20)$$

$$\frac{d_m}{1 + a' \exp \frac{0.25\delta^2}{}} \quad (3.25)$$

$$a' = \frac{d_m - d_{50}}{d_{50}} \quad (3.22)$$

$$\delta = \frac{0.907}{\ln\left[\frac{d_{90}}{d_m - d_{90}} - \frac{d_m - d_{50}}{d_{50}}\right]} \quad (3.23)$$

$$d_m = d_{50}\left[\frac{d_{50}(d_{90} + d_{10}) - 2\, d_{90}\, d_{10}}{d_{50}^2 - d_{90}\, d_{10}}\right] \quad (3.24)$$

Log-normal $\frac{\delta}{\sqrt{\pi}} \exp(-\delta^2 r^2)$ (3.26)

Table 3.2. Continued

Distribution	dυ/dr		Mean Diameter d_{32}
	where: $r = \ln \frac{d}{d_{vg}}$	(3.27)	$\exp(\ln d_{vg} + 2.5\ln^2 SG)$ (3.30)
	$\delta = \frac{0.394}{\log 10 (\frac{d_{90}}{d_{vg}})}$	(3.28)	
	$S.G. = d_{84.14}/d_{50}$	(3.29)	
Gal-or et al (71)	$4(\frac{\delta^3}{\pi})^{0.5} r^2 (\exp - \delta r^2)$	(3.31)	
	where:		
	$r = d$	(3.32)	
	$\delta = (\frac{4}{\sqrt{\pi}} r_\upsilon^3)^{2/3}$	(3.33)	
	$r_\upsilon = (\frac{\Sigma n_i r_i}{N})^{1/3}$	(3.34)	

Table 3.2. Continued

Distribution	dυ/dr	Mean Diameter d_{32}
Rosin-Rammler (73)	$\frac{\delta (r)^{\delta - 1}}{(\bar{r})^{\delta}} \exp\left(-\frac{r}{\bar{r}}\right)$ (3.36)	
	$r = d$ (3.37)	$\frac{\bar{r}}{\Gamma\left(1 - \frac{1}{\delta}\right)}$ (3.38)
	$\bar{r}$ = value of r at 36.8% on the Rosin Rammler graph plot	

3.4. COALESCENCE FUNDAMENTALS

Coalescence in agitated columns induces fusion of two or more macroscopic quantities of the same substance. The coalescence rate depends on the system properties, drop size, and coalescence mechanism. There are three separate mechanisms in any column:

a) Drop interface coalescence

b) Drop-drop coalescence

c) Drop-solid surface coalescence.

Case (a) occurs in the settling section and is preceded by flocculation and inter-drop coalescence. Case (b) may, or may not, occur in the mixing section, as well as in the settling section, when a layer of uncoalesced drops accumulates. Case (c) is a special case of drop coalescence on the internals or the column wall, if wetted by the dispersed phase.

Coalescence generally occurs in three steps:

a) flocculation of drops,

b) collision between drops and drainage of the continuous phase film between them until it reaches a critical thickness,

c) rupture of this film.

The coalescence time depends on steps (b) and (c) so that factors affecting these steps control the coalescence process. These factors are summarised in Table 3.3 (74).

An understanding of coalescence in high shear fields is important in the design of mechanically-agitated extractors where equilibrium between coalescence and droplet break-up establishes the mean drop size. As the shear rate increases (even when droplets collide) the probability for coalescence decreases as the contact time becomes less than the film drainage time required to cause coalescence.

Table 3.3 Factors Affecting Coalescence Time (74)

Variable (increasing)	Effect on coalescence time	Explanation in terms of effect on continuous film drainage rate
1. Drop size	Longer	More of the continuous phase film.
2. Distance of fall	Longer	Drop 'bounces' and film is replaced.
3. Interfacial tension	Shorter	More rigid drop, less continuous phase in films.
4. Phase $\Delta\rho$	Longer	More drop deformation, more continuous phase film.
5. Phase viscosity ratio $\frac{\mu_{drop}}{\mu_{continuous}}$	Shorter	Either less continuous phase in film or higher drainage rate.
6. Temperature	Shorter	Increase in phase viscosity ratio.
7. Temperature gradients	Shorter	Film distorts.
8. Curvature of interface towards drop:		
a) concave	Longer	More continuous phase in film.
b) convex	Shorter	Less continuous phase in film.
9. Presence of a third component		
a) stabiliser	Longer	Forms 'skin' around drop, film drainage inhibited.
b) mass transfer into drop	Longer	Sets-up interfacial tension gradients which oppose flow of film.
c) mass transfer out of drop	Shorter	Sets-up interfacial tension gradients which assist flow of film.

3.4.1. Drop-Drop Coalescence

The extent to which inter droplet coalescence occurs in an extractor in conjunction with subsequent break-up by turbulence results in the drop size distribution. Hence it determines the interfacial area. It may also lead to an enhancement of mass transfer rate. Coalescence occurs either between two or more drops of various sizes or between the drops and a plane interface and the ease with which it occurs can have a marked influence on extractor performance.

Coalescence on the column internals eg. due to dirty or dispersed phase wetted walls, is undesirable as this will result in rapid formation of large drops of dispersed phase. This may lead to a reduction in the interfacial area and drop residence time and consequently a significant reduction in mass transfer.

In systems in which mass transfer is taking place, coalescence is favoured when the direction of transfer is from the dispersed to the continuous phase and hindered when it is in the opposite direction (75, 76). Furthermore, since the effect is usually a function of solution concentration, Sauter mean drop size would be expected to vary with contactor height.

There is little data on coalescence in agitated columns. In a pilot scale RDC with the system kerosene-water, Davies et al (75) found that drop-drop coalescence was not significant at a hold-up of about 10%, whereas Misek (66) asserted that at high hold-ups of about 18% drop-drop coalescence occurred. Later Mumford (9) found that inter droplet coalescence was significant only at high hold-ups approaching flooding.

From a theoretical approach, Howarth (77) developed an equation to relate the frequency of coalescence with hold-up in a homogeneous isotropic turbulent flow:

$$\alpha = \left(\frac{24 \times C\bar{V}^2}{d^3}\right)^{0.5} \cdot \exp\left(-3\,W^2/4\bar{V}^2\right) \qquad (3.39)$$

where α is the coalescence frequency, x is the hold-up, C is the distance between the centres of the drop, V^2 is the mean square Langrangian turbulent velocity fluctuation, W is the critical approach velocity and d is the drop diameter. Although equation 3.39 showed good agreement with Madden and Damarell's (78) observation, for water drops dispersed in toluene in an agitated tank, the assumptions made in the derivation seriously limit the application to real situations (9).

Misek (79) in a later study characterised the dispersion by hydraulic mean drop diameter and assumed that these drops exactly followed the turbulent fluctuations in the continuous phase and that every collision of drops resulted in coalescence. Since drop- drop coalescence may either occur in the bulk of liquid or at the column wall, Misek (79) proposed a different expression for each case. For coalescence in the bulk liquid,

$$\ln \frac{d}{d_o} = K_1 (n' d^3) V_o^{1/2} \left(\frac{D\rho}{\mu}\right)^{1/2} = K_2 \cdot x \left(\frac{\sigma}{d_o \rho}\right)^{1/4} \left(\frac{D\rho}{\mu}\right)^{1/2}$$

$$= Z_1 \cdot x \qquad (3.40)$$

For drop coalescence at the column wall

$$\ln \frac{d}{d_o} = K_3 (n' d^3) V_o \left(\frac{D\rho}{\mu}\right) = K_4 \cdot x \left(\frac{\sigma}{d\rho}\right)^{1/2} \cdot \left(\frac{D\rho}{\mu}\right)$$

$$= Z_2 \cdot x \qquad (3.41)$$

The coefficients Z_1, Z_2 were determined indirectly based on phase flow rate measurements using Misek's equation

$$\frac{V_d}{x} + \frac{V_c}{1-x} = V_N (1-x) \exp. \left[x \left(\frac{Z}{\alpha} - 4.1\right)\right] \qquad (3.42)$$

Drop size d_o was calculated from the terminal falling velocities of solid spheres. Fair agreement was obtained with this equation for a number of binary systems in various column designs. It was found to have a value of 1.59×10^{-2} independent of agitator type. However, it is questionable whether coalescence characteristics in columns as different as the RDC and Oldshue-Rushton can be described by a single equation.

In a practical extraction operation coalescence of one drop with another may happen at an early stage in the drop life while the solute concentration is high. However, in the absence of subsequent redispersion, coalescence also leads to a reduction in dispersed phase hold-up, which may override the effects of the induced mixing.

Jeffreys and Lawson (80) studied the behaviour of coalescing single drops with a benzene-acetone-water system. They measured the coalescence times of aqueous drops at an oil-water interface. The authors observed an increase in coalescence rate with transfer of solute from drops to the continuous phase.

Smith et al (81) carried out a study of coalescence of liquid drops of several systems in extractors. They used a theoretical analysis to formulate a hypothetical mechanism for coalescence proposed by previous investigators (45, 82). Their observation was similar to that of Groothius and Zuiderweg (83), the region between the drops and between drops and the interface was more concentrated in solute than a region remote from these areas when transfer of mass was from the drops to the continuous phase. When the transfer of mass was vice versa, the regions between the drops and interface were preferentially depleted in solute and coalescence became less likely, Figure 3.2.

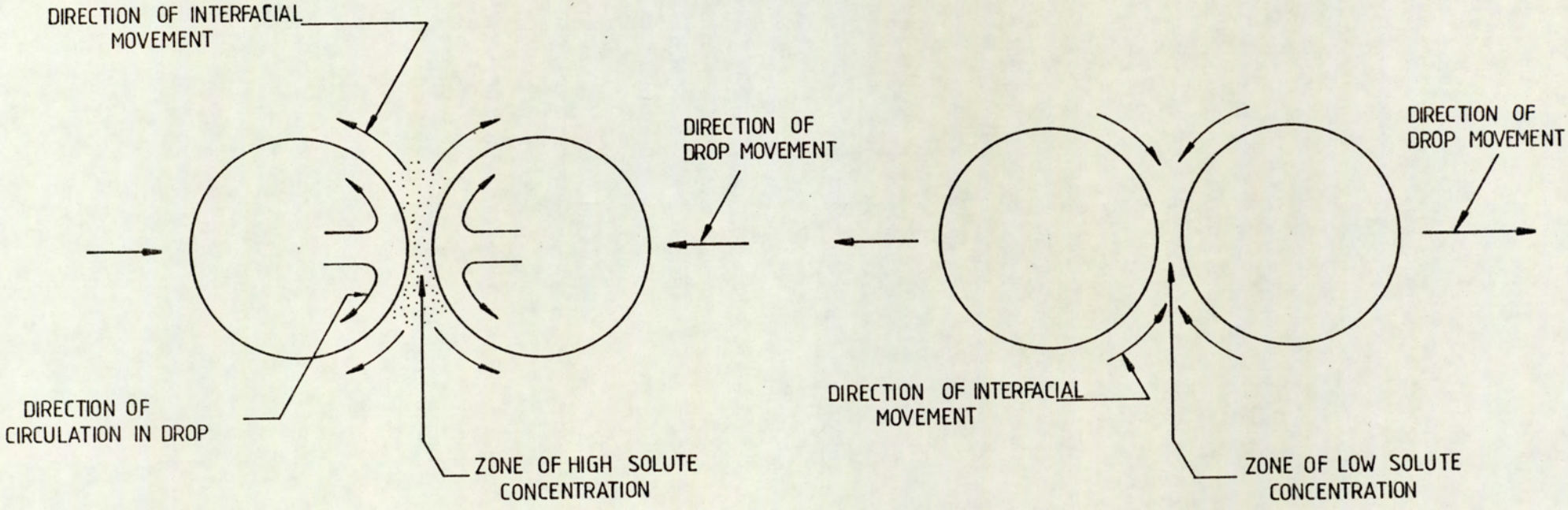

Transfer of material from the dispersed phase to the continuous phase.

Transfer of material from the continuous phase to the dispersed phase.

Figure 3·2 Effect of solute transfer on interdrop coalescense (81)

4. MASS TRANSFER IN LIQUID-LIQUID SYSTEMS

4.1. INTRODUCTION

The rate of mass transfer in any extractor depends on the overall mass transfer coefficient, the interfacial area, and the driving force, as expressed by equation 1.1. The rate of mass transfer cannot be predicted directly, and is usually calculated on the basis of correlations for the mass transfer coefficients.

The overall mass transfer coefficient depends on the rate of diffusion inside, across the interface, and outside the droplet. The life of an individual droplet inside the contactor - assuming no interdrop coalescence prior to phase separation - comprises the following stages:

a) Time of formation at the distributor.

b) Residence time during passage through the continuous phase.

c) Time of flocculation, interdrop and drop-interface coalescence.

Different degrees of mass transfer occur in each stage and since the mechanisms differ they should be considered separately.

4.2. PHASE EQUILIBRIA

The term "phase equilibrium" implies a condition of equilibrium between two or more phases ie. no tendency towards change with time. Equilibrium between mechanically separable phases is a part of the basis for most of the operations involved in chemical engineering. Most of the separations require a favourable relationship between the equilibrium states of two phases for their success. Liquid extraction involves the use of systems composed of at least three substances, and

although for the most part the insoluble phases are chemically very different, generally all three components appear at least to some extent in both phases.

Although the equipment in a plant or laboratory rarely operates at a state of equilibrium between the phases, it is essential to know the relationship between the phases at equilibrium for process understanding. The phase equilibria for a two phase system may be based on the equilibrium relation between both phases as:

$$y = m.x \qquad (4.1)$$

The distribution coefficient ratio m, has been found to be linear at low concentrations for most systems (8). Ternary liquid-liquid equilibria may be conveniently represented on a triangular diagram, either on equilateral or by rectangular coordinates (82, 83).

To determine phase equilibria, the main factors to be considered are the solubility and solute distribution. Mutual solubility curves are usually determined through cloud point using the cell and method recommended by Bonner and Smith (2).

For a given apparatus the following factors are important to determine the liquid-liquid equilibria:

- the purity of material used,
- temperature regulation,
- true equilibrium attainment,
- sampling methods,
- analyses or detection of equilibrium

A conventionally agitated two-phase system containing a known amount of solute may take up to 4 hours to reach equilibrium. The temperature must be

maintained constant. Samples are then taken from both phases and analysed by refractometer, spectro-photometer or torsion balance. By plotting the equilibrium compositions of the solute in the heavy phase against that in the light phase, the relevant slope gives the value of the distribution coefficient m.

Details of the apparatus required and of experimental techniques for satisfactory determination of phase equilibria are given in references (2,8,136,226, 87).

4.3. MASS TRANSFER DURING DROP FORMATION

The drop size and hold-up determine the surface area over which mass transfer takes place. Investigations on drop formation in the absence of mass transfer may not provide accurate information for use in design, as uncertainty exists regarding the mutual influence of the variables, such as concentration, density, viscosity and interfacial tension.

Many workers have determined the extent of mass transfer during initial drop formation. Sherwood (84) stated that 40% of the mass transfer to, or from a drop occurred during drop formation. If this is correct, there would be advantages in forming the drop repeatedly in extraction equipment, suggesting that plate type columns, or columns agitated and arranged to promote repetitive drop coalescence and redispersion are to be preferred (on efficiency grounds alone) to packed or spray columns.

However, West and Conway (85) reported that the maximum amount of mass transfer during drop formation was only 14%. Licht and Pansing (86) found that 7% occurred during drop formation. Recent investigations (38, 88, 89) have shown that about 10% of the extraction occurs during the formation period. It is important to establish whether 40% or 7% of the mass tranfer takes place during drop formation, since this may establish whether plate or packed columns, or an agitated column, is to be

preferred for a specific extraction operation. This is of course of less concern when, as in the present study, or with Scheibel or Oldshue-Rushton type or pulsed packed columns, the mass transfer during drop travel through the continuous phase is enhanced by the application of turbulence. However, Sawistowski (89) demonstrated that the prediction of the precise extraction rate during drop formation is difficult, because of the rapid changes which take place in interfacial tension and in the interfacial area of the droplet during this period.

Despite these difficulties many mathematicial models have been proposed to predict dispersed phase mass transfer rates during drop-formation. These are summarised in Table 4.1. All the expressions describe diffusion mass transfer and are based on one of the following theoretical models:

1) The model of an ageing rigid boundary layer which increases in surface area.
2) In the ageing boundary layer, the concentration gradient increases, because of the increase in surface area due to stretching; this is known as "the balloon model".
3) The boundary layer ages as with a rigid layer, surface is increased by addition of fresh surface elements: "The fresh surface model".
4) For the boundary layer a flow pattern has been developed in which a varying rate of stretching occurs.

Various modifications of the models are possible. In deriving the mathematical expressions for mass transfer, the following conditions have been assumed in all cases:

i) The interfacial concentration is that at saturation.
ii) Mass is transported by diffusion perpendicular to the interface.

Table 4.1 Models For Mass Transfer During Drop Formation

Authors	Correlation	Equation Number
Licht and Pensing (86)	$K_{df} = \frac{6}{7} (D_d/\pi t_f)^{1/2}$	4.1
Heertjes et al (90)	$K_{df} = \frac{24}{7} (D_d/\pi t_f)^{1/2}$	4.2
Groothuis and Kramer (45)	$K_{df} = \frac{4}{3} (D_d/\pi t_f)^{1/2}$	4.3
Coulson and Skinner (91)	$K_{df} = 2\sqrt{\frac{3}{5}} (D_d/\pi t_f)^{1/2}$	4.6
Heertjes and De Nie (92)	$K_{df} = 2\ [r_o/a_d + 2/3]\ [D_d/\pi t_f]^{1/2}$	4.5
Heertjes and De Nie (39)	$K_{df} = \frac{14}{3}\ [r_o/a_d + 1/3]\ [D_d/\pi t_f]^{1/2}$	4.6
Ilkovic (93)	$K_{df} = 1.31\ (D_d/\pi t_f)^{1/2}$	4.7
Angelo et al (88)	$K_{df} = \frac{2}{\tau} \sqrt{\tau}\ (D_d/\pi t_f)^{1/2}$	4.8

iii) The process of diffusion is slow compared with the process of drop growth.

iv) Variations in the diffusion coefficient in the direction of flow can be neglected.

The mathematical expressions given in equations 4.2, 4.3, 4.4 and 4.7 in Table 4.1 were tested by Skelland and Minhas (94) and found to predict considerably lower mass transfer rates than experimentally observed values. This was due to the lack of allowance in the models for internal circulation, interfacial turbulence, and disturbances caused by drop detachment. They therefore, proposed a modified expression which includes other parameters, eg. density, viscosity and interfacial tension.

$$K_{df} = 0.0432 \frac{d}{t_f} \left(\frac{V_N^2}{d_g} \right)^{0.089} \left(\frac{d^2}{t_f D_d} \right)^{-0.334} \left(\frac{\mu_d}{\sqrt{\rho_d d \sigma}} \right)^{-0.601} \qquad (4.9)$$

This correlation represents the overall mass transfer occuring during drop formation, which includes mass transfer during drop growth, during the detachment of the drop, and the influence of the rest of the drop. The average absolute deviation from the experimental values was approximately 25%. This model did not consider the rate of formation as one of the variables affecting mass transfer, whereas Heertjes (92) and Coulson and Skinner (91) observed mass transfer at high frequencies of drop formation. However, all models lead to a similar type of expression, describing the efficiency as proportional to the square root of the time of formation:

$$E_f = F\left(\frac{D_d\, t_f}{\pi}\right)^{1/2} \qquad (4.10)$$

in which E_f = the efficiency during drop formation.

D_d = Diffusion Coefficient.

t_f = time of drop formation of the drop.

F = proportionality constant, which depends on the model used and on the surface area-volume relation of the growing drop.

Values of the factor F for the four models are given in Table 4.2 for the simplified case of a spherical drop of diameter d.

Table 4.2 Values of the Factor F

Model	F. $\frac{d}{6}$
1	0.86
2	1.13
3	1.48
4	1.78 front
	1.31 equator
	0.50 rear

At a moderate formation rate the following expression of Popovich et al (95), based on the fresh surface model can be used for the prediction of mass transfer rate,

$$E_f\ V_{dr} = \frac{4n}{2n+1} \int_0^1 \{(1-y^2)dy\ (C^* - C_o)$$

$$\left(\frac{D_d}{\pi}\right)^{0.5} B_p t^{(2n+1)/2}\} \qquad (4.11)$$

where n and B_p are defined by: the surface area $A = B_p t^n$ and $y = (1 - t/t_l)^{1/2}$; t is the time at which a fresh surface element is formed and t_l, that when the mass transfer is considered. The above model is applicable to drops with a moderate rate of formation given by:

$$1.286 \times 10^6 \leq \left(\frac{d^2}{t_f D_d}\right) \leq 12.31 \times 10^4$$

For the special case of a spherical drop the equation reduces to:

$$E_f = \left(\frac{A_R}{2\,V_{dr}} + \frac{4}{3} B\right) \left[\frac{D\,t_f}{\pi}\right]^{0.5} \qquad (4.12)$$

In the case of formation at high speed, ie. Re > 40, large contributions to mass transfer are caused by strong circulation in the drop. For circulating drops Johnson et al (96) showed that the amount of transfer taking place during formation could be estimated by the correlation:

$$E_f = \frac{20.6}{d} \cdot \left[\frac{\pi}{D.\,t_f}\right]^{0.5} \qquad (4.13)$$

In an agitated column the formation of drops at the inlet distributor may not be correlated by the above equation if turbulence from the agitated section extends to the orifices eg. if less than one compartment height separates the distributor from the first agitated compartment.

4.4. MASS TRANSFER DURING DROP-RISE

Mass transfer during drop rise in the continuous phase is significantly influenced by the hydrodynamic state of the drop, ie. whether it is stagnant, circulating or oscillating. Circulation or oscillation results in intense mixing inside the drop, resulting in a high rate of mass transfer to, or from, the drop. Conversely, a stagnant drop, in which internal mixing is completely inhibited, has a lower mass transfer rate. Whether a drop is stagnant, circulatory or oscillatory depends upon its Reynolds number Re defined as:

$$Re = \frac{d.v.\rho}{\mu_c} \qquad (4.14)$$

Oscillation starts when the droplet Reynolds number exceeds 200 as discussed later. Below this circulation predominates (97). The amount of mass transfer during release was reported by Licht and Conway (98) to be of the same magnitude as that for the period of drop formation, whereas Popovich et al (95) concluded that drop release had no effect at all. The different conclusions may be attributed to the fact that in the later work, the main resistance to mass transfer was in the continuous phase. Marsh and Heideger (100) deduced that a high contribution to mass transfer occured during release. In a recent contribution Heertjes and de Nie (92) showed that, for isobutanol drops in

water, the mass transfer coefficient during release was six times greater than the value for the preceding period. However, confirmation of this awaits further work with other liquid- liquid systems.

4.4.1. Mass Transfer in the Dispersed Phase

Studies of the mechanism of mass transfer inside droplets in liquid-liquid systems during drop travel have compared experimental rates of mass transfer to rates predicted by various mathematical models. In many cases the experimentally determined rate has been greater than that predicted (87, 91, 99). The different models have been presented in the form of an extraction efficiency, E_m, or an internal mass transfer coefficient, k_d and the basic assumptions, common to all models are that the drop is spherical and of constant volume and that the solute concentration is sufficiently dilute for the physical properties to be essentially constant. When the major resistance to mass transfer is in the dispersed phase, the overall transfer rate will be controlled by the transfer mechanism inside the drop and this is influenced by the hydrodynamics of the system.

The dispersed phase mass transfer coefficient depends upon the size of the drop and the physical properties of the system. Mass transfer within the drops is characterised for three different types of drop namely: stagnant, circulating and oscillating drops, where the droplet Reynolds number may be used as a rough guide to determine the hydrodynamic state of the drops.

4.4.1.1. Stagnant Drops

These are generally very small drops, ie. < 2mm diameter but in the presence of surface active agents larger drops may behave as stagnant drops. Drop Reynolds

number is between 10 and 50. The liquid inside the drop is stagnant and mass transfer either into or out of the drop takes place initially by molecular diffusion and the mass transfer coefficient is best estimated by Newman's relation (101).

$$E = 1 - \frac{6}{\pi^2} \sum_{n=1}^{\infty} \exp\left(\frac{-4.\, n^2 D_d \pi^2 .t}{d^2_p}\right) \qquad (4.15)$$

where D_d = diffusivity of the solute in the liquid inside the drop

d_p = Drop size

n = integer

Vermeulen (102) found that Newman's model could be closely approximated by an empirical expression by taking the first term in equation 4.15 and neglecting the ratio $(6/\pi^2)$. Thus for n = 1

$$E_m = \left[1 - \exp \frac{-4\pi^2 \; D_d.t}{d_p{}^2}\right]^{0.5} \qquad (4.16)$$

which for values of $E_m < 0.5$, reduces by a series expansion neglecting higher order terms to:

$$E_m = \pi \left(\frac{4\, D_d t}{d^2_p}\right)^{0.5} \qquad (4.17)$$

Correlation for the mass transfer coefficient based on a linear concentration difference driving force was proposed by Treybal (8):

$$k_{d.s} = \frac{2.\pi^2 D_d}{3\, d_s} \qquad (4.18)$$

4.4.1.2. Circulating Drops

Experimental studies indicate that the rate of mass transfer is greater when circulation occurs. The circulating droplets are those in which the fluid inside the drop is in a state of rapid circulation, where the Reynolds number of the drop exceed 50. As the circulating velocity is increased, liquid at the centre of the drop is rapidly transferred to the surface. Furthermore, the circulating pattern encourages mixing, so that the driving force increases, with the result that the mass transfer coefficient is about 5 times greater than for stagnant drops.

There are numerous correlations to estimate the mass transfer coefficient of circulating drops but the one found most reliable is that due to Kronig and Brink (103). They derived a relation for a droplet with internal circulation based on Hadamard (104) flow pattern assuming that the time of circulation is small compared to the time of solute diffusion and that the continuous phase resistance is negligible. They obtained the expression:

$$E_m = 1 - \frac{3}{8} \sum_{n=1}^{\infty} A^2_n \exp\left\{-\lambda_n \frac{64\, D_d t}{d_p^2}\right\} \qquad (4.19)$$

where A_n and λ_n are eigenvalues.

Heertjes et al (90) presented values of A_n and λ_n for values of n from 1 to 7. Calderbank et al (105) suggested an empirical approximation to equation 4.19

$$E_m = \left[1 - \exp\left(-\pi^2 \frac{4\bar{R}.D_d t.}{d^2_p} \right) \right] \qquad (4.20)$$

where $\bar{R}$ is the dimensionless correlation factor of the molecular diffusivity, is equal to 2.25.

Under laminar circulation, Kronig and Brink proposed an approximate expression for mass transfer coefficient for circulating droplets,

$$k_{d.c} \cong \frac{17.9\, D_d}{d_c} \qquad (4.21)$$

For the case of turbulent circulation, Handlos and Baron (106) proposed the correlation:

$$k_d = \frac{0.00375\, V_t}{(1 + \mu_d/\mu_c)} \qquad (4.22)$$

Equation (4.22) has been verified experimentally by Skelland and Wellek (107) and Johnson and Hamielec (96). Olander (108) reported some deviation when using Handlos and Baron's model for cases involving short contact times. This was due to the fact that in the derivation of equation (4.22) only the first term of the series which appears in the mathematical expression had been used. This is permissible for long contact times only. Thus Olander proposed a correlation for the calculated mass transfer coefficient (108).

$$k_d = 0.972\, k_{HB} + 0.075 \frac{d}{t} \qquad (4.23)$$

where k_{HB} is the mass transfer coefficient calculated by means of the Handlos and Baron model. Equation 4.23 is for cases where the resistance in the continuous phase is zero.

4.4.1.3. Oscillating Drops

In general at low continuous phase viscosities, when the drop Reynolds number exceeds 200 the drop oscillates, throughout its existence, and the frequency of oscillation is sustained to give intense mixing of the liquid inside the drop. Furthermore, as the drop shape changes from a prolate spheroid to an oblate spheroid, the interfacial surface stretches. Thus a sphere of given volume has the minimum surface and therefore any departure from sphericity increases the surface area thereby enhancing the opportunities for elements of the liquid inside the drop to rise to the surface thereby facilitating mass transfer. There are two basic models to correlate the mass transfer coefficient of oscillating drops, due to Rose and Kintner (97) and Angelo and Lightfoot (88). Rose and Kintner applied a variation of the film theory to mass transfer within oscillating droplets. The Rose and Kintner model is supported by extensive experimental results and is the one recommended for the evaluation of the oscillating drop mass transfer coefficient. This model considers the amplitude and frequency of single drop oscillation. The final equations are,

$$E_m = 1 - \exp\left[\frac{-2\pi D_E}{V}\int \frac{1}{f_1(t)}\left\{\left(\frac{3V}{4\pi w}\right)^2 + \frac{1}{2\alpha}\ln\frac{1+\alpha}{1-\alpha} + \omega\right\} dt\right] \qquad (4.24)$$

where $$\alpha = \frac{w - (3v/4\pi w)^2}{w} \qquad (4.25)$$

$$w = [a_o + a_p \{\sin 0.5\,\omega t\}]^2 \tag{4.26}$$

$$f_1(t) = \frac{a_o^2 b - (a - x_o)^2 (b_o - x_o) - 2abx_o + bx_o^2}{a^2 - 2a\,x_o - x_o^2} = x \tag{4.27}$$

$$a = a_o + a_p \{\sin 0.5\,\omega t\} \tag{4.28}$$

and

$$b = \frac{3V}{4\pi a^2} \tag{4.29}$$

The correlation proposed by Rose and Kintner for the dispersed phase mass transfer coefficient is (97),

$$k_d = 0.45.\,(D_d\omega)^{0.5} \tag{4.30}$$

where D_d = Diffusivity of the solute in the dispersed phase.

ω = The frequency of the oscillating drop.

The frequency of oscillation is predicted with the Schroeder and Kintner (131) modification of Lamb's (233) equation:

$$\omega^2 = \frac{\sigma b}{r^3}\left[\frac{n(n-1)(n+1)(n+2)}{(n+1)\rho_d + n\rho_c}\right] \tag{4.31}$$

σ = interfacial tension of the system

b = a coefficient related to the drop size to the power 0.225

while:
$$b = \frac{d_p^{0.225}}{1.242} \tag{4.32}$$

ρ_d, ρ_c = densities of the dispersed and continuous phase

n, the mode of oscillation, for rigid body motion n = 0.1. For fluid oscillating drops n > 1.

In Kintner's work which was carried out with Reynolds number close to 200, n was equal to 2. In the majority of situations which should be designed into extraction equipment n = 2. The maximum value of n is 4, but under these conditions the oscillating drops are in danger of breakage resulting in the production of a myriad of stagnant drops and a significant reduction in mass transfer rate coupled with coalescence problems at the phase separation interface ie. an increased flocculation - coalescence zone height.

Angelo et al (88) also based their model on surface stretch and internal mixing of the drop. The empirical relation for k_d is given as:

$$k_{d.o} = \left[\frac{4 D_d \omega (1 + \varepsilon_o)}{\pi} \right]^{0.5} \tag{4.33}$$

where ω is the frequency and ε_o is a dimensionless factor for the amplitude, which is given by:

$$\varepsilon_o = \varepsilon + \frac{3}{8} \varepsilon^2 \tag{4.34}$$

$$\varepsilon = \left(\frac{A_{max}}{A_o}\right)^{-1} \tag{4.35}$$

$$A = A_o (1 + \varepsilon \sin^2 \omega t) \tag{4.36}$$

The overall mass transfer coefficient is given by:

$$K_d = k_d \left[\frac{1}{\left[1 + m \left(\frac{D_d}{D_c}\right)^{0.5}\right]} \right] \tag{4.37}$$

4.4.2. Mass Transfer in the Continuous Phase

The continuous phase mass transfer coefficient may be evaluated in terms of the resistance in the film surrounding the drop through which the transfer takes place by molecular diffusion. The overall mass transfer process between dispersed and continuous phase, includes the contribution of mass transfer in the continuous phase. This is very difficult to predict due to the wake of the drop. Thus the process has often been described as an overall process for the whole drop, using a partial coefficient of mass transfer k_c.

Numerous investigations have been performed to derive a theoretical, or empirical, correlation for the continuous phase mass transfer coefficient. Summaries of these investigations can be found in the work of Linton et al (109), Sideman et al (110) and Griffith (111).

The different mechanisms of mass transfer in the continuous phase from, or to, a droplet are dependent on the droplet's hydrodynamic state as considered below.

4.4.2.1. From, and to, Stagnant Droplets

For the case of a stagnant drop, theoretical analysis by Garner and Suckling (112) and Garner and Jenson (113) based on the boundary layer theory, have shown that the rate of mass transfer can be correlated by a general equation:

$$Sh = A + C\ Re^{m}\ .\ Sc^{n} \qquad (4.38)$$

where A, C, m and n are constants. Examples from the literature are reproduced in Table 4.3.

4.4.2.2. From, and to, Circulating Droplets

The correlations proposed to describe mass transfer in this case are similar to those given for stagnant drops ie. k_c found via a Sherwood number relation. These expressions are given in Table 4.3. Many studies (114, 96, 103) have indicated that the continuous phase mass transfer coefficient is increased when circulation occurs inside the drop due to reduction in the boundary layer thickness. In Equation 4.42 the proportionality constant may be lower than 1.13 because of the existence of a wake under particular conditions. Thus Garner and Tayeban (114) proposed Equation 4.43 with a constant of 0.6. In another study Garner (118), using a partially miscible binary liquid-liquid system of low interfacial tension, observed that the exponent on the Schmidt group for stagnant drops is 0.33, and for fully circulating flow 0.5. Hence they proposed Equation 4.44 with an exponent of 0.42 on the Schmidt number.

In a recent study by Mekasut et al (119) on the transfer of iodine from an aqueous continuous phase to carbon tetrachloride drops the resistance to mass transfer was assumed to be solely in the continuous phase. The Sherwood number was

Table 4.3 Correlations for Continuous Phase Mass Transfer Coefficient

Author and Reference	Correlation	Equation Number	Hydrodynamic state of drops	Comment
Linton and Sutherland (109)	$Sh_c = 0.0582\,(Re)^{0.5}\,(Sc)^{0.33}$	4.39	Stagnant	Ignores diffusion and wake effect.
Rowe et al (115)	$Sh_c = 2 + 0.76\,(Re)^{0.5}\,(Sc)^{0.33}$	4.40	Stagnant	Account for discussion process.
Kinard et al (116)	$Sh_c = 2 + (Sh_n) + 0.45\,(Re)^{0.5}\,(Sc)^{0.33}$	4.41	Stagnant	Include diffusion process and wake effect.
Boussinesq (117)	$Sh_c = 1.13\,(Re)^{0.5}\,(Sc)^{0.5}$	4.42	Circulating	Claimed to be valid for many systems.
Garner and Tayeban (114)	$Sh_c = 0.6\,(Re)^{0.5}\,(Sc)^{0.5}$	4.43	Circulating	Inapplicable to Re >450
Garner et al (118)	$Sh_c = -126 + 1.8\,(Re)^{0.5}\,(Sc)^{0.42}$	4.44	Circulating	For partially miscible binary system of low interfacial tensions.
Mekasut et al (119)	$Sh_c = 1.04\,(Ga)^{0.49}$	4.45	Circulating	Ga is Galileo number $Ga = d^3 \rho_c^2 g/\mu_c^2$
Garner and Tayeban (114)	$Sh_c = 50 + 0.0085\,(Re)\,(Sc)^{0.7}$	4.46	Oscillating	Successfully used by Thorsen et al (58)
Yamaguchi et al (120)	$Sh_c = 1.4\,(\bar{Re})^{0.5}\,(Sc)^{0.5}$	4.47	Oscillating	$\bar{Re} = \rho_c \omega d_e^2/\mu_c$
Mekasut et al (119)	$Sh_c = 6.74\,(Ga)^{0.34}$	4.48	Oscillating	Ignores the effect of frequency of oscillation.

correlated with Galileo number ($Ga = d^3 \rho_c^2 g/\mu^2_c$) in equation 4.45 for drop diameters <0.265cm.

4.4.2.3. From, and to, Oscillating Drops

Various workers (107, 96, 121) have used correlations to estimate mass transfer rates during oscillation, which causes higher mass transfer rates than circulation (97, 114). The continuous phase mass transfer coefficient was correlated universally by Garner et al (114). They reported a Schmidt number exponent > 0.5, because for oscillating drops, there is less dependence on diffusivity (122). Yamaguchi et al (120) proposed equation 4.47 with a modified Reynolds number $\bar{Re} = \dfrac{\rho_e \omega d^2_e}{\mu_c}$ which neglects the drop velocity.

Galor and Hoelscher (71) derived a mathematical model for unsteady-state mass transfer. Inter-actions within a swarm of drops and the effect of drop size distribution, have been taken into account. From their equation k_c should be linearly proportional to a mean drop size diameter $(d_{32})^{0.5}$.

$$k_c = 0.371 \left\{ \frac{D_d (\rho_c - \rho_d) g}{2\mu_c + 3\mu_d} (1/2\, d_{32}) \right\}^{1/2} \qquad (4.49)$$

Hughmark (123) concluded that for a swarm of drops in a system for which the ratio of viscosities of the continuous to the dispersed phase is <1.0, the mass transfer coefficient for the continuous phase is the same as for single drops. For (μ_c/μ_d) for ratios > 1.0, an interaction effect in the continuous phase has to be recognised.

Finally a new approach was used by Mekasut et al (119) who correlated the Sherwood number with the Galileo number in equation 4.45 to predict the mass transfer coefficient of the continuous phase of the oscillating drop. Hendrix et al (124) observed that oscillation of drops resulted in irregular oscillation of the wake and that the wake diminished rapidly and did not follow the drop closely.

4.5. MASS TRANSFER DURING COALESCENCE

Each drop leaving the last compartment of an RDC is required to flocculate and then coalesce. Some mass transfer occurs during this process. Various workers have found that coalescence rates are greatly affected by the presence of mass transfer. These rates were also dependent on the direction of transfer. Groothuis and Zuiderweg (83) observed enhanced coalescence when transfer was from the dispersed phase to the continuous phase. This was considered to be due to the Marangoni effect which was subsequently confirmed by Jeffreys and Lawson (80), Sawistowski (125) and from work in agitated columns by Al-Hemeri (33) and Arnold (126, 127). This observation is only applicable however, if the solute decreases the interfacial tension, since McFerrin and Davidson (128) using the system water-di-isopropylamine-salt, in which the solute salt increased the interfacial tension, found that transfer into the drop aided coalescence and out of the drop it was hindered.

Johnson and Hamielec (96) derived an expression for K_{dc} for the simplified case of a drop coalescing immediately upon reaching the boundary between the phases:

$$K_{dc} = \left(\frac{D_d}{\pi t_f} \right)^{0.5} \qquad (4.50)$$

Penetration theory was assumed to hold for the process. Similar results were reported by Licht and Conway (98) and Coulson and Skinner (91) but, Skelland and Minhas (94)

subsequently criticized the above models, and concluded that the amount of mass transfer during coalescence is insignificant compared to that during drop formation. Their experimental data for mass transfer coefficient during coalescence was correlated by:

$$\frac{K_{dc}\, t_f}{d} = 0.1727 \left(\frac{\mu_d}{\mu_d D_d} \right)^{-1.115} \left(\frac{\Delta\rho g d^2}{\sigma} \right)^{1.302} \left(\frac{V^2_t\, t_f}{D_d} \right)^{0.146} \tag{4.51}$$

The average absolute deviation from the data was approximately 25%.

Skelland and Minhas's (94) observation of insignificant mass transfer on coalescence at the interface has been confirmed by Heertjes and De Nie (39, 129) who argued that drainage of drop contents in a homosphere does not allow entrainment of continuous phase in the homosphere. Furthermore coalescence is so rapid (occupying only about 3×10^{-2} sec) that no substantial mass transfer is to be expected. This is particularly true in the case of agitated columns, where efficient mass transfer takes place in the column proper.

4.6. THE OVERALL MASS TRANSFER COEFFICIENT

The overall resistance to mass transfer is calculated as the sum of the resistances of the individual phases, where the interfacial resistance is generally neglected. The resistance to transfer in one of the phases is often predominant and the design equations can then be based on the coefficient in that phase only. A criterion, as to which phase is controlling, requires the knowledge of the time taken for the concentration of the drop to change by 95%, using the equation derived by Crank (130)

$$\frac{Q_t}{Q_o} = 1 - \frac{6}{\pi^2} \left[\frac{1}{n^2} \exp\left(- \frac{4 D_d n^2 \pi^2 t}{d^2} \right) \right] \tag{4.52}$$

or the experimentally modified version proposed by Calderbank and Korchinski (105) for the dispersed phase

$$\frac{Q_t}{Q_o} = 1 - \exp\left[-2.25\left(\frac{4D_d\pi^2 t}{d^2}\right)\right] \qquad (4.53)$$

and for the continuous phase

$$\frac{Q_t}{Q_o} = 1 - \mathrm{erf}\left[\frac{x}{\sqrt{4 D_c t}}\right] \qquad (4.54)$$

In the majority of industrial extractors the continuous phase coefficient would be expected to control the rate of extraction.

In the present work the calculated mass transfer coefficients, in Section 8, were based on the models listed in Table 4.4.

4.7. INTERFACIAL TURBULENCE

The various kinds of small flows generated at the interface, and in the layers immediately adjacent to it, are grouped together as 'interfacial turbulence'. It induces a substantial increase in the rates of mass transfer between two phases. Thus transfer rates may be much higher than predicted from a proper combination of single-phase rate coefficients on the assumption of a quiescent interface.

Interfacial turbulence covers many aspects of interfacial films, eg. interfacial gradient (Marangoni effect), or density gradient (Rayleigh effect) and cellular convection currents in the vicinity of the interface (132), but the influence of the interfacial tension gradient has been studied most frequently. Thomson (133) was the first to observe the

Table 4.4 Mass Transfer Coefficient Models

State of Droplet	Reynolds Number	Dispersed Phase Coefficient Model	Equation Number	Continuous Phase Coefficient Model	Equation Number
Stagnant	Re < 10	$k_{d.s} = \frac{4\pi^2 D_d}{3d_s}$	(4.18)	$Sh_{c.s} = 2.076\,(Re)^{0.5}\,(Sc)^{0.3}$	(4.40)
		Treybal (1963)		Rowe (1965)	
Circu-lating	10 > Re < 200	$k_{d.c} = \frac{17.9 D_d}{d_c}$	(4.21)	$Sh_{c.c} = -126 + 1.8\,(Re)^{0.5}\,(Sc)^{0.42}$	(4.44)
		Kronig and Brink (1960)		Garner-Foord Tayeban (1959)	
Oscill-ating	Re > 200	$k_{d.o} = 0.45\,(\omega D_d)^{0.5}$	(4.30)		
		Rose and Kinter (1966)		$Sh_{c.o} = 50 + 0.0085\,(Re)\,(Sc)^{0.7}$	(4.46)
				Garner-Tayeban (1960)	
		$k_{d.o} = \sqrt{\frac{4\omega D_d (1+\varepsilon_o)}{\pi}}$	(4.33)		
		Where $\varepsilon_o = \varepsilon + \frac{3}{8}\varepsilon^2$	(4.34)		
		Angelo-Lightfoot (1966)			

existence of spontaneous interfacial convection. Later Marangoni (134) observed that liquids of lower surface tension will spread on liquid of higher surface tension. This phenomenon was observed with miscible liquid as well as with immiscible and partially miscible liquid pairs and is referred to as the Marangoni effect. In the case of the Marangoni effect, the amount of solute transferred is proportional to the square root of the contact time (135). Considerable research has been carried out on the theoretical aspects of interfacial turbulence (132, 135, 125), but until now there have been no studies on the experimental aspects because of the difficulties of quantifying turbulence, the incomplete state of the data on interfacial tension in contrast to mass transfer rate data, and the dependence of interfacial turbulence on conditions of flow of the bulk phase within apparatus.

Theoretical studies of this phenomenon were presented by Pearson (137) and by Sternling and Scriven (138). Sternling and Scriven (138) in their analysis of this phenomenon, suggest that interfacial turbulence may be promoted by:

1) Transfer of solute out of the phase of higher viscosity.
2) Transfer of solute out of the phase in which its diffusivity is lower.
3) Large differences in the kinematic viscosity and solute diffusivity between the two phases.
4) Large concentration gradients near the interface.
5) Strong variation of interfacial tension with solute concentration.
6) Absence of surface active-agents, and
7) Highly dispersed systems with large interfacial area.

While the model of Sternling and Scriven is a radically simplified one, it serves remarkably well to predict the creation, propagation and damping of turbulence. Orell and Westwater (139) used Schlieren photographic methods and have confirmed some of the above conditions.

Sherwood and Wei (140) showed that the most pronounced interfacial turbulence is observed when a chemical reaction is simultaneous with mass transfer, as in the extraction of acetic acid from benzene droplets by water containing ammonia.

Haydon (141) developed a theory implying that spontaneous interfacial turbulence should occur with transfer of solute in either direction. Maroudas and Sawistowiski (142, 143) found their experimental results agreed with Haydon's theory. They also concluded that Sternling and Scriven's theory is too simple to give a reliable criterion of interfacial instability. This resulted from their finding that the intensity of interfacial turbulence during the transfer of phenol and propronic acid between carbon tetrachloride and water was higher when the transfer was into the aqueous phase, in which the kinematic viscosity is higher and diffusivity is lower.

Finally, Davies (144) reported that for the extraction of acetic acid from benzene drops rising through water, the rate of mass transfer was faster by a factor of 5.9, if 5% butanol was initially present in the benzene. This arose because butanol caused spontaneous interfacial turbulence which accelerated the transfer of acetic acid. With 10% of butanol in benzene, the acetic acid transfer is 8.8 times faster than without the butanol (85).

4.8. EFFECT OF IMPURITIES

The presence of impurities or of surface active material has a marked effect on drop characteristics and hence on contactor efficiency and capacity. If interfacial tension is reduced it results in smaller droplets; retardation of coalescence has a similar effect (145). Interfacial compressibility also decreases, thus adversely affecting surface renewal. In addition, surface viscosity increases, and tends to slow down any movement of the interface. The amount of surface-active agent present may be so small that no measurable change in any physical property can be detected. This is particularly

true if the agent is a finely divided solid (144). Even a few parts per million of the surfactant are sometimes sufficient to cause a very radical change in mass transfer to or from drops (146). This is important since traces of surfactants are common in commercial liquid-liquid extraction operation. Garner and Hale (147), Garner and Skelland (148) and others have shown that rate of mass transfer can be substantially reduced by the presence of such impurities, since they accumulate at the interface between dispersed and continuous phases. This inhibits circulation within the drops, changes the pattern of drop oscillation, sets up mechanical barriers to transfer across the interface, and modifies the shape of the drops.

The presence of surfactant directly influences the interface as well as drop size and movement. The lowered interfacial tension results in smaller droplets and retardation of coalescence has a similar effect (145). In a spray column, hold-up has been found to increase by a factor of 2 to 2.5 for a coalescing system and 1.4 to 1.6 for a non-coalescing system (149). Surfactants retard circulation in droplets, the agent being collected like a cap at the rear of the drop.

Reman (29) reported that when extracting heavy distillates with furfural, emulsification caused by pitch contamination may reduce RDC capacity by a factor of 2.5. The absence of droplet coalescence in RDC's during the extraction of phenols from a continuous aqueous phase with Fenosolvan or benzene has been attributed to the presence of surface active agents (150).

4.9. APPLICABILITY OF SINGLE DROP MASS TRANSFER MODELS FOR THE DESIGN OF AGITATED EXTRACTORS

The application of single drop mass transfer correlations to agitated extractors may, above a minimum hold-up, be of limited value due to the complex interactions between drops of different sizes in the swarm. The basic differences may be

summarised as follows:

- In the case of single drop mass transfer a reasonably-accurate estimate may be made for the driving force. Difficulties arise with a swarm of drops, due to the mixing action of the rotors and back-mixing of the two phases.
- Generally in a swarm of drops, the mass transfer coefficients are higher than those predicted from single drop models. This is due to the phenomena of coalescence - redispersion and associated surface renewal effects, which predominate in agitated extractors.
- Drop break-up may lead to a higher surface area but a lower mass transfer coefficient, due to change in modes of mass transfer.
- A wide range of drop sizes may exist resulting in different modes of mass transfer and also a residence time distribution.

In industrial contactors important effects may also arise due to the presence of impurities and surface active agents. Hence single drop models presented in sections 4.4.1 and 4.4.2, and based on pure systems under ideal conditions, will seldom apply in practice. The significance of some of these effects (151, 152) is a central consideration in the present study as described in Sections 4.7 and 4.8 and to back mixing (Chapter 6).

5. FUNDAMENTALS AND PERFORMANCE OF THE RDC

The RDC was first introduced in 1951 by Reman (6). A sketch of the apparatus is shown in Figure 5.1. It consists of a number of rotating discs centered between stator rings which form the compartments.

The dense phase is introduced into the top of the column and the light phase into the bottom, so that, counter current flow is established by gravity. In modern designs (153, 33), one of the phases is dispersed at either the top or bottom of the column by means of a distributor. This has been found to provide a saving in the effective column height (154). Flat rotor discs without protrusions are generally used to create uniform shearing conditions and hence obtain as small a spread in droplet size as possible. The requisite size of droplets in the effective length of the contactor is maintained by variation of the rotor speed.

The important column variables that affect the performance of a rotating disc contactor for a given extraction system are the column diameter D, the rotor diameter R, the stator opening S, the compartment height H and the speed of rotation of the discs N. These parameters and the flow rates of the liquid phases affect the hold-up of the dispersed phase, flooding rates of the two phases, residence times of the liquids, drop size and drop size distribution and mass transfer rates (155).

For optimum design the column should have the following ratios (23, 76, 156, 66, 157, 158).

$$\frac{\text{Stator diameter (S)}}{\text{Column diameter (D)}} = 0.66 \text{ to } 0.75$$

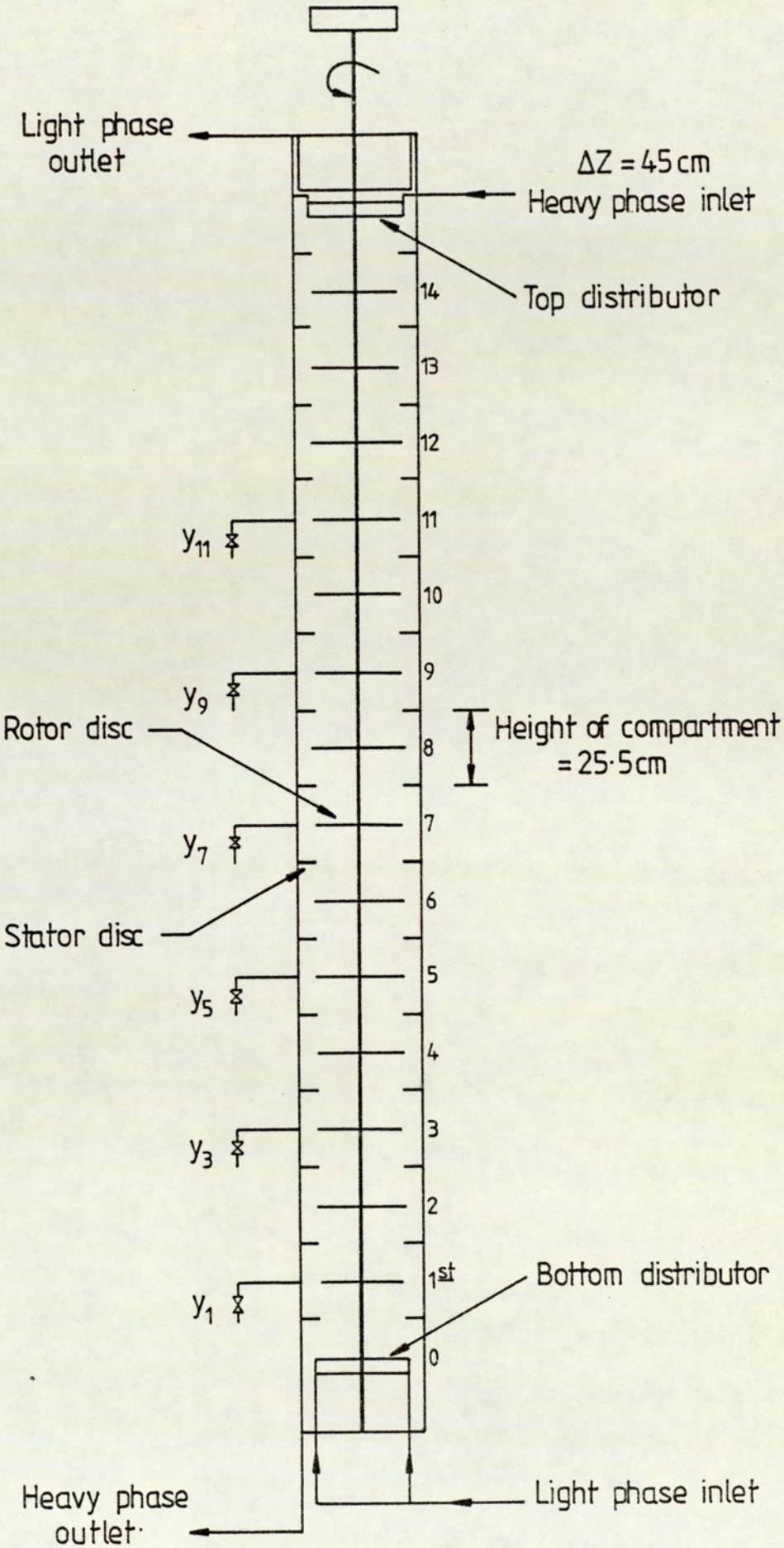

Figure 5·1 R.D.C. Column Arrangement

$$\frac{\text{Disc diameter (R)}}{\text{Column diameter (D)}} = 0.5 \text{ to } 0.66$$

$$\frac{\text{Compartment height (H)}}{\text{Column diameter (D)}} = 0.33 \text{ to } 0.5$$

However, these ratios pertaining to the choice of column geometry may be varied slightly to provide flexibility in design. Such variations may be used to alter the column flow capacity and mass transfer efficiency. For example, increasing the rotor diameter decreases the column throughput but increases the efficiency. Increase in stator ring opening or compartment height will increase the volumetric capacity but decrease the efficiency of the contactor.

Numerous modifications have been proposed in an attempt to improve the RDC's capacity and efficiency. The Asymmetric Rotating Disc-Extractor (159) is the most important modification of the RDC and was developed by Misek and co-workers (12). The main difference from the RDC is that the shaft is placed off-centre. A transfer zone is located at the side of the column, providing a path to the mixing chambers above and below the one being considered. It is claimed that this arrangement considerably reduces unfavourable flow such as axial mixing. An approximate relation for the estimation of extractor capacity has been published (57, 14). One known application is in Caprolactam recovery but several are claimed to be in operation (13).

Another modified RDC designed by Reman (160) has two rotors in the column shell. This is claimed to minimise instability of the vortex flow pattern in large diameter columns. Another design incorporating perforated disc rotors has been tested on a pilot scale (161, 162). For the extraction of acetic acid from a dilute (3-5% w/w) dispersed benzene solution by a continuous aqueous phase it gave three times the mass transfer of a conventional RDC of the same geometry. This was attributed to the

substantial reduction in average drop size. However, a significant reduction in capacity was also observed. The experiments were carried out at low rotor speeds between 140 to 350 rpm, with discs 52mm in diameter. Under these conditions axial mixing effects were insignificant; these may be troublesome at higher rotor speeds.

Another modified RDC in which the stator rings were omitted and the discs were of two sizes, with the larger discs perforated, has been employed by Sokov et al (163). For the extraction of aromatics, this design was claimed to give both a fourfold increase in capacity and improved efficiencies at low rotor speeds compared with the RDC.

Various other extractors are not simple modifications of one of the more common designs but a combination of more than one type. Perhaps the most important extractor of this kind is the Kuhni Column (18) which incorporates features of the RDC, the sieve plate and Oldshue-Rushton columns. The column consists of a cylindrical shell with a larger diameter at the top and bottom, to assist settling. It is divided into compartments by plates perforated only at the centre so that flow from one compartment to the next is directed towards the agitator. Each compartment has four vertical baffles and is agitated by an impeller, sandwiched between two washer type discs. Such a design would give a low volumetric capacity.

Another extractor combination is the Ziehl extractor (16), which is a combination of three types, viz the RDC, the mixer settler and the pulsating column. It consists of a vertical cylindrical column terminating at the top and bottom in vessels of considerably larger diameter, to assist settling. The stirring mechanism consists of a shaft fitted with a number of star shaped impellers, which give the column a free cross sectional area of 65-75% and permits very large volumetric throughputs to be handled. The shaft imparts both a rotary and a reciprocating motion to the impellers. However, the standard RDC remains by far the most common and probably, if the rotor speed is

variable, the most versatile extractor of its type.

5.1 FLOW CHARACTERISTICS

Reman (6) observed that the flow pattern in an RDC is essentially toroidal as shown in Figure 5.2 and causes recirculation and backmixing of both liquids within each compartment. The agitation pattern imposed by the rotating disc is rather complex. The whole liquid contents rotate in the same direction as the rotor but horizontal vortices are also created between two adjacent stator rings (Figure 5.2). Such a vortex starts from the tip of the rotor disc and flows outwards to the shell, where it is deflected by the shell and the stator ring and returns to the rotor shaft. The combination of the horizontal rotation and this vortex flow results in a toroidal flow in each compartment. The overall flow of the liquids in an RDC is counter-current, being established by virtue of the difference in densities of the two phases. Reman (6) suggested that the flow pattern consists of a rotation of the whole mass of liquid and that superimposed upon this rotation is a slower movement of liquid from the shaft towards the wall of the contactor in the vicinity of the discs, and from the wall to the shaft in the vicinity of the stator rings.

A similar flow pattern was also reported by Kung and Beckmann (157) but they observed that backmixing became insignificant below an impeller Reynold's number of 7.5×10^4. This is illustrated in Figure 5.3 and the backmixing flow pattern is shown in Figure 5.4. In a later study Mumford (67) found that a critical minimum rotor speed existed, below which a layer of dispersed phase droplets built up beneath the rotor discs.

The energy transferred from the rotor discs to the liquid creates a rather uniform turbulence in the liquid phase and this appears to be beneficial for obtaining a high mass transfer rate, that is high efficiencies.

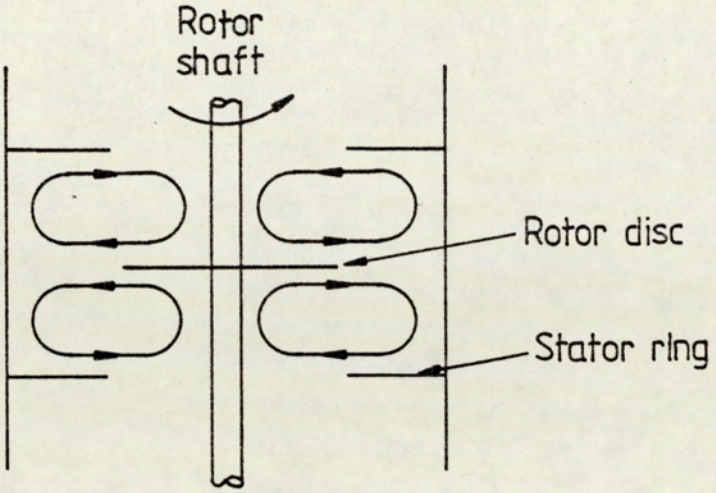

Figure 5·2 Predicted flow pattern in a RDC (6)

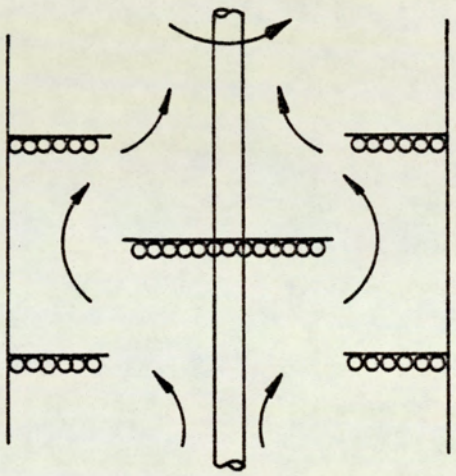

Figure 5·3 Observed dispersed flow pattern in a RDC at $R_e < 7{\cdot}5 \times 10^4$. Toluene - water system

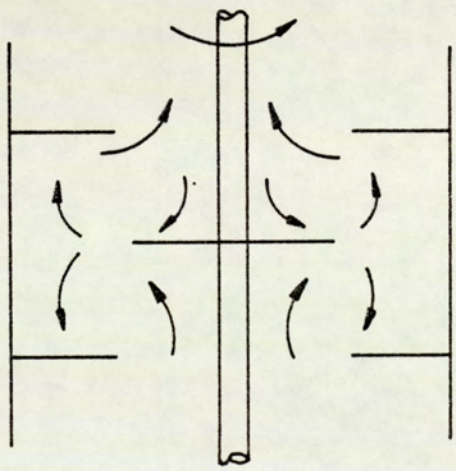

Figure 5·4 Observed dispersed phase flow pattern in a RDC at $R_e > 7{\cdot}5 \times 10^4$. Toluene - water system.

5.2 HYDRODYNAMICS

5.2.1 Hold-up

The hold-up of an extraction apparatus, equal to the ratio of the dispersed phase to the total volume of liquid in the apparatus (ie. volume fraction), is one of its most important hydrodynamic characteristics. It may also be considered as the fraction of the cross-sectional area of the column occupied by the dispersed phase.

The dispersed phase hold-up is usually used for the estimation of interfacial area for mass transfer calculations, based on the fact that under steady-state operating conditions the hold-up is proportional to the interfacial area. Correspondingly, the efficiency of mass transfer is a function of hold-up. The interfacial area in Equation 1.1 is estimated as the product of the drop surface area and the number of drops in the column. To determine the interfacial area of the dispersion either of the following should be known:

i) the drop residence time in the extractor, or,

ii) the fraction of the column volume occupied by the dispersed phase ie. the dispersed phase hold-up.

In agitated contactors, the residence time distribution is rather complex and dispersed phase hold-up is therefore usually used for the estimation of interfacial area. The interfacial area is expressed in terms of hold-up by:

$$a = \frac{6x}{d_{32}} \qquad (5.1)$$

Hold-up increases with increasing rotor speed and dispersed phase flow rate (66, 67). Logsdail et al (156) studied various two phase systems in the RDC and were the first to introduce the concept of dispersed phase hold-up for the characterisation of column hydrodynamics and thus the empirical approach to column design. These authors modified the concept of relating the slip velocity V_s of the dispersed phase to the hold-up (164, 165, 166) by:

$$V_s = \frac{V_d}{x} + \frac{V_c}{(1 - x)} \qquad (5.2)$$

to

$$V_N (1 - x) = \frac{V_d}{x} + \frac{V_c}{(1 - x)} \qquad (5.3)$$

V_N is the characteristic velocity, defined as the mean relative velocity of the drops at substantially zero flow rates and at rotor speed N.

Many correlations have been published relating the dispersed phase hold-up to the characteristic velocity with additional factors for column size (157), constriction (76) and droplet coalescence and break-up (66, 167). All these correlations are summarised in Table 5.1. Many correlations were subsequently developed to relate V_N to system and column properties, these are summarized in Table 5.2.

The majority of research regarding hold-up has been conducted on the basis of Pratt's (168) characteristic velocity. Unfortunately however correlations for the characteristic velocity achieved in spray or packed columns have been applied without question to the RDC in which the velocities of drop travel are a function of external energy input.

Table 5.1 Correlations of Dispersed Phase Hold-up in an RDC

Author & Reference	Correlation	Column Diameter (cm)	Remarks
Logsdail et al (156)	$\frac{V_d}{x} + \frac{V_c}{1-x} = V_N(1-x)$	7.62	
Kung & Beckmann (157)	$\frac{V_d}{x} + k_1\frac{V_c}{1-x} = V_N(1-x)$	15.24	$k_1 = 2.1$ for $\frac{S-R}{D} < \frac{1}{24}$ $k_1 = 1.0$ for $\frac{S-R}{D} > \frac{1}{24}$
Strand et al (76)	$\frac{V_d}{x} + \frac{V_c}{1-x} = C_R\, V_N(1-x)$	15.24 106.68	C_R = minimum constriction factor dependent on column geometry
Misek (66, 167)	$\frac{V_d}{x} + \frac{V_c}{1-x} = V_N(1-x)\exp\left[\left(\frac{Z}{\alpha} - 4.1\right)x\right]$	25.0 50.0	Z = coalescence correction factor
	$Z = 1.59 \times (10^{-2})\left[\frac{D\rho_c}{\mu_c}\left(\frac{\sigma}{\rho_c d_o}\right)^{0.5}\right]^{0.5}$		α = backmixing correction factor
	$\alpha = f(d_o.V_N.\rho_c/\mu_c)$		d_o = mean drop size.

Table 5.2 Correlation of Characteristic Velocity in an RDC

Author & Reference	Correlation	Column Diameter (cm)	Remarks
Logsdail et al (156)	$\frac{V_N \mu_c}{\sigma} = 0.012 \left[\frac{\Delta\rho}{\rho c}\right]^{0.9} \left[\frac{g_c}{RN^2}\right]^{1.0} \left[\frac{S}{R}\right]^{2.3} \left[\frac{H}{R}\right]^{0.9} \left[\frac{R}{D}\right]^{2.7}$	7.6	
Kung & Beckmann (157)	$\frac{V_N \mu_c}{c} = k \left[\frac{\Delta\rho}{\rho_c}\right]^{0.9} \left[\frac{g_c}{RN^2}\right]^{1.0} \left[\frac{S}{R}\right]^{2.3} \left[\frac{H}{R}\right]^{0.9} \left[\frac{R}{D}\right]^{2.6}$	15.0	$k = 0.012$ for $\frac{S-R}{D} > \frac{1}{24}$ $k = 0.0225$ for $\frac{S-R}{D} < \frac{1}{24}$
Laddha et al (171)	$\bar{V}_N = 0.01 \left[\frac{\sigma \Delta\rho g_c}{\rho c}\right]^{0.25} \left[\frac{g_c}{RN^2}\right]^{1.0} \left[\frac{\sigma^3 \rho c}{\mu_4 g_c}\right]^{0.25} \left[\frac{\Delta\rho}{\rho_c}\right]^{0.5} \left[\frac{H}{R}\right]^{0.9} \left[\frac{S}{R}\right]^{2.1} \left[\frac{R}{D}\right]^{2.4}$		
Jeffreys et al (65)	$\frac{V_N \mu_c}{\sigma} = 6.24 \times 10^{-3} \left[\frac{\Delta\rho}{\rho_c}\right]^{0.783} \left[\frac{g_c}{RN^2}\right]^{0.234} \left[\frac{S}{R}\right]^{1.778} \left[\frac{H}{R}\right]^{1.362} \left[\frac{R}{D}\right]^{1.922}$	45.0	For large column only.
Jeffreys et al (65)	$\frac{V_N \mu_c}{\sigma} = 4.45 \times 10^{-4} \left[\frac{\Delta\rho}{\rho_c}\right]^{-0.941} \left[\frac{g_c}{RN^2}\right]^{0.205} \left[\frac{S}{R}\right]^{1.601} \left[\frac{H}{R}\right]^{0.689} \left[\frac{R}{D}\right]^{1.786}$	7.6 15.0 45.0	Logsdail's and Kung's data are used in the correlation.

Kasatkin et al (169) proposed a correlation for hold-up by means of dimensional analysis; however, it presents difficulties in treating the dimensionless terms. Later an experimental investigation was undertaken by Murakami et al (170) into the relationship between the dispersed phase hold-up and the operating conditions and column geometry which is more realistic for estimating the hold-up in a RDC. Very recently, Jeffreys et al (65) proposed a more practical correlation over a wide range of column diameters (5.0cm to 45cm) for different liquid systems. Table 5.3 shows the dimensional analysis correlations of the dispersed phase hold-up.

5.2.2. Hold-up Profile

Hold-up in the RDC varies in both the radial and axial direction (23, 157, 156, 76). The variation in the radial direction is generally insignificant in small columns (33). In the axial direciton, the hold-up with a light dispersed phase was found to increase up the column, probably because a finite time is required for drop break-up. Towards the end of the column, the hold-up decreased; this may be due to the competing effects of axial diffusion of drops in the contact zone and of drop discharge into the settling zone from the top compartment.

Similar results were reported by Rozkos (172) in an industrial RDC. From the results reproduced in Figures 5.5 and 5.6, the maximum hold-up point corresponded to approximately the middle part of the column. In each case, the hold-up showed a maximum which increased with rotor speed.

Rod (154), later, presented a mathematical model describing the longitudinal hold-up profile by considering the two mechanisms influencing hold-up: the break-up of drops in the mixed section and the longitudinal mixing of the dispersion. Earlier findings of Strand et al (76) were that the hold-up increased to a maximum value at about half-way up the column and then decreased towards the top.

Table 5.3 Dimensional Analysis Correlations of the Dispersed Phase Hold-up

Author & Reference	Correlation	Column Diameter (cm)	Remarks
Kasatkin et al (169)	$x = 1.58 \left[\frac{NR}{V_c}\right]^{1.0} \left[\frac{V_d}{V_c}\right]^{0.96} \left[\frac{S^2 - R^2}{D^2}\right]^{-0.7} \left[\frac{H}{H}\right]^{-0.426} \left[\frac{\Delta\rho}{\rho_c}\right]^{-1.31} \left[\frac{\rho_c V_c D}{\mu_c}\right]^{-0.13} \left[\frac{\rho_c D V_c}{\sigma}\right]^{0.245} \left[\frac{V_c^2}{g_c D}\right]^{0.96}$	5.4	H = total column height
Murakami et al (170)	$x = 3.3 \left[\frac{ND}{V_c}\right]^{0.55} \left[\frac{V_d}{V_c}\right]^{0.80} \left[\frac{S^2 - R^2}{D^2}\right]^{-0.30} \left[\frac{H}{D}\right]^{-0.66} \left[\frac{R}{D}\right]^{0.40} \left[\frac{\Delta\rho}{\rho c}\right]^{-0.13} \left[\frac{\rho_c D V_c}{\sigma}\right]^{0.18} \left[\frac{V_c^2}{g_c D}\right]^{0.60}$	7.9, 10.5 30.0	
Jeffreys et al (65)	$x = 1.05 \times 10^{14} \left[\frac{NS}{V_c}\right]^{0.521} \left[\frac{V_d}{V_c}\right]^{0.775} \left[\frac{S^2 - R^2}{D}\right]^{-0.187} \left[\frac{H}{D}\right]^{-0.873} \left[\frac{R}{D}\right]^{-0.201} \left[\frac{\Delta\rho}{\rho}\right]^{4.843} \left[\frac{\rho_c D V_c}{\sigma}\right]^{1.082} \left[\frac{V_c^2}{gD}\right]^{0.892} \left[\frac{\rho_c V_c D}{\mu_c}\right]^{-2.367}$	7.62 15.24 45.0	

furfural $q_c = 24 m^3/hr$
oil $q_d = 118 m^3/hr$
D = 160 cm H_C = 705 cm

Figure 5·5

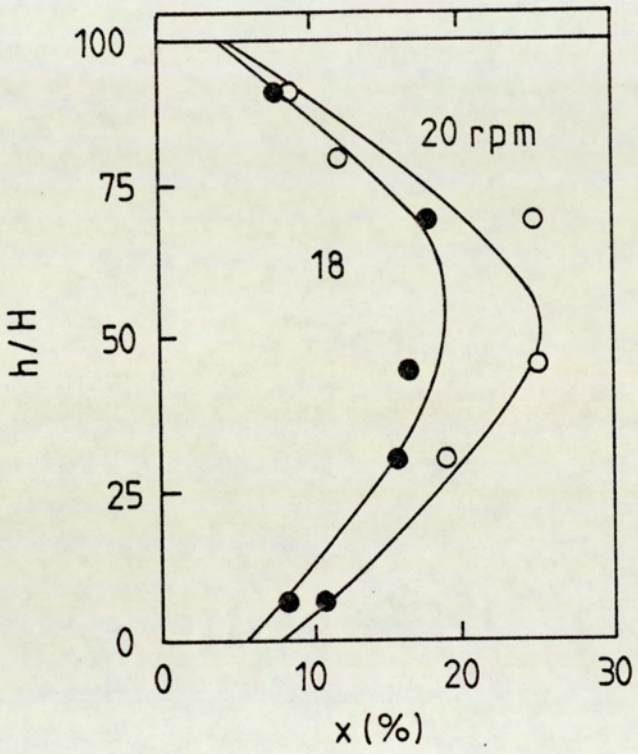

water $q_c = 45 m^3/hr$
butylacetate $q_d = 45 m^3/hr$
D = 200 cm H_C = 950 cm

Figure 5·6

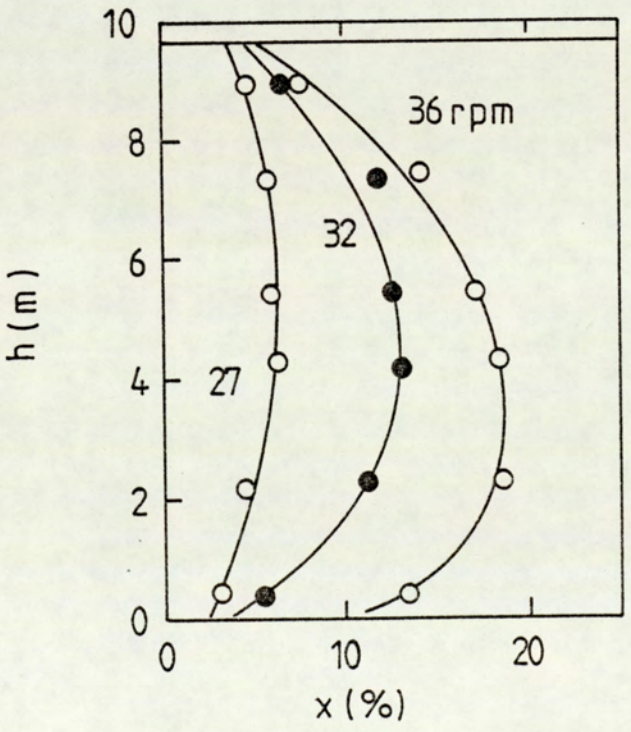

Hold-up profile in a RDC (172)

Al-Hemiri (33) operated a 10.2cm RDC and proposed the correlation:

$$x = \{0.0013\,N + 0.38\,(V_d - 1) - 1\}\,(h - h^2) + 0.076\,(1 + \frac{1}{V_d}) \quad (5.4)$$

Where x is the hold-up at height h in the column. The results are shown in Figure 5.7. Analysis of the work of Rod (154) and Mumford (67), however, reveals that the above results may only be true at low values of dispersed phase flow rate and rotor speeds.

5.2.3. Limiting Capacity of the RDC

The values of the limiting flow velocities of the dispersed and continuous phases, termed the 'flooding point', are extremely important in extractor design since it is the only information required to estimate the extractor diameter. Flooding is a typical hydrodynamic phenomenon particularly associated with differential contactors, in which for each flow rate of one phase, there is a corresponding maximum practical flow rate of the other phase. This maximum depends upon the system properties and the design of the contactor. Flow in excess of the maximum causes either of the liquids to be rejected by the equipment, which is then said to be 'flooded'. Therefore in the design of an RDC to avoid flooding it is necessary to predict the column cross-sectional area correctly for a maximum flow rate of dispersed phase for a particular flow rate of the continuous phase at each rotor speed.

Any increase in flow velocity above the maximum leads to one of the following:

i) the entrainment of the dispersed phase into the continuous phase (true flooding.

ii) the occurence of phase inversion, ie. the dispersed phase changes into the continuous phase and vice versa.

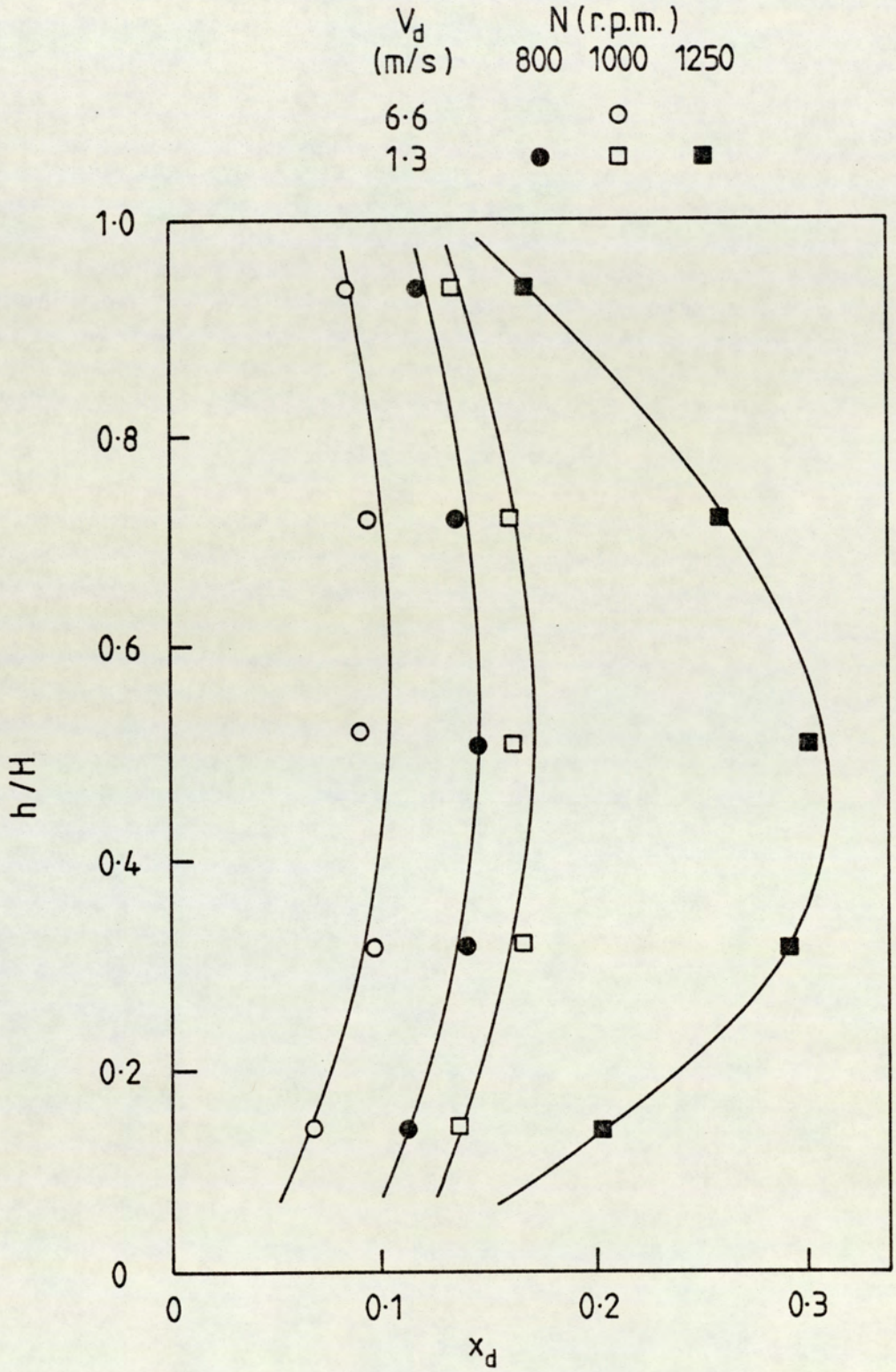

Figure 5·7 Hold-up profile in 10 cm diameter R.D.C. (33)

Knowledge of the flooding point will enable flooding to be avoided and also ensure that the preferred direction of mass transfer is maintained.

The study of dispersed phase hold-up for the characterisation of column hydrodynamics has shown (164, 19) that hold-up is related to the superficial phase velocities V_d and V_c by:

$$\frac{V_d}{x} + \frac{V_c}{1-x} = V_N (1-x) \qquad (5.3)$$

Re-arranging and differentiating

$$V_c = V_N (1-x^2) - \frac{1-x}{x} V_d$$

$$\frac{dV_c}{dx} = 2 V_N (x-1) + \frac{V_d}{x^2} \qquad (5.5)$$

$$V_d = V_N \cdot x(1-x) - \frac{x}{1-x} V_c$$

$$\frac{dV_d}{dx} = V_N \cdot (1-2x) - \frac{V_c}{(1-x)^2} \qquad (5.6)$$

At the flooding point, the flow rates reach their maximum values, hence,

$$\frac{dV_c}{dx} = \phi \quad \text{and} \quad \frac{dV_d}{dx} = \phi$$

Therefore equations (5.5) and (5.6) can be re-written as:

$$(V_d)f = 2V_N \cdot x_f^2 (1 - x_f) \tag{5.7}$$

$$(V_c)f = V_N (1 - 2x_f)(1 - x_f)^2 \tag{5.8}$$

Eliminating V_N between equations 5.7 and 5.8 yields an relationship between x_f and the flow rate $V_{d.f}/V_{c.f} = L$

Thus;

$$x_f = \frac{(L^2 + 8L)^{0.5} - 3L}{4(1 - L)} \tag{5.9}$$

Recently Baird et al (173) proposed

$$x_f = \frac{(9L^2 + 54L + 1)^{0.5} - 7L - 1}{10(1 - L)} \tag{5.10}$$

Reman (6, 23, 29, 174) studied the effect of the different variables on the limiting capacity which was found to decrease with increasing rotor speed, disc diameter and flow rate ratio V_d/V_c, but to increase with increasing stator opening and

compartment height. Successful correlation of capacity data was obtained by taking the energy input per unit volume $\frac{N^3 R^5}{HD^2}$ as determining the drop size of the dispersed phase. To allow for the effect of constrictions or settling of the drops, the capacity values were divided by a factor C_R. An approximate guide to operating range is presented in Figure 5.8 (175). Similar work was carried out by Strand et al (76) who included a constriction factor defined as the minimum of the three area ratios $(\frac{S}{D})^2$, $\{1 - (\frac{R}{D})^2\}$ and $\frac{S+R}{D}\sqrt{(\frac{S-R}{D})^2 + (\frac{H}{D})^2}$ in their analysis, and found the procedure to be valid for columns up to 106.68cm in diameter. Misek (167) calculated the limiting values of hold-up using a similar procedure to that of Logsdail et al (156). Misek proposed an expression for hold-up at flooding in an RDC.

$$\frac{V_{d.f}}{V_{c.f}} = \frac{2 x_f^2 \{(1 - x_f) + (Z/\alpha - 4.1)(x_f - (x_f^2/2) - \frac{1}{2}\}}{(1 - x_f^2)\{(1 - 2 x_f) + (Z/\alpha - 4.1)(x_f - x_f^2)\}} \qquad (5.11)$$

at Z values, ranging from 2.26 to 6.105.

5.2.4 Phase Inversion

Phase inversion is the phenomenon of interchange of phases in a liquid-liquid dispersion so that the dispersed phase becomes continuous and vice-versa under conditions determined by system properties, phase ratio and energy input.

The limiting capacity has recently been defined either by flooding or phase inversion (6, 15, 17) depending on the system characteristics, column design geometry, material of construction and operating parameters.

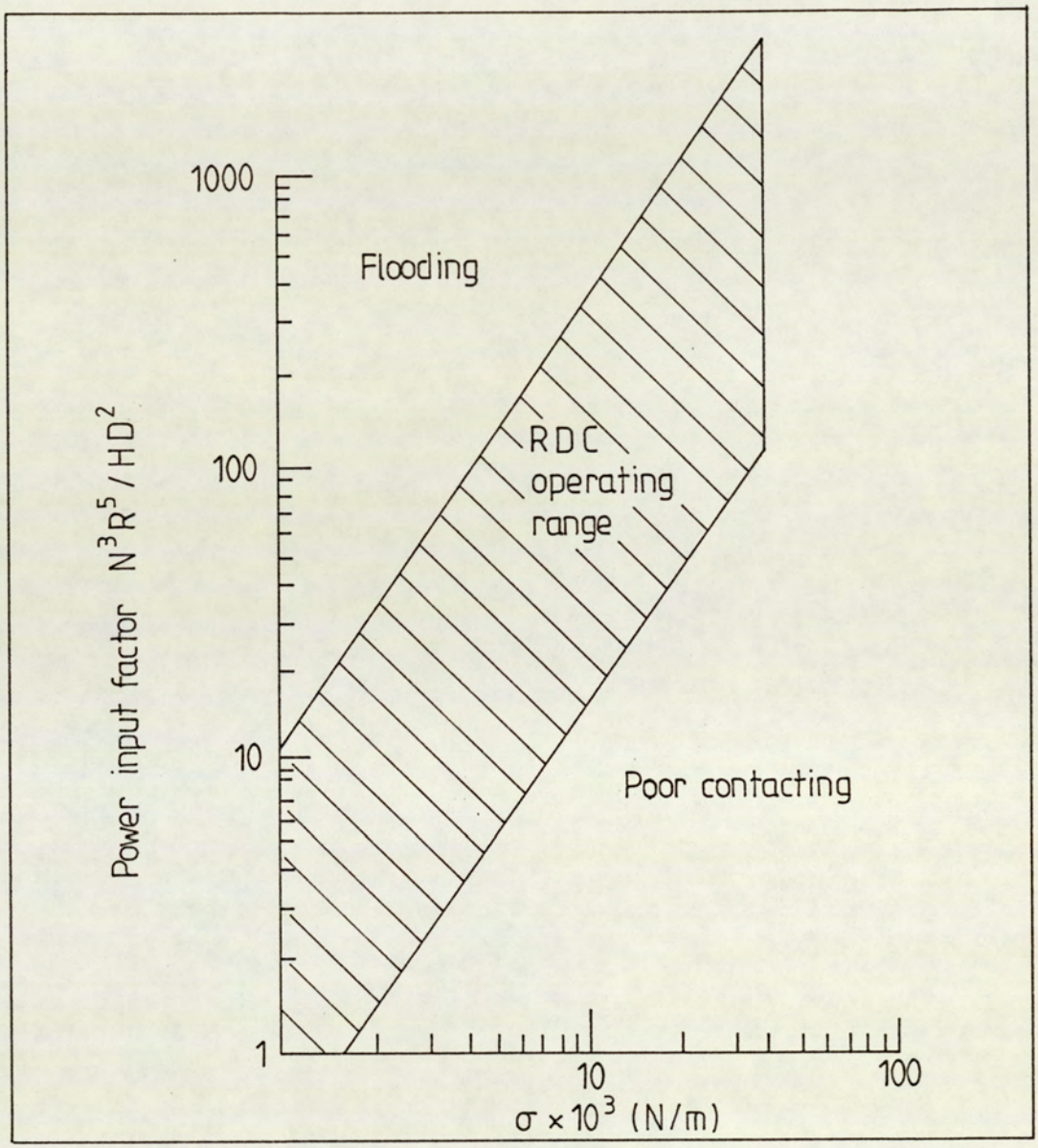

Figure 5·8 RDC Power input group operating range (175)

Under certain conditions when the dynamic equilibrium between droplet break-up and coalescence is shifted towards the later, phase inversion may occur. The inversion characteristics in a stirred tank were found to be critically affected by rate of energy input, interfacial tension, viscosity and the density ratio of the phases (176, 177). For example, the lower the interfacial tension, the greater was the resistance of the system to inversion. Clarke and Sawistowski (178), however, suggested recently that drop size rather than interfacial tension is critical in inversion. Phase inversion studies in continuous counter-current systems have to date been very limited.

Al-Hemiri (33) observed at specific operating conditions that the onset of phase inversion occurred in the bottom compartment giving rise to very large slug; this possessed a high terminal velocity and travelled up the column and eventually dispersed in the upper compartments. With further increase in the dispersed phase flow the effect was repeated at an increased frequency until all compartments reached their critical phase inversion hold-ups. Complete inversion was then obtained in the mixing section with the column still operating counter-currently. Typical results are illustrated in Figure 5.9. The following model was proposed for hold-up at inversion.

$$\frac{V_c}{V_d} = \frac{1}{K}\left\{1 - 1.5\left(\frac{1}{x_i}\right) + 0.5\left(\frac{1}{x_i^2}\right)\right\} \qquad (5.12)$$

where K is a geometric constant.

$$K = 1.0 \text{ at } \frac{S-R}{D} > \frac{1}{24}$$

$$K = 2.1 \text{ at } \frac{S-R}{D} < \frac{1}{24}$$

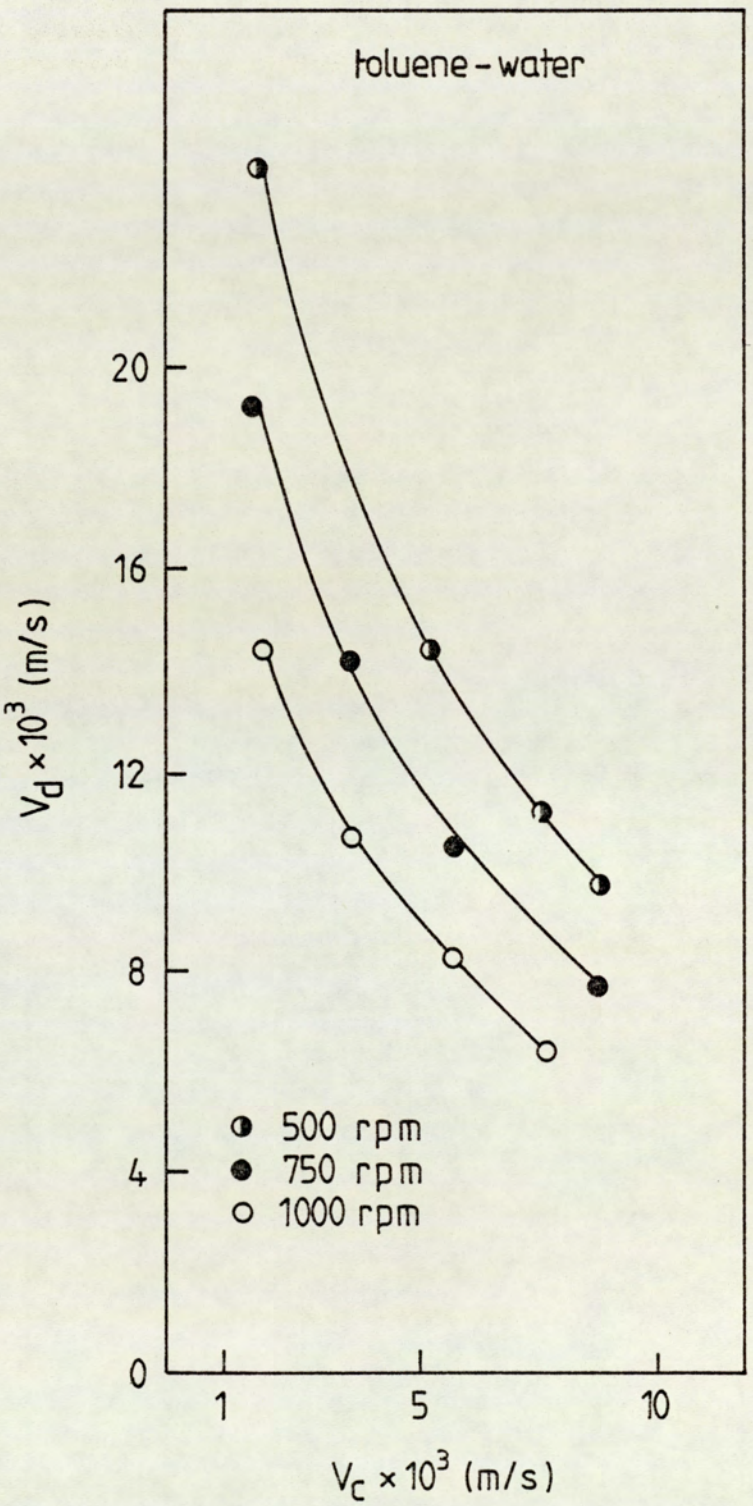

Figure 5·9 Dispersed phase flow (V_d) vs Continuous phase flow (V_c) at onset of inversion.

Sarkar's (179) analysis based on a 10cm diameter RDC revealed that a high hold-up (> 40%) of dispersed phase is an essential criterion for phase inversion. Using the systems butyl-acetate-water and toluene-water he was able to generate phase inversion but, contrary to Al-Hemiri's observation, it was a cyclic phonomenon, similar to that reported by Arnold (126) in an Oldshue-Rushton column. Phases in each unit mixing section inverted and re-inverted on a time cycle. Further work (180) using the RDC has confirmed the cyclic phase inversion mode. A model for predicting hold-up values at phase inversion in an RDC was proposed:

$$\frac{V_{c,i}}{V_{d,i}} = \frac{(1 - x_i)(3 - 4x_i)}{x_i (4x_i - 2)} \qquad (5.13)$$

which may be expressed as:

$$Rr = 1 - \left(\frac{a}{x_i}\right) + \sum_{k=2,\, j=1}^{k/j} (b)^k \frac{K}{(x_i)^j} \qquad (5.14)$$

where $Rr = \frac{V_{c,i}}{V_{d,i}}$, $a = 1.5$, $b = 0.5$

x_i = hold-up at inversion

The model was tested for $Rr < 1.0$ and was found to be in good agreement with experimental results.

The time for re-appearance of the inversion slug in a compartment was correlated by,

$$t = 0.048\ (Z)^{0.66}\ (x)^{0.33}\ (D_{tr})^{-1.0} \qquad (5.15)$$

where

Z = compartment volume

D_{tr} = drop diffusion coefficient. The value of D_{tr} may be predicted from the expression:

$$D_{tr} = \alpha\ (\bar{\varepsilon})^{0.33}\ (\lambda)^{1.33} \qquad (5.16)$$

where α = contant dependent on the continuous phase density.

$\bar{\varepsilon}$ = energy input per unit mass

λ = eddy length

These studies were the first to characterise inversion in agitated columns. The deviation of experimentally determined times, from those predicted by this correlation was within 25%; at higher energy input rate the deviation was negligible.

5.3. WETTING EFFECTS

The terms wetting and non-wetting are generally used to describe whether or not a given liquid spreads on a particular solid surface. The effect of the wetting characteristics of the column walls and internals upon column performance is an important consideration in design and scale-up and has pronounced effects upon the limiting throughputs (20). The performance of a large column may be significantly different from a laboratory column, with the same liquid system due to differences in the materials of construction and the frequency, and thoroughness, of cleaning.

In many instances when a liquid is placed upon a surface it will not completely wet it but remain as a drop with a certain angle of contact exhibited between the liquid

and the solid. The spreading coefficient is defined in terms of the contact angle and the surface tension of the liquid (181). High surface energy materials, eg. most metals and glass, are wetted by liquids with high surface tension such as water or glycerine, whilst low surface energy materials, eg. plastics, are wetted by liquids with low surface tension including most organic liquids.

Since the efficiency of mass transfer in an extractor depends upon interfacial area and turbulence in either or both phases, the degree of wetting exhibited by column internals, ie. walls, stators, rotors, packing etc, may have a significant effect. Conflicting results have been reported (182, 183, 184, 20, 185), but it is generally accepted that the best efficiency is obtained when the continuous phase wets the column internals. In an RDC with dispersed phase wetted internals, Davies, et al (75) found that the transfer rate of phenol from a dispersed aqueous phase to a kerosene phase was less than that achieved using a conventional RDC. In practical equipment, it has frequently been observed that preferential wetting of the column internals by the continuous phase deteriorated with time. This resulted in a change in the mode of operation of the equipment, possibly at the expense of extraction efficiency.

The effects were noted in a laboratory scale pulsed plate column by Coggan (20), who observed different types of dispersion at different times. These are represented in Figure 5.10.

In a later study, using an aqueous continuous phase and an organic dispersion in an RDC, a variation was observed in the wetting properties in the form of increased coalescence of dispersed phase on the glass and stainless steel column internals. This was attributed to the deposition of dirt or impurities on the column internals (9).

Al-Hemiri (33) studied the effect of wetting with a range of systems and various rotor designs, such as stainless steel or p.t.f.e. discs or poly-propylene cones,

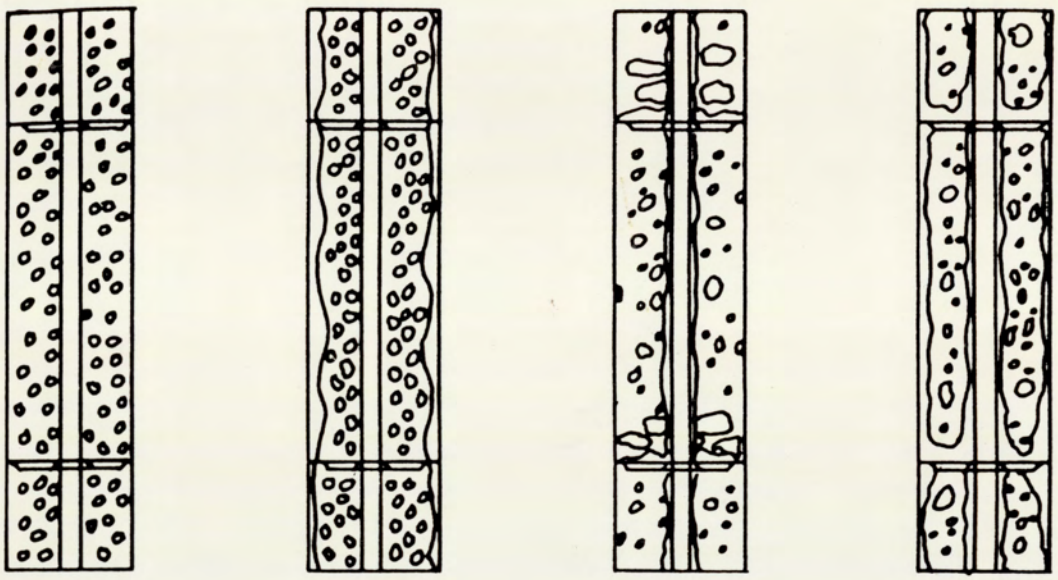

(columns shown in half-section)

Type I	Non-coalescing dispersion. The discontinuous phase wets none of the surfaces in the column and does not coalesce.
Type II	Wall-coalescing dispersion. The discontinuous phase wets the column wall and forms a continuous moving layer.
Type III	Plate-coalescing dispersion. The discontinuous phase wets the plate cartridge but not the wall. Droplets are large.
Type IV	Plate and wall coalescing. The discontinuous phase wets all the surfaces within the column and coalesces rapidly on contact. It runs down (or up) the column wall and the cartridge tie rod.

Figure 5.10 Effect of Wetting on the Type of Dispersions (20)

in a 10cm diameter RDC with stainless steel stators. Comparison of results for wetted and non-wetted rotors demonstrated that:

i) Average hold-up decreased with the wetted rotors.

ii) Phase inversion instead of flooding, defined the limiting capacity with wetted rotors.

iii) Under non-mass transfer conditons a different drop break-up mechanism, involving sheet and ligament disruption, existed with wetted rotors.

iv) For the system studied, ie. toluene-acetone-water no significant difference was observed between the efficiency of wetted and non-wetted rotors.

Although it appears from the above work that rotor wettability has no significant effect on mass transfer efficiency, the possibility remains of higher mass transfer rates due to coalescence and redispersion phenomena in wetted disc columns. Even if the mass transfer efficiency in a wetted disc column is only equivalent to that in a conventional column, the higher volumetric capacity, due to the larger coalesced drops rising faster (33), would give a better overall column performance.

5.4. POWER CONSUMPTION OF THE RDC

The sizing of the driving unit is an important step in the design of an RDC. Reman and Van de Vusse (31) considered power requirements on the basis of mixing. The results were in the form of a relation between the Power number

$$Np = \frac{P}{N^3 R^5 \rho} \qquad (5.17)$$

and the Reynolds number for mixing

$$Re_M = \frac{R^2 N \rho}{\mu} \qquad (5.18)$$

Using this correlation the power requirements for a full-size extractor could be found from pilot plant work.

In a later study Misek (186) analysed the results of previous authors and obtained a common relation of the form

$$N_p = B.Re_M^A \qquad (5.19)$$

where A and B were constants determined experimentally as,

i) In the laminar region, where $Re_M < 6.74 \times 10^4$

$A = -0.568$, $B = 6.78$

ii) In the turbulent region, where $Re_M > 6.74 \times 10^4$

$A = -0.155$, $B = 0.068$

The power consumption data of Reman et al (31) are about three times higher than those predicted by Misek (186). This was explained on the basis that the results obtained by Reman were on a full-scale plant and probably included all power losses due to friction and bearings, whereas Misek's results were on a pilot plant. The results obtained by Misek are shown in Figure 5.11.

5.5. MASS TRANSFER EFFICIENCY

Many studies have been made of the effect of the different parameters on the efficiency of the RDC. Reman and Olney (23) investigated the influence of important variables on efficiency. It was found that efficiency increased with:

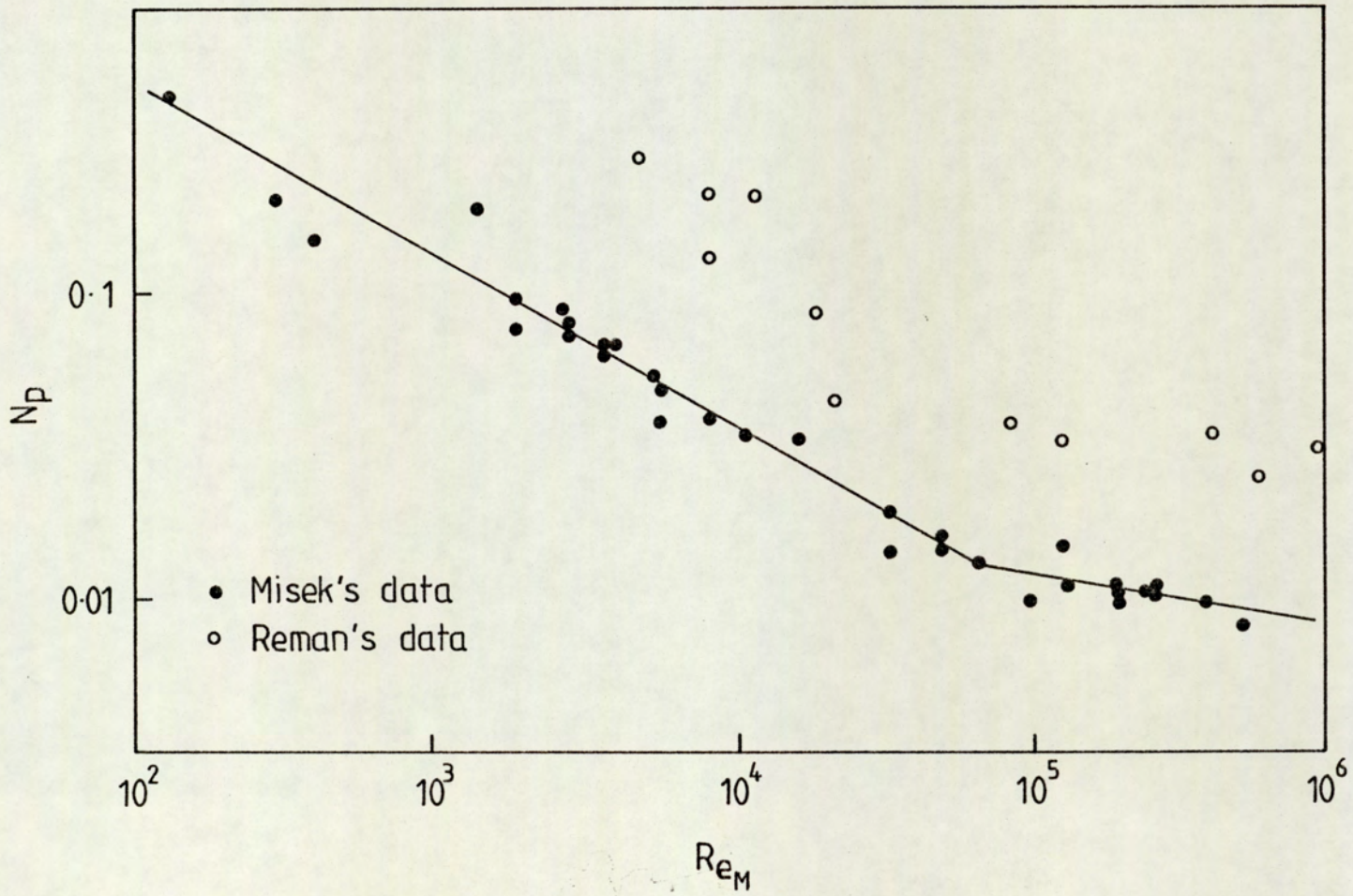

Figure 5·11 Power required for agitation in a RDC (186)

a) increasing rotor speed

b) increasing ratio of dispersed to continuous flow

c) increasing rotor disc diameter

d) decreasing stator opening

e) decreasing compartment height

f) increasing specific load. However, under conditions that noticeable back-mixing occurs, the reverse effect may occur.

However, in certain cases increase in rotor speed, reduced the efficiency, due to back-mixing. This was observed earlier by Vermijs and Kramers (158). Data was interpreted by plotting the efficiency, defined as number of stages per metre of column height, versus power input as illustrated in Figure 5.12.

Later Logsdail et al (156) employed the system toluene-acetone-water and butylacetate-acetone-water with the water as continuous phase and acetone as the solute, and produced a correlation to calculate the mass transfer coefficient or HTU of the form:

$$\left[\frac{(H.TU)_{oc}}{V_c}\left(\frac{g^2\rho_c}{\mu_c}\right)^{1/3}\right] x = \left[\frac{x}{K_{oc}^{a}}\left(\frac{g^2\rho_c}{\mu_c}\right)^{1/3}\right] = K\left[\frac{\mu_c g}{V^3 N (1-x)^3 \rho_c}\right]^{2m/3}\left(\frac{\Delta\rho}{\rho_c}\right)^{2(m-1)/3} \tag{5.20}$$

In this expression, the constant K and the exponent m are determined from model tests with a small scale column.

In a study by Al-Hemiri (33), mass transfer data were interpreted by comparing observed mass transfer coefficients with calculated values assuming stagnant, circulating, oscillating drops and fresh surface models (45). Generally, best agreement was obtained with the last two models. It was suggested that the total mass transfer comprised the net effect of a large number of oscillations and complete cycles of

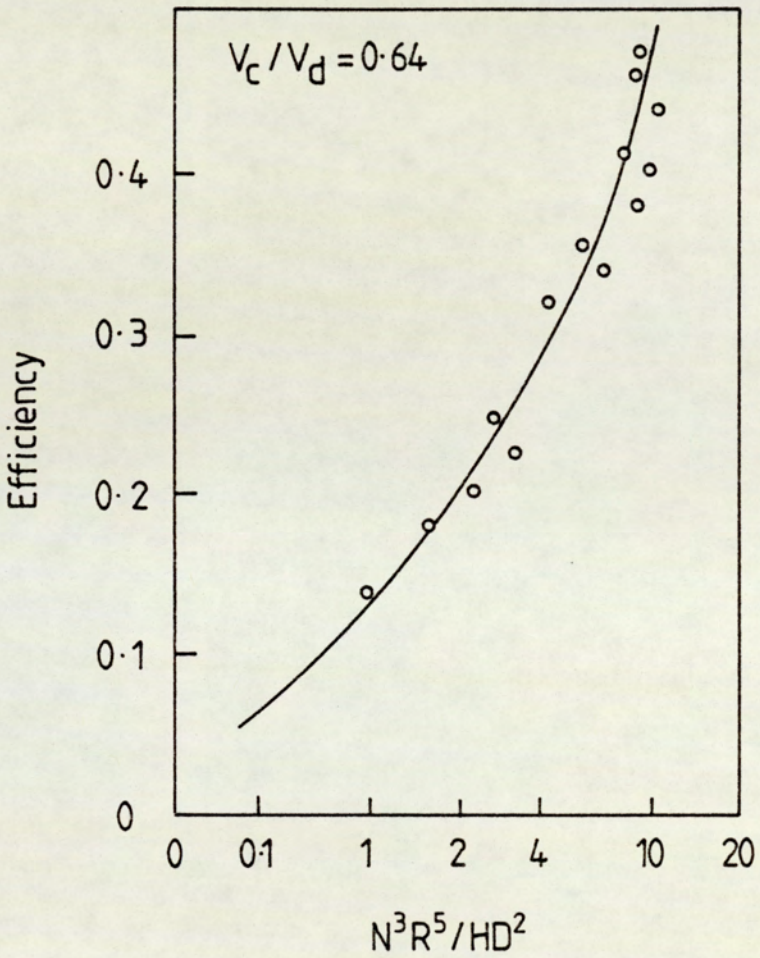

Figure 5·12 R D C Efficiency for system Water-Kerosene-Butylamine (23)

formation and coalescence. On that basis the following expression was developed:

$$\sum_{n=1}^{n} \left[\sum_{i=1}^{i} \int \left(\frac{dc}{c - c^*} \right)_i \right]_n = \sum_{n=1}^{n} \left[\sum_{i=1}^{i} A_i/V_i \int K_i \, dt \right]_n \qquad (5.21)$$

where i refers to any particular phenomenon; ie. drop formation, free rise etc, and n is the total number of compartments. The above mass transfer model was however, based on single drop correlations and therefore its applicability to an agitated swarm of drops is of doubtful validity, ie. it neglects interdrop interactions or coalescence-redispersion.

In a recent study of an RDC, Laddha et al (171) reported a critical rotor speed and distinguished between two operating regions. For operation below and above the critical rotor speed respectively they proposed the following correlations,

Region 1 correlation, below critical rotor speed:

$$K_{od}.a = c.x\,(1 - x) \left(\frac{g^3 \Delta\rho^3}{\sigma \rho^2_c} \right)^{1/4} (\psi_1)^{-1} \qquad (5.22)$$

where the value of the constant c = 0.068

and $$\psi_1 = [(Sc)_d^{1/2} + m\,(Sc)_c^{1/2}] \qquad (5.23)$$

Region 2 correlation above the critical rotor speed:

$$K_{od}.a = 0.95 \times (1 - x) \left(\frac{g^3 \Delta\rho^3}{\sigma \rho^2_c} \right)^{1/4} Fr.^{1/2}.\ \psi_1^{-1}\, \psi_2^{1/2} \qquad (5.24)$$

where ψ_2 is the physical property group, given by:

$$\psi_2 = \left(\frac{\sigma^3 \rho_c}{\mu_c^4 g}\right)^{1/4} \left(\frac{\Delta\rho}{\rho_c}\right)^{0.6} \qquad (5.25)$$

6. AXIAL MIXING

6.1. INTRODUCTION

Axial mixing occurs in one dimensional flow systems (such as counter-current extraction columns) when pockets of fluid move at velocities differing randomly from the mean velocity. This spread of velocities is caused by eddying or entrainment of one phase in the other. Obviously any backward movement must be accompanied by a corresponding forward movement if the fluid is incompressible (187). Axial mixing flatterns the concentration profiles along the column length and hence reduces the mass transfer and therefore must be taken into account in plant design.

Considerable back mixing of the continuous phase in rotating disc contactors has been observed by many authors (76, 188, 189, 190, 191, 192). Axial mixing has an important effect upon extraction efficiency, especially with agitated columns such as the RDC. Even under optimum conditions the stage efficiency of these columns has been stated to be low, usually < 25%, due to axial mixing (188). Under some conditions axial mixing effects have been reported in some cases to be equivalent to up to 70% of the total working height of the extractor (193).

Many investigations have been undertaken to determine axial mixing effects, usually presented in the form of axial mixing coefficients, E_c for the continuous phase and E_d for the dispersed phase. The axial mixing coefficient E, can be considered to be similar to the molecular diffusion coefficient D in Fick's law so that the rate of axial mixing would be

$$N_A = -E \frac{dc}{dz} \qquad (6.1)$$

On this basis the use of E_c and E_d are shown in Figure 6.1.

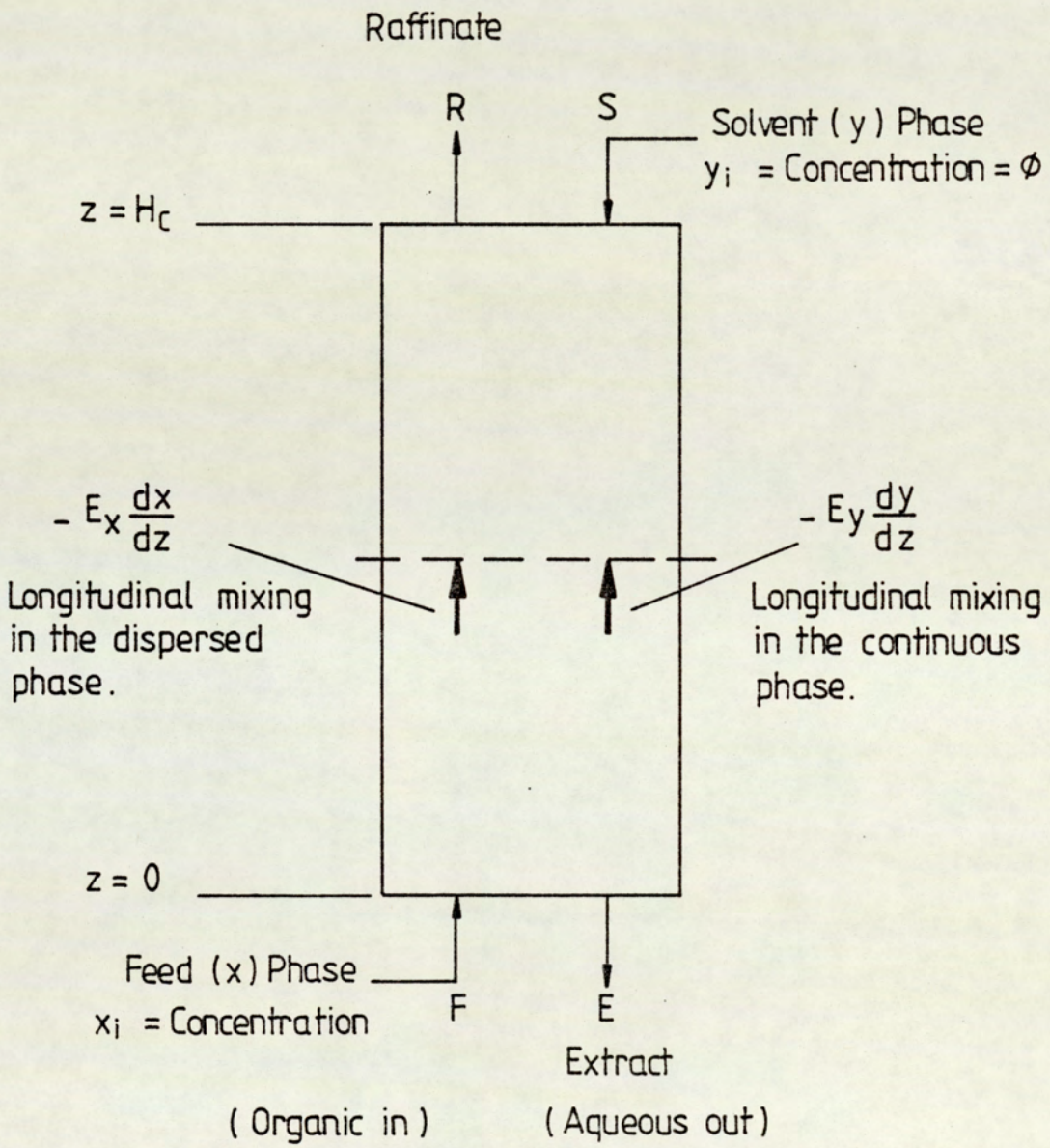

Figure 6·1 Nomenclature for Back-mixing Model.

Studies of RDC columns (158, 194, 188) have demonstrated extensive axial mixing under conditions suitable for intensive mass transfer. The design of counter-current separation processes is usually based on the idealised assumption of piston-flow conditions for both phases. However, this assumption is only valid if the velocities of all particles of each phase in any cross-section of the separation column are equal. In the case of extraction columns this assumption is inapplicable (195, 196, 197). During studies of the efficiency of packed and spray extraction columns considerable longitudinal mixing of the continuous phase was observed. This non-ideal behaviour is referred to variously as axial mixing, longitudinal diffusion, back mixing, entrainment or eddy diffusion.

Despite the realisation that back mixing decreases extraction performance, little mention of it appeared in the literature until 1950. Morello and Poffenberger (37) and Geankoplis and Hixon (196) noted the existence of back mixing, especially in spray columns. However, its significance for extraction performance, was not clearly stated until 1952 (198). Later work (90, 199, 197) included experimental measurements of concentration gradients in columns in which there was appreciable back mixing of the continuous phase.

All this work was carried out in spray or packed columns. In 1954 Vermijs et al (158) noted some effects of back mixing in an RDC. In no case, however, was there any attempt to characterise quantitatively the axial mixing in either phase. Most experimental studies have been carried out in small laboratory contactors with diameters less than 300mm which is a rather narrow region for scaling-up purposes, and little is known of the quantitative variation of the phenomenon with scale for columns > 300mm diameter. In general however the unfavourable flow patterns resulting in axial mixing would be expected to be increased in larger diameter columns, or indeed as between RDC's of similar diameter in a column with increased stator gap, Figure 6.2.

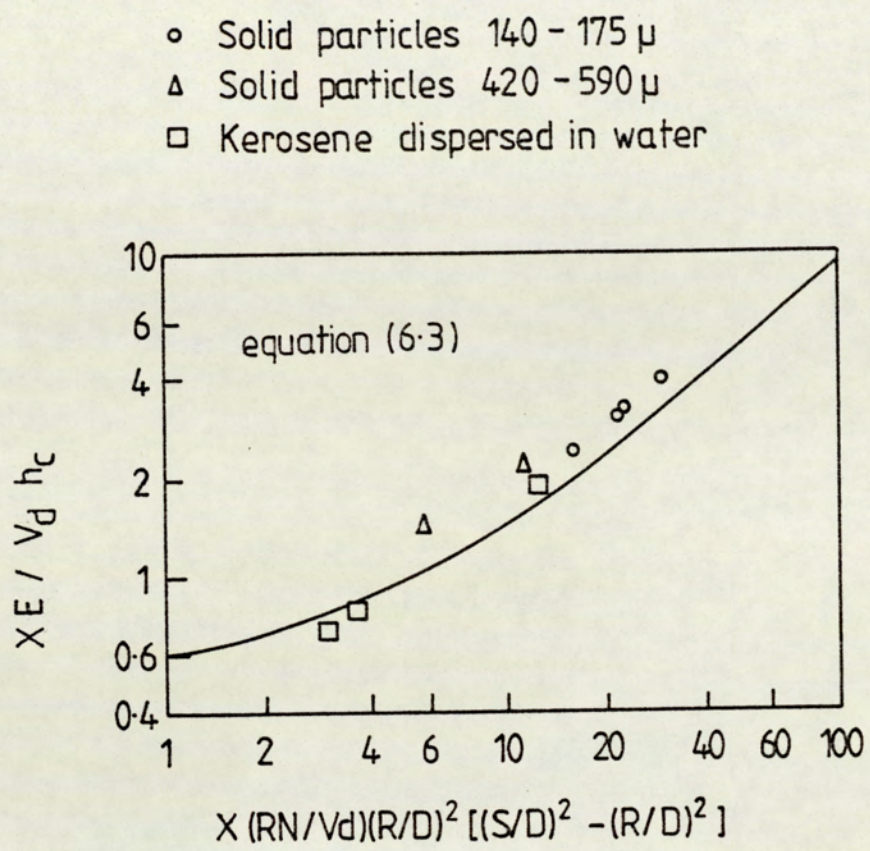

Figure 6·2 Dispersed-phase axial diffusion 15 cm diameter RDC (76)

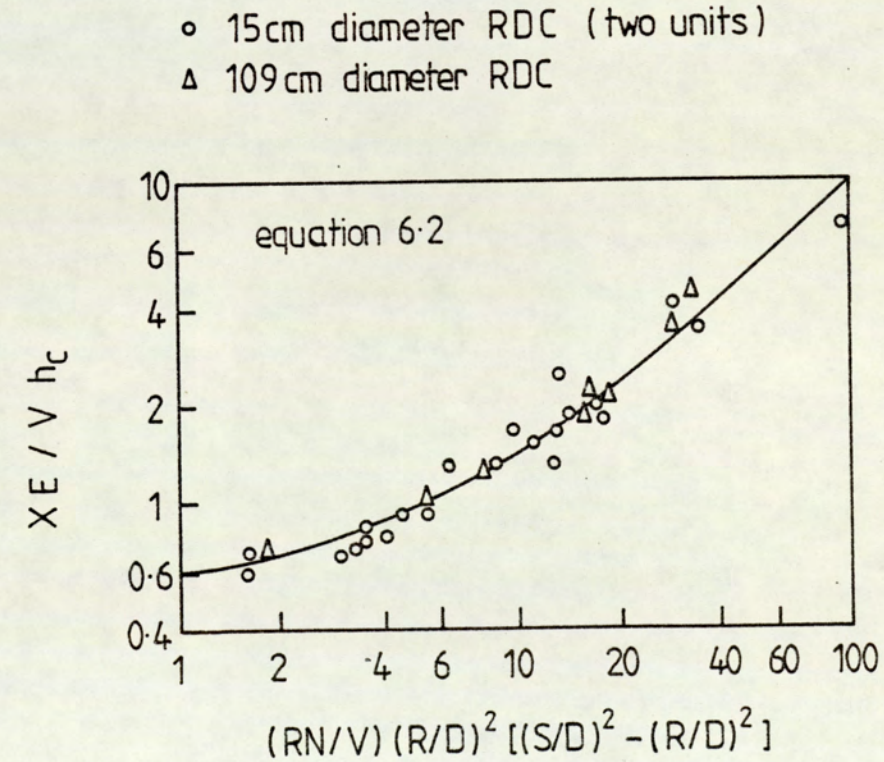

Figure 6·3 Axial diffusion, single-phase flow. RN/V > 30 (76)

Most axial mixing investigations have involved the use of tracer techniques to measure back mixing in the phase in which the tracer is selected to be soluble. Several attempts have been made to correlate the axial mixing coefficient E_c in an RDC with column geometry as well as operating para meters (V_c, V_d, and N). The usual correlations are listed in Table 6.1 and are based on either of two mathematical models, the diffusion model or the back flow model which are discussed in Section 6.2.

Strand et al (76) considered the overall axial mixing process in the continuous phase to be made up of two main components, an eddy or back mixing contribution, and a Taylor type diffusion, or channelling phenomenon which was present especially in the forward direction.

Values of the axial mixing coefficients in both phases have been reported for 15.2cm and 105cm diameter RDC columns. E_c was correlated by,

$$\frac{E_c\,(1-x)}{V_c.H} = 0.5 + 0.09\,(1-x)\left(\frac{R.N}{V_c}\right)\left[\frac{R}{D}\right]^2\left[\left(\frac{S}{D}\right) - \left(\frac{R}{D}\right)^2\right] \quad (6.2)$$

For the dispersed phase, E_d was given by:

$$\frac{E_d.x}{V_d.H} = 0.5 + 0.09\left(\frac{R.N}{V_d}\right)\left[\frac{R}{D}\right]^2\left[\left(\frac{S}{D}\right)^2 - \left(\frac{R}{D}\right)^2\right] \quad (6.3)$$

Equation 6.3 gave only fair agreement with experimental results for a 15.2cm RDC while equation 6.2 gave better agreement, as shown in Figures 6.2 and 6.3.

Table 6.1 Continuous Phase Axial Mixing Correlations for the RDC

Eqn. No.	Author and Reference	Column Diameter (cm)	Correlation	Comment
I	Westerterp et al (189)	4.1 - 5.0	$\frac{E_c}{V_c H} = \{0.5 + 6.5 \times 10^{-3} \frac{RN}{V_c}\} \frac{1}{N_c}$	Diffusion Model
II	Strand et al (76)	10 - 10.5	$\frac{E_c (1-x)}{V_c H} = 0.5 + 0.09 (1-x) \frac{RN}{V_c} \{\frac{R}{D}\}^2 \{(\frac{S}{D})^2 - (\frac{R}{D})^2\}$	Diffusion Model
III	Stemerding et al (202)	6.4 - 218	$\frac{E_c}{V_c H} = 0.5 + 0.012 \frac{RN}{V_c} \{\frac{S}{D}\}^2$	Back-flow Model
IV	Miyauchi et al (206)	10 - 30	$\frac{E_c}{V_c H} = 0.5 + 4.3 \times 10^3 \frac{RN}{V_c} \{\frac{D}{H}\}^{.5} \{\frac{D}{S}\}^{0.25}$	
			For $\frac{R^2 N \rho}{\mu} > 1.2 \times 10^5$	Back-flow Model
			$\frac{E_c}{V_c H} = 0.5 + 4.5 \times 10^{-2} \frac{RN}{V_c} \{\frac{D}{H}\}^{0.5} \{\frac{D}{S}\}^{0.25} (\frac{R^2 N \rho}{\mu})^{0.2}$	
			For $< 1.2 \times 10^5$	
V	Misek (205)		$\frac{E_c}{V_c H} = 0.5 + \{\frac{RN}{V_c}\} \{-0.00212 + 0.00434 (\frac{S}{D})^2 + 0.0264 (\frac{R}{D})^2\}$	Diffusion Model

Table 6.1 Continued....

Eqn. No.	Author and Reference	Column Diameter (cm)	Correlations	Comments
VI	Pebalk et al (209)	5.6	$\frac{E_c}{V_c H} = 0.54 + \left\{\frac{RN}{V_c}\right\} 0.0103 \left\{\frac{S}{D}\right\}^2$ For $1.6 \times 10^4 < \frac{RN\rho}{\mu} < 8 \times 10^4$	
VII	Bruin (191)	14 - 96	$\frac{E_c}{V_c H} = 0.5 + \left\{\frac{D-S}{2H}\right\} \left\{\frac{\mu}{DV_c\rho}\right\} + 0.033 \left\{\frac{2H}{R}\right\}^{0.16} + 0.0102 \left\{\frac{NR}{V_c}\right\}$	
VIII	Murakami et al (212)	7.9 - 30	$\frac{E_c}{V_c H} = 0.5 + 0.18 \left\{\frac{RN}{V_c}\right\}^{0.8} \left\{\frac{V_d}{Vc}\right\}^{0.4} \left\{\frac{S^2 - R^2}{D^2}\right\}^{0.6} \left\{\frac{H}{D}\right\}^{-0.4} \left\{\frac{R}{D}\right\}^{2.5}$	Back-flow Model
IX	Marr and Moser (213)	4 - 40	$\frac{E_c}{V_c H} = 0.37 + 0.121 \left\{\frac{S}{D}\right\}2 \left\{\frac{D}{H}\right\}^{0.33} \left\{\frac{R^2 N\rho}{\mu}\right\}^{0.83} / \left\{\frac{V_c D\rho}{\mu}\right\}$	
X	Blazej et al (69, 192)	10	$\frac{E_c}{V_c H} = 3.23 \times 10 \left\{\frac{RN(1-x)}{V_c}\right\}^{-1.73} \left\{\frac{V_d(1-x)}{V_c}\right\}^{0.443} \left\{\frac{\rho N_c V_c}{\mu_c(1-x)}\right\}^{-1.34}$	Diffusion Model

Table 6.1 Continued....

Eqn. No.	Author and Reference	Column Diameter (cm)	Correlations	Comments
XI	Venkatara-mana et al (211)	3.5 - 218	$\frac{E_c}{V_c H} = 0.5 + 0.028 \left\{\frac{RN}{V_c}\right\} \left\{\frac{S - 0.5D}{D}\right\}$	Diffusion Model
			$\frac{E_c}{V_c H} = 0.5 + 0.028 \left\{\frac{Re_R}{Re_D}\right\} \left\{\left(\frac{S}{R}\right) - 0.5 \left(\frac{D}{R}\right)\right\}$	Back flow Model
XII	Zhang et al (214)	10	$\frac{E_c}{V_c H} = 0.5 + 0.0204 \left\{\frac{S}{D}\right\}^{1.75} \left\{\frac{D}{H}\right\}^{6.5} \left\{\frac{\mu_D + \mu_c}{\mu_c}\right\}^{0.52} \left\{\frac{RN}{V_c}\right\}^{0.74}$ With solute transfer	
XIII	Lu et al (215)	14.2	$\frac{E_c}{V_c H} = 0.5 + 0.004 \left\{\frac{RN}{V_c}\right\} + 5.62 \left\{\frac{RN}{V_c}\right\}^{-1}$	

Westerterp and Landsman (189) in their analysis of experimental results from two small RDC columns, of 4.1 and 5.0cm diameter, showed that data on axial mixing coefficients at constant rotor speed indicated a linear relationship with liquid velocity. Their results, as well as those obtained from an earlier study (200) in a 10cm diameter column, were well correlated by:

$$P_e = \frac{2n}{1 + 13 \times 10^{-3} (N.R/V_c)} \qquad (6.4)$$

This was further verified by Westerterp and Mayburg (201) in separate experiments on a 50cm RDC using the steady state injection technique to determine the back mixing coefficient.

Stemerding et al (202) observed that the axial mixing coefficient E_c for the continuous phase may be correlated by,

$$E_c = K_1 V_c + K_2.N \qquad (6.5)$$

where $K_1 = 0.5H$ for limited rotor speeds and K_2 includes a geometry factor. Equation 6.5 may be compared with the following relationship between E_c and the back flow due to the rotor F_B from the back flow model derived by Misek and Rod (203):

$$\frac{E_c}{V_c.H} = 0.5 + \frac{F_B}{V_c} \qquad (6.6)$$

Stemerding et al indicated that F_B, the mean actual rate of interstage mixing per unit area

of column cross-section, may be taken as proportional to S^2, the area of stator ring opening and RN the pumping effect of the rotor,; it is also inversely proportional to the area of cross-section of the column:

$$F_B \sim RN \left(\frac{S}{D}\right)^2 \tag{6.7}$$

They derived a back flow model and proposed equation III in Table 6.1.

In an industrial scale RDC column 100cm in diameter, Misek and Roskos (204) found that values of axial diffusivities were only 27 to 55% of the values predicted by the Strand et al correlations. Therefore Misek (205) proposed the following equation for the continuous phase; and equation V in Table 6.1.

$$F_B = K_4 NR \tag{6.8}$$

where

$$K_4 = -0.001212 + 0.00434 \left(\frac{S}{D}\right)^2 + 0.0264 \left(\frac{R}{D}\right)^2 \tag{6.9}$$

Stainthorp and Sudall (188) determined back mixing in both phases using a 3.5cm diameter RDC under mass transfer conditions. They reported that values of continuous phase back mixing coefficient E_c were about 15% higher than those predicted by the correlation of Strand et al (76) and values of dispersed phase back mixing were inapplicable.

Although the above studies covered a wide range of column size, little account was taken, experimentally, of the effect of changes in column geometry. This was considered in a study of continuous phase axial mixing carried out by Miyauchi et al (206). The results were obtained using injection of tracer into one phase in the system.

They proposed equation IV in Table 6.1. The axial mixing coefficients were related to the rates of interstage mixing using the conversion relationship (equation 6.6) and it was observed that the back flow factor F_B was influenced by the rotor diameter and speed of rotation. Miyauchi et al (206), from a semi-theoretical analysis, postulated that the back flow factor F_B could be related to the power number (N_P) by the equation:

$$\frac{F_B}{RN} = 0.017\,(N_P)^{1/3}\left(\frac{D}{H}\right)^{1/2}\left(\frac{S}{D}\right)^{2} \qquad (6.10)$$

where $N_P = \dfrac{P}{\rho_m N^3 R^5}$ and P is the power consumed per compartment as estimated by Nece and Daily (207). Equation IV was shown to correlate the data of Miyauchi et al (206), for RDC as well as Oldshue-Rushton (208) columns, and the data of Westerterp et al (189) and Stemerding et al (202).

Pebalk et al (209) determined the continuous phase axial mixing coefficient using a 56mm diameter column and a pulse input of tracer. Based on the back flow model he proposed equation VI in Table 6.1.

Bruin (191) studied the effects of geometry on axial mixing of the continuous phase in RDC's ranging from 14 to 96cm diameter using single phase flow of water at zero and finite rotor speeds and a pulse of tracer. Based on the diffusion model equation VII in Table 6.1 was proposed. He concluded that the axial mixing coefficient E_c at zero speed was proportional to liquid superficial velocity and to compartment height. At low rotor speeds it was proportional to liquid superficial velocity, rotor speed, and stator diameter.

A clear limitation of operating a column and measuring axial mixing, with only the continuous phase present is that it does not represent practical conditions. The flow of the phases is interactive (in the limit resulting in flooding) and therefore difficult to extrapolate from single phase data. Columns of less than 15cm diameter do not exhibit significant axial mixing; columns of more than 45cm diameter may, depending on operating conditions, include large axial mixing effects.

More recently Elenkov et al (210) studied axial mixing in a 5.1cm diameter RDC using both single phase and two phase flow. When compared with the Strand et al relationship (76), their data showed considerable deviation. They observed that E_c values obtained in single phase flow experiments were two-fold higher than the data obtained in two-phase flow experiments. This is contrary to the observations of other reported investigations (188, 202).

Blazej et al (69, 192) proposed a correlation to estimate the axial mixing in the continuous phase E_c and another correlation to estimate the dispersed phase coefficient E_d, based upon work using a laboratory scale RDC column of 6.5cm diameter. They compared their data with other workers' correlations and found that the Strand (76) relation was the most convenient for E_d, inspite of the fact that it was originally derived for the continuous phase.

Venkataramana et al (211) studied axial mixing in the continuous phase in two RDC columns each of 90cm height and of 7.62cm and 10cm diameter respectively, and proposed the following correlation for the axial mixing effect,

$$\frac{E_c}{V_c.H} = 0.5 + 0.028 \left(\frac{RN}{V_c}\right) \left[\frac{S - 0.5D}{D}\right] \qquad (6.11)$$

$$= 0.5 + 0.028 \left[\frac{Re_R}{Re_D}\right] \left[\frac{S}{R} - 0.5 \frac{D}{R}\right] \qquad (6.12)$$

They compared experimental data with the predicted values from their correlations as well as from other correlations (76, 189, 202, 205, 206). Predicted values from their correlation showed better agreement with experimental values than did those predicted from other correlations.

Murakami and Misonou (212) have derived a correlation on the basis of dimensional analysis for the back mixing flow ratio of the continuous phase F_B, as a function of operating conditions and geometry of an RDC. This was claimed to give good agreement with experimental results. Using the back flow model they proposed Equation VIII in Table 6.1.

Marr and Moser (213) investigated axial mixing of the continuous phase in a 56mm diameter column using single phase flow. On the basis of the diffusion model they proposed Equation IX in Table 6.1.

Zhang et al (214) studied continuous phase axial mixing in a 10cm diameter column using the system kerosene/water containing some glycerol. They employed the diffusion model using a pulse input of dye tracer. For mass transfer conditions they proposed Equation XII in Table 6.1, concluding that E_c depends not only on rotor speed, V_c and column geometry but also on V_d. The disc Reynolds number has no influence on the axial mixing and is not therefore included in Equation XII.

Finally, Lu et al (215) studied the effect of dispersed phase flow on E_c. Experimental results indicated that the axial mixing of the continuous phase could be increased or decreased with dispersed phase flow under different operating conditions.

Equations were developed to predict the effect of dispersed phase flow on the axial mixing of continuous phase. They proposed Equation XIII in Table 6.1.

6.2. MODELS DESCRIBING THE PERFORMANCE OF AN EXTRACTION COLUMN

It has been common practice in the past to design extraction columns assuming perfect counter-current plug flow for both phases. The extraction rate in this simplest form is expressed as:

$$N = k_d (x - x_i) \tag{6.13}$$

$$= -k_c (y - y_i) \tag{6.14}$$

where N is the number of moles transferred across a unit area per unit time and x_i, y_i are the concentration of solute in the raffinate and extract phases at the interface respectively. If the concentrations x_i, y_i are in equilibrium and the distribution coefficient is defined as

$$m = \left(\frac{y_i}{x_i}\right)^* = \text{a const.} \tag{6.15}$$

Then it is possible to formulate equations 6.13 and 6.14 as:

$$N = K (x - x^*) \tag{6.16}$$

where K is the overall mass transfer coefficient. K is expressed in terms of the individual resistances in the two phases as:

$$\frac{1}{K_c} = \frac{1}{k_c} + \frac{m}{k_d} \tag{6.17}$$

and $$\frac{1}{K_d} = \frac{1}{k_d} + \frac{1}{mk_c} \qquad (6.18)$$

where $$x^* = \frac{y}{m} \qquad (6.19)$$

Equations 6.17 and 6.18 are often applied under conditions where m is not constant and even when equation 6.19 is not completely valid.

The simplest mass transfer model is that which neglects axial mixing assuming piston flow of phases through the column. This case is shown diagramatically in Figure 6.4. Nowadays however, it is accepted that considerable deviations from plug flow exist in the column flow patterns; these cause an appreciable reduction in the driving force ΔC and hence, of column performance. The effect on the driving force and the concentration profiles is illustrated in Figure 6.5 which demonstrates a sudden concentration change at each inlet and a zero concentration slope at each outlet. Both the true driving force, taking into account axial mixing, and the apparent driving force, without making such allowance - ie. the case of piston flow - can be seen.

Misek and Rod (203) have shown that the mass transfer process can be better represented by models which take axial mixing into account. Four such models will be discussed; these are shown diagramatically in Figures 6.6., 6.7, 6.8 and 6.9.

6.2.1. Stage Model

The stage model is the simplest to describe mass transfer with axial mixing in a counter-current column (203). The model is represented in Figure 6.6. It is assumed that each stage is perfectly mixed, so that the solute concentration in streams leaving any

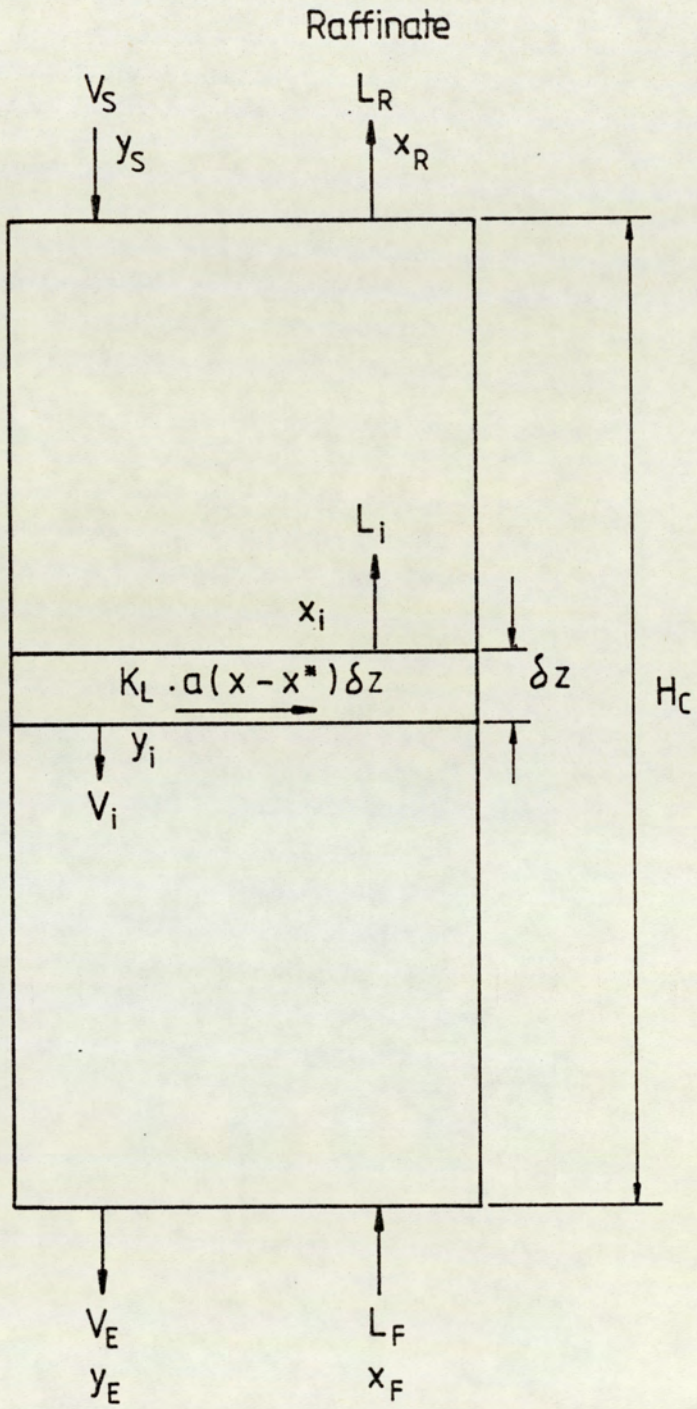

Figure 6·4 Piston Flow Model

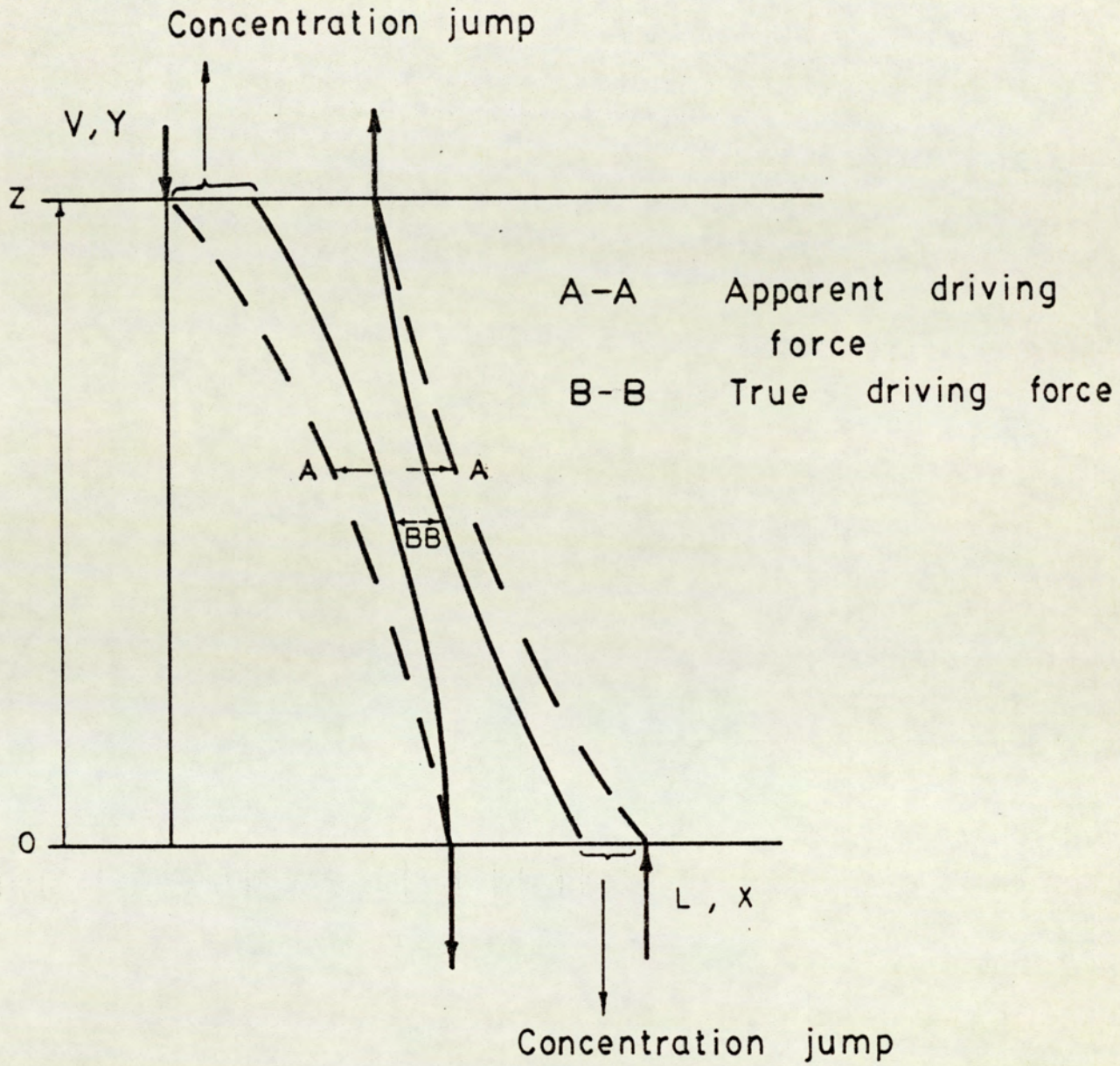

Figure 6·5 Effect of Axial Mixing on Concentration Profiles in the column

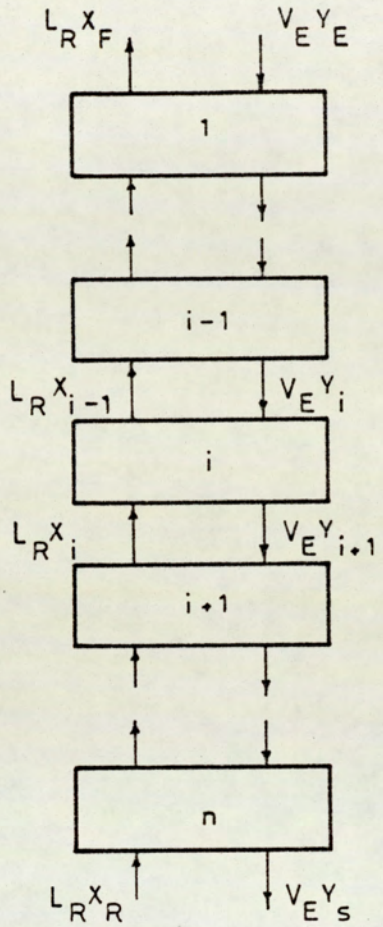

Fig. 6.6 Stage Flow Model

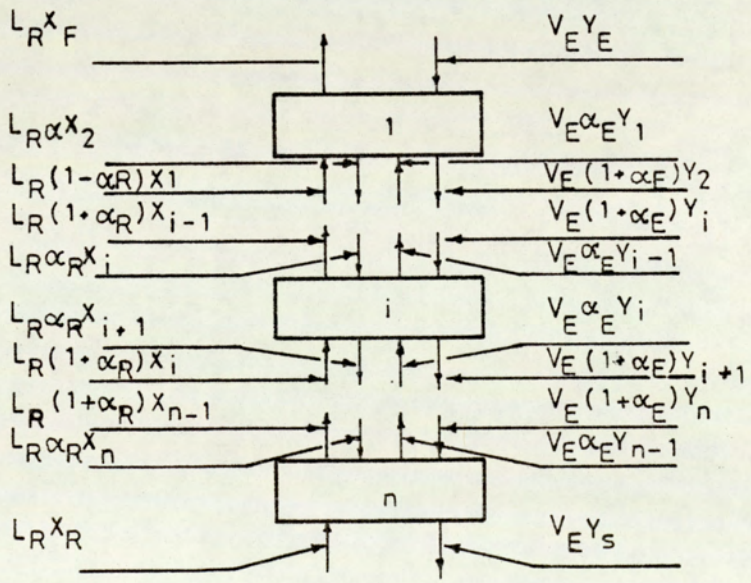

Fig. 6.7 Back Flow Model

stage are identical with the solute concentration in that phase throughout the stage. Axial mixing is characterised only by the number of stages required. The concentration profile is described approximately and the use of this model is only recommended for cases where the extent of back mixing in both phases is similar and where its influence on mass transfer is not high, such as in a mixer settler chain, in which entrainment is the main cause (216).

Miyauchi et al (217) suggest that the following conditions must apply for the stage model to be used,

a) Inter droplet coalescence is a frequent event,

or, b) Inter droplet coalescence is not a frequent event, but the drop size distribution is narrow, hold-up x and mass transfer coefficient K should be constant.

The model is limited in application due to the assumption of equal mixing in both phases.

A material balance on the ith stage is described by (203, 192),

$$L_R (x_i - x_{i-1}) = V_E (y_{i+1} - y_i) \qquad (6.20)$$

and the mass transfer in the ith stage by:

$$x_i - x_{i-1} = \frac{k_x .a.h}{L_R} (x_i - x_i^*) \qquad (6.21)$$

The boundary conditions being,

$$x_O = x_F \qquad y_1 = y_E$$

$$x_n = x_R \qquad y_{n+1} = y_S$$

The analytical solution of the finite difference equations 6.20 and 6.21 for the linear case has been given by Sleicher (218). A graphical solution is necessary for the non-linear case.

6.2.2. Back Flow Model

This model (219, 218) may describe flow conditions in a counter current extractor, when one phase is entrained in the main flow of the other in a stagewise system as shown in Figure 6.7.

A material balance on the ith stage is represented by:

$$L_R [(1 - \alpha_R)\ x_{i-1} - (1 + 2\alpha_R)\ x_i + \alpha_R\ x_{i+1}] =$$

$$V_E [-\alpha_E y_{i-1} + (1 - 2\alpha_E)\ y_i - (1 + \alpha_E)\ y_{i+1}] = Nh.a \qquad (6.22)$$

and the mass transfer is described by the relation

$$N = K_R\ (x_i - x_i^*) \qquad (6.23)$$

The governing finite difference equation is obtained by a combination of equations 6.22 and 6.23. The boundary conditions result from balances around the end stages:

for i = 1 $$L_R\ (x_F - x_1) + L_R\ (x_2 - x_1) = K_R\ a(x_1 - x_1^*)h \qquad (6.24)$$

$$y_1 = y_E$$

for i = n $$L_R\ (x_{n-1} - x_n) + L_R \alpha_R\ (x_{n-1} - x_n) = K_R.a.-(x_n - x_n^*)h \qquad (6.25)$$

$$x_n = x_R$$

Hartland and Mecklenburg (219) have given the solution for the simple linear case. For the general case solution involves a graphic-numerical procedure (220).

6.2.3. Diffusion Model

For a continuous counter-current differential extraction column in which the change in concentration takes place along the column axis, an analogy to Fick's law of diffusion can be used to describe axial mixing. This model describes solute transfer within the phase from loci of higher concentration to those of lower concentration as a diffusional process, ie. the mass flux is proportional to concentration gradient. From Figure 6.8 a material balance over height element ΔZ for raffinate and extract phases yields,

$$E_x \frac{d^2x}{dz^2} - L\frac{dx}{dz} = -E_y \frac{d^2y}{dz^2} - V\frac{dy}{dz} = K_R.a.(x - x^*) = N.a \quad (6.26)$$

The mass transfer between the phases is given by:

$$N = K_R (x - x^*) \quad (6.27)$$

The boundary conditions are obtained by performing material balances for both ends of the column, thus (221):

$$L.x_F = L.x - E_x \frac{dx}{dz} \; ; \; \frac{dy}{dz} = 0 \text{ at } z = 0$$

$$V.Y_S = V.Y + E_y \frac{dy}{dz} \; ; \; \frac{dx}{dz} = 0 \text{ at } z = h_c$$

Outside the mass transfer zone, the axial mixing coefficients E_x, E_y are considered to be equal to zero. Again the general case may be solved by a numeric-graphical method

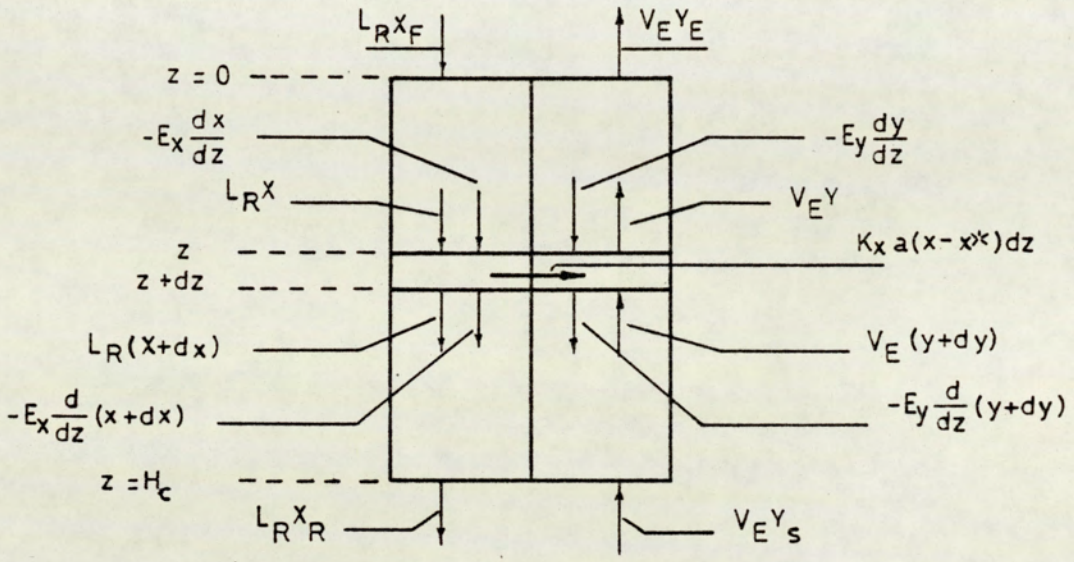

Fig. 6.8 Diffusion Model

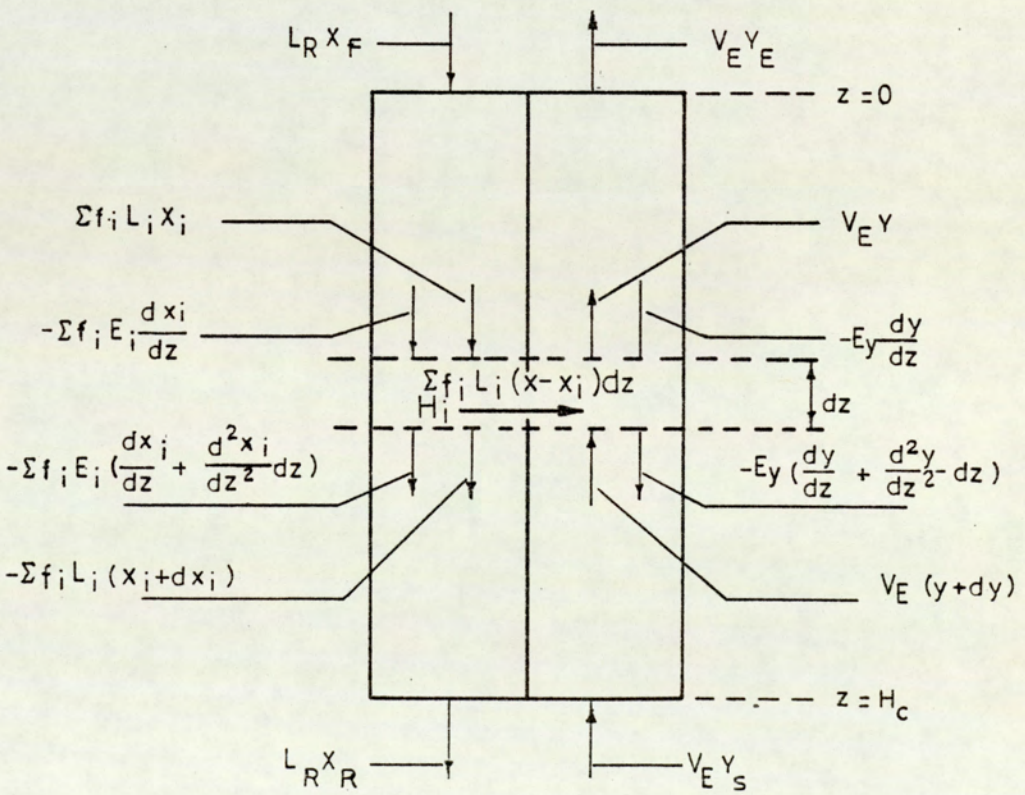

Fig. 6.9 Combined. Model with Forward mixing

(203). Several solutions have been obtained (218, 219) for the linear case.

6.2.4. Combined Model with Forward Mixing

Recent work on logitudinal mixing in the dispersed phase (52) has indicated that neither the diffusion nor the back flow model adequately describe the mixing of the dispersed phase when this phase has a significant polydisperse character and coalescence - redispersion occurs. This situation is applicable when a solvent is dispersed in a mechanically agitated column extractor operating with a high hold-up. Since under these conditions drops of differing sizes have different velocities, which influences the residence time distribution, another mechanism of axial mixing takes place. It is termed (205) "forward mixing" to distinguish it from back mixing, where displacement of fluid elements occurs in a backward direction with respect to normal flow in the equipment. Thus the combined model takes account of both mechanisms of longitudinal mixing.

One such model describing mass transfer in an RDC has been proposed by Olney (52) considering the effect of polydispersity. Whilst no analytical solution has been proposed for this model due to the complexity involved, a calculation procedure similar to that for the diffusion model has been adopted by Misek (203) to solve the general case.

6.3. APPLICATION TO THE RDC

The suitability of any particular model to describe the extraction process in an extractor will depend on the difference between the real situation and the apparent one on which the model is based. Thus a diffusion model is more applicable to a spray column and a back flow model to a mixer-settler.

Conditions in an RDC would be expected to fall between the two limits, ie. discrete stage and plug flow, spray column operation. In this study the diffusion model has been used. To apply the methods of calculation outlined above the true values of the coefficients of mass transfer and the experimental values of the axial mixing and axial mixing coefficients are required for the appropriate conditions.

The extent of axial mixing in an extractor can be evaluated by several methods. However the most straight-forward method is to measure the concentration of a solute along the column during steady-state operation.

6.4. GRAPHICAL METHOD OF BACK MIXING CALCULATION IN AN RDC BASED ON DIFFUSION MODEL

The object of the following calculation is the construction of the true operating line on the basis of mass balances over small portions of column height, where mass transfer, including back mixing is taken into account. Various models have been developed to describe axial mixing effects in counter-current flow equipment. The model most widely used in designing solvent extraction apparatus is probably the diffusion model developed by Sleicher (218), Miyauchi (217) and Rod (220). Such an approach is justified for the continuous phase (222).

The method of calculation is based on the diffusion model shown in Figure 6.10. The formation of the model, with a graphical description given by Figure 6.10 is based on the following assumptions:

- The dispersed phase can be considered as a second continuous phase.
- Deviation from plug flow may be characterised for the whole column by a constant axial eddy diffusivity, E.
- Mean velocity and concentration of each phase are constant across the column diameter.

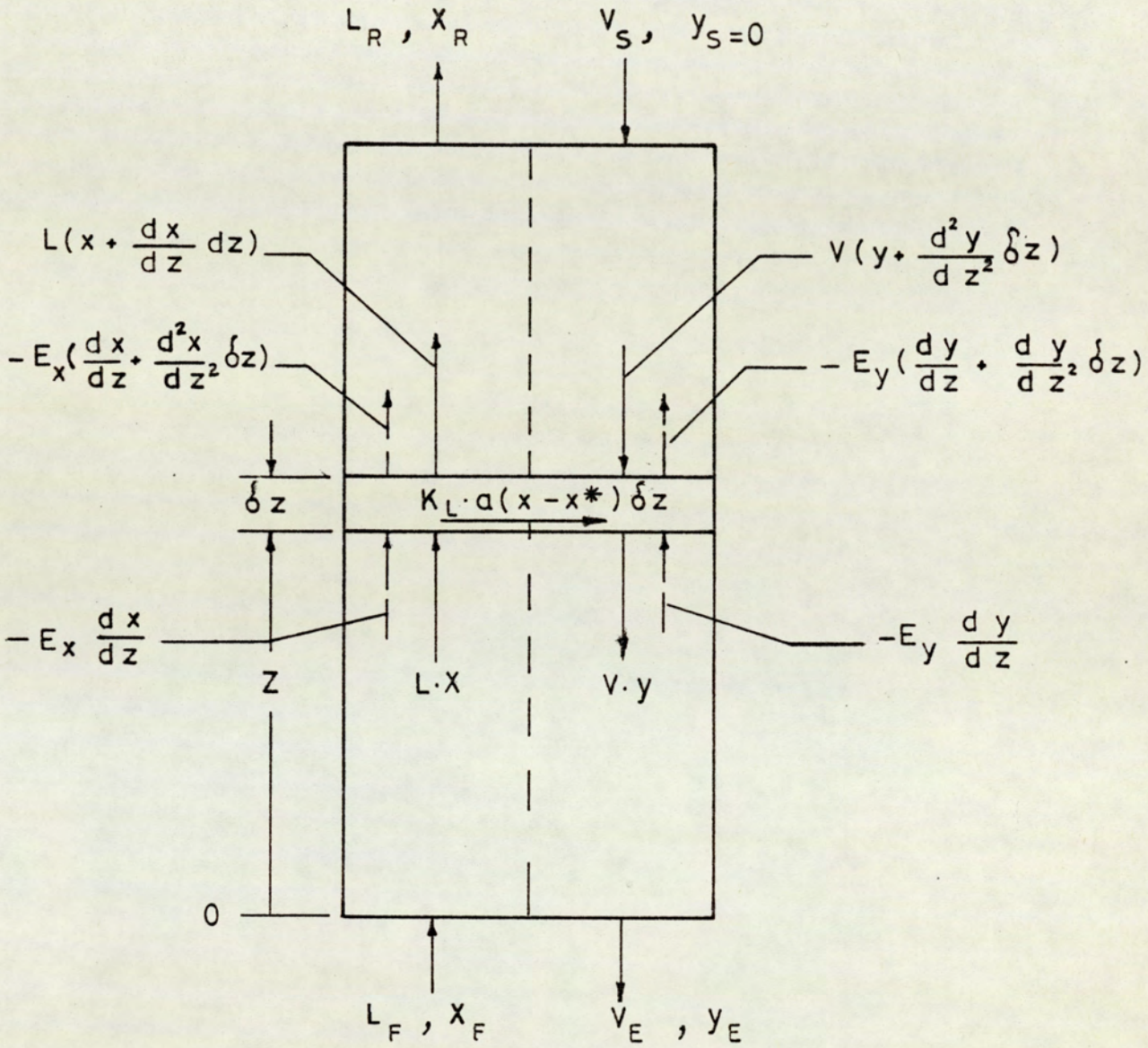

Figure 6.10 Diffusion Model of Back Mixing

- Solvents are immiscible.
- Volumetric flowrates of solvent and feed raffinate do not change with column height.
- The volumetric overall mass transfer coefficients $K_L.a$ or $K_V.a$ are constant throughout the column.
- There is a smooth variation in concentration profile.
- The inlet streams have uniform concentration without axial mixing.

At steady state the mass balance over an infinitesimal column height interval dz are for the extract and raffinate phases,

Extract Phase:

$$-E_y \frac{dv}{dz} + V\left(y + \frac{dv}{dz}dz\right) = V.y - \left(\frac{dy}{dz} + \frac{d^2y}{dz^2}dz\right) - K_V.a\,(y^* - y)\,dz \qquad (6.28)$$

$$E_y \frac{d^2y}{dz^2} - V\frac{dy}{dz} = K_V.a\,(y^* - y) \qquad (6.29)$$

Raffinate Phase:

$$L.x - E_x \frac{dx}{dz} = L\left(x + \frac{dx}{dz}dz\right) - E_x\left(\frac{dx}{dz} + \frac{d^2x}{dz^2}dz\right) + K_L.a\,(x - x^*)\,dz \qquad (6.30)$$

$$E_x \frac{d^2x}{dz^2} - L\frac{dx}{dz} = K_L.a\,(x - x^*) \qquad (6.31)$$

An overall mass balance on the bottom section of the column is:

$$L_F.x_F + V.y = L.x - E_x \frac{dx}{dz} + V_E.y_E - E_y \frac{dy}{dz} \qquad (6.32)$$

$$L_F.x_F - V_E.y_E = L\left(x - \frac{E_x}{L}\frac{dx}{dz}\right) - V\left(y + \frac{E_y}{V}\frac{dy}{dz}\right) \qquad (6.33)$$

= The net flow of solute per unit cross section of the column.

The graphical presentation of equation 6.33 is the operating line of the column.

Let $$X = x - \frac{E_x}{L}\frac{dx}{dz} \qquad (6.34)$$

$$Y = y + \frac{E_y}{V}\frac{dy}{dz} \qquad (6.35)$$

$$\frac{dX}{dz} = \frac{dx}{dz} - \frac{E_x}{L}\frac{d^2x}{dz^2} = -\frac{K_L.a}{L}(x_i - x_i^*) \qquad (6.36)$$

Substituting the differentials dx, dy, dz by finite differences Δx, Δy, Δz:

$$\frac{\Delta x}{\Delta z} = -\frac{K_L.a}{L}(x_i - x_i^*) \qquad (6.37)$$

$$\Delta x_i = -\frac{K_L.a.\Delta z}{L}(x_i - x_i^*) \qquad (6.38)$$

From equation 6.35

$$Y_{i+1} = y_{i+1} + \frac{E_y . \Delta yi}{V . \Delta z} \qquad (6.39)$$

$$Y_{i+1} - y_i = y_{i+1} + \frac{E_y . \Delta y_i}{V . \Delta z} - yi$$

$$= \Delta y_i \left(1 + \frac{E_y}{V.\Delta z}\right) \qquad (6.40)$$

$$\Delta yi = \frac{1}{1 + \frac{E_y}{V.\Delta z}} (Y_{i+1} - y_i) \qquad (6.41)$$

$$\Delta yi = - \frac{1}{1 + \frac{E_y}{V.\Delta z}} (y_i - Y_{i+1}) \qquad (6.42)$$

Equations 6.38 and 6.42 constitute the basic relationship for the graphical construction of the operating line.

From the graph in Figure 6.11 it follows that back mixing causes a lowering of driving force expressed as $(x_i - x_i^*)$; thus a greater column height is needed to achieve the desired separation. As the degree of back mixing increases, the operating line approaches the equilibrium line until they coincide. In this case the separation is no longer possible with columns of finite height.

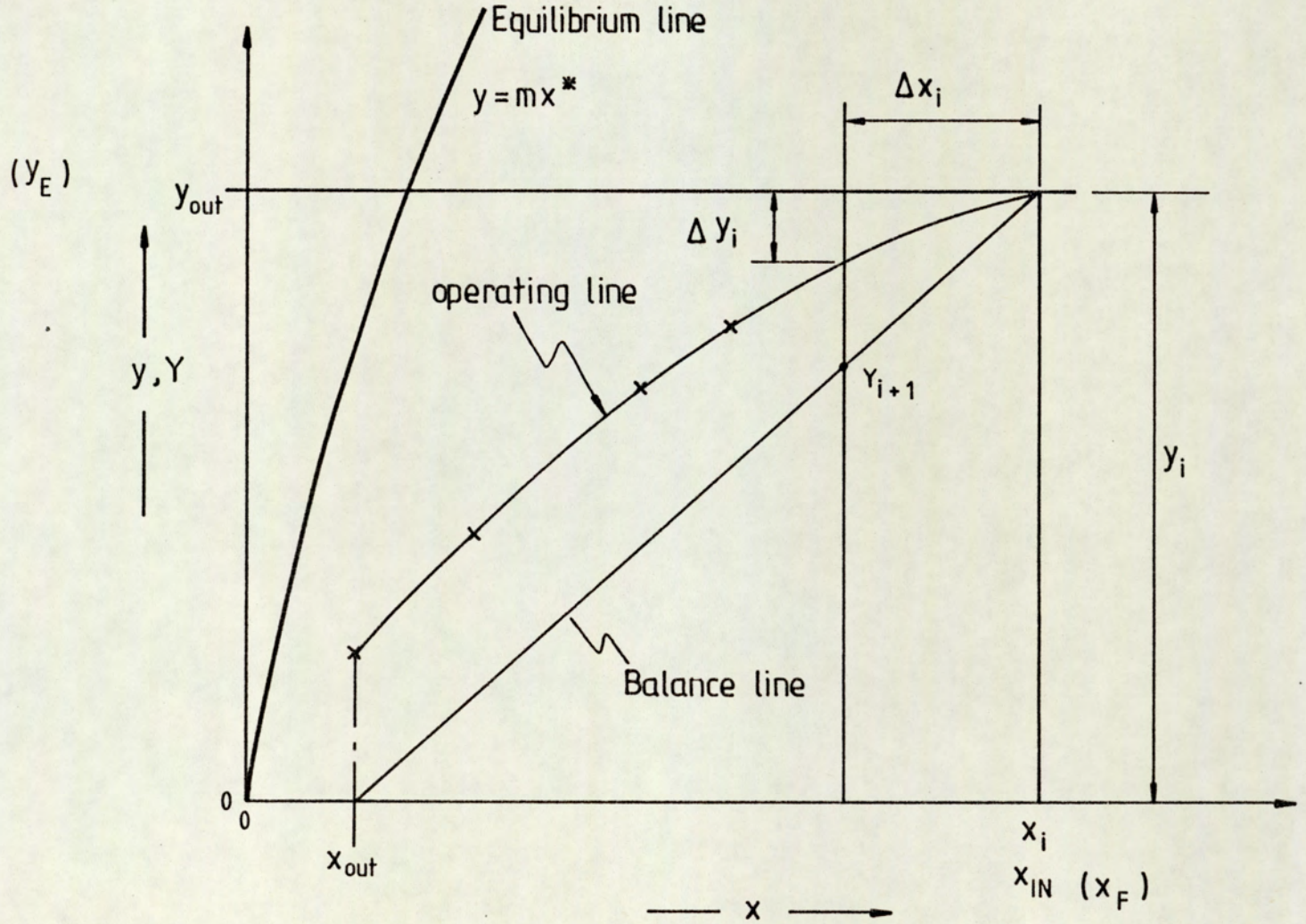

Figure 6·11 The Distribution Diagram with operating line in case of existing Back mixing in continuous phase.

7. EXPERIMENTAL INVESTIGATION

The objectives of the experimental investigation were:

a) To determine the extent of axial mixing effects in a large scale, 0.45m diameter, RDC when operating near to the practical limits. This was considered more representative of RDC's in use in industry, since axial mixing effects may be negligible in small columns (1).

b) To correlate hydrodynamics and mass transfer efficiency of this RDC with operating parameters, viz V_d, V_c, N and ΔC. This was an extension of the study of Al-Aswad (99, 65) with the aim of studying operation at higher holdups and evaluating the applicability of the drop size distribution-related, mass transfer calculation method referred to in section 8.2.2. An inherent part of this investigation was to determine the actual volumetric capacity of the column (ie. flooding conditions) not previously studied in detail (99).

7.1. DESCRIPTION OF EQUIPMENT

The flow diagram of the equipment is shown in Figure 7.1. The general arrangement is shown in Figure 7.2. The process lines, feed and receiver tanks were arranged so that the column was accessible from all sides to facilitate sampling and photography. The control valves were arranged within easy reach. Drain points were located at the lowest points in the system for complete drainage. The control valves and instrumentation were located on the first floor of the plant so that the system could be operated by one person. The basic equipment was originally constructed by Khandelwal (223) and subsequently modified by Al-Aswad (99). The column dimensions are listed

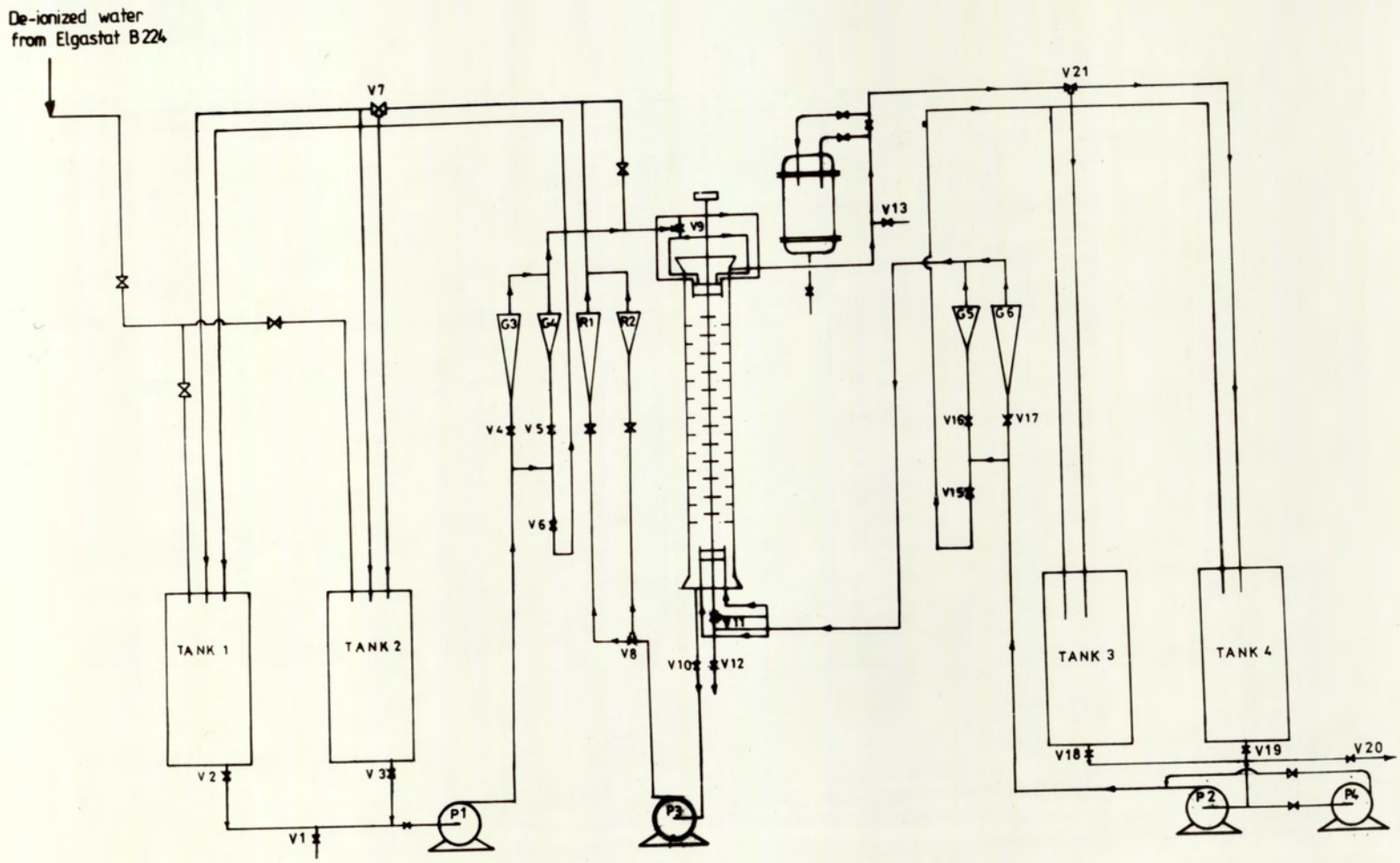

Figure 7.1 Flow Diagram of Apparatus

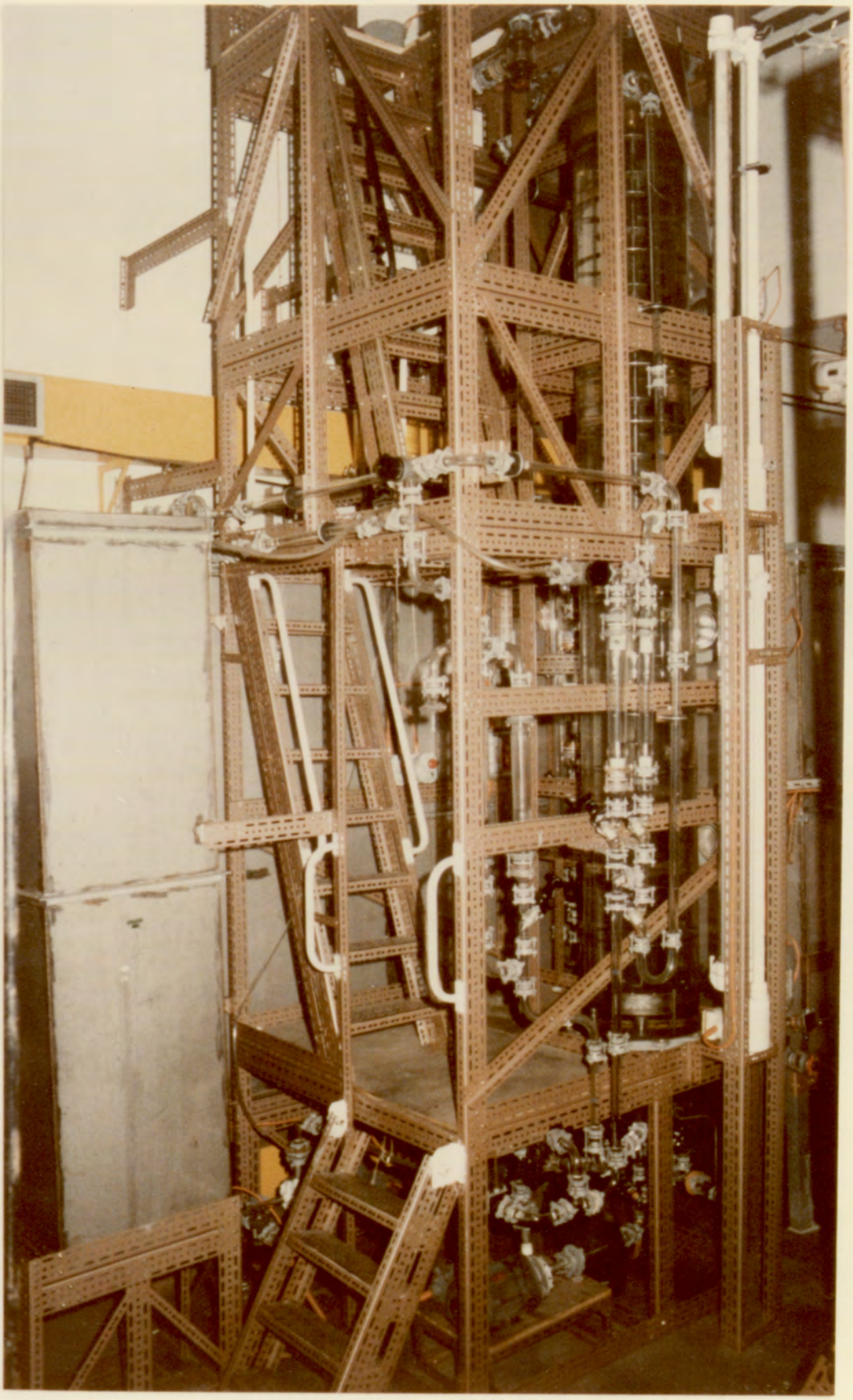

Figure 7.2 GENERAL ARRANGEMENT OF EQUIPMENT

in Table 7.1.

The dimensions were generally in accordance with published design criteria (23, 76, 156, 66, 157, 158). The column consisted of two 2 metre high, standard 450mm diameter QVF industrial glass sections divided into 14 compartments. Nine sample points were provided over the column height including one at the inlet and one at the outlet. Each sample point comprised a 10mm diameter hole fitted with a 6mm diameter tube with a quick-acting toggle valve. The column internals, were fabricated from 18/8 stainless steel.

The stators were supported by means of four equispaced 6mm diameter stainless steel rods. Each rotor disc was fixed to the shaft by means of grub screw through its collar; this was counter-sunk into the collar to eliminate any effect on the pattern of agitation. The discs had straight edges since discs with sharp edges tend to increase axial mixing effects (66). The bottom plate was drilled and incorporated pipes for the bottom distributor inlets and outlets as shown in Figure 7.3. Distributor plates were located at the top and at the bottom of the column. The shaft was fabricated from 22.4mm o.d. stainless steel rod in two sections threaded at the centre. It was supported at three points, at the top and bottom distributors and in the centre, by means of p.t.f.e. bearings (Figure 7.4). The support plates at the bottom and in the column centre were fabricated from 6.35mm thick stainless steel.

The heavy aqueous phase could be introduced into the top of the column either via a side entry, (if it was to form a continuum), or through the top distributor plate. This was to facilitate operation with the heavy phase constituting either the continuous or dispersed phase. The stainless steel bottom distributor was "water wetted" which is recommended for organic phase inlet into an aqueous continuous phase, and the polypropylene top distributor was "organic wetted" for introduction of aqueous phase into organic phase.

into organic phase.

Table 7.1 Dimensions of RDC

Variables or Parts	Dimensions
Column inside diameter (D)	0.45m
Column Height (h_c)	4.3m
Stator diameter (opening) (S)	0.3775m
Disc diameter (R)	0.225m
Disc and Stator thickness	0.002m
Compartment height (H)	0.225m
Number of compartments	14
S/D	0.75
R/D	0.5
H/D	0.5

As shown in Figure 7.5 the top distributor holder was constructed of 10 gauge stainless steel, but the perforated plate was of 6.4mm thick polypropylene, with 1.6mm size holes drilled at a 10mm triangular pitch.

The bottom distributor plate shown in Figure 7.3 was designed on the conventional basis using the correlation by Treybal (8). The distributor plate diameter

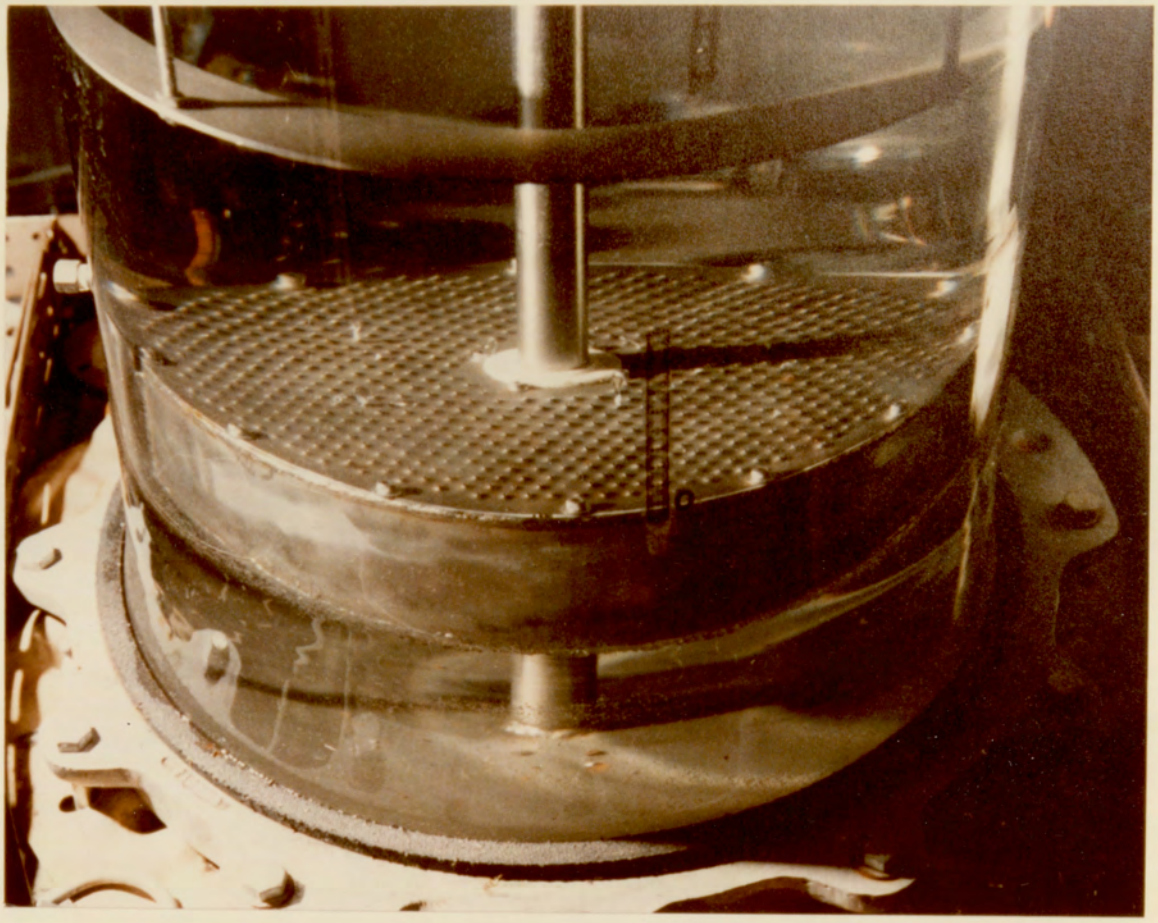

Figure 7.3 BOTTOM DISTRIBUTION PLATE
700 Holes, 1.6 m.m. diameter
Drilled and Punched on a
10 m.m. Triangular Pitch inside
a 305 m.m. diameter.

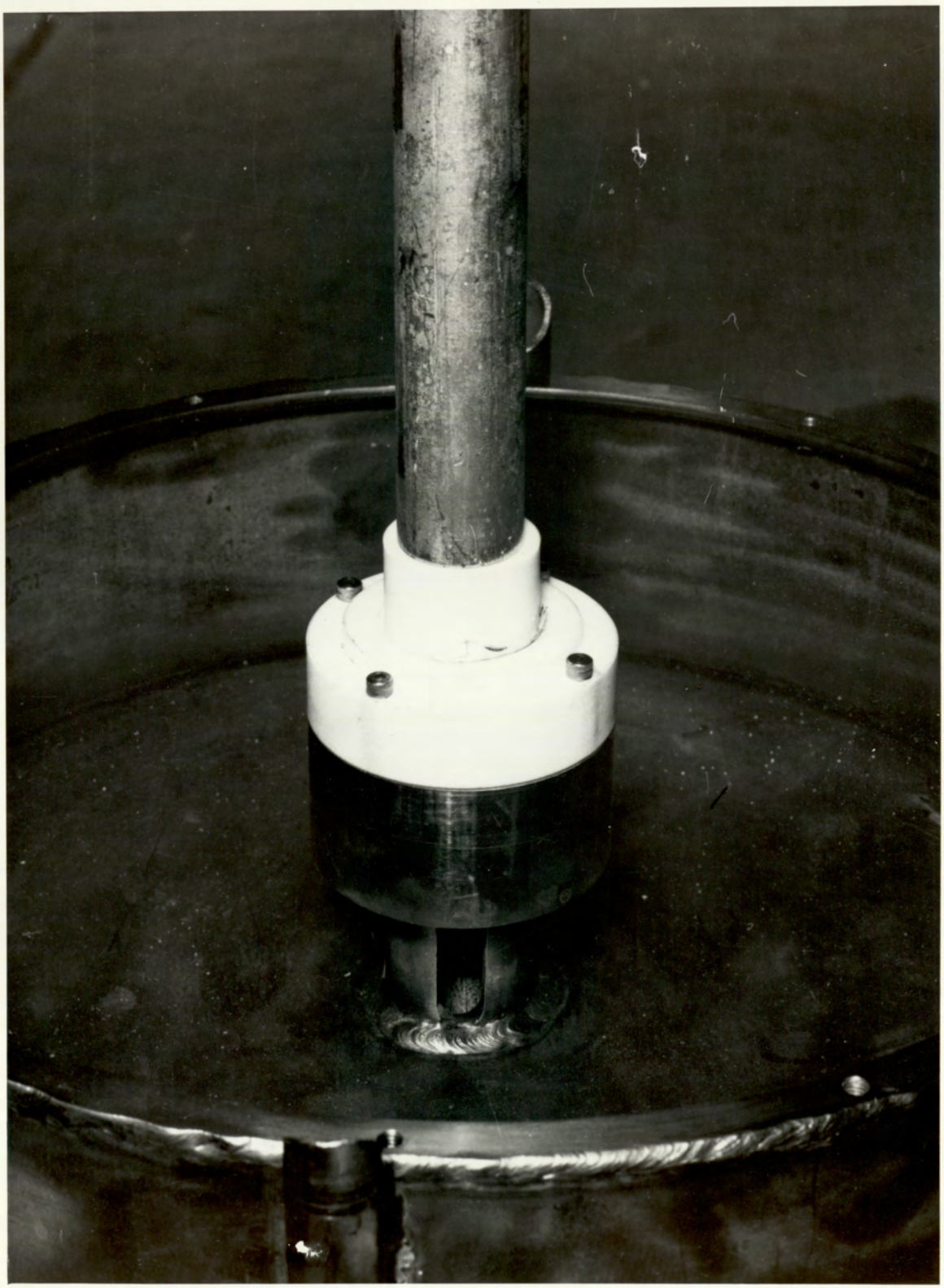

Figure 7.4 The Bottom Distributor with Plate Removed

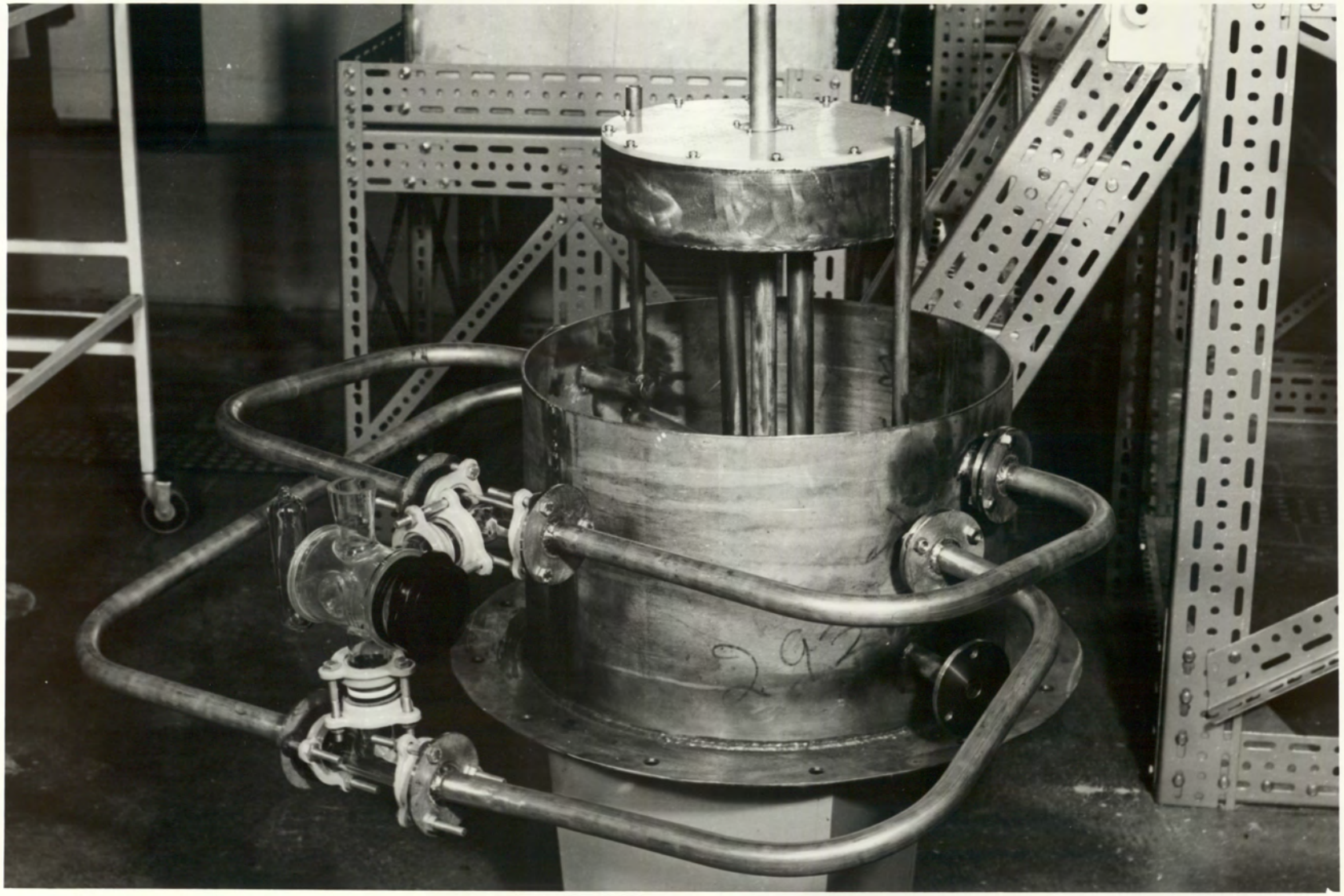

Figure 7.5 Top Stainless Steel Section in Inverted Position Outside the Column

triangular pitch. The holes were drilled under size 1.2mm and then centre punched to the correct size. This provided an upward projection around the periphery of each hole and hence more uniform droplets. The disperser was located 225mm above the bottom s.s. plate to minimise the effects of heavier phase out flow on droplet formation.

The distributor plate was located 200mm below the first compartment, so that initial droplet formation was substantially but, in the event, not entirely unaffected by agitation. As shown in Figure 7.5 a 300mm long and 450mm diameter stainless steel section, fabricated from 10 gauge sheet, provided the light phase coalescence section and incorporated outlets, heavy phase inlets, support for bearings and the top distributor. The light phase was withdrawn 75mm below the top bearing, thus leaving a dead space to avoid the need for a mechanical seal on the agitator shaft. A pair of self-lubricated, thrust bearings were provided at the top to retain and to support the weight of the shaft.

7.1.1. Associated Equipment

The shaft was driven by a 0.25 HP, 240 volt single phase AC variable speed flame-proof electric motor. The speed of the motor was controlled by means of a gear box and could be varied from 100 to 400 rpm. The speed of rotation was measured by a Comark electronic tachometer covering the range 0-3000 rpm used in association with a photo-electronic probe located on the shaft at the top of the column.

As shown in Figure 7.1 four stainless steel rectangular tanks, each with dimensions of 3.44m x 1.22m x .61m, and a capacity of 2500 litres were used as feed tanks and receivers. A recycle line for each phase was provided for use during feed preparation, and for mutual saturation of the phases by recirculation in a closed loop.

The heavy phase was transferred by means of two PVC flame-proof pumps each capable of supplying 50-100 litre/min. against a head of 6m-3m. The first pump was used to feed the column while the second was used to return the continuous phase from the bottom of the column to the reservoir. In the hydrodynamic (non-mass transfer) study the second pump was also used to recirculate the continuous phase to the top of the column. A third pump of 120 litres per min. capacity was originally used for the light phase. This pump was found to be under-sized for flooding experiments. For this purpose a new pump with a capacity of 100 litres/min was therefore parallel installed.

Dispersed phase flow rates was measured by two rotameters with stainless steel floats and a maximum capacity of 160 litres/min. and 60 litres/min. respectively installed in parallel to provide fine control. Continuous phase flow rates at the inlet and outlet were measured using two rotameters with stainless steel floats, and a capacity of 100 litres/min. and 50 litre/min. respectively installed in parallel to obtain fine control.

The equipment was located in an isolated pilot plant room provided with flame-proof switch gear and lighting and an effective high and low level extraction system. The ambient temperature was generally between 18^{o}C and 20^{o}C.

The RDC used in the present work was essentially that used by Al-Aswad (99) but with some important modifications. To increase flexibility in operating and to achieve an increased volumetric capacity, the process lines were repiped. A new pump for Clairsol was contructed. This booster pump was essential to provide higher dispersed phase flow rates to run the plant at its limiting capacity for flooding runs. At the top of the plant an external settler, Figure 7.6, was installed at the column light phase outlet. This addition was necessary to eliminate any heavy phase carry-over, especially in flooding runs in which some loss of heavy phase via the top of the column was unavoidable. A section of the column is illustrated in Figure 7.7.

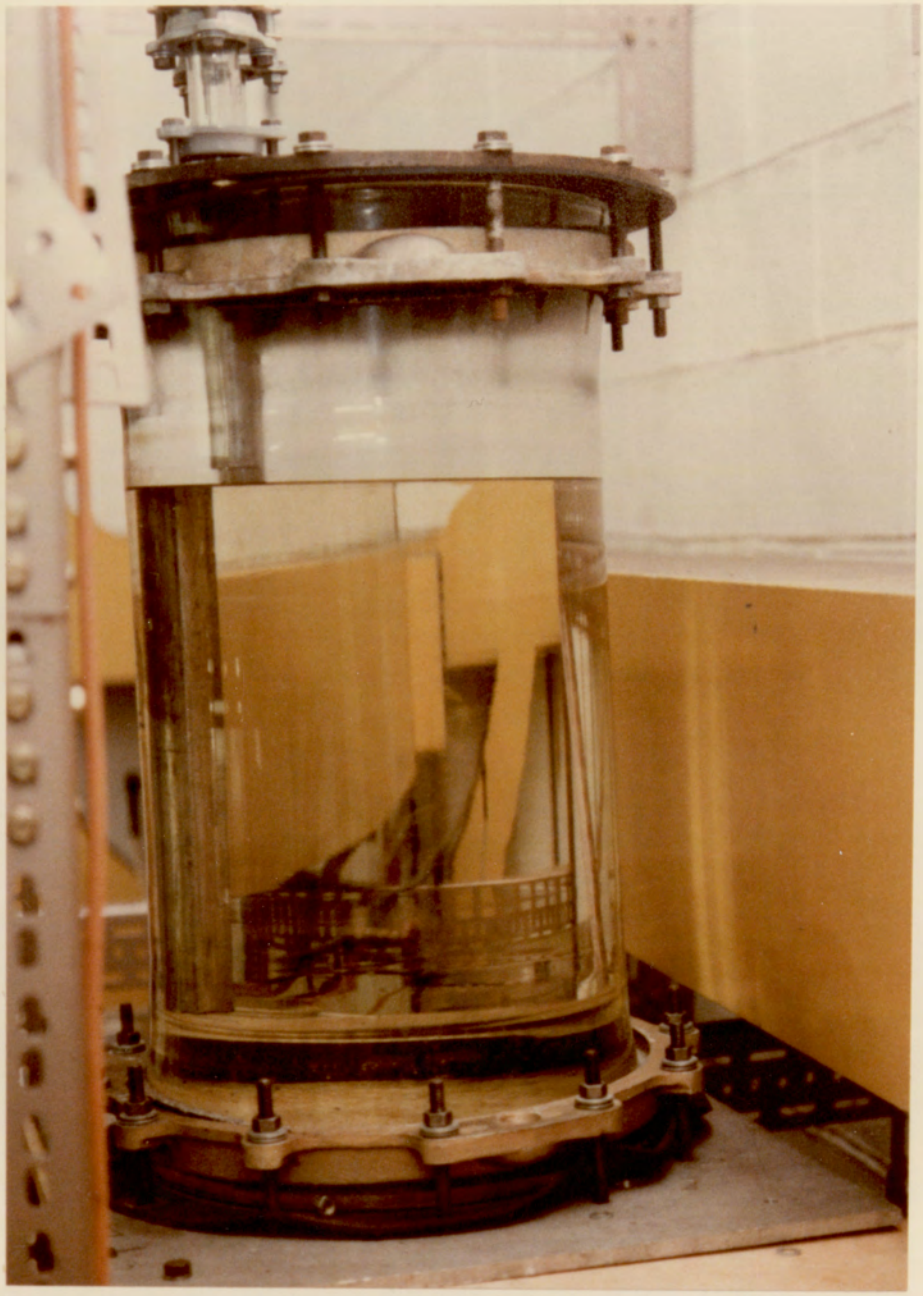

Figure 7.6 EXTERNAL SETTLER VESSEL
350 m.m. by 600 m.m. high.

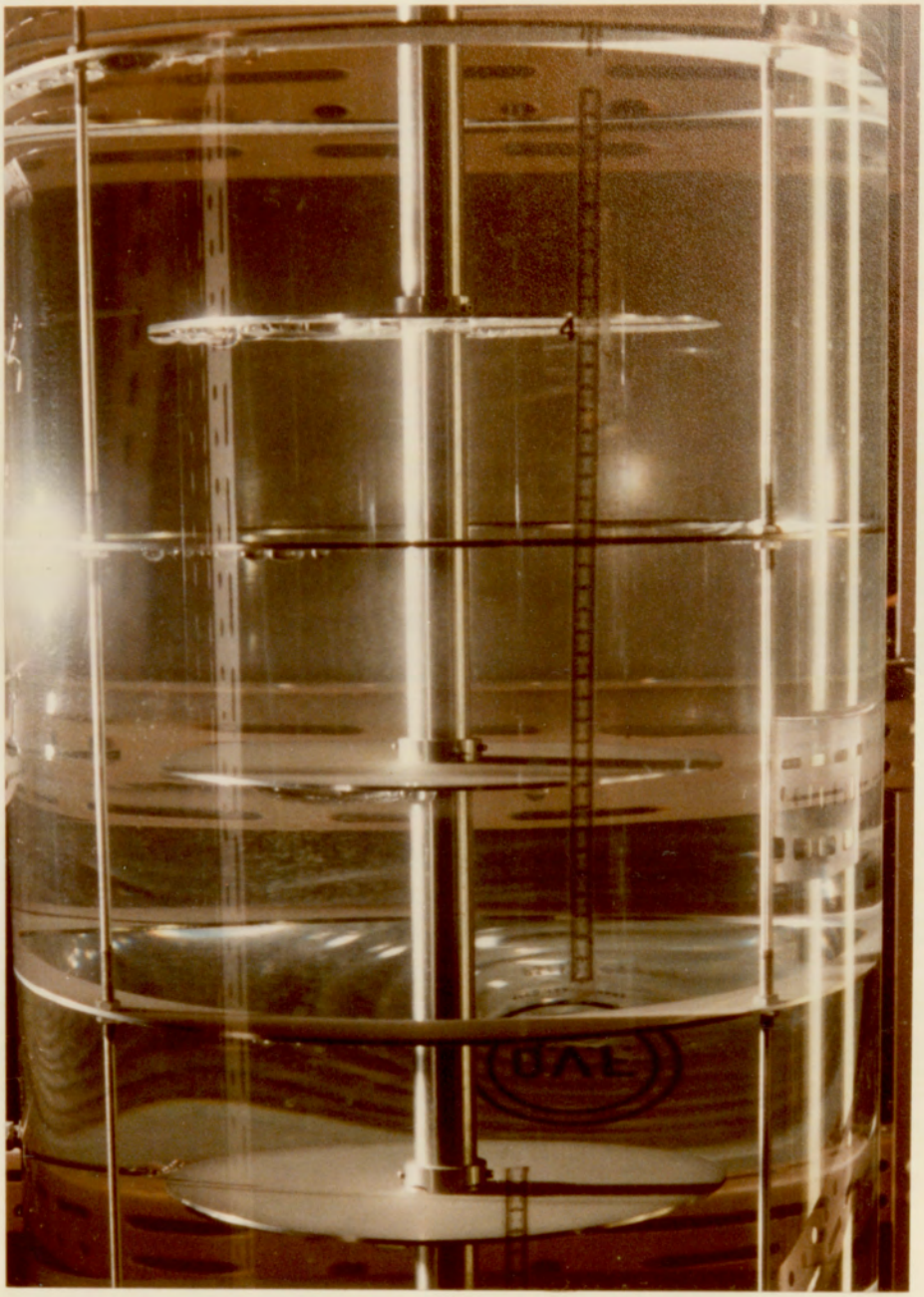

Figure 7.7 ILLUSTRATION OF R.D.C. COLUMN SECTION

During operation the criterion for steady state hydrodynamic conditions was taken as a steady interface level, the attainment of which needed on average approximately 5 minutes depending on operating variables, Appendix 7. To reach such a state during mass transfer experiments before samples could be taken, a total displacement of 2.5 times dispersed phase volume was required.

7.2. SELECTION OF LIQUID-LIQUID SYSTEM

The storage and use of relatively large quantities of solvent, ie. about 1000 litres at any time, required a low-cost solvent to a fixed specification. Therefore the liquid system selected for study was Clairsol-350, acetone-water. The physical properties of this system are given in Appendix 2. The selection was based, in general, on the following considerations.

1. Low volatility of Clairsol-350 and relatively low toxicity. Flash point over 71°C and hence a reduced fire hazard compared with other commercially available solvents. The low volatility resulted in both low vapour concentrations in the plant during open handling operations and low solvent losses.

2. Availability and cost.

3. The availability of results on Clairsol-350 from other studies for comparison (99).

4. The kinematic viscosity was in the range of 2-3 Cs, interfacial tension with water in the range of 25-45 dyne/cm, and the density 0.785 g/cm^3 of Clairsol-350 provided a system of the type ideal for operation with an agitated column (223).

De-ionised water constituted the aqueous phase instead of tap water. This was obtained by passing mains water through an Elgastat B224 de-ioniser, Appendix 1. Using de-ionised water was intended to reduce stagnant drop behaviour by avoiding the presence of metallic ions existing in tap water, which act as surfactants and have a barrier effect on mass transfer.

7.3. EXPERIMENTAL TECHNIQUES

7.3.1. Cleaning Procedure

Cleanliness is an important factor affecting liquid extraction column operation since surfactants, or oil and grease, can easily be dissolved, by one of the phases. These result in changes in the physical properties of the system and may lead to inconsistencies in the experimental data and results. Suspended solids, eg. interfacial scum or corrosion products, may act similarly. Therefore, prior to experiments, all the column internals, the transfer lines and the storage tanks were carefully cleaned with a 2 per cent V/V solution of "Decon 90" decontaminant in de-ionised water. The column was filled with this solution and left overnight. Next morning it was pumped through all parts of the plant, for about 2 hours with the agitator running, and then drained. The equipment was then flushed with tap water several times and finally rinsed with the continuous phase (de-ionised water). Great care was taken to effectively drain all low points and pipe sections to avoid any retention of surfactant. Care was taken to ensure that all sample points were well-flushed.

The use of de-ionised water for the final wash and in operation was found to reduce the accumulation of interfacial dirt or rag between the two liquids. The storage tanks were cleaned in a similar manner.

7.3.2. System Purity Checks

The system purity was checked at regular intervals during the experimentation by measuring relevant system properties, ie. density, viscosity, interfacial tension and individual surface tension of the component liquids. Due to scale of operation some change in the system properties was unavoidable, but generally no significant discrepancies were observed ie. less than 5%. Whenever a significant discrepancy in the values of the system properties was observed, the liquids were discarded, followed by complete equipment washing using the method already described.

7.3.3. Measurement and Calibration Techniques

There are a number of methods available to determine the concentration of acetone in the organic dispersed and aqueous continuous phase, eg. by measurement of the refractive index, relative absorbance or via surface tension. In this work solute concentrations were determined by using the refractive index technique.

An Abbe A60 refractometer with temperature control was used and calibrated to five decimal places, to measure the acetone concentration in the samples of the aqueous continuous phase as well as in the dispersed phase. Temperature was controlled at 20°C ± 1°C by means of a Townson and Mercer temperature control circulating unit. Accurate calibration curves were obtained for refractive index vs. solute concentration, by measuring the indices for solutions made up to known concentration. These are given in Appendix 3. Only small quantities of liquid under test ie. 10 mls, were required for this method.

7.3.4. Experimental Mass Transfer Operations

Experimental runs involving the transfer of solute from the dispersed phase to the aqueous continuous phase were performed at 80% of flooding rate and below. De-ionised water comprised the extract phase in all cases. The solute concentration in the raffinate was restricted to 4% by weight to avoid scum formation. The initial concentration of acetone in the aqueous phase was always 0%.

In consecutive runs a precalculated amount of acetone was added to the raffinate to reach the desired initial concentration. This procedure was adopted to avoid the need for batch distillation to recover large quantities of Clairsol.

Before each experiment the phases were mutually saturated by circulating each phase in a closed loop for a period of at least 3 hours. Afterwards they were left overnight to settle and separate. Feed solutions were made up to the required solute concentration by the addition of a calculated amount of 'Analar' acetone. Each experiment was run with fresh water as solvent.

Operating rotor speeds were selected between two values. The minimum speed at which drops became trapped beneath the rotating discs and stator rings, as described in section 5.1, was 100 rpm. The maximum speed without generation of a secondary dispersion of Clairsol in water was 350 rpm. Therefore speeds were selected between these in order to characterise column performance with the system studied.

Two samples were taken from the feed tank via a sample valve for initial concentration measurement. The column was then filled with continuous phase and the rotor speed adjusted to the required value. The continuous phase inlet and outlet values were then adjusted to give the required continuous phase flow through the column. Dispersed phase was then introduced and this displaced the interface level at the top of

the column. This level was maintained by adjustment of the continuous phase outlet valve. Steady state operation was judged to have been achieved when at least two consecutive samples from every sample point gave the same solute concentration (within the limit of analytical accuracy). After steady-state conditions were reached, depending on flow rates and hold-up, duplicate samples were withdrawn. Hold-up and drop size were measured as described earlier. Measurements of drop size distribution were made for compartments 1, 3, 5, 6, 7, 9 and 11. Results of mass transfer runs were evaluated as discussed in Chapter 8.

7.3.5. Photography and Associated Techniques

For this work, photographs of the droplet swarm were taken using two still cameras, a Nikkormat FTN 35mm with a 55mm micro-Nikkor lens and an Asahi Pentax Spotmatic ESII with a 100mm Macro Takumar lens. For most cases lightingwas provided by a simple 1000 watt photoflood lamp placed directly behind the compartment.

Ilford XP1 400 ASA films were used in all cases. Aperture openings, shutter speeds and focal lengths were adjusted accordingly. In most cases a shutter speed of 1/1000 of a second was found to give the best results especially at high rotor speeds. The aperture varied between f4 and f22 according to the amount of light passing through the column. Three photographs of the drop swarms were taken of each event, after steady state had been attained.

Drop size measurements were taken from prints with approximately 1 to 2 times magnification. A Carl Zeiss T4.I.3 particle size analyser was used to analyse the photographs. Ellipsoids were recorded as spheres of equivalent diameter. The number of drops measured for each run for the different compartments varied from 300 to 950, but this was reduced to 250 to 350 drops counted in a random manner.

8. RESULTS AND DISCUSSION

8.1. NON-MASS TRANSFER STUDIES

8.1.1 Flooding

Flooding rates represent the maximum volumetric capacity of an extraction column under a given set of operating conditions. Flooding in this work was characterised by the complete rejection of the dispersed phase, as a dense layer of drops just above the distributor, which is the conventional flooding phenomena (223, 33, 76).

The hold-up (ie. volume fraction) of the dispersed phase is a key variable for flooding and mass transfer characteristics. The available interfacial area in a dispersion is related to hold-up by,

$$a = \frac{6x}{d_{32}} \qquad (8.1)$$

Near to the flooding point the hold-up tends to increase in an unstable manner.

Separate runs were carried out to measure flooding rate. Before starting a run the phases were mutually saturated in the absence of mass transfer. Flooding was determined by fixing the rotor speed and continuous phase flow rate and then increasing the dispersed phase flow rate incrementally until flooding occurred.

With the original equipment arrangement, operation of the column at maximum flow rates did not result in flooding although a relatively high hold-up was apparent, indicative of 'incipient flooding'. A booster pump was therefore necessary, as described earlier, to raise the dispersed phase flow rates to reach flooding. By operating

the column with higher dispersed phase flow rates after a while an accumulation of drops was observed under the stator (ie. >3cm) in the bottom compartment together with back flow to the distributor. This level of drops beneath the stator increased; as the drops could not escape readily the hold-up increased further until suddenly flooding occurred. At this point the dispersed phase was rejected and entrained in the continuous phase exit flow. The extent of back mixing was so marked as to cause entrainment of continuous phase in the return line of the dispersed phase to the external settler. A number of relatively large drops were observed in the bottom compartment due to coalescence. Conditions just before flooding are illustrated in Figures 8.1 and 8.2. The local velocities of the smaller drops were much less than the continuous phase, so they were carried out with that phase.

Samples were taken from the third compartment to measure local hold-up at the flooding point. A minimum of two readings were taken for each point; a variation of only $\pm 3\%$ was observed between each determination. (This compartment was selected for convenience since at true flooding the hold-up should be independent of position in the column.)

Hold-up at the flooding point can be estimated by equation (5.9)

$$x_f = \frac{(L^2 + 8L)^{0.5} - 3L}{4(1 - L)} \qquad (5.9)$$

The characteristic velocity can be determined according to equation (5.7)

$$V_{d.f} = 2V_N \, x_f^2 \, (1 - x_f) \qquad (5.7)$$

A plot of $V_{d.f}$ against $x_f^2 (1 - x_f)$ can therefore be expected to yield straight lines through the origin. This approach has been popular because flooding rates can be estimated from only two parameters, viz the flow rate ratio L and the characteristic

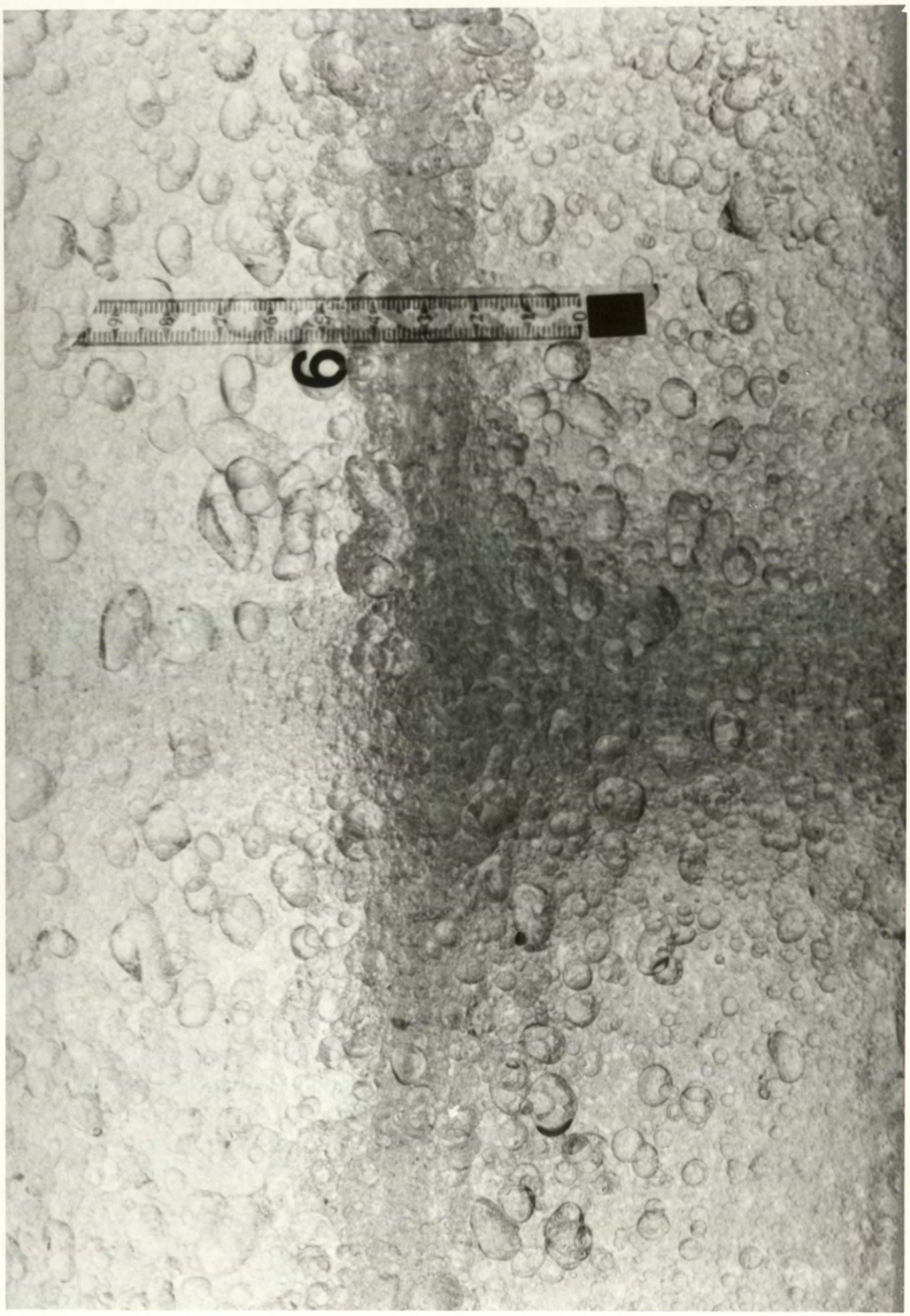

Figure 8.1 Conditions Just Prior to Flooding

Mass Transfer d → c

Initial Acetone Concentration = 0.78

V_c = 0.8 cm/s , V_d = 0.63 cm/s

N = 300 r.p.m.

Compartment No. 6

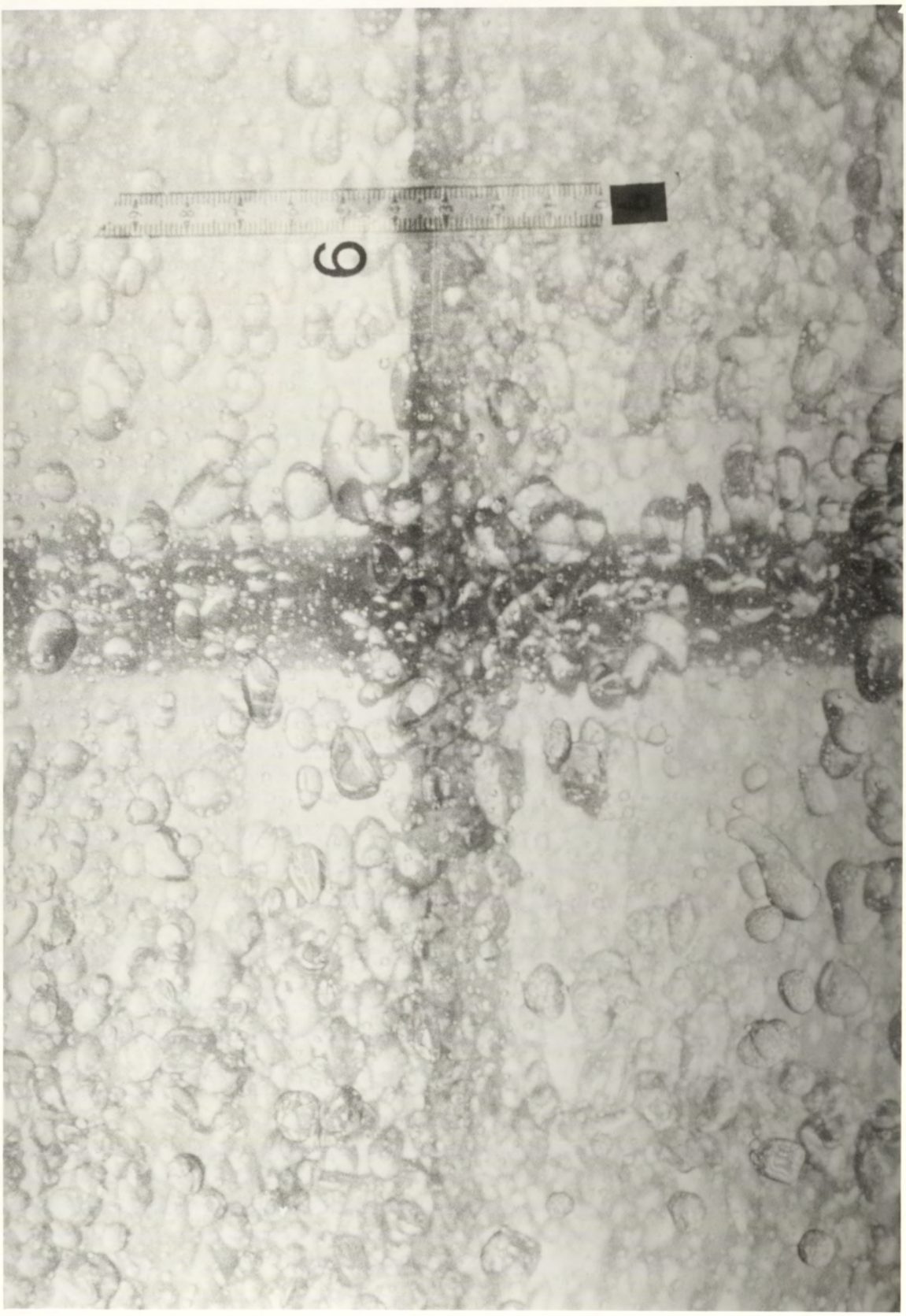

Figure 8.2 Conditions Just Prior to Flooding

Mass Transfer d → c
Initial Acetone Concentration = 0.78%
V_c = 0.8 cm/s , V_d = 0.63 cm/s
N = 0 r.p.m.
Compartment No. 6

velocity V_N. The approach has been applied successfully to characterise flooding in an RDC (166, 167).

Table 8.1 Experimental Flooding Data

$V_{c.f}$ (cm/s)	V_{df} (cm/s)	$x_f^2 (1 - x_f)$	$(V_d/V_c)_f$	x_f (%)
0.7	0.765	0.076	1.09	33.9
0.775	0.68	0.071	0.88	32.5
0.84	0.635	0.067	0.75	31.2

The experimental flooding data used to plot Figures 8.3 and 8.4 are given in Table 8.1. These data have been used to test Logsdail et al's flooding relation (156). Values of the characteristic velocity V_N were obtained from the slope of the line shown in Figure 8.4 equal to 2 V_N. Equation (5.9) appears satisfactory for hold-up calculation at flooding since the experimental data lay relatively close to calculated ones. However the calculated hold-up values were between 15% and 26% less than the experimental values. The complex mixing pattern induced by the rotating discs, which does not receive any consideration in the derivation of Equation 5.9, may be one explanation for this. Figure 8.3 demonstrates that, surprisingly, the column volumetric capacity was almost 25% greater than reported by Al-Aswad (99).

8.1.2. Hold-up

In this work the average value of the dispersed phase hold-up was measured for each individual run and, as expected, was found to increase with increasing flow rates.

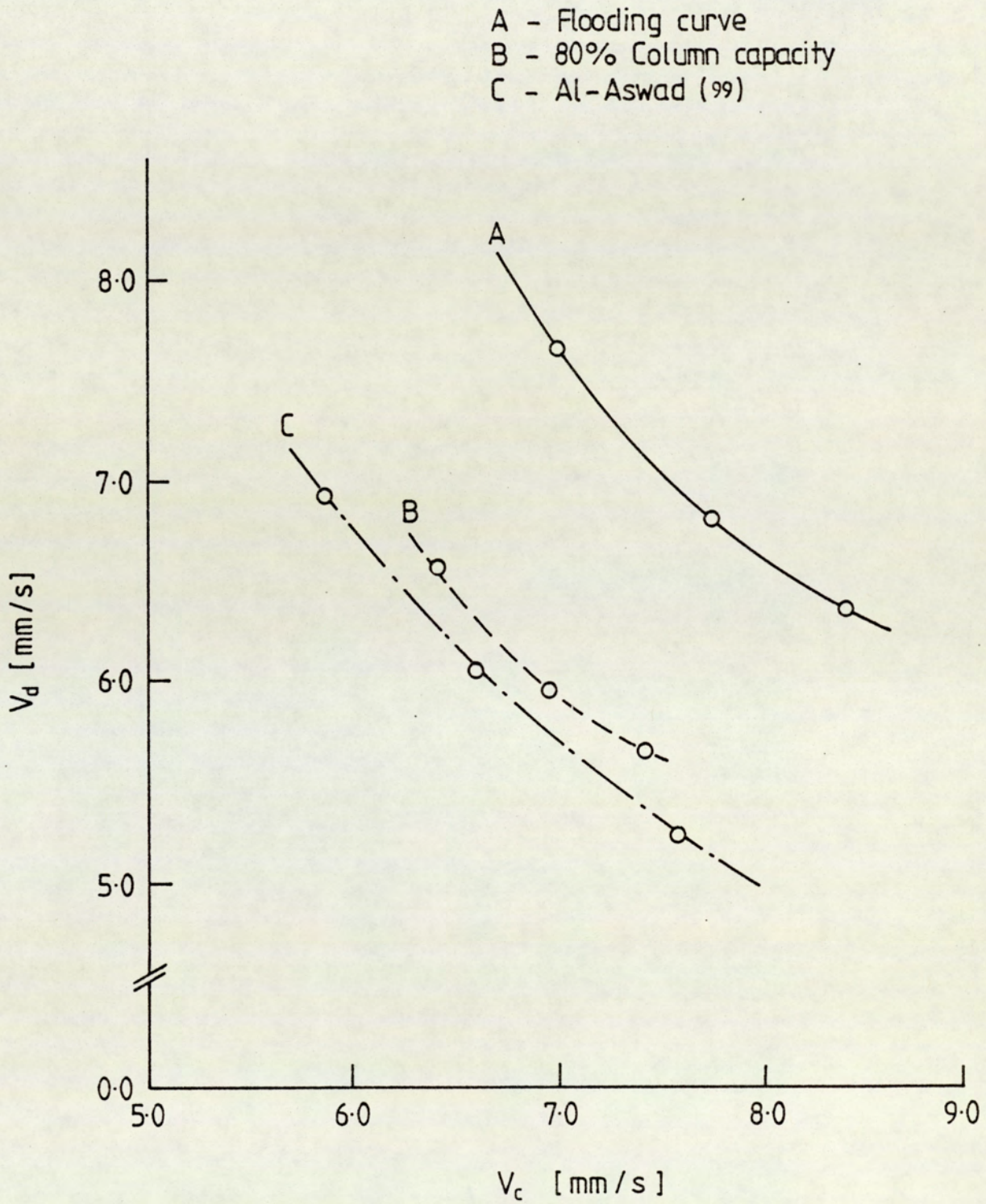

Figure 8·3 Flooding Curves at Rotor Speed of 300 rpm.

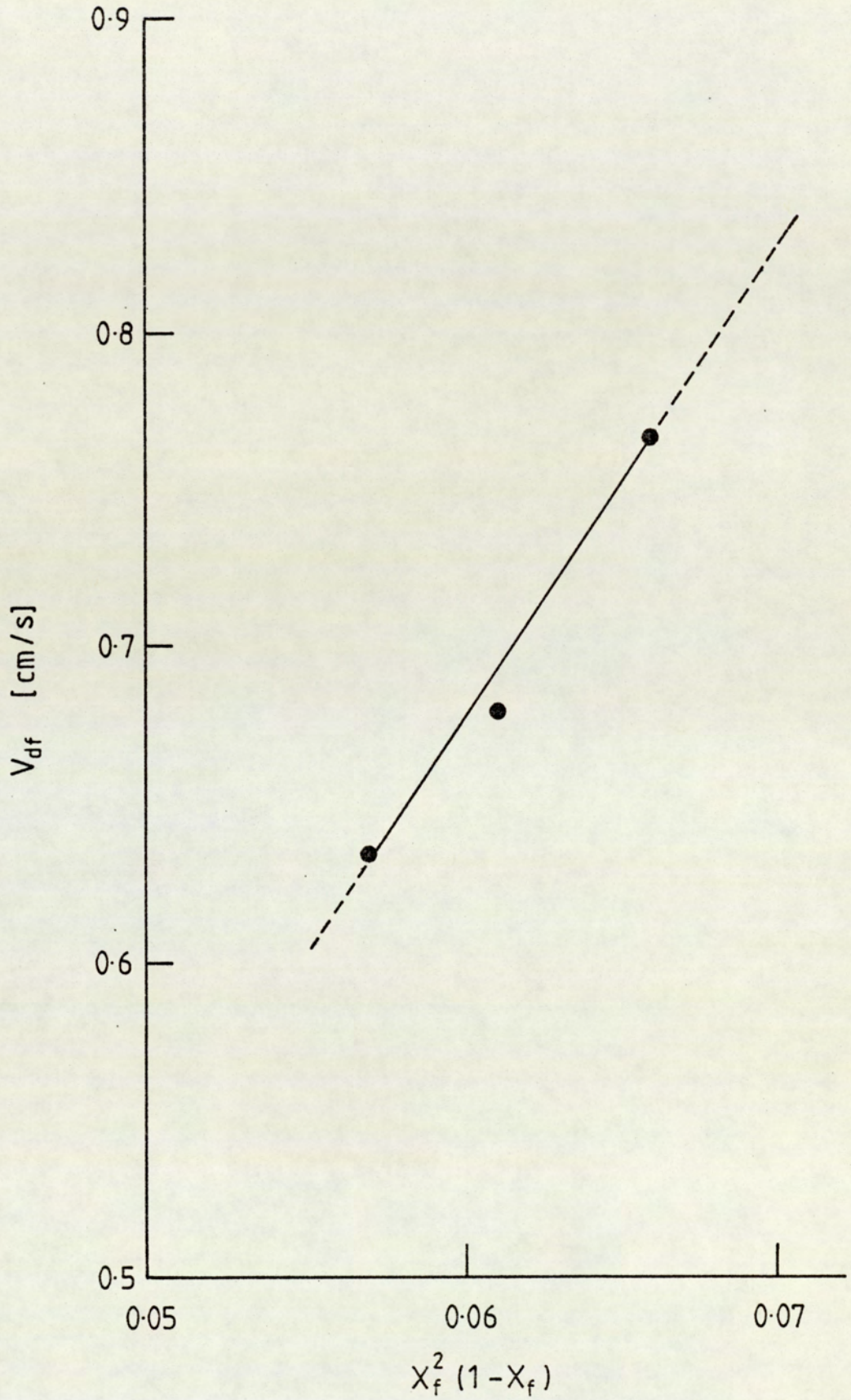

Figure 8·4 Correlation of Flooding Data at Rotor Speed 300 rpm.

Under equivalent operating conditions, ie. equal flowrates and rotor speeds, the values of average hold-up determined under mass transfer conditions (dispersed to continuous phase) as described in Section 8.2 were lower than those under non-mass transfer conditions. This was in agreement with the observed drop sizes, that is with mass transfer taking place from the dispersed to continuous phase, the Sauter mean drop sizes were larger due to enhanced interdroplet coalescence. (In the case of mass transfer from the continuous phase to the dispersed phase, it would be expected that higher hold-ups would be obtained due to the absence of coalescence resulting in smaller drops with larger residence times. Thus, neglecting any changes due to overall lowering of interfacial tension by the presence of solute, the drop size and hold-up should approximate to the non-mass transfer case.)

8.1.3. Mean Drop Size

The observed Sauter mean drop size diameters d_{32} under mass transfer conditions with solute transfer from the dispersed to the continuous phase, were found to be larger than those in non-mass transfer experiments for the same conditions of flow rate and rotor speed (Figures 8.5 and 8.6). This was attributable to the action of transferred acetone from the dispersed to the continuous phase resulting in an enhanced rate of inter droplet coalescence which increased the drop size. This may be explained by the proposal by Smith et al (81), considering two drops separated by a continuous phase, that in such a case coalescence between drops is more likely, because the continuous phase between them receives solute from both drops and concentration tends to rise more quickly than in other regions around them, and within each drop the solute concentration should decrease slightly slower than in the facing region. As a result the interfacial tension in the facing region will be less, which will promote coalescence leading to larger drops.

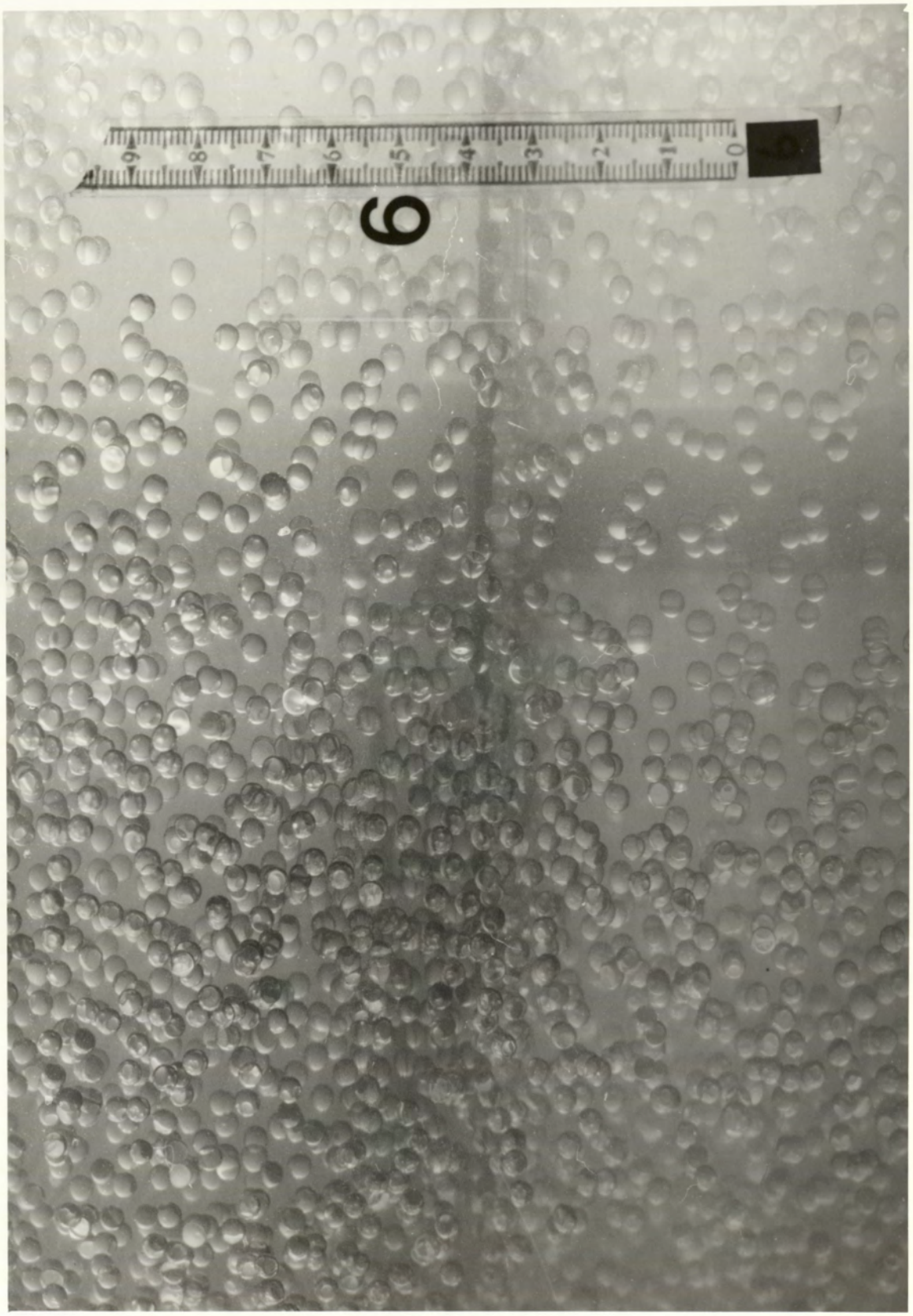

Figure 8.5 Drop Size Distribution Under Non-Mass Transfer Conditions

V_c = 0.3145 cm/s , V_d = 0.25 cm/s

N = 100 r.p.m.

Figure 8.6 Drop Size Distribution with Acetone Transfer from Dispersed to Continuous Phase

V_c = 0.3145 cm/s , V_d = 0.25 cm/s

N = 100 r.p.m.

Many correlations have been proposed to predict the drop size (76, 66, 54). However, most of these correlations were derived from small scale columns (<20cm) and with binary systems. Therefore they would not be expected to correlate data for large scale columns and large differences were in fact observed. Al-Aswad's correlation was more reliable due to the scale of column used but even this predicted lower values of d_{32}.

$$\frac{d_{32}}{D} = 5.52 \times 10^{-8}\left(\frac{V_d.H.\rho_c}{\mu_c.x}\right)^{1.14}\left(\frac{N^2D^3\rho_c}{\sigma}\right)^{-0.14}\left(\frac{V_d^2}{g_c.D.x^2}\right)^{-0.38}\left(\frac{n}{Nc}\right)^{-0.06} \qquad (8.2)$$

The deviation was between 22% and 86%. Such a deviation could be anticipated between the experimental results with mass transfer and those predicted from the above equation based on non-mass transfer conditions.

The drop size decreased with increasing rotor speed. This would be expected since an increase in rotor speed causes more drops to break up and the proportion of the small droplets will be greater (Figure 8.7).

For various rotor speeds with constant flow rates the different mean drop sizes, under mass transfer conditions, were determined from the bottom to the top of the column, Figure 8.8. The trend of mean drop size up the column was as follows:

For Rpm =100 little change in d_{32}

Rpm = 200 d_{32} decreasing

Rpm = 300 d_{32} decreasing

The critical rotor speed, above which operation of this RDC was practicable appeared to be 100 rpm. Below this the energy input was not sufficient to overcome the interfacial tension (171).

a) N = 300 r.p.m.

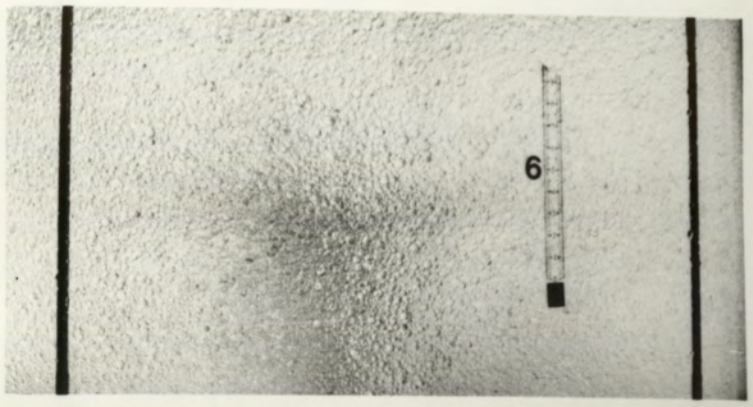

b) N = 200 r.p.m.

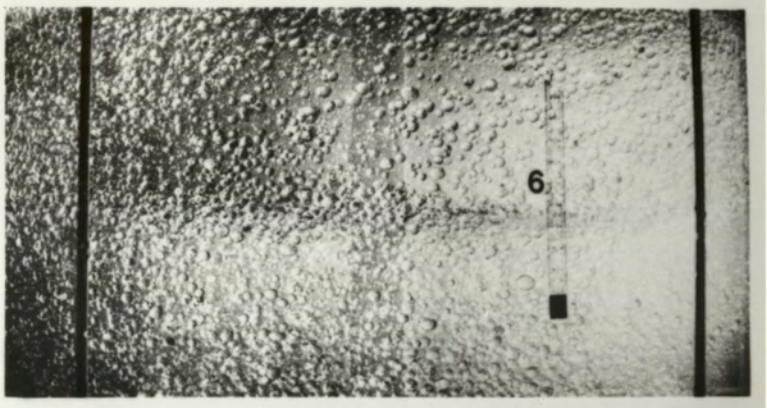

c) 100 r.p.m.

Figure 8.7 Drop Size Distribution Variation with Rotor Speed in Compartment No. 6

Mass Transfer d → c

Initial Acetone Concentration = 0.5%

V_c = 0.3145 cm/s , V_d = 0.25 cm/s

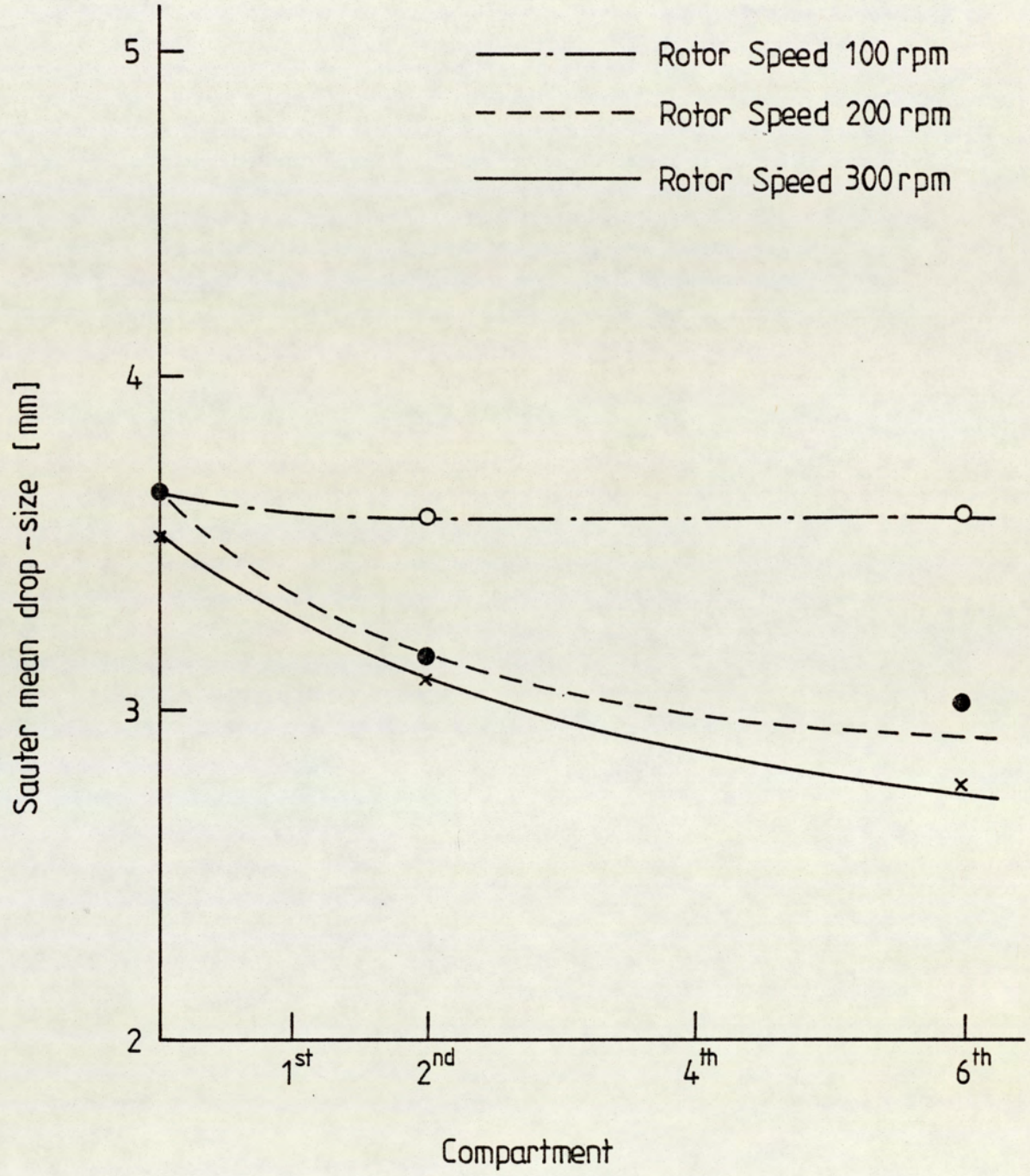

Figure 8·8 Drop-size Profile along Column length

For rotor speed below the critical rotor speed the rate of coalescence overcomes the rate of drop break up resulting in larger mean drop sizes as the swarm of drops rises through the column. For rotor speeds of 100 rpm, and above, the situation is vice versa, because of a reduction in, or complete absence of, coalescence (Figure 8.9). A typical illustration of drops behaviour in the bottom compartment is shown in Figure 8.10.

8.1.4. Drop Size Distribution

Figures V and VI in Appendix 4 show the drop size distribution as drop cumulative volumes, as well as drop cumulative area, versus drop diameter for the sixth compartment at a rotor speed of 300 rpm. The cumulative volumes, of the drop size sample were calculated as:

$$\upsilon_v = \Sigma n_i \left(\frac{\pi}{6} d_i^3\right) \tag{8.3}$$

$$\upsilon_a = \Sigma n_i \pi d_i^2 \tag{8.4}$$

A sample calculation for drop size distribution is given in Appendix 4. Log-probability graph paper was used to plot the drop size cumulative volume, as well as area, versus drop diameter. From these graphs the upper limit distribution parameters proposed by Mugele et al (70), d_m, $\bar{a}$, δ can be obtained:

$$d_m = \frac{d_{50}(d_{90} + d_{10}) - 2d_{90}d_{10}}{d_{50}^2 - d_{90}d_{10}} . d_{50} \tag{3.24}$$

$$\bar{a} = \frac{d_m - d_{50}}{d_{50}} \tag{3.22}$$

a)

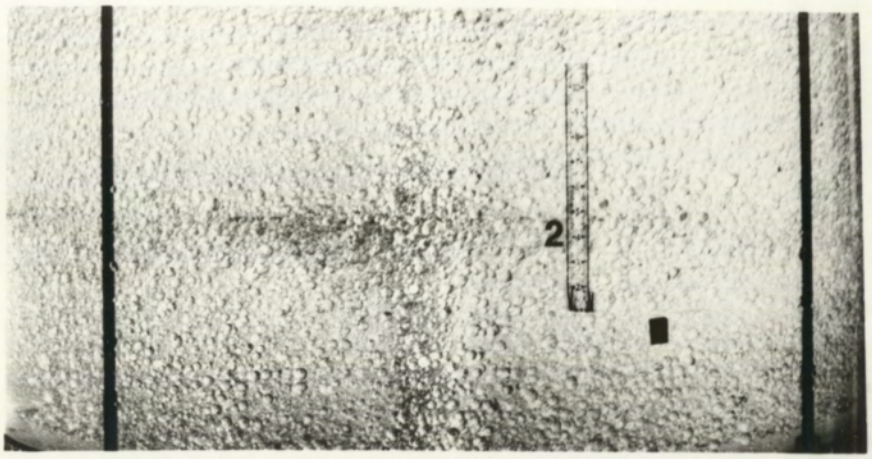

b)

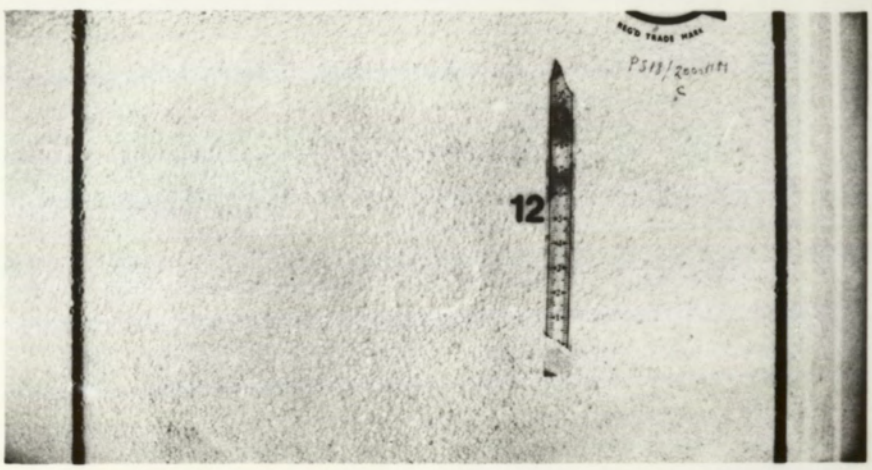

Figure 8.9 Drop Size Distribution Variation with Height

a) Compartment No. 2

b) Compartment No. 12

Mass Transfer d → c

Initial Acetone Concentration 0.75%

V_c = 0.3145 cm/s , V_d = 0.25 cm/s

N = 300 r.p.m.

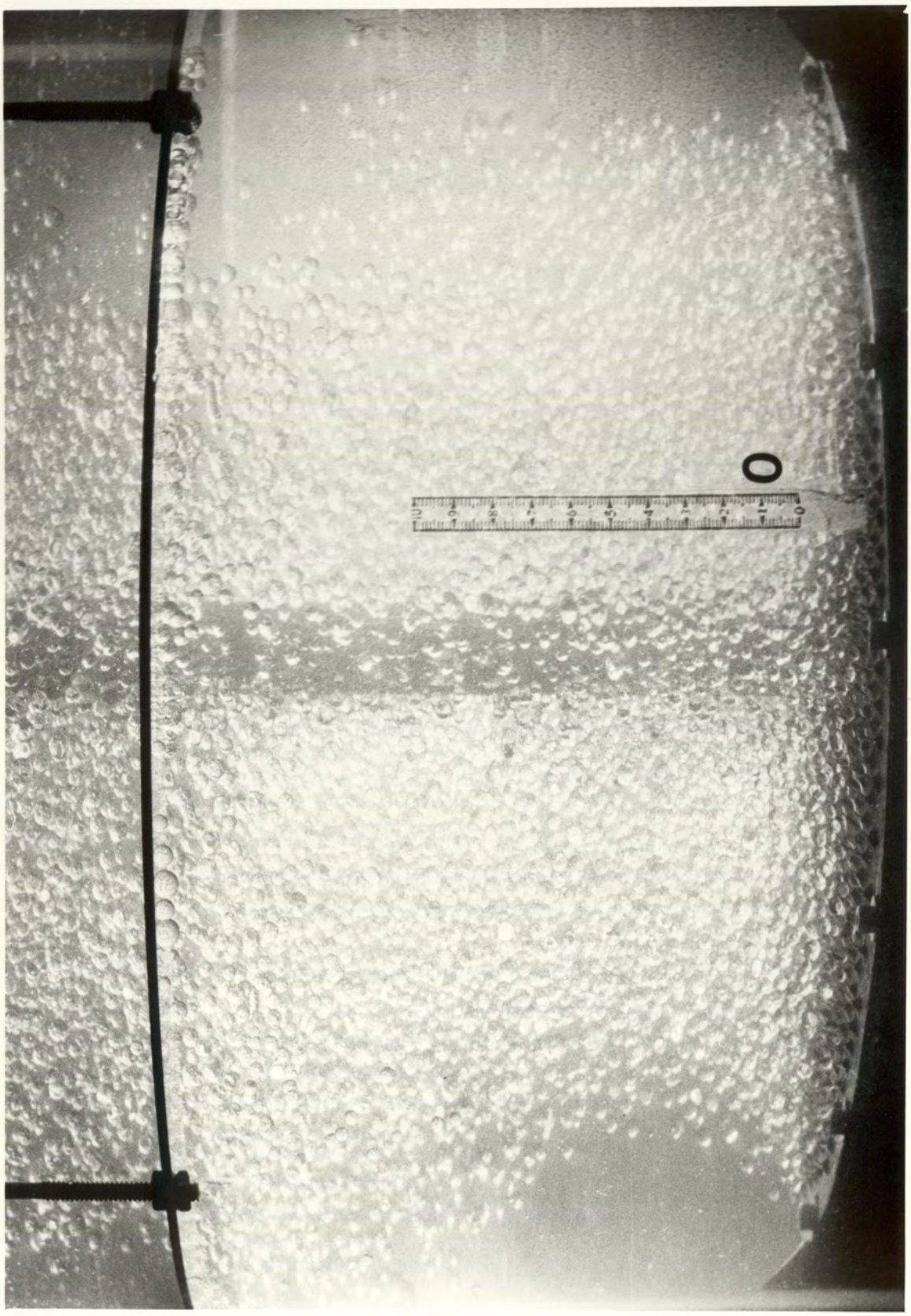

Figure 8.10 Drop Formation from Distribution

V_c = 0.3145 cm/s , V_d = 0.24 cm/s

The dead-zones at the periphery are typical of the operating conditions.

$$\delta = \frac{0.907}{\ln\left[\frac{d_{90}}{d_m - d_{90}} - \frac{d_m - d_{50}}{d_{50}}\right]} \qquad (3.23)$$

As shown in Appendix 4, Tables IVa and b, the range of the observed drop sizes, was between 1.7 and 8.9mm. This range is slightly wider on the large drop size side than observed in a previous study (99), but is as reported by other workers (52, 63). The wider range was due to mass transfer operations, in which coalescence would be enhanced, resulting in a larger drop regime.

The shape of the drop size distribution curve is similar to that reported by Olney (52) and Jeffreys et al(65).

Figures 8.11 and 8.12 show good agreement between experimental results and the Upper Limit distribution predicted by Mugele-Evans (70). This agreement is demonstrated by comparison between the Sauter mean drop diameter,

$$d_{32} = \frac{\Sigma n_i d_i^3}{\Sigma n_i d_i^2} \qquad (8.5)$$

and d_{32} calculated from Mugele-Evans (70) equation.

$$d_{32_M} = \frac{d_m}{1 + a' e^{0.25\delta^{-2}}} \qquad (8.6)$$

The index δ, determines the spread of the distribution, a smaller value indicates a wider range of drop sizes.Both d_{32} and $d_{32\,M}$ are in good agreement (Appendix 4).

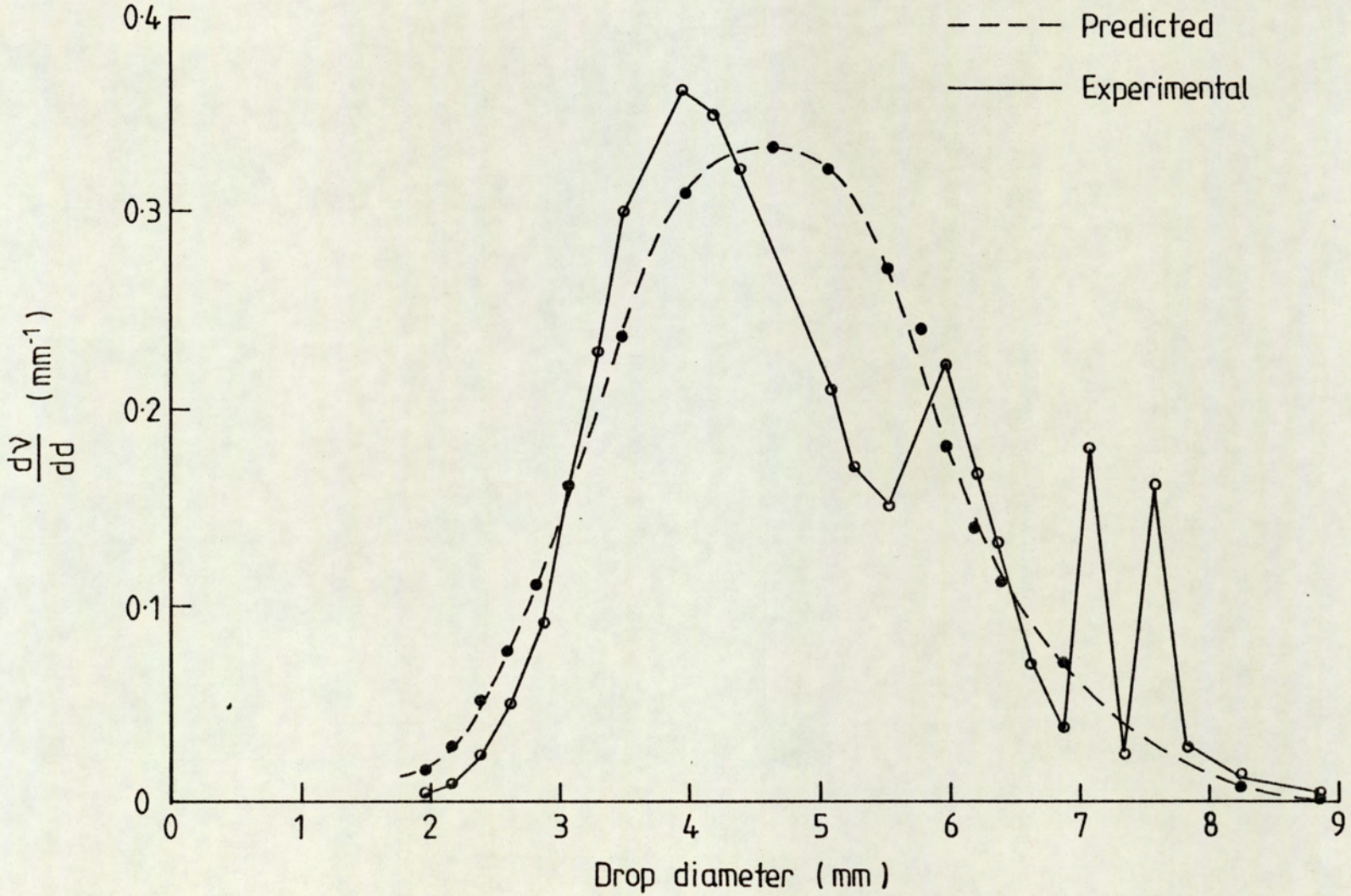

Figure 8·11 Comparison of experimental and predicted upper-limit drop size distribution (Volume basis)

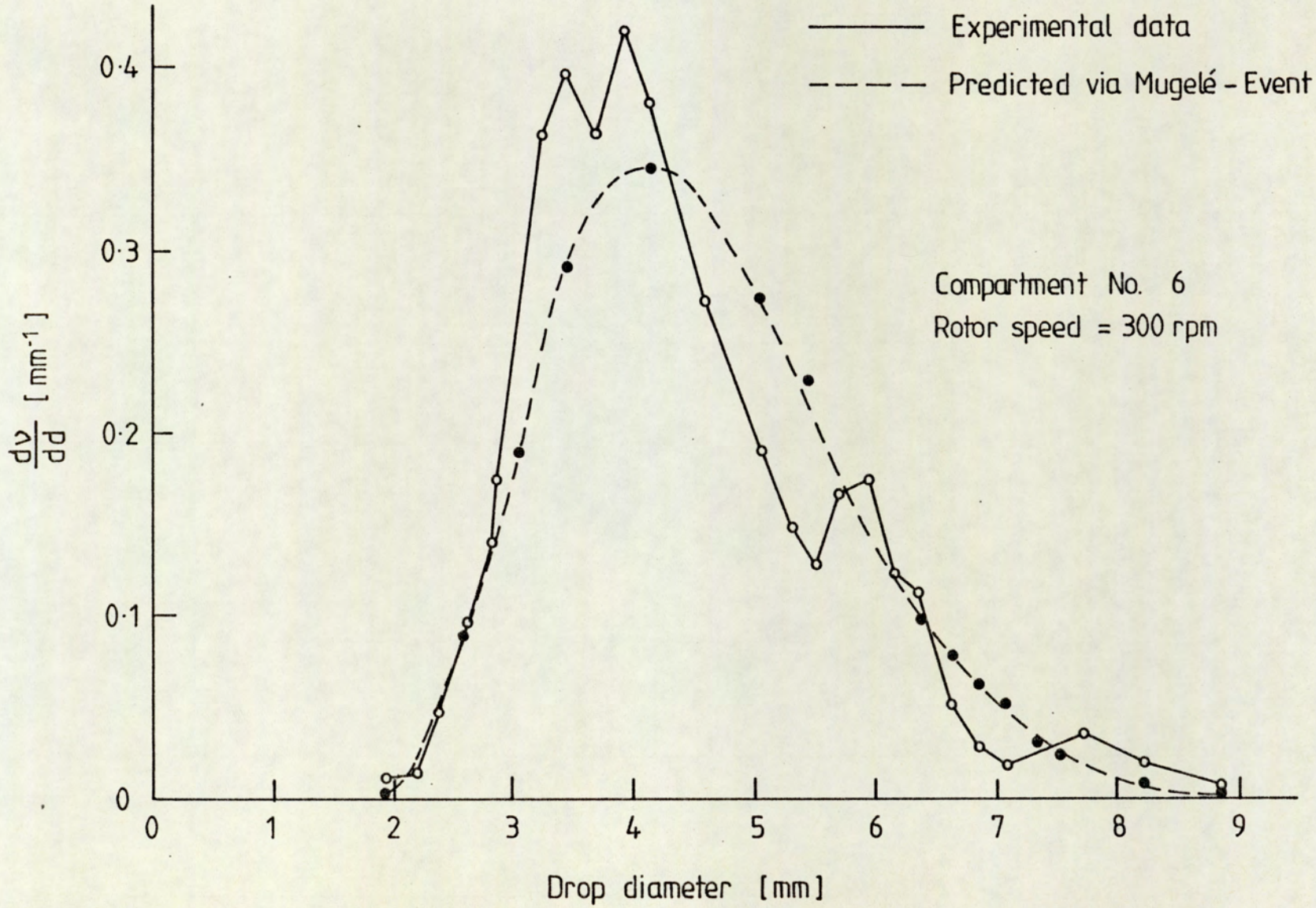

Figure 8·12 Comparison of Experimental and Predicted Upper Limit Drop-size Distribution on Area-Basis.

The importance of accounting for change in drop size distribution under the practical conditions when mass transfer is taking place is illustrated by Figures 8.5 and 8.6. These clearly show the larger drop sizes associated with mass transfer from the dispersed to continuous phase, and hence the reduced interfacial area compared with non-mass transfer operation under otherwise similar conditions.

8.2. MASS TRANSFER STUDIES

The column's extraction efficiency, and its hydrodynamic behaviour under mass transfer conditions, were determined at different solute concentrations in the feed stream. The conditions are summarised in Table 8.2. All mass transfer runs were carried out at 80% and below of flooding flowrate, previously assessed under the same operating conditions. Most of the runs were carried out with relatively low flow rates where no significant back mixing was detectable. Even in subsequent runs with high flow rates the axial mixing was virtually negligible except in one with the highest flow rates achievable. The feed concentration of solute was restricted to 4% to avoid scum formation and deposition (223).

The efficient design of an RDC requires a knowledge of the overall mass transfer coefficient for the systems involved. In this study this was calculated as described in Section 8.2.1.

8.2.1. Experimental Overall Mass Transfer Coefficient

The overall experimental mass transfer coefficient was calculated for each run using the common equation

$$N = K.A.\Delta C_m \qquad (1.1)$$

where N is the mass transfer rate calculated from a mass balance across the column. A is

Table 8.2. Summary of Experimental Conditions

System: Clairsol - 350 (dispersed) - Acetone --> De-ionised Water.

Run No.	RPM	V_c (cm/s)	V_d (cm/s)	x_{in} ($\times 10^{-2}$)	x_{out} ($\times 10^{-2}$)	y_{in} ($\times 10^{-2}$)	y_{out} ($\times 10^{-2}$)
1	200	0.3145	0.25	3.3	1.3	0.00	1.6
2	300	0.3145	0.25	3.3	1.05	0.00	1.8
3	200	0.3145	0.25	2.0	0.6	0.00	1.1
4	300	0.3145	0.25	2.0	0.56	0.00	1.15
5	200	0.2	0.15	1.1	0.16	0.00	0.7
6	300	0.2	0.15	1.1	0.16	0.00	0.7
7	200	0.3145	0.25	2.6	0.96	0.00	1.3
8	300	0.3145	0.25	2.6	0.8	0.00	1.4
9	300	0.3145	0.25	4.0	0.125	0.00	3.1
10	300	0.16	0.63	4.0	0.29	0.00	4.2
11	300	0.615	0.63	2.4	0.16	0.00	2.3
12	300	0.75	0.60	4.0	1.0	0.00	1.8
13	300	0.8	0.565	2.1	0.1	0.00	1.4
14	300	0.84	0.55	2.5	0.2	0.00	1.6

the total surface area in the column, estimated from the equation,

$$a = \frac{6x}{d_{32}} \tag{8.1}$$

where a is the interfacial area per unit of column volume, hence

$$A = a.V \tag{8.7}$$

where V is the total column volume.

Simpson's rule was applied to determine the actual mean driving force ΔC_m by using the acetone concentration profile along the column. Acetone concentration was measured in samples of the continuous phase taken from compartment numbers 1, 3, 5, 7, 9 and 11 and the column inlet and outlet streams. The mean driving force in each compartment could hence be determined as Δy_1, Δy_3, Δy_5, Δy_7, Δy_9 etc respectively, where

$$\Delta y_i = y_i^* - y_i \tag{8.8}$$

and y is the acetone concentration in the aqueous phase.

Simpson's rule is as follows:

$$\Delta y_m = \frac{1}{20} \{\Delta y_{in} + \Delta y_{out} + 4\,\Delta y_1 + 2\,\Delta y_3 + 4\,\Delta y_5 + 2\,\Delta y_7 + 4\,\Delta y_9 + 2\,\Delta y_{11}\} \tag{8.9}$$

Δy_m was then converted to ΔC_m by multiplying it by extract phase density. The overall experimental mass transfer coefficient can be calculated as:

$$K_{exp} = \frac{N}{A.\,\Delta C_m} \tag{8.10}$$

* The subscripts on y refer to the compartment numbers - Figure 5.1.

Table 8.3 shows the results of overall mass transfer coefficients. A sample calculation is given in Appendix 5.i and the results are discussed in Section 8.2.4.

8.2.2. Theoretical Overall Mass Transfer Coefficient

A method of calculation was used which applied the drop size distribution diagram to estimate the volume as well as the area percentage of stagnant, circulating and oscillating drops in the drop sample population (typical drop size distribution diagrams are shown in the Appendices, Figures V and VI). Individual mass transfer coefficients were evaluated for related drop regimes applying different single drop model mass transfer coefficient models from Table 4.4. The overall mass transfer coefficient K_{cal} was calculated as the fractional sum of the individual coefficients and their proportion in the drop population.

The different drop regimes are characterised by the following Reynolds number ranges,

Stagnant drops	$Re < 10$
Circulating drops	$10 < Re < 200$
Oscillating drops	$Re > 200$

where drop Reynolds number is

$$Re = \frac{d.V_s.\rho_c}{\mu_c} \qquad (8.11)$$

where d is the drop diameter and V_s is the slip velocity, determined by applying Misek's equation (171)

$$V_s = \frac{V_d}{x} + \frac{V_c}{1 - x} \qquad (5.2)$$

Table 8.3. Experimentally Determined K_{exp} Based Upon Estimated d_{32} Values.

Run No	N (g/s)	x (%)	H_E (cm)	d_{32} (cm)	a (cm^2/cm^3)	A (cm^2)	$(\Delta C)_m$ (g/cm^3)	K_{exp} (cm/s) x 10^{-4}	K.a (s^{-1}) $\times 10^{-4}$
1	7.9	3.9	320	0.35	0.67	340896	0.15	1.6	1.1
2	9	4.8	313.5	0.32	0 .9	448618.5	0.13	1.5	1.4
3	5.5	2.1	315	0.49	0.26	128718.5	0.11	3.8	1
4	5.75	4.3	312	0.36	0.72	357177.6	0.077	2.1	1.5
5	2	2.2	340	0.55	0.22	117949	0.035	4.3	0.9
6	2.2	5.1	284	0.37	0.83	374794.8	0.037	1.6	1.3
7	6.5	5	370	0.48	0.64	376512	0.13	1.3	0.8
8	7	5.3	380	0.33	0.96	580032	0.12	1	0.96
9	15.5	5.5	407	0.46	0.72	464251	0.116	2.8	2
10	9.9	7	373.5	0.6	0.69	408579.1	0.23	1.1	0.7
11	22.5	17.6	321.5	0.36	2.9	1513107.6	0.073	1.7	4.9
12	21.4	17	267.5	0.34	3	1275975	0.14	1.2	3.6
13	17.8	15	361	0.28	3.15	1808068.5	0.07	1.4	4.4
14	21.3	14.7	363	0.44	2.1	1180575	0.097	1.9	4.0

NB. The derived values (a and A) are listed as calculated; this does not imply a higher degree of accuracy than the measured values ie. 2 or 3 significant figures.

The maximum diameter of the stagnant drop regime in the whole drop population can be found by setting

$$Re = 10 \qquad 10 = \frac{d_s V_s \rho_c}{\mu_c} \tag{8.12}$$

where d_s is the maximum diameter in the stagnant drop regime. Similarly the maximum diameter in the oscillating drop regime is found by setting,

$$Re = 200 \qquad 200 = \frac{d_o V_s \rho_c}{\mu_c} \tag{8.13}$$

The circulating drop regime is that between d_s and d_o. The data in Table 8.4 shows that d_s was too small to be included; hence the drop population was considered to contain only circulating and oscillating drops with d_o as the boundary between the regimes. Once the maximum drop size for each drop regime has been estimated, the mean drop size can be found, and the mean overall mass transfer coefficient for the particular drop regime calculated from the single drop correlations in Table 4.4.

The overall mass transfer coefficient is the fractional sum of the individual overall mass transfer coefficients of each drop regime in proportion to either the volume fraction or the area fraction of that regime in the drop population in the column.

Thus the calculated overall mass transfer coefficient for the column based on volume fraction is:

$$(K_{cal})_v = (K_s)_v P_s + (K_c)_v P_c + (K_o)_v P_o \tag{8.14}$$

where P_s, P_c P_o are the volume fraction of drops in the stagnant, circulating and oscillating drop regimes respectively, and K_s, K_c, K_o are the overall mass transfer coefficients relating to each regime.

Table 8.4. Results of Calculation of V_s, d_s, d_o.

Run No.	V_c (cm/s)	V_d (cm/s)	x (%)	V_s (cm/s)	d_s (cm)	d_o (cm)
1	0.3145	0.25	3.9	6.7	0.019	0.38
2	0.3145	0.25	4.8	5.5	0.023	0.46
3	0.3145	0.25	2.1	12.2	0.01	0.21
4	0.3145	0.25	3.2	8.1	0.016	0.36
5	0.2	0.15	2.2	7.02	0.018	0.36
6	0.2	0.15	5.1	3.96	0.04	0.64
7	0.3145	0.25	4.5	5.9	0.022	0.43
8	0.3145	0.25	5.3	5.03	0.026	0.52
9	0.3145	0.25	5.5	4.88	0.021	0.41
10	0.16	0.63	7	9.2	0.014	0.28
11	0.615	0.63	17.6	4.25	0.03	0.6
12	0.75	0.6	17	4.4	0.029	0.57
13	0.8	0.565	14.7	4.7	0.027	0.54
14	0.84	0.55	15	4.6	0.028	0.56

The calculated overall mass transfer coefficient for the column based on area fraction is:

$$(K_{cal})_a = (K_s)_a a_s + (K_c)_a a_c + (K_o)_a a_o \qquad (8.15)$$

where a_s, a_c, a_o are the area fractions of drops in the related drop regime.

1. Circulating Drop Regime

The individual mass transfer coefficients of the dispersed and continuous phase for the circulating drops, based on volume as well as area fractions, were calculated as follows.

a) Dispersed phase mass transfer coefficient was estimated by the Kronig and Brink (103) correlation

$$k_d \simeq \frac{17.9\, D_d}{\bar{d}_c} \qquad (4.21)$$

where $\bar{d}_c$ is the circulating drop mid-sector diameter obtained from the relevant drop size distribution diagram, and D_d is the molecular diffusion of acetone in the dispersed phase, estimated by the correlation of Wilke et al (225).

b) Continuous phase mass transfer coefficient was estimated by the correlation of Garner et al (118)

$$\frac{k_{c.c} \cdot \bar{d}_c}{D_c} = -126 + 1.8\ (Re)^{0.5}\ (Sc)^{0.42} \qquad (4.44)$$

where D_c is the molecular diffusion of acetone in the continuous phase estimated in a similar manner to D_d.

The overall mass transfer coefficient of the circulating drops $K_{o.c}$ can be obtained by using,

$$\frac{1}{K_{o.c}} = \frac{1}{k_{c.c}} + \frac{1}{m.k_{d.c}}$$

Results of the circulating drop coefficients are listed in Table 8.5.

2. Oscillating Drop Regime

The rest of the drop population was considered to comprise oscillating drops. The individual mass transfer coefficients for the dispersed and continuous phases for this drop regime were calculated as follows:

a) Dispersed phase mass transfer coefficient. There are two basic models to correlate the mass transfer coefficient:

i) Firstly by Rose and Kintner's (97) equation:

$$k_{d.o} = 0.45\ (D_d.\omega)^{0.5} \qquad (4.30)$$

ii) Secondly by Angelo and Lightfoot's (88) equation:

$$k_{d.o} = \left[\frac{4\, D_d\, \omega\, (1+\varepsilon_o)}{\pi}\right]^{0.5} \qquad (4.33)$$

where $\varepsilon_o = \varepsilon + \frac{3}{8}\varepsilon^2$ (4.34) and ε is the eccentricity estimated from Al-Hassan's (122) correlation as:

$$\varepsilon = 0.434 \left(\frac{\omega.d_o}{V_s}\right)^{-0.46} \left(\frac{\bar{d}_o\, V_s^2\, \rho_c}{\sigma}\right)^{-0.53} \left(\frac{\mu\, V_s}{\sigma}\right)^{-0.11} \qquad (8.16)$$

Table 8.5. Theoretical Mass Transfer Coefficients of Circulating Drops

Run No	$k_{d.c}$ (cm/s)	$k_{c.c}$ (cm/s)	$K_{o.c}$ (cm/s)	P_c (%)
1	7.7×10^{-6}	11×10^{-4}	0.95×10^{-6}	0.65
2	8×10^{-6}	10×10^{-4}	1.1×10^{-6}	0.8
3	14.5×10^{-6}	20×10^{-4}	2×10^{-6}	0.005
4	9.3×10^{-6}	13.2×10^{-4}	1.3×10^{-6}	0.29
5	7.7×10^{-6}	11×10^{-4}	1.1×10^{-6}	0.085
6	6.9×10^{-6}	6.7×10^{-4}	0.94×10^{-6}	0.96
7	7.3×10^{-6}	9.9×10^{-4}	1×10^{-6}	0.42
8	7.2×10^{-6}	9.6×10^{-4}	0.98×10^{-6}	0.85
9	6.6×10^{-6}	8.6×10^{-4}	0.9×10^{-6}	0.36
10	9×10^{-6}	14×10^{-4}	1.25×10^{-6}	0.046
11	6.8×10^{-6}	11.5×10^{-4}	0.9×10^{-6}	0.9
12	6.3×10^{-6}	7.9×10^{-4}	0.86×10^{-6}	0.84
13	5.6×10^{-6}	6.7×10^{-4}	0.77×10^{-6}	0.73
14	5.8×10^{-6}	7.8×10^{-4}	0.79×10^{-6}	0.6

where $\bar{d}o$ is the oscillating drop mid-sector diameter.

b) Continuous phase mass transfer coefficient was estimated by Garner and Tayeban's (114) correlation (4.46),

$$\frac{k_{c.o}\,\bar{d}o}{D_c} = 50 + 0.0085\ Re\ Sc^{0.7} \qquad (4.46)$$

The overall mass transfer coefficient of the oscillating drops $K_{o.o}$ was predicted from,

i) $$\frac{1}{K_{o.o}} = \frac{1}{k_{c.o}} + \frac{1}{mk_{d.o}}$$

where $k_{d.o}$ is the dispersed phase coefficient calculated by Rose and Kintner's (97) equation 4.30.

ii) By Angelo et al (88)

$$K_{o.o} = k_{d.o}\ \frac{1}{1 + m\left(\frac{D_d}{D_c}\right)^{0.5}} \qquad (4.37)$$

where $k_{d.o}$ is the dispersed phase mass transfer coefficient calculated by Angelo's (88) equation (4.33). Results of the oscillating drop coefficients calculated by both methods are listed in Table 8.6. This method of calculation was used to calculate $(K_{cal})_a$ as well as $(K_{cal})_v$ using the relevant drop size distribution diagram.

Where $P_o = 1 - P_c$ (8.17)

and $a_o = 1 - a_c$ (8.18)

Table 8.6. Theoretical Mass Transfer Coefficients of Oscillating Drops

Run No	$k_{d.o}$ (I) (cm/s)	$k_{c.o}$ (cm/s)	$K_{o.o}$ (I) (cm/s)	$k_{d.o}$ (II) (cm/s)	$K_{o.o}$ (II) (cm/s)	P_o (%)
1	1.4×10^{-3}	1.9×10^{-3}	1.7×10^{-4}	4.5×10^{-3}	4.7×10^{-4}	0.35
2	1.53×10^{-3}	1.5×10^{-3}	1.8×10^{-4}	4.3×10^{-3}	4.6×10^{-4}	0.2
3	1.3×10^{-3}	3.4×10^{-3}	1.7×10^{-4}	3.2×10^{-3}	3.9×10^{-4}	0.995
4	1.7×10^{-3}	2.3×10^{-3}	2.1×10^{-4}	5.3×10^{-3}	5.5×10^{-4}	0.71
5	$1.5 \times 10_{-3}$	2×10^{-3}	1.9×10^{-4}	4.5×10^{-3}	4.7×10^{-4}	0.915
6	1.28×10^{-3}	1.12×10^{-3}	1.52×10^{-4}	4.25×10^{-3}	4.8×10^{-4}	0.04
7	1.4×10^{-3}	1.6×10^{-3}	1.7×10^{-4}	4.3×10^{-3}	4.3×10^{-4}	0.58
8	1.5×10^{-3}	1.4×10^{-3}	1.6×10^{-4}	5×10^{-3}	4.6×10^{-4}	0.15
9	1.48×10^{-3}	1.37×10^{-3}	1.8×10^{-4}	3.8×10^{-3}	5.4×10^{-4}	0.64
10	1.3×10^{-3}	2.6×10^{-3}	1.65×10^{-4}	3.4×10^{-3}	3.9×10^{-4}	0.954
11	1.4×10^{-3}	2.3×10^{-3}	1.8×10^{-4}	4.1×10^{-3}	4.5×10^{-4}	0.1
12	1.3×10^{-3}	1.2×10^{-3}	1.6×10^{-4}	3.8×10^{-3}	3.6×10^{-4}	0.16
13	1.25×10^{-3}	1.3×10^{-3}	1.5×10^{-4}	3.4×10^{-3}	3.8×10^{-4}	0.27
14	1.2×10^{-3}	1.3×10^{-3}	1.4×10^{-4}	3.3×10^{-3}	3.5×10^{-4}	0.4

I Based on Equation (4.30)

II Based on Equation (4.33)

Two values of $(K_{cal})_v$ as well as $(K_{cal})_a$ were obtained from each run. These corresponded with the two values of $K_{o.o}$, the first based on Rose and Kintner (97) and Garner et al's (114) correlations, and the second based on Angelo et al's (88) correlation. The K_{cal} values together with the experimental values are presented in Table 8.7. A sample calculation is given in Appendix 5.ii.

8.2.3. Axial Mixing

Quantitative studies of continuous phase back mixing for column design purposes or for evaluation of column efficiency, have generally been carried out with single phase flow based on values from some form of stimulus-response technique involving introduction of a tracer and measurement of the response rather than measurement of concentration profile under operating conditions as used in this study. This technique has the great advantage of being applicable to full-scale industrial installations without requiring any disruption of production or possible introduction of impurities making it ideal for evaluation of the performance of existing plant (229).

Treatment of Results

The experimental data related only to continuous phase samples. Therefore the theory, given in Chapter 6, must be extended in order to evaluate E_x and E_y.

A mass balance over the lower section of column of height z, Figure 8.13, yields,

$$L_F x_F - V_E y_E = L\left[x - \frac{E_x}{L}\frac{dx}{dz}\right] - V\left[y + \frac{E_y}{V}\frac{dy}{dz}\right] \qquad (6.33)$$

where L,V are flowrates of the dispersed and continuous phases respectively per unit of column cross-section (cm/s).

Table 8.7. Comparison Between K_{exp} and K_{cal} using (i) a Volume Basis and (ii) an Area Basis.

Run No	K_{exp} x 10^{-4} (cm/s)	Rose & Kintner		Angelo et al	
		Volume	Area	Volume	Area
		$(K_{cal})^{I}_{v}$ x 10^{-4} (cm/s)	$(K_{cal})^{I}_{a}$ x 10^{-4} (cm/s)	$(K_{cal})^{II}_{v}$ x 10^{-4} (cm/s)	$(K_{cal})^{II}_{a}$ x 10^{-4} (cm/s)
1	1.6	0.6	0.4	1.7	1.2
2	1.5	0.5	0.4	1.2	1
3	3.8	1.7	1.7	4.7	4.6
4	2.1	1.5	1.2	3.9	3.1
5	4.3	1.7	1.6	4.3	4.0
6	1.6	0.07	0.04	0.2	0.1
7	1.3	1.0	0.6	2.6	1.6
8	1.0	0.27	0.1	0.7	0.4
9	2.8	1.15	0.94	3.5	3.1
10	1.1	1.5	1.4	3.7	3.5
11	1.7	0.19	0.22	0.46	0.54
12	1.2	0.2	0.13	0.4	0.3
13	1.4	0.4	0.29	1.0	0.65
14	1.9	0.6	0.4	1.4	1.1

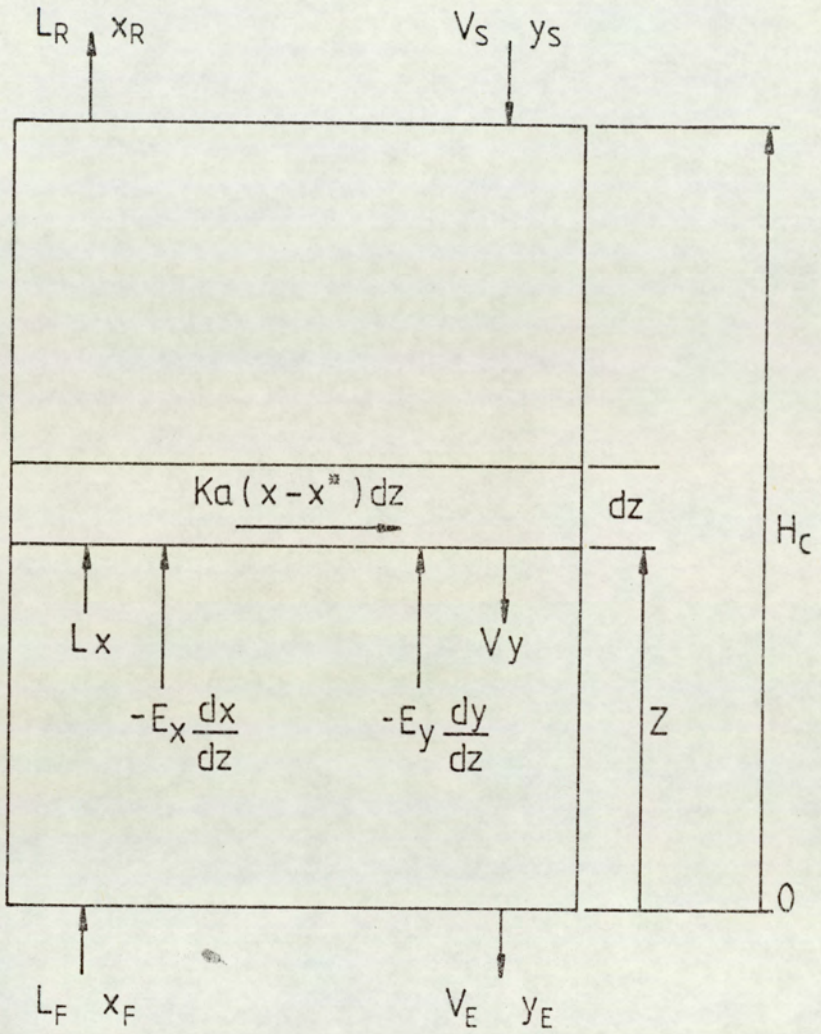

Figure 8·13 Basis for Axial Mixing Calculations.

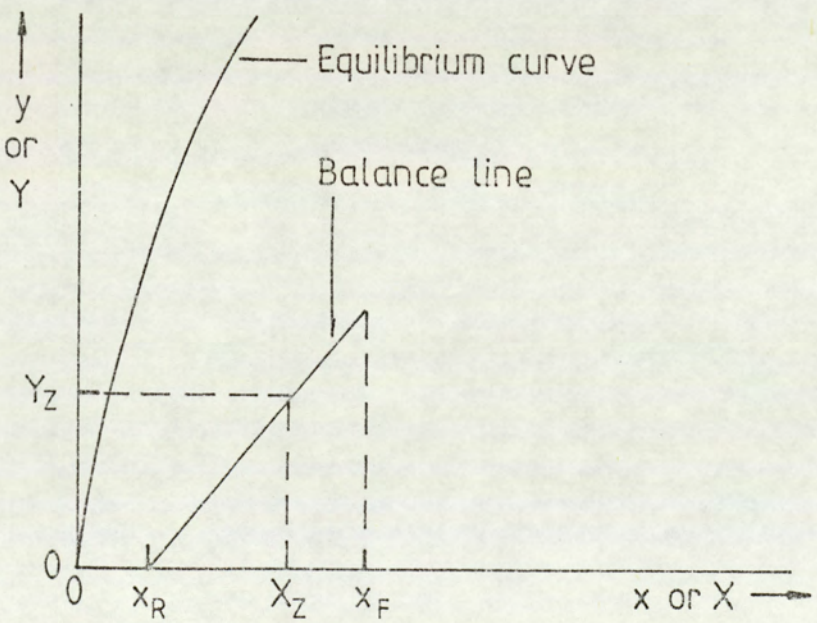

Figure 8·14 Distribution diagram.

Let $$X = x - \frac{E_x}{L}\frac{dx}{dz} \qquad (6.34)$$

and $$Y = y + \frac{E_y}{V}\frac{dy}{dz} \qquad (6.35)$$

When $E_x = E_y = 0$, X and Y are 'plug flow' compositions. From analysis of samples of continuous phase withdrawn at points 1, 3, 5, 7, 9 and 11 from the column base during steady-state operation, y is known along the length of the column. The 'plug flow' gradients can be evaluated from the slope of the plug flow operating line (balance line). The coordinates of the balance line can be obtained by the following procedure. Since, as shown in Figure 8.15, the Clairsol and water were for all practical purposes completely immiscible within the experimental range studied L and V at any plane in the column can be estimated.

$$L \cong \frac{L_F + L_R}{2} = L_F \cong L_R \text{ and } V = \frac{V_S + V_E}{2} \cong V_E \cong V_S$$

Then at any plane z, X_z and Y_z can be obtained from the distribution diagram as shown in Figure 8.14.

Then $$Y_z = y_z + \frac{E_y}{V}\frac{dy}{dz} \qquad (8.19a)$$

in Equation 6.35, Y_z, y_z, V are known and $\left.\frac{dy}{dz}\right|_z$ can be estimated from the distribution diagram so that E_y can be evaluated:

$$E_y = \frac{(Y_z - y_z)\,V_s}{\left.\frac{dy}{dz}\right|_z} \qquad (8.19b)$$

Figure 8.15 Solubility and Equilibrium Data for Clairsol-Acetone-Water

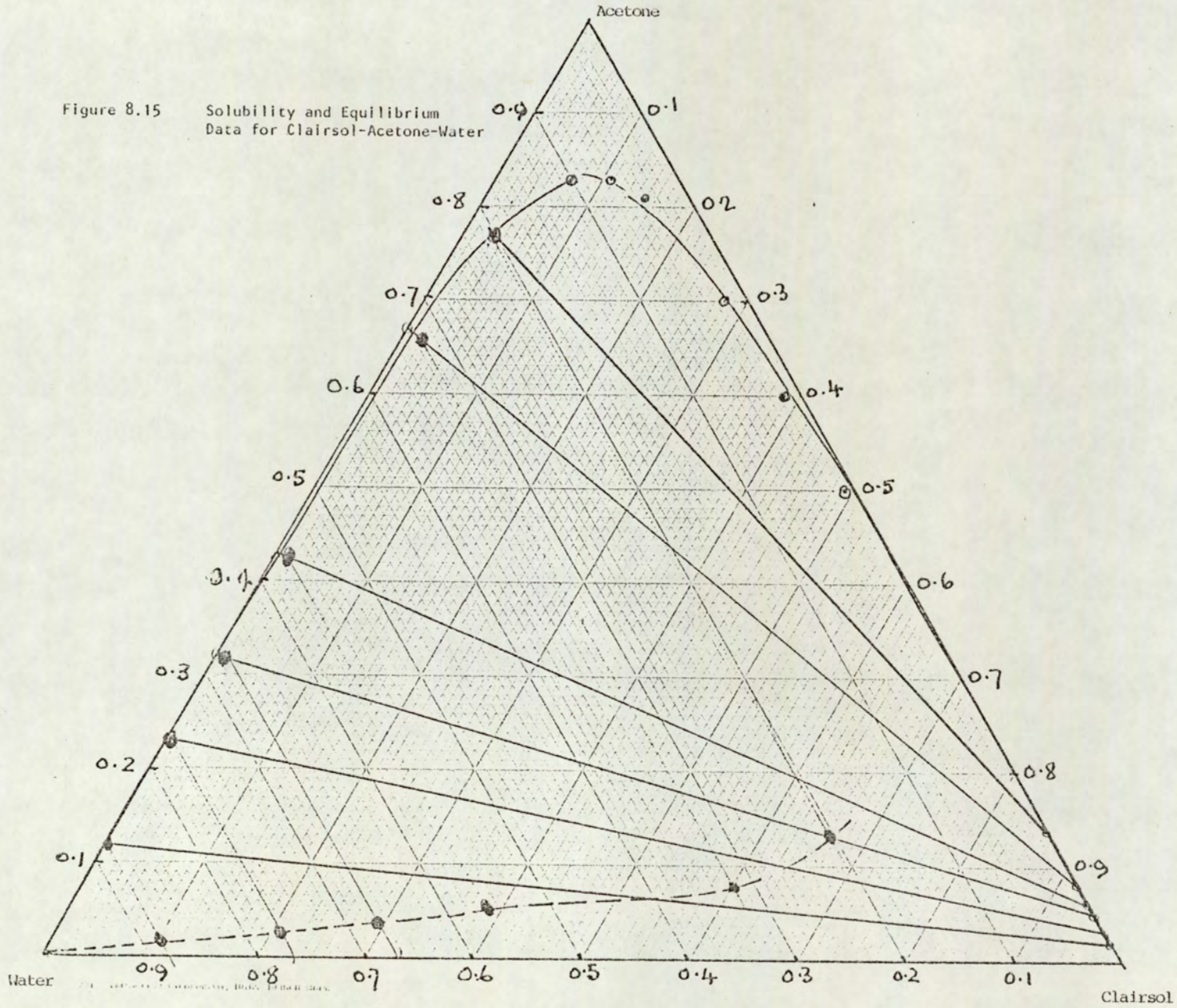

Furthermore

$$\frac{dX}{dz} = -\frac{Ka'}{L'}(x - x^*) \qquad (8.19c)$$

$\frac{dX}{dz}$ can be obtained from the slope of the balance line with respect to z

K can be obtained from drop characteristics (in this case based upon Δy,

using the method given in Section 8.2.1 it can be converted via m) cm/s.

a' the interfacial area per unit of column height (cm^2/cm) can be obtained from the drop size and hold-up.

L' volumetric flowrate of the dispersed phase (cm^3/s).

x* can be obtained from the equilibrium curve and hence x can be evaluated from Equation 8.19c. Then it follows that

$$E_x = \frac{L'(X - x)}{dx/dz}\Bigg|_z \qquad (8.19d)$$

Results

The plots of experimental data for runs 1-6 and 9-12 showed that ,within the limits of experimental error, the balance lines coincided with the experimentally-determined operating curves obtained from the values of x estimated by the procedure described in Section 8.2.3 from the experimentally determined y value. Thus there are only small back mixing effects under these operating conditions. In runs 7, 8, 13 and 14 the operating curve was estimated to be above the balance line and the results were therefore analysed by the procedure described.

A typical calculation based on Run 7 is included in Appendix 6A and the calculated E_y and E_x values for Runs 7, 8, 13 and 14 are summarised in Table 8.8a.

For completeness a specimen calculation for the estimation of E_y and E_x in Run 5, showing that they both approximate to zero, is also included in Appendix 6b. E_y for Run 8 was slightly larger than for Run 7; this is explained by the higher rotor speed, ie 300 rpm compared with 200 rpm, with the same values of V_c and V_d. E_y's for Run 13 and 14 were much larger than in earlier runs due to these being at the maximum practical operating V_c and V_d values.

Whilst E_y's represent average values over the column height, it can be seen from Table 8.8a that there were maxima corresponding to the middle of the column. If continuous phase back mixing is caused predominantly by entrainment by droplets then this would be expected, since hold-up's reach a maximum near the middle of the column. E_x approximated to zero in all cases indicating that , with the column geometry and rotor speeds studied here, droplets were not significantly back mixed prior to flooding.

Table 8.8a Calculated Back Mixing Coefficients

Sample Point Number	E_y (Run 7) (cm^2/s)	E_y (Run 8) (cm^2/s)	E_y (Run 13) (cm^2/s)	E_y (Run 14) (cm^2/s)
11	3.9	9.08	9.1	8.4
9	5.7	9.5	30.5	20.2
7	9.3	10.2	24.2	23.5
5	12.4	10.0	17	33.6
3	1.5	9.3	16.3	28
1	0	7.8	14.5	14

Comparison of the experimental E_y and E_x values and those predicted from the literature for small columns showed that the values were of similar order, Table 8.8b. With other column designs, involving larger stator openings, finite E_x values would be expected.

Table 8.8b Predicted axial mixing coefficient E_c values under experimental conditions and Experimental E_{exp} values.

Run No.	V_c (cm/s)	rpm	E_c (cm^2/s)	E_{exp} (cm^2/s)
1	0.3145	200	4.86	0
2	0.3145	300	5.52	0
3	0.3145	200	4.86	0
4	0.3145	300	5.52	0
5	0.2	200	3.57	0
6	0.2	200	4.23	0
7	0.3145	200	4.86	6.6
8	0.3145	300	5.52	9.3
9	0.3145	300	5.52	0
10	0.16	300	3.78	0
11	0.615	300	8.9	0
12	0.75	300	10.42	0
13	0.8	300	10.98	18.6
14	0.84	300	11.43	21.3

8.2.4. Comparison of Experimental and Theoretical Mass Transfer Coefficient

8.2.4.1. Effect of Operating Variables

Over the range of variables studied, the experimental mass transfer coefficient decreased with increase in rotor speed at any fixed combination of initial solute concentration and flow rates - Table 8.2. On the other hand the rate of mass transfer increased with rotor speed - Table 8.3. This arose because the higher rotor speed resulted in relatively small oscillating drops which possessed an increased interfacial area resulting in a larger rate of mass transfer compared with the oscillating drops generated by lower rotor speed. The calculated interfacial area was found to increase rapidly as rotor speed increased ie. from 24% to 68.5% for rotor speeds between 200 and 300 rpm. The rate of mass transfer increased with increase in either phase flow rate. For example Runs 5 and 6 with relatively low flow rates produced the lowest rate of mass transfer compared with other runs (Table 8.3).

Hold-up in the absence of mass transfer was considerably higher than with mass transfer. The reason for this, as described in Section 8.1.2, was the enhanced coalescence with mass transfer resulting in larger drops with higher mean rise velocities. Therefore uncorrected hold-up values obtained under non mass transfer conditions should not be used to predict practical values during mass transfer from dispersed to continuous phase.

From Table 8.4 the trend is clearly for slip velocity V_s to decrease with increase in rotor speed. This is due to the increase in energy expended on drop-breakup, with increased speed resulting in smaller drops with reduced terminal velocities. The experimental overall mass transfer coefficient decreased with increase in combined phases flowrates eg. capacity Table 8.9.

Table 8.9 Experimental Mass Transfer Coefficients and Column Capacity

Run No.	R.p.m.	$V_c + V_d$ (cm/s)	K_{exp} x 10^{-4} (cm/s)
6	300	3.5	1.6
2	300	5.65	1.5
10	300	7.9	1.1
5	200	3.5	4.3
1	200	5.65	1.6

Direct comparison of these results with those of Al-Aswad is not possible because of different V_c and V_d values however in general they were between 3% and 51% greater than in the study of Al-Aswad (99) as shown in Table 8.10. Part of the difference may be accounted for by the use of de-ionised water as the continuous phase in the present work rather than Birmingham mains water, since the dissolved

ions and contaminants (eg. surfactants) in tap water would be expected to inhibit mass transfer.

Table 8.10 Comparison of volumetric overall mass transfer coefficients.
(nb. Direct comparison is not possible due to differing V_c, V_d values)

		x_{in}		Ka (s^{-1})	
Run No.	rpm	This Work x 10^{-2}	Previous Work x 10^{-2}	This Work x 10^{-4}	Previous Work x 10^{-4}
1	200	3.3	3.03	1.1	0.625
2	300	3.3	3.03	1.4	0.683
3	200	2.0	3.96	1	0.87
4	300	2.0	3.96	1.5	0.87
7	200	2.6	4.91	0.8	0.79
8	300	2.6	4.91	0.96	0.93

8.2.4.2. Comparison Between the Experimental and Theoretical Mass Transfer Coefficient

All results are summarised in Table 8.7. Specimen calculations are included in Appendix 5. The comparison between K_{exp} and the various theoretical overall coefficients is shown in Table 8.11.

A wide divergency was found between the experimental mass transfer coefficient K_{exp} and either $(K_{cal})_a$ or $(K_{cal})_v$ particularly at high flowrates of both phases. The explanation for the higher experimental mass transfer coefficients compared with the calculated mass transfer coefficients is that a large proportion of the drop swarm considered to fall within the range of circulating drops would, in reality, be oscillating

Table 8.11 Comparison Between Experimental and Theoretical Mass Transfer Coefficients

Run No	K_{exp} x 10^{-4} (cm/s)	$K_{exp}/(K_{cal})^{I}_{v}$	$K_{exp}/(K_{cal})^{I}_{a}$	$K_{exp}/(K_{o.o})^{I}$	$K_{exp}/(K_{cal})^{II}_{v}$	$K_{exp}/(K_{cal})^{II}_{a}$
1	1.6	2.6	4	0.92	0.9	1.3
2	1.5	3	3.75	1.22	1.25	1.5
3	3.9	2.3	2.3	0.44	0.83	0.84
4	2.1	1.4	1.75	1.0	0.54	0.7
5	4.3	2.5	2.6	0.43	1.0	1.1
6	1.6	23.15	40.3	1.05	7.96	15.2
7	1.3	1.3	2.1	1.3	0.5	0.8
8	1	3.7	10	1.79	1.4	2.5
9	2.8	11.6	7	0.64	1.75	2.5
10	1.1	0.7	0.8	1.54	0.3	0.3
11	1.7	8.9	7.7	1.04	3.7	3.1
12	1.2	6	9.2	1.48	3	4
13	1.45	3.5	5	0.97	1.45	2.2
14	1.9	3.1	4.7	0.76	1.3	1.7

due to,

a) Drop interaction, ie. the inducement of oscillation in one drop due to others,

and more particularly,

b) The drop velocity being much higher locally in the region of the discs, rather than the slip velocity used in calculating K_{cal}.

Generally the predicted mass transfer coefficients are based on single drops of liquid under conditions such that they neither collide nor coalesce and when the stream lines around individual drops are not disturbed. This is not analogous to the conditions in a large-scale, agitated extractor with relatively high hold-ups.

The biggest deviation between experimental and calculated overall mass transfer coefficients was, as expected, with those runs with high hold-ups, since conditions were furthest from the single drop situation. Conditions in these runs (11 to 14) resulted in a high theoretical circulating drop fraction but a long residence time in the column, and hence a higher volumetric mass transfer coefficient.

The analysis given in 8.2.2 with the individual drop coefficients related to their respective fraction, gives the best practical method of calculation of the overall mass transfer coefficient. However, even allowing that the mechanism does not involve coalescence and redispersion (111), with the RDC there is a fundamental weakness in predicting individual drop film coefficients, k_c or k_d, based upon Reynolds numbers with the slip velocity representing the velocity. In the turbulence, drops move at a range of velocities for limited periods and it is these local velocities which determine short-term drop behaviour (51). For example the maximum velocity a drop could ever attain is the disc tip velocity, which is much higher than the assumed slip velocity.

A theoretical analysis of mass transfer coefficient predictions which account for both drop size and local drop velocity distributions would be extremely complex taking into account the probability of drops of different sizes travelling at different local velocities for different periods, any effects due to interdrop reactions would still require consideration. The approach to be adopted may make use of the fact that drop local velocity is a resultant of the three velocity components axial (w), radial (u) and circumferential ϕ which are expressed as:

$$u = r\omega F(\zeta)$$

$$v = r\omega G(\zeta)$$

$$\text{and } w = \sqrt{r\omega}\, H(\zeta)$$

By means of these equations and Cochrans (228) data functions F, G and H can be evaluated and the value of the resultant velocity across a drop can be found for any location beneath the disc (51). The local velocity is proportional to the effective radius from the disc. The velocity component w, normal to the disc is small (of the order of $\sqrt{r\omega}$) and can be neglected. Since the motion of drops beneath the disc tends to involve acceleration until the tip is reached followed by deceleration (51) as a first approximation the average drop velocity can be taken as $V = 0.5\ V_T$. The effect which this higher assumed mean drop velocity has on k_c was therefore evaluated and the corresponding calculated K values are given in Table 8.12.

The data in Table 8.12 shows that although the overall mass transfer coefficient K based on $V = 0.5\ V_T$ is somewhat larger it still does not approach K_{exp}. The explanation for this is that k_d is the controlling coefficient (by comparison $k_c \cong 10^{-3}$, $k_d \cong 10^{-6}$). Hence a better prediction of K requires a better correlation for k_d which takes account of Re and the increased tendency to oscillation due to the effect of

Table 8.12. Comparison of Mass Transfer Coefficients

Run No	K $V = V_S$ (cm/s) x 10^{-4}	K $V = 0.5V_T$ (cm/s) x 10^{-4}	K_{exp} (cm/s) x 10^{-4}
1	0.6	0.67	1.6
2	0.5	0.53	1.5
3	1.7	1.8	3.8
4	1.5	1.6	2.1
5	1.7	1.9	4.3
6	0.07	0.07	1.6
7	1.0	1.1	1.3
8	0.27	0.32	1.0
9	1.15	1.3	2.8
10	1.5	1.7	1.1
11	0.19	0.2	1.7
12	0.2	0.3	1.2
13	0.4	0.5	1.4
14	0.6	0.65	1.9

neighbouring drops.

In summary whereas some proportion of the drops in an RDC would, on the basis of Reynold's number predicted using the slip velocity V_S, not be oscillating (or indeed with different systems and drop size distributions even be stagnant) the position in practice is more favourable. If the drops do not break up (which would be reflected in the diameter) the effect of agitation in causing drops to distort and oscillate, is not reflected in single drop correlations based upon Reynold's values predicted using V_S. Therefore it is to be expected that, as in Table 8.7, experimental overall mass transfer coefficient (K_{exp})values would be significantly greater than those predicted by the method in section 8.2.2.

It follows that, provided an efficient distributor is used, operation of an RDC with a rotor speed less than that causing any break-up of drops will be more efficient than a comparable plate-column.

8.2.5 Basis for Preferring Volume Fractions or Area Fractions

In any extractor in which all the drops are not oscillating the reason for preferring a volume basis can be explained as follows. The calculated overall mass transfer coefficient for an extraction on an incremental area basis is:

$$(K_{cal})_a = a_s . K_s . + a_c K_c + a_o K_o \qquad (8.15)$$

where a_s, a_c, a_o are the interfacial area fractions of drops in the stagnant, circulating and oscillating drop regimes respectively and K_s, K_c, K_o are the overall mass transfer coefficients corresponding to each regime.

Examination of mass transfer coefficients shows that in all the experimental runs in this work d > 0.2cm and hence Re > 50 so that only the circulating and oscillating drop fractions need be considered.

The area fractions of both regimes are:

$$a_c = \frac{6 P_c}{d_c} \tag{8.19}$$

$$a_o = \frac{6 P_o}{d_o} \tag{8.20}$$

The average drop diameter for the circulating regime is approximately half the average drop diameter in the oscillating regime.

$$a_o = \frac{6 P_o}{d_o} = \frac{6 P_o}{2 d_c} \tag{8.21}$$

Division of Equation 8.19 by Equation 8.21 gives;

$$\frac{a_c}{a_o} = \frac{6 P_c/d_c}{3 P_o/d_c} = \frac{2 P_c}{P_o} \tag{8.22}$$

The rate of mass transfer corresponding to each regime is:

$$N_{Ac} = K_c \cdot a_c \cdot (\Delta c)_c \tag{8.23}$$

$$N_{Ao} = K_o \cdot a_o \cdot (\Delta c)_o \tag{8.24}$$

From earlier studies the mass transfer coefficient of an oscillating drop is of the order of five-fold greater than that of a circulating drop,

$$K_o \sim 5\,K_c \tag{8.25}$$

The ratio of the rates of mass transfer to, or from, the circulating as well as the oscillating drops is:

$$\frac{N_c}{N_o} = \frac{K_c.\,a_c.\,(\Delta c)_c}{5\,K_c.\,a_o.\,(\Delta c)_o} = \frac{2}{5}\left[\frac{P_c}{P_o}\right]\left[\frac{\Delta C_c}{\Delta C_o}\right]$$

$$= \frac{P_c}{P_o}\left[\frac{2\,\Delta C_c}{5\,\Delta C_o}\right] \tag{8.26}$$

It is not possible to estimate the ratio of the driving forces; hence it is preferable to base the mass transfer fractions on volume fractions rather than area fractions.

The data in Table 8.7 shows that mass transfer coefficients based upon an area basis and on a volume basis are, for all practical purposes, indistinguishable, thus substantiating the assumption proposed by Al-Aswad et al (232).

However in the situation where very many small, theoretically stagnant drops may be present and the turbulence does not cause them to oscillate (eg. a low interfacial tension system subjected to only moderate turbulence) the area fraction would be preferable.

8.3. ALLOWANCE FOR PRACTICALITIES OF COLUMN PERFORMANCE IN DESIGN

Volumetric capacity is obviously one important feature of RDC performance. It is normally expressed as the sum of the superficial velocities of the two phases. The maximum liquid loading above which flooding will occur appears to be satisfactorily correlated by means of Equations 5.7 and 5.9.

Except as it appeared under the range of operating conditions in this work, compared with Al-Aswad (99), the use of the Sauter mean drop size instead of the drop size distribution may be unrealistic, in view of the possible different mass transfer mechanisms, and lead to a significant error. (Results based on mean drop size in this work show considerable deviations from experimental data.) Therefore it is recommended that predicted distribution data based on Mugele-Evans Upper Limit Distribution should be used predicted from d_{32} correlations.

Wettability of column internals has a very pronounced effect on column performance. It is generally accepted that the best efficiency of mass transfer is obtained when the continuous phase wets the internals. Otherwise there is increased coalescence of the dispersed phase on the glass or metal column internals. Although it appears from Al-Hemiri's (33) work on a 10cm diameter RDC with stainless steel stators, that rotor wettability has no appreciable effect on mass transfer efficiency, the possibility remains of higher mass transfer rates due to coalescence and redispersion phenomena in wetted disc columns, since in the system used by Al-Hemiri the controlling resistance to mass transfer was in the continuous phase. Wetting in an RDC affects the break-up mechanism, thus affecting both volumetric capacity and efficiency; in fact the large coalesced drops in a wetted disc column tends to give an improved volumetric capacity (33).

The column geometry for an RDC can be based in the range shown below depending on whether a high volumetric capacity or the most efficient mass transfer is required.

RDC - Internal Components	High Volumetric Capacity Lowest Mass Transfer Efficiency	Lowest Volumetric Capacity Highest Mass Transfer Efficiency
R/D	0.5	0.66
H/D	0.5	0.33
S/D	0.75	0.66

Clearly the column used in this work was in the first category where the ratio R/D was at the lower end of the optimum range, the ratio of H/D was at the upper end of the optimum range, and the ratio of S/D at the upper end of the optimum range.

In cases where phase separation limits volumetric capacity the type of external settler used in this work eliminated any heavy phase carry-over at flooding or at high flow rate. It also aided visualisation or control of the interface level.

Apart from external settlers, for which a wide range of designs are available (8), knitted mesh packings are probably the most convenient coalescing aids. Their use with primary dispersions was studied by Thomas and Mumford (230), who confirmed that for maximum efficiency, the coalescer material should be preferentially wetted by the dispersed phase. Further design recommendations are referred to in the literature (231).

9. CONCLUSIONS AND RECOMMENDATIONS FOR FURTHER WORK

9.1 CONCLUSIONS

1. Operation of an RDC at relatively high flowrates, ie. at 80% of flooding, results in increased hold-ups and is associated with higher volumetric overall mass transfer coefficients $(Ka)_{exp}$. Hence the RDC column is most efficient when operated near its maximum volumetric capacity. The phenomenon of flooding, rather than phase inversion, was the best criteria for defining limiting capacity. Hold-up at flooding could be predicted from Logsdail's flooding equation (5.12), but values were between 15% and 26% less than the experimental ones.

Increasing rotor speed resulted in an increase in overall mass transfer coefficient (Ka).

2. Drop size, drop distribution and hold-up were all different under conditions of mass transfer from the dispersed to continuous phase compared with non-mass transfer conditions. For example compared with non-mass transfer conditions d_{32} was approximately 22.8% greater and hold-up was 57% less. Therefore data obtained under non-mass transfer conditions should be applied with caution in extractor design when transfer is from the dispersed to continuous phase. Drop size distributions were measured experimentally and the best fit of all data (in the presence or absence of mass transfer) was given by Mugele-Evans' Upper Limit compared to the Log-Normal distribution.

3. In the calculation of mass transfer performance use of a mean concentration driving force, calculated by Simpson's Rule, gave a more precise overall mass transfer

coefficient, than use of a log-mean driving force.

Drop size distribution should normally be included in calculations of theoretical mass transfer coefficients, as outlined in 8.1.4, since this gives more reliable results compared with the assumption of mass transfer based on a mean drop size.

4. With the particular system and range of operating parameters (N = 200 to 300 rpm, V_c = 1.6cm/s to 8.4cm/s, V_d = 1.5cm/s to 6.3cm/s, acetone concentration 1.1 x 10^{-2} w/w to 4 x 10^{-2} w/w) covered in this study the calculated overall mass transfer coefficients for oscillating drops based on Equation 1.3 produced the closest fit to the experimental overall mass transfer coefficients. Hence using the oscillating single drops calculation as in section 8.2.2 will probably be more reliable for calculation and design of large agitated columns. This is in agreement with Gasmelseed's (227) recent observations on a small-scale Scheibel column for extraction with the system water-acetic acid-n-butanol-n hexane with stage efficiencies between 60%-70%. However with the system used in the present study K_{exp} exceeded K predicted using the Rose and Kintner correlations for oscillating drops.

Because all the drops apparently oscillated the novel method used to calculate overall mass transfer coefficient on an area basis $(K_{cal})_a$, (ie. the relative contribution from different drop regime fractions on an area basis) or on a volume basis, $(K_{cal})_v$ was not properly tested and similar results were obtained in both cases. However this approach is likely to be appropriate for other extractor types eg. spray columns, or packed columns in which circulating or stagnant drops may be present the Rose and Kintner correlations for usual oscillating drops which gave a closer approximation than those of Angelo et al.

5. Generally above an rpm of 100 the mean drop size decreased with column height, eg. by approximately 45% over the effective height. Hence the selection of a 'typical' compartment for drop-size prediction during design could introduce significant errors. A check should therefore be made, as in this work, with eg. the highest and lowest d_{32} values.

6. The new procedure for the calculation of axial mixing coefficients E_x and E_y, based on continuous phase concentrations determined along the column height, outlined in section 8.2.3 appears promising for analysis of axial mixing characteristics in real situations, ie in the presence of dispersed phase. The results showed that, under the conditions of operation used, there was negligible dispersed phase back-mixing ie $E_x \rightarrow 0$. The levels of continuous phase back-mixing were relatively small but comparable with those predicted from published correlations.

7. At relatively high rotor speed (>300 rpm) very small drops were observed rotating around the bottom distributor. This has not been reported previously. With the system Clairsol-350 and de-ionised water, it was probably, due to Clairsol drops breaking up into small drops which were subjected to back mixing bringing them into the lower compartment. After a period of time such small drops would be carried-over with the continuous phase to form a haze (secondary dispersion) within the continuous phase.

9.2 RECOMMENDATIONS FOR FURTHER WORK

1. To study hydrodynamics and mass transfer in the existing column with the same organic phase as the continuous phase, and with the aqueous phase dispersed. (The drop size distributions and hold-ups in this case should approximate more closely to non-mass transfer conditions.)

2. Phase flowrates have a significant effect upon experimental mass transfer coefficients but, with the system studied, a negligible effect regarding K_{cal}. Therefore existing correlations should be modified, based on further results, to include phase flowrate variations. Such correlations would be more reliable for column design.

3. To investigate continuous phase axial mixing effects when solute transfer is from continuous to dispersed phase.

Alternatively by choosing a system of higher interfacial tension it would be possible to operate at rotor speeds > 300 rpm whilst still generating drops of similar size to those in this study ie. avoiding secondary haze formation.

Tracer injection studies are not recommended since (i) contaminants would alter the interfacial tension of the system and (ii) considerable expense would be involved in purification of the Clairsol.

APPENDICES

APPENDIX 1

ELGASTAT B224

SPECIFICATION

Dimensions	Height 1.095m
	Depth 0.225m
	Width 0.225m
Weight	23kg
Electrical Supply	240 Volts (50HZ single phase).

RAIN WATER SUPPLY

Cold potable water free of suspended solids. Maximum input pressure 4.5 bar (70 p.s.i.).

TYPICAL TREATED WATER ANALYSIS IN P.P.M. (mg/l)

Copper, lead, trace metals	0.0006
Iron	0.0005
Ammonia, sulphate	0.002
Chloride	0.015
Sodium	1.0
Silica	As influent
Free carbon dioxide	As influent
T.D.S.	5-10
pH	5.0-6.0
Electrical resistivity	50-15 µs (0.02-0.07 meg ohm cm)

FLOWRATE

Up to 360 litre per hour.

APPENDIX 2

SYSTEM PHYSICAL PROPERTIES

i) Clairsol-350 as the industrial grade with following properties:

Density	0.783 g/cm^3 at 20° C
Surface Tension	26.7 dynes/cm at 20°C
Interfacial Tension with De-ionised water	35.5 dynes/cm at 20°C
Kinematic Viscosity	2.3 cs at 20°C
Refractive Index	1.43920
Average Molecular Weight	160-170 g/g mole
Aromatic Content	0.1 (% w/w)
Flash Point	71°C
Boiling Range	205-230°C

ii) De-ionised Water

Density	0.9983 g/cm^3
Surface Tension	71.5 dynes/cm
Kinematic Viscosity	0.01 cs at 20°C
Refractive Index	1.3326

iii) Acetone-Analar

Density	0.789-0.791 g/cm^3 at 20°C
Boiling Range (95%)	56.0-56.5°C

CONTENTS OF APPENDIX 3

APPENDIX 3a

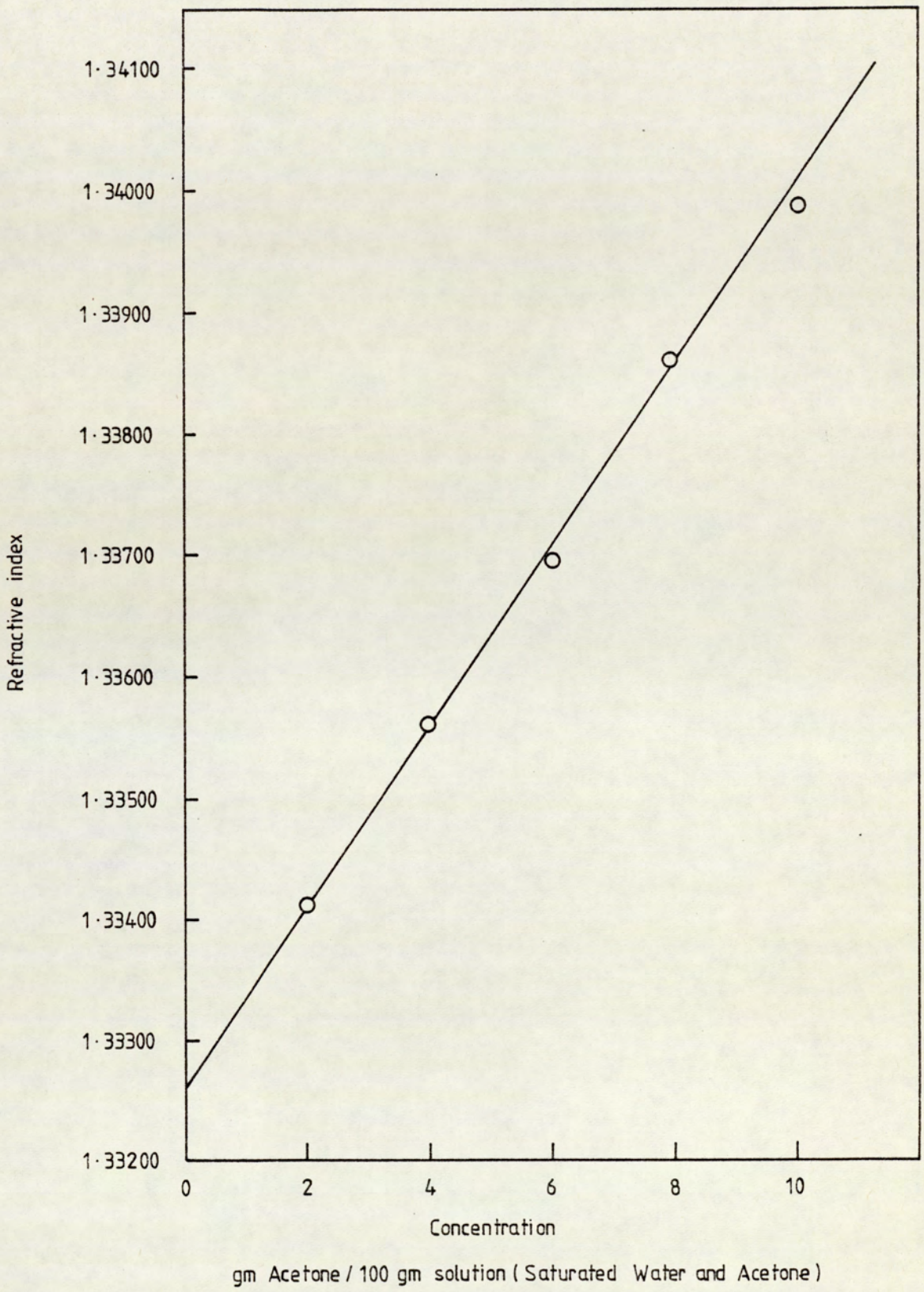

Figure I Calibration curve for Refractive index vs Weight percent Clairsol Saturated Water and Acetone at 20°C.

APPENDIX 3b

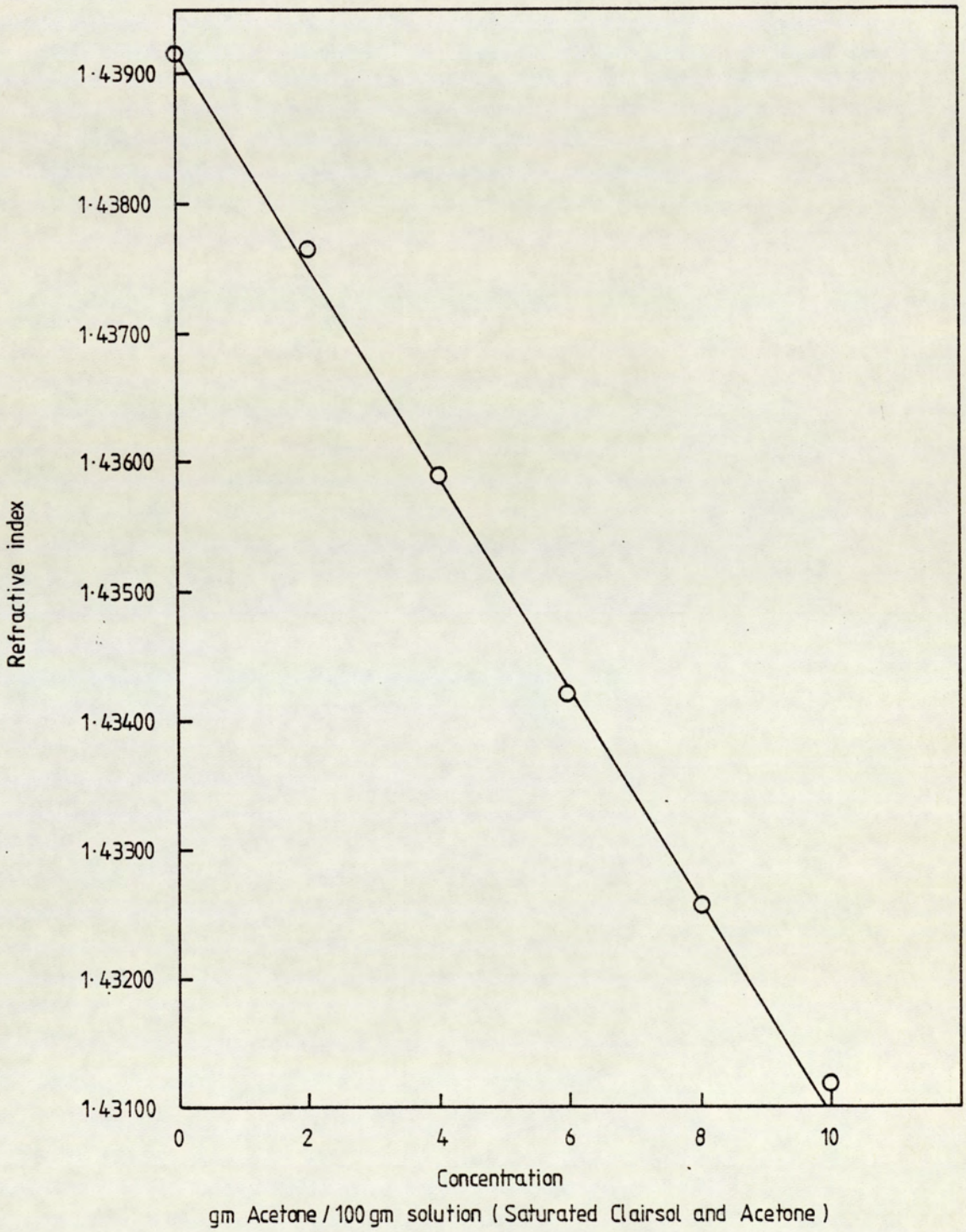

Figure II Calibration curve for Refractive index vs Weight percent Water Saturated Clairsol and Acetone at 20°C.

APPENDIX 3c

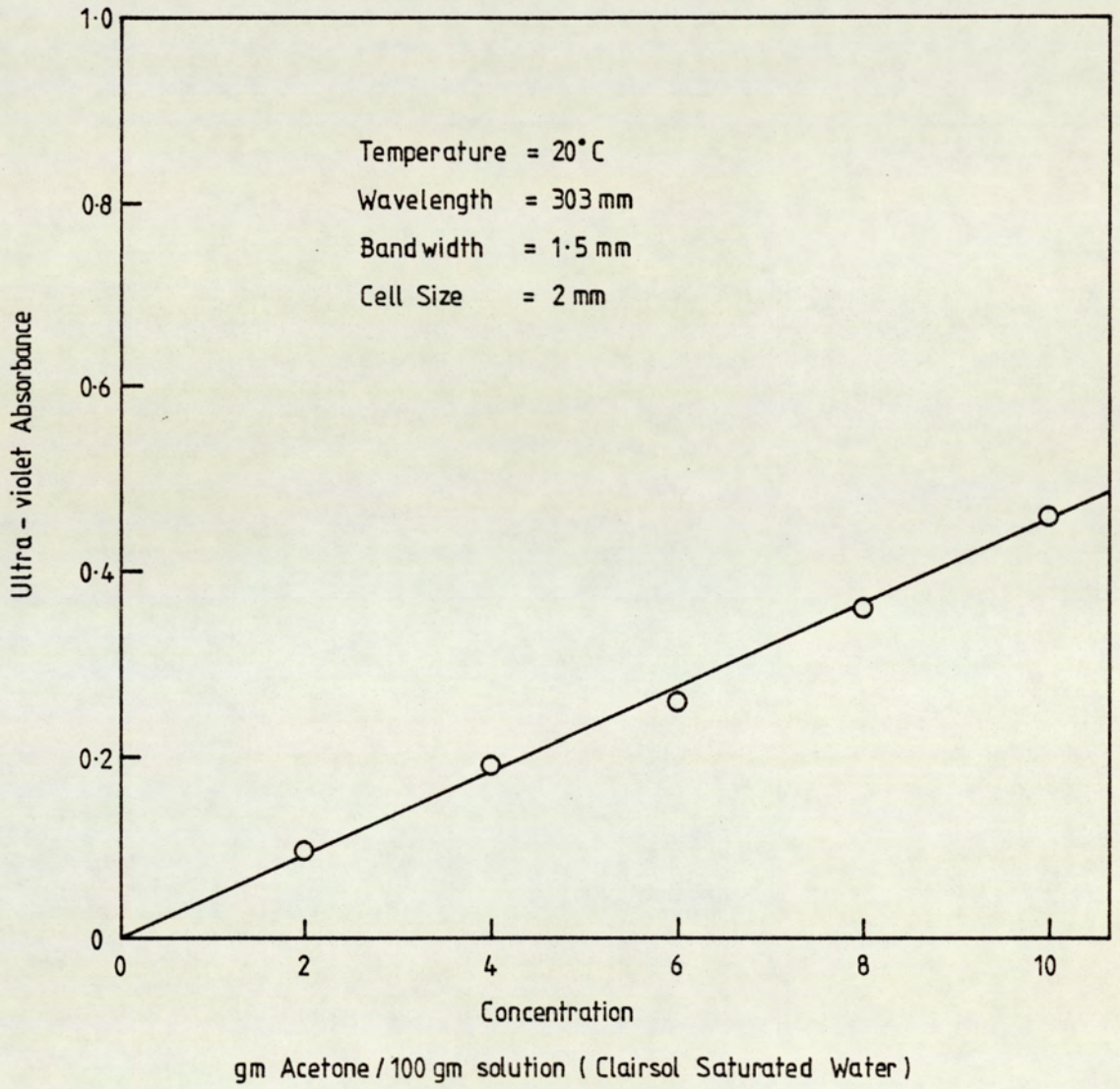

Figure III Calibration curve of Acetone in Clairsol Saturated Water vs. Ultra-violet Absorbance.

APPENDIX 3d

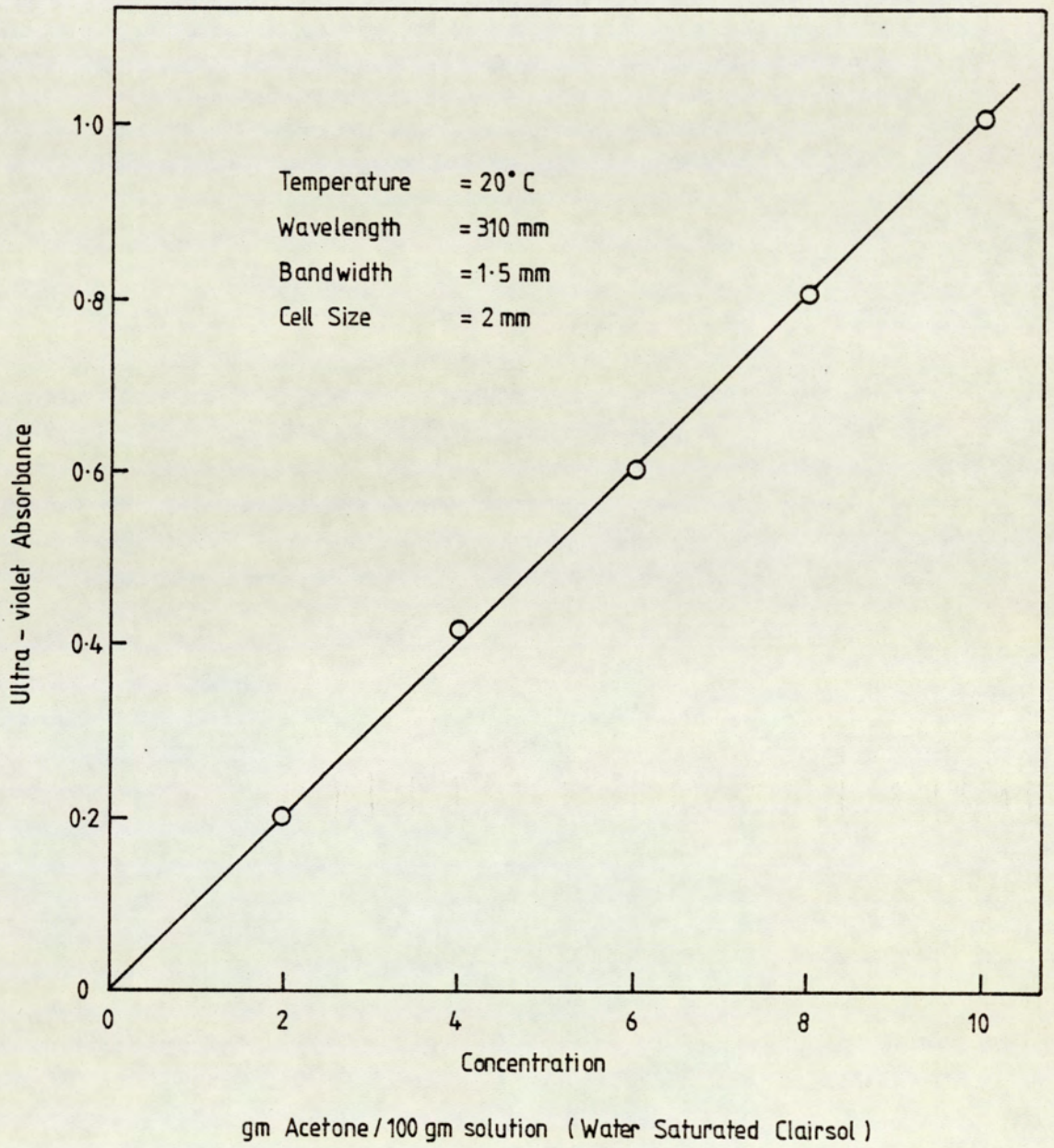

Figure IV Calibration curve of Acetone in Water Saturated Clairsol phase vs. Ultra - violet Absorbance.

APPENDIX 4

i) Sample Calculation of Drop Size d_{32} and Drop Size Distribution

(Basis Run No 9)

For: Compartment 6

Rotor Speed 300 rpm

Magnification 1.22

Hold-up 5.5%

i) Drop size count

$$d_{act} = \frac{d_{obs}}{\text{Magnification}}$$

$$d_{32} = \frac{\Sigma n_i d_i^3}{\Sigma n_i d_i^2} \qquad (8.5)$$

ii) Drop size distribution

Cumulative drop volume:

$$\upsilon_i = \Sigma ni \frac{\pi}{6} d_i^3 \qquad (8.3)$$

% cumulative drop volume:

$$\%\upsilon_i = \frac{\upsilon_i}{\upsilon \text{ total}} \times 100$$

$$\frac{d\upsilon}{dd} = \frac{\upsilon_{f,i} - \upsilon_{f,i-1}}{d_i - d_{i-1}}$$

where υ_f is the fractional cumulative drop volume

$$\upsilon_{f,i} = \frac{\upsilon_i}{\upsilon_{total}}$$

Table IV.a shows the drop size distribution results.

$$d_{32} = 4.6mm$$

The volumetric drop size distribution curve is shown in Figure V, from which the following are obtained:

at $\upsilon\% = 10$ $\quad d_{10} = 3.2mm$

$\upsilon\% = 50$ $\quad d_{50} = 4.8mm$

$\upsilon\% = 90$ $\quad d_{90} = 6.6mm$

$$\frac{d_m}{d_{50}} = \frac{d_{50}(d_{90} + d_{10}) - 2d_{90}d_{10}}{d_{50}^2 - d_{90}d_{10}} \qquad (3.24)$$

$$\frac{d_m}{4.8} = \frac{4.8\ (6.6 + 3.2) - 2 \times 6.6 \times 3.2}{(4.8)^2 - 6.6 \times 3.2}$$

$$d_m = 12mm$$

$$a' = \frac{d_m - d_{50}}{d_{50}} \qquad (3.22)$$

$$= \frac{12 - 4.8}{4.8}$$

$$= 1.5$$

$$\delta = \frac{0.907}{\ln \frac{d_{90}}{d_m - d_{90}} \cdot \frac{d_m - d_{50}}{d_{50}}} \qquad (3.23)$$

$$= \frac{0.907}{\ln \frac{6.6}{12 - 6.6} \times \frac{12 - 4.8}{4.8}}$$

$$= 1.49$$

d_{32_M} calculated from equation proposed by Mugele and Evans (70)

$$d_{32_M} = \frac{d_m}{1 + a' \cdot e^{0.25\ \delta^{-2}}} \qquad (8.6)$$

$$= \frac{12}{1 + 1.5 \times e^{0.25 \times 1.5^{-2}}}$$

$$= 4.5\text{mm}$$

which is in excellent agreement with d_{32}.

Table IV.a Drop Size Distribution Results (Volume - Basis)
N = 300 RPM (Run No 9)

d_{obs} (mm)	d_{act} (mm)	n	$n\,d_a^2$ $(mm)^2$	$n.\,\pi d_a^3$ $(mm)^2$	υ_v $(mm)^3$	υ_v %	$\frac{d\upsilon_v}{dd}$ (mm^{-1})
1.42	1.74	3	9.06	15.75	8.24	0 .028	
1.6	1.96	8	30.72	60.24	39.74	0.105	0.004
1.78	2.17	10	47.1	102.2	93.19	0.25	0.007
1.97	2.40	29	167.04	400.8	302.79	0.8	0.024
2.15	2.62	43	294.98	773.14	707.14	1.8	0.049
2.34	2.85	62	503.44	1435.3	1457.8	3.86	0.087
2.52	3.07	87	819.54	2516.9	2774.14	7.35	0.159
2.70	3.24	117	1265.94	4166.4	4953.15	13.13	0.263
2.89	3.53	117	1457.82	5146.8	7644.94	20.26	0.297
3.07	3.75	98	1251.34	4692.9	10099.4	26.77	0.296
3.26	3.98	95	1504.8	5988.8	13231.5	35.07	0.361
3.44	4.2	74	1305.36	5482.7	16098.9	42.67	0.345
3.62	4.42	59	1152.86	5094.7	18763.4	49.7	0.321
3.81	4.65	45	972.9	4524.3	21129.6	56	0.273
3.99	4.87	9	213.5	1039.5	21673.25	57.5	0.065
4.78	5.10	26	676.3	3448.9	23477.02	62.2	0.207
4.36	5.32	18	509.4	2710.3	24894.48	65.9	0.17
4.54	5.54	14	429.66	2380.4	26139.43	69.3	0.15
4.73	5.77	18	599.22	3457.8	27847.9	74.08	0.208
4.91	6.00	17	612.0	3672	29868.3	79.2	0.221
5.10	6.22	11	425.6	3647	31252.72	82.84	0.165
5.26	6.42	9	370.98	2381.5	32498.24	86.14	0.164
5.46	6.66	4	177.4	1181.6	33116.24	87.73	0.068
5.65	6.89	2	94.94	651.2	33458.37	88.7	0.039
5.83	7.11	8	40.44	2875.4	34962.23	92.7	0.181
5.02	7.34	1	53.88	395.45	35169.05	93.2	0.024
6.20	7.56	6	342.9	259.5	36524.9	96.8	0.164
6.38	7.78	1	60.53	470.9	36771.2	97.5	0.0295
6.75	8.27	2	135.8	1118.96	37356.4	99.02	0.033
7.30	8.91	1	79.4	707.35	37726.37	100	0.0146
Σ	–	–	985	15604.8	72134.7	37726.37	–	–

Table IV.b Drop Size Distribution Results (Area - Basis)
N = 300 RPM (Run No 9)

d_{obs} (mm)	d_{act} (mm)	n	$n\,d_a^2$ $(mm)^2$	$n.\,\pi d_a^2$ $(mm)^2$	υ_A $(mm)^2$	υ_A %	$\frac{d\upsilon_A}{dd}$ (mm^{-1})
1.42	1.74	3	9.06	28.45	28.45	0.058	
1.6	1.96	8	30.72	96.46	129.9	0.225	0.0089
1.78	2.17	10	47.1	9.8	274.7	0.56	0.0145
1.97	2.40	29	167.04	5.4	799.1	1.63	0.0465
2.15	2.62	43	294.98	92.2	1725.3	3.5	0.0976
2.34	2.85	62	503.44	1580.8	3306.1	6.75	0.1413
2.52	3.07	87	819.54	2573.4	5879.5	12	0.0808
2.70	3.24	117	1265.94	3975	9854.5	20	0.3636
2.89	3.53	117	1457.82	4577.6	14432.03	29.5	0.3958
3.07	3.75	98	1251.34	3929.2	18361.2	37.5	0.3636
3.26	3.98	95	1504.8	4725	23086.2	47.15	0.41956
3.44	4.2	74	1305.36	4098.8	27185	55.5	0.3795
3.62	4.42	59	1152.86	3619.9	30805	62.9	0.3363
3.81	4.65	45	972.9	3054.9	33859.9	69.15	0.06136
3.99	4.87	9	213.5	670.3	34530.21	70.5	0.06136
4.78	5.10	26	676.3	2123.5	36653.7	74.86	0.18956
4.36	5.32	18	509.4	1599.5	38253.2	78.13	0.1486
4.54	5.54	14	429.66	1349	39602.2	80.9	0.1259
4.73	5.77	18	599.22	1881.6	41483.76	84.7	0.1652
4.91	6.00	17	612.0	1921.7	43405.4	88.7	0.1739
5.10	6.22	11	425.6	1336.4	44741.8	91.4	0.1227
5.26	6.42	9	370.98	1164.9	45906.7	93.8	0.10909
5.46	6.66	4	177.4	557.2	46463.8	94.9	0.0458
5.65	6.89	2	94.94	298.1	46761.9	95.5	0.02608
5.83	7.11	8	40.44	126.98	46888.9	95.8	0.0163
5.02	7.34	1	53.88	169.18	47018.06	96	0.00867
6.20	7.56	6	342.9	1076.7	48094.76	98	0.0909
6.38	7.78	1	60.53	190	48284.76	98.6	0.033
6.75	8.27	2	135.8	426.4	48711.16	99.5	0.0195
7.30	8.91	1	79.4	249.3	48960.46	100	0.0079
Σ -	-	985	-	-	48960.46	-	-

CONTENTS OF APPENDIX 5

i) Experimental Overall Mass Transfer Coefficient k_{exp}

ii) Calculated Overall Mass Transfer Coefficient k_{cal}

APPENDIX 5

i) Calculation of Experimental Overall Mass Transfer Coefficient

(Example based on Run No 12; results listed in Table 8.3 to 8.7)

The overall experimental mass transfer coefficient under each set of operating conditions was calculated using the equation:

$$N = K A (\Delta C)_m \qquad (1.1)$$

Hold-up , x = 17%

Sauter mean diameter d_{32} = 0.24cm

Continuous phase superficial velocity V_c = 0.75 $\frac{cm}{s}$

Dispersed phase superficial velocity V_d = 0.6 $\frac{cm}{s}$

Rotor speed in rpm = 300

Column cross sectional area = 45cm

Effective column height = 267.5cm

$y = mx^*$ The equilibrium line equation is shown in Appendix 6, Figure VIII.

where m = 7.3

	y_i	y^*	$\Delta y_i = y^* - y_i$	zi (#)
Bottom	0.018	0.292	0.274	$z_0 = 0.00$
Compact 1.	0.015	0.219	0.204	$z_1 = 45$
3.	0.01	0.16425	0.154	$z_3 = 90$
5.	0.007	0.136875	0.13	$z_5 = 135$
7.	0.005	0.118625	0.114	$z_7 = 180$
9.	0.003	0.01	0.097	$z_9 = 225$
11.	0.001	0.082	0.081	$z_{11} = 270$
Top	0.00	0.073	0.073	

(#) $\Delta z = 45cm$ = constant along the column height

The mean driving force Δy_m was estimated by applying Simpson's rule as:

$$\Delta y_m = \frac{1}{20} \{\Delta y_{bottom} + \Delta y_{top} + 4(\Delta y_1 + \Delta y_5 + \Delta y_9) + 2(\Delta y_3 + \Delta y_7 + \Delta y_{11})\}$$

$$= \frac{1}{20} \{0.274 + 0.073 + +4\,(-204 + 0.13 + 0.097) + + 2(0.154 + 0.114 + 0.081)\}$$

$$= 0.138 \ \frac{\text{g acetone}}{\text{100 g aqueous solution}}$$

$$\Delta c_m = 0.138 \times 0.9983$$

$$= 0.138 \ \frac{\text{g acetone}}{\text{cm}^3 \text{ solution}}$$

$$\text{The specific interfacial area, } a = \frac{6x}{d_{32}} \qquad (8.1)$$

$$= \frac{6 \times 0.17}{0.34}$$

$$= 3.0 \ \frac{\text{cm}^2}{\text{cm}^3}$$

Total interfacial area, A = a x V, where V is the effective column volume.

$$A = 3 \times 267.5 \times 1590 = 1275\ 975 \text{ cm}^2$$

The rate of mass transfer in the column = N

$$= Q_c \cdot \rho_c \cdot (y_{out} - y_{in}) = Q_d \cdot \rho_d \cdot (x_{in} - x_{out})$$

$$= 0.75 \times 1590 \times 0.9983 \ (0.018 - 0.0)$$

$$= 21.43 \text{g/cm}$$

$$K_{exp} = \frac{N}{A \ (\Delta C)_m} \qquad (8.10)$$

$$= \frac{21.43}{1275\,975 \times 0.138}$$

$$= 1.2 \times 10^{-4}\ \text{cm/s}$$

ii) **Sample Calculation of the Theoretical Overall Mass Transfer Coefficient**

(Example based on Run No 9)

The slip velocity of the dispersed phase in the RDC was estimated by applying Equation (111),

$$V_s = \frac{V_d}{x} + \frac{V_c}{1 - x} \qquad (5.2)$$

Dispersed phase flow rate = 24000 cm^3/min

Since D = 45cm,

Dispersed phase vertical velocity $V_d = \frac{24000}{60 \times 1590} = 0.25$ cm/s

Continuous phase flow rate = 30000 cm^3/min

Continuous phase vertical velocity $V_c = \frac{24000}{60 \times 1590} = 0.3145$ cm/s

$$V_s = \frac{0.25}{0.055} + \frac{0.3145}{1 - 0.055}$$

$$= 4.88 \times 10^{-2}\ \text{m/s}$$

The maximum diameter of the stagnant drops, d_s, in the whole drop population was found by setting Re = 10

$$Re = \frac{d_s \cdot V_s \cdot \rho_c}{\mu_c} = 10$$

$$\therefore \quad d_s = \frac{10 \times 0.01}{0.9983 \times 4.88}$$

$$= 0.021 \times 10^{-2} \text{ m}$$

The maximum diameter of the oscillating drops was found by setting Re = 200

$$do = \frac{200 \times 0.01}{0.9983 \times 4.88}$$

$$= 0.41 \times 10^{-2} \text{ m}$$

The circulating drops population is between d_s and d_o.

Table 8.4 shows that d_s is too small to be included in the calculation. Hence, the drop population is considered to contain only circulating and oscillating drop regimes; d_o is the boundary between these regimes.

From the drop size distribution diagrams Figures V and VI, the fractional population of circulating and oscillating drops based either on volume or area fractions will be as follows:

$$P_c = 0.36 \qquad P_o = 1 - 0.36 = 0.64$$

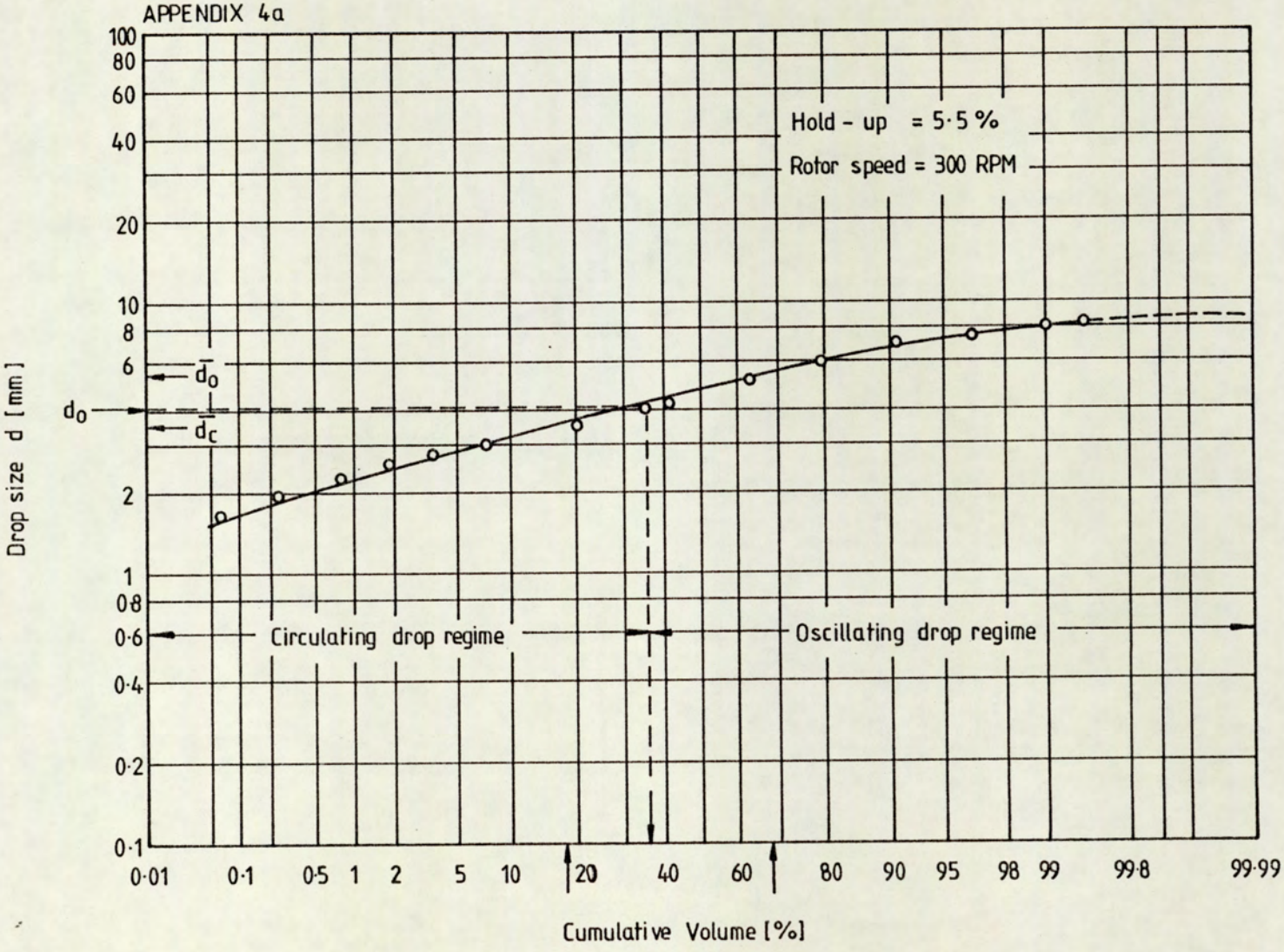

Figure V Drop size distribution for Compartment 6 (Run No. 9) Volume Basis

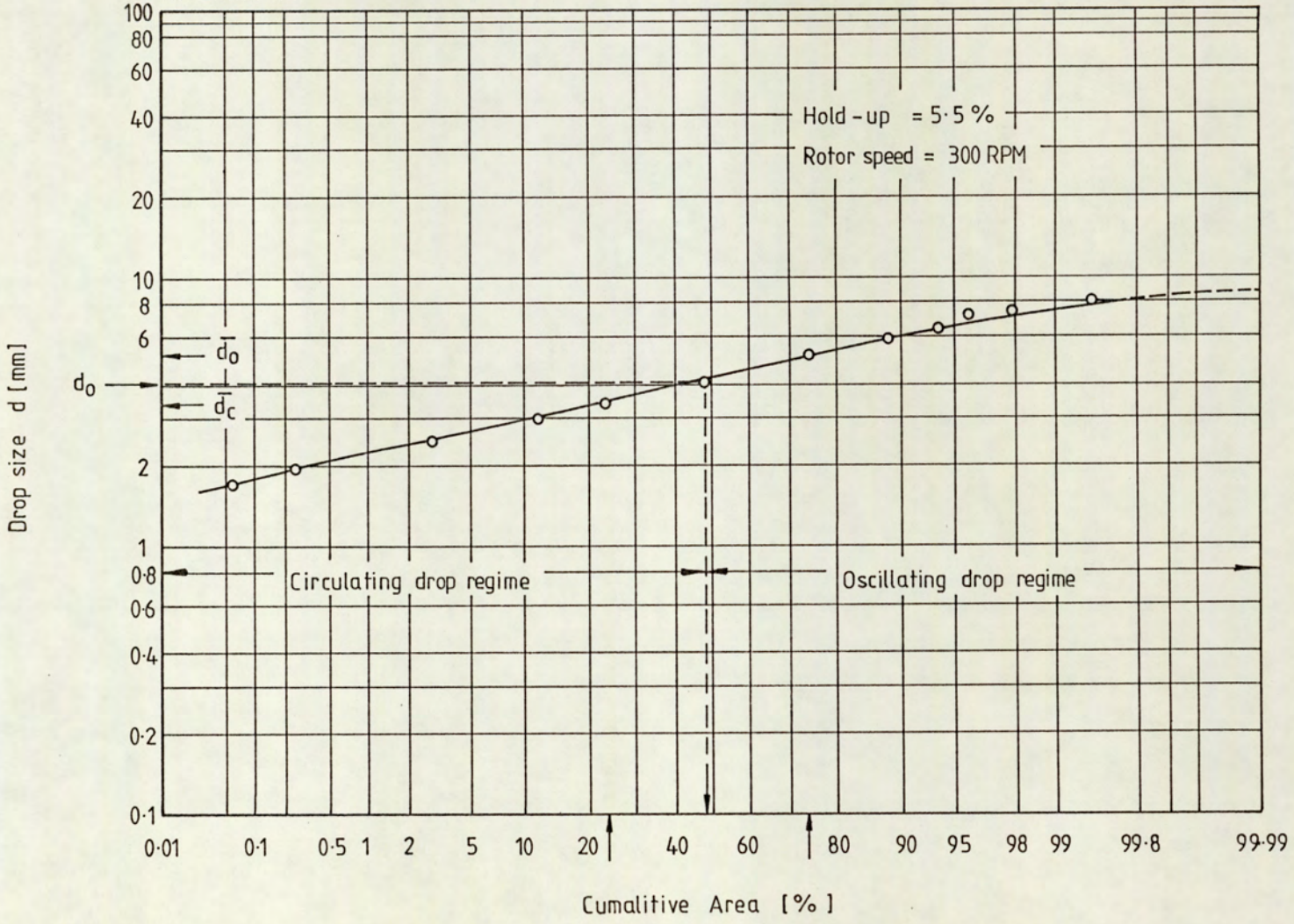

Figure VI Drop size distribution for Compartment 6 (Run No. 9) Area Basis

and $a_c = 0.48$ $a_o = 1 - 0.48 = 0.52$

1) Circulating Drop Regime

a) Dispersed phase mass transfer coefficient was estimated from Kronig and Brink (103),

$$k_{d.c} \cong \frac{17.9 \times D_d}{\bar{d}_c} \qquad (4.21)$$

where $(\bar{d}_c)_v = 0.35\text{cm}$ and

$(\bar{d}_c)_a = 0.34\text{cm}$

from drop size distribution diagrams Figures V and VI

$D_d = 1.298 \times 10^{-7}$ cm/s for diffusion of acetone in Clairsol.

$$\therefore (k_{d.c})_v = \frac{17.9 \times 1.298 \times 10^{-7}}{0.35}$$

$$= 6.6 \times 10^{-6} \text{ cm/s}$$

b) Continuous phase mass transfer coefficient was estimated by Garner et al (118) correlation,

$$Sh = \frac{k_{c.c} \times \bar{d}_c}{D_c} = -126 + 1.8\ Re^{0.5}\ Sc^{0.42} \qquad (4.44)$$

$D_c = 1.119 \times 10^{-7}$ cm^2/s for diffusion of acetone in water.

$$\frac{k_{c.c} \times 0.35}{1.119 \times 10^{-7}} = -126 + 1.8 \left(\frac{0.35 \times 4.88 \times 0.9983}{0.01}\right)^{0.5} \times \left(\frac{0.01}{0.9983 \times 1.119 \times 10^{-7}}\right)^{0.42}$$

$$\therefore \quad k_{c.c} = 8.6 \times 10^{-4} \text{ cm/s}$$

c) Overall mass transfer coefficient of the circulating drops,

$$\frac{1}{K_{o.c}} = \frac{1}{k_{c.c}} + \frac{1}{m.\, k_{d.c}}$$

$$= \frac{1}{8.6 \times 10^{-4}} + \frac{1}{0.136 \times 6.6 \times 10^{-6}}$$

$$K_{o.c} = 0.9 \times 10^{-6} \text{ cm/s}$$

2) Oscillating Drop Regime.

a) Dispersed phase mass transfer coefficient was firstly estimated by Rose and Kintner (97) correlation,

$$k_{d.o} = 0.45 \, (D_d . \omega)^{0.5} \tag{4.30}$$

where

$$\omega^2 = \frac{n \sigma b}{r^3} \left[\frac{(n-1)(n+1)(n+2)}{(n+1)\rho_d + n\rho_c}\right] \tag{4.31}$$

where, $n = 2$ and $b = \dfrac{\bar{d}_o^{0.225}}{1.242}$ (4.32)

$(\bar{d}_o)_v = 0.54$ cm

$(\bar{d}_o)_a = 0.51$ cm

from drop size distribution diagrams Figures V and VI.

$$b = \frac{(0.54)^{0.225}}{1.242} = 0.7$$

$$r = \frac{0.54}{2} = 0.27$$

$$\omega^2 = \frac{2 \times 35.5 \times 0.70}{(0.27)^3}\left[\frac{(2-1)\ (2+1)\ (2+2)}{(2+1)\ 0.783 + 2 \times 0.9983}\right]$$

$$\omega = 83.5\ \text{sec}^{-1}$$

$$\therefore\ k_{d.o} = 0.45\ (1.298 \times 10^{-7} \times 83.5)^{0.5}$$

$$= 1.48 \times 10^{-3}\ \text{cm/s}$$

Secondly by Angelo et al (88) Equation,

$$k_{d.o} = \left[\frac{4\omega D_d\ (1 + \varepsilon_o)}{\pi}\right]^{0.5} \quad (4.33)$$

where $\varepsilon_o = \varepsilon + \frac{3}{8}\varepsilon^2$ (4.34)

$$\varepsilon = 0.434 \left(\frac{\omega.\bar{d}_o}{Vs}\right)^{-0.46} \left(\frac{\bar{d}_o V_s^2 \rho_c}{\sigma}\right)^{-0.53} \left(\frac{\mu V_s}{\sigma}\right)^{-0.11} \quad (8.16)$$

$$= 0.434 \left(\frac{83.4 \times 0.54}{4.88}\right)^{-0.46} \left(\frac{0.54 \times (4.88)^2 \times 0.9983}{35.5}\right)^{-0.53}$$

$$\left(\frac{0.01 \times 4.88}{35.5}\right)^{-0.11}$$

$$= 0.55$$

$$\varepsilon_o = 0.55 + 3/8\,(0.55)^2$$

$$= 0.66$$

$$\therefore \; k_{d.o} = \left[\frac{4 \times 1.298 \times 10^{-7} \times 83.5\,(1 + 0.66)}{\pi}\right]^{0.5}$$

$$= 4.8 \times 10^{-3} \text{ cm/s}$$

b) Continuous phase mass transfer coefficient was estimated by Garner et al (114) correlation,

$$\frac{k_{c.o} \times \bar{d}_o}{D_c} = 50 + 0.0085 \quad Re \,.\, Sc^{0.7} \quad (4.46)$$

$$\frac{k_{c.o} \times 0.54}{1.119 \times 10^{-7}} = 50 + 0.0085\left(\frac{0.54 \times 4.88 \times 0.9983}{0.01}\right)$$

$$\left(\frac{0.01}{0.9983 \times 1.119 \times 10^{-7}}\right)^{0.7}$$

$$k_{c.o} = 1.37 \times 10^{-3} \text{ cm/s}$$

c) The overall mass transfer coefficient of oscillating drops,

i) Firstly by Rose and Kintner (97) and Garner et al (114),

$$\frac{1}{K_{o.o}} = \frac{1}{k_{c.o}} + \frac{1}{m.k_{d.o}}$$

$$= \frac{1}{1.37 \times 10^{-3}} + \frac{1}{0.136 \times 1.48 \times 10^{-3}}$$

$$(K_{o.o})_v^I = 1.8 \times 10^{-4} \text{ cm/s}$$

ii) Secondly by Angelo et al (88) correlation,

$$K_{o.o} = k_{d.o}\left[\frac{1}{1 + m\left(\frac{D_d}{D_c}\right)^{0.5}}\right] \quad (4.37)$$

$$= 4.8 \times 10^{-3}\left[\frac{1}{1 + 7.3\left(\frac{1.290 \times 10\text{-}7}{1.119 \times 10\text{-}7}\right)^{0.5}}\right]$$

$$(K_{o.o})^{II} = 5.4 \times 10^{-4} \text{ cm/s}$$

Hence the theoretical overall mass transfer coefficients for the whole drop population on the basis of volume and on the basis of area are respectively,

$$(K_{cal})_v = (K_{o.c})_v \cdot P_c + (K_{o.o})_v \cdot P_o \qquad (8.14)$$

$$(K_{cal})_a = (K_{o.c})_a \cdot a_c + (K_{o.o})_a \cdot a_o \qquad (8.15)$$

$$(K_{cal})^{I}_v = 0.9 \times 10^{-6} \times 0.36 + 1.8 \times 10^{-4} \times 0.64$$

$$= 1.15 \times 10^{-4} \text{ cm/s}$$

$$(k_{cal})^{II}_v = 0.9 \times 10^{-6} \times 0.36 + 5.4 \times 10^{-4} \times 0.64$$

$$= 3.5 \times 10^{-4} \text{ cm/s}$$

$$(K_{cal})^{I}_a = 0.9 \times 10^{-6} \times 0.48 + 1.8 \times 10^{-4} \times 0.52$$

$$= 0.94 \times 10^{-4} \text{ cm/s}$$

$$(k_{cal})^{II}_a = 0.9 \times 10^{-6} \times 0.48 + 5.4 \times 10^{-4} \times 0.52$$

$$= 3.1 \times 10^{-4} \text{ cm/s}$$

I Rose and Kintner and Garner et ai correlations (97, 114)

II Angelo et al correlation (88)

APPENDIX 6a

Specimen Calculation of Back Mixing Coefficients Run 7

Refer to Figure VIII

a) Continuous phase back mixing coefficient E_x

Considering sample point 11

$$Y_{11} = y_{11} + \frac{Ey_{11}}{V} \frac{dy}{dz} \qquad (8.19a)$$

Y_{11} = 0.0035 from the balance line

y_{11} = 0.004 from experiment

(This data point, together with those calculated below, is plotted versus z in Figure VII)

$$\frac{dy}{dz} = \frac{0.004}{100} = 0.00004$$

Hence,

$$0.0035 = 0.004 - \frac{Ey_{11}}{0.3145} \times 0.00004$$

or

$$Ey_{11} = \frac{0.3145\ (0.004 - 0.0035)}{0.00004} \qquad (8.19b)$$

$$= 3.9\ cm^2/s$$

Considering sample point 9

Y_9 = 0.0052

y_9 = 0.006

$$\frac{dy}{dz} = \frac{0.006 - 0.004}{45} = 0.000044$$

Hence,

$$0.0053 = 0.006 - \frac{Ey_9}{0.3145} \times 0.000044$$

$$Ey_9 = \frac{0.3145\,(0.006 - 0.0052)}{0.000044} = 5.7 cm^2/s$$

Considering sample point 7

$$Y_7 = 0.0067$$

$$y_7 = 0.008$$

$$\frac{dy}{dz} = \frac{0.008 - 0.006}{45} = 0.000044$$

$$0.0067 = 0.008 + \frac{Ey_7}{0.3145} \times 0.000044$$

Hence,

$$Ey_7 = \frac{0.3145\,(0.008 - 0.0067)}{0.000044}$$

$$= 9.3 cm^2/s$$

Considering sample point 5

$$Y_5 = 0.0082$$

$$y_5 = 0.0095$$

$$\frac{dy}{dz} = \frac{0.0095 - 0.008}{45} = 0.000033$$

$$0.0082 = 0.0095 - \frac{Ey_5}{0.3145} \times 0.000033$$

Hence,

$$Ey_5 = \frac{0.3145\ (0.0095 - 0.0082)}{0.000033}$$

$$= 12.4 cm^2/s$$

Considering sample point 3

$$Y_3 = 0.0098$$

$$y_3 = 0.105$$

$$\frac{dy}{dz} = \frac{(0.0105 - 0.0095)}{45} = 0.000021$$

$$0.0098 = 0.0105 - \frac{Ey_3}{0.3145} \times 0.000021$$

$$Ey_3 = \frac{0.3145\ (0.105 - 0.0098)}{0.000021}$$

$$= 1.5 cm^2/s$$

The average value of back mixing coefficient is $6.6 cm^2/s$.

Individual values show that back mixing coefficient approximates to a maximum in the middle of the column and minimum values at the column ends.

b) Dispersed phase back mixing coefficient E_x

$$\frac{dX}{dz} = - \frac{Ka'}{L'} (x - x^*) \qquad (8.19c)$$

$$\frac{dX}{dz} = - \left(\frac{0.26 - 0.0096}{370}\right) = 0.00004$$

from the balance line

$$Ka' = 1.3 \times 10^{-4} \times 7.3 \times 0.64 \times 1590$$

$= 0.97 cm^2/s$

$L' = 0.25 \times 1590 = 397.5 cm^3/s$

Considering sample point 7

$$x^*_7 = 0.001$$

$$-0.00004 \times \frac{397.5}{0.97} = 0.001 - x_7$$

$$x_7 = 0.0164 + 0.001 = 0.0174$$

Considering sample point 9

$$x^*_9 = 0.0008$$

$$x_9 = 0.0164 + 0.0008 = 0.172$$

$$E_x = \frac{L'(X - x)}{dx/dz} \qquad (8.19 d)$$

$$\frac{dx}{dz} = \frac{x_7 - x_9}{45} = \frac{0.0174 - 0.0172}{45} = 0.000\,0044$$

$$E_{x9} = \frac{397.5\,(0.0171 - 0.0172)}{0.000\,0044} \cong 0$$

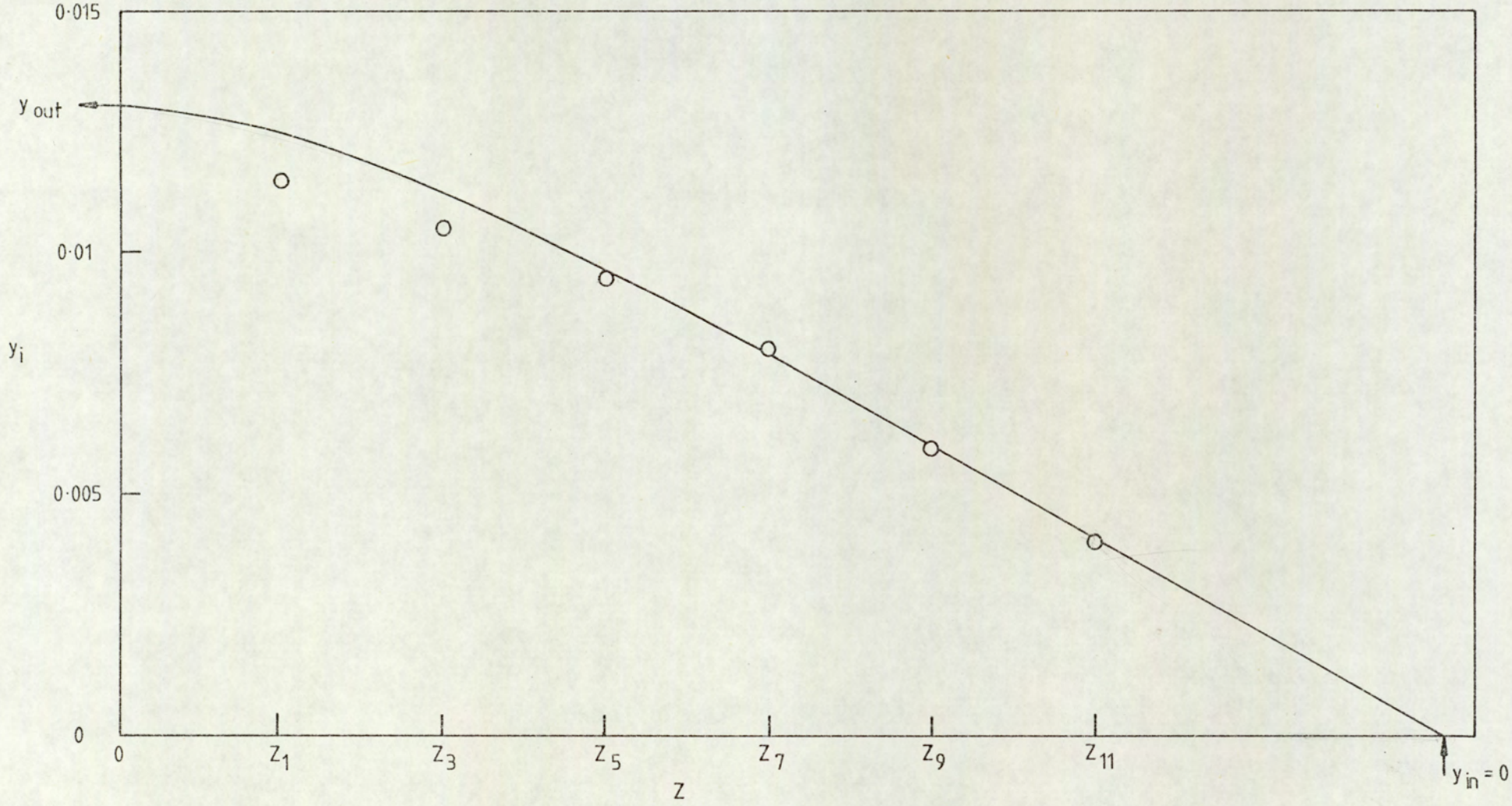

Figure VII Concentration profile along column length for Back mixing determination (Run No 7)

APPENDIX 6b

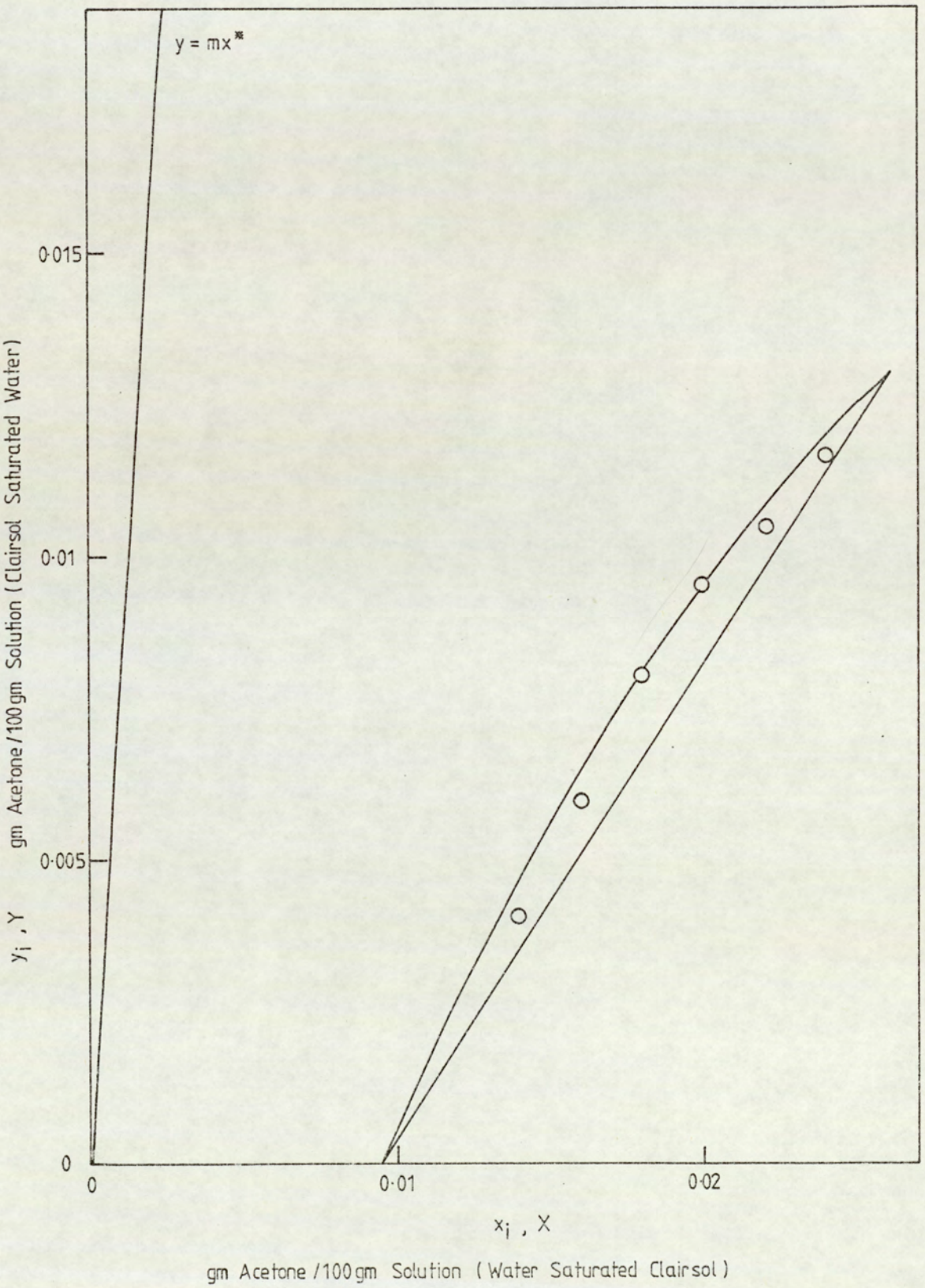

Figure VIII Operating curve profile along column length for Back mixing determination (Run No.7)

APPENDIX 6b

Specimen Calculation of Back Mixing Coefficients Run 5

a) Continuous phase back mixing coefficient E_y

Considering sample point 11

$$Y_{11} \cong y_{11} = 0.0015$$

$$\frac{dy}{dz} = \frac{0.0015 - 0}{70} = 0.00002$$

$$0.0015 = 0.0015 - \frac{Ey_{11}}{0.2} \times 0.00002$$

$$Ey_{11} = \frac{0.2\,(0.0015 - 0.0015)}{0.00002} = 0 \qquad (8.19b)$$

Results calculated for other sampling points also approximate to zero (Figure IX)

b) Dispersed phase back mixing coefficient E_x

$$\frac{dX}{dz} = -\frac{Ka'}{L'}(x - x^*)$$

$$\frac{dX}{dz} = \frac{0.011 - 0.0016}{340} = 0.000027$$

$$Ka' = 4.3 \times 10^{-4} \times 7.3 \times 0.22 \times 1590$$

$$= 1.1 cm^2/s$$

$$L' = 0.15 \times 1590 = 238.5 cm^3/s$$

$$\frac{-0.000027 \times 238.5}{1.1} = x^* - x$$

Considering sample point 7

$$x^* = 0.0004$$

$$x = 0.00625$$

Considering sample point 9

$$x^* = 0.003$$

$$x = 0.00615$$

$$\frac{dy}{dz} = \frac{0.00625 - 0.00615}{45} = 0.00\ 0002$$

$$E_x = \frac{238.5\ (0.0063 - 0.00625)}{0.00\ 0002} \cong 0$$

APPENDIX 6c

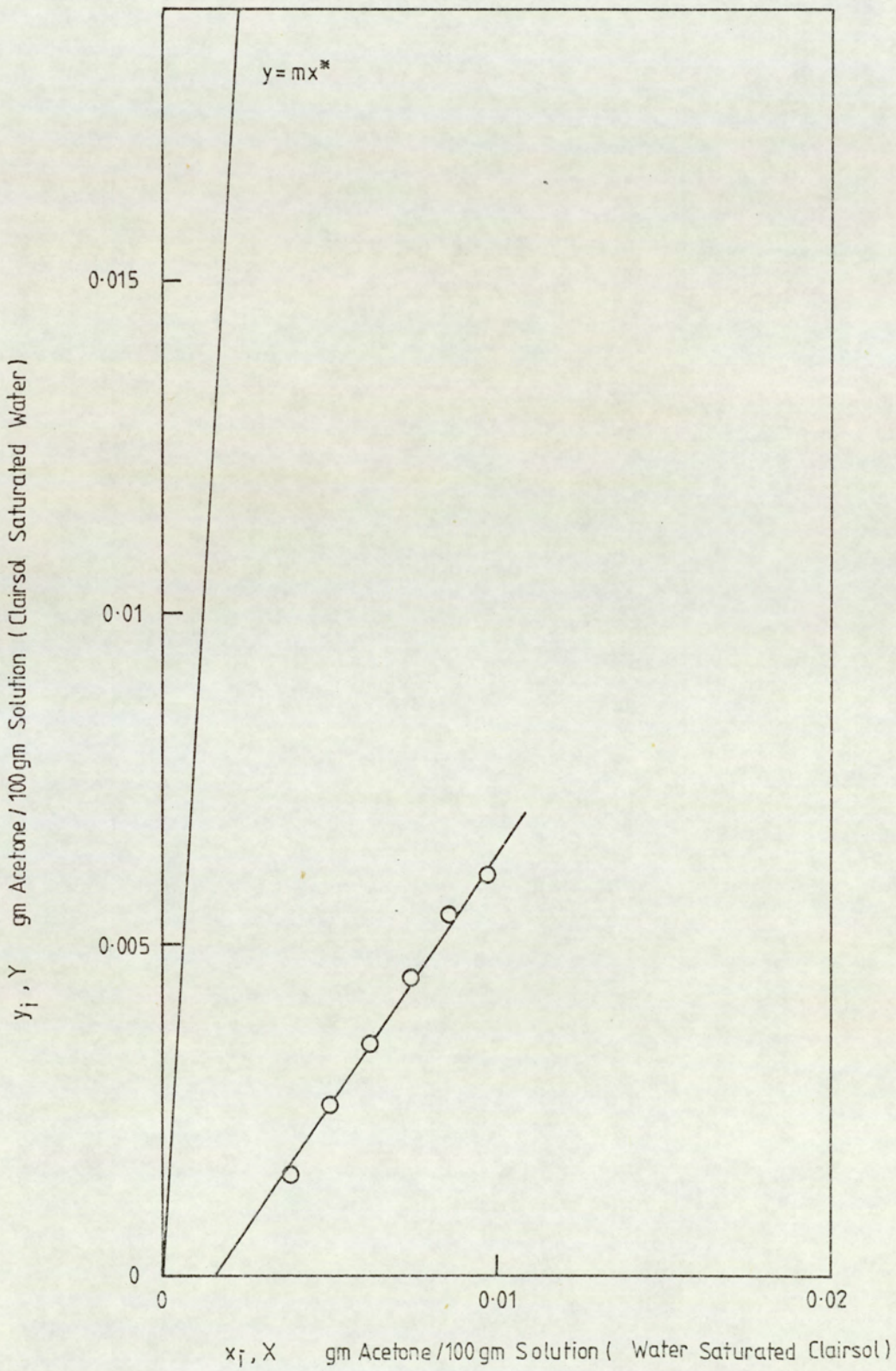

Figure IX Operating curve profile along column length for Back mixing determination.

APPENDIX 7

Calculation of Time to Steady State

(Run No 9)

$$V_d = 0.25 \frac{cm}{s} \quad \text{-----> Feed flow rate} = 400 \frac{cm^3}{s}$$

$$x = 0.055$$

$$h_{eff} = 407mm$$

$$\text{Column effective volume} = \frac{\pi}{4} D^2 \times h_{eff}$$

$$= \frac{\pi}{4} (45)^2 \times 407$$

$$= 646.98 \text{ litres}$$

Volume of Clairsol in column is:

$$= 646.98 \times 0.055$$

$$= 35.58 \text{ litres}$$

Clairsol volume necessary to reach steady state is:

$$= 35.58 \times 2.5$$

$$= 88.96 \text{ litres}$$

Minimum time required for steady state after which samples can be taken is:

$$\frac{88960}{400} = 222.4 \text{ seconds}$$

$$= 3.7 \text{ minutes}$$

$$\cong 4 \text{ minutes}$$

On this basis, as described in Chapter 7, a minimum of 5 minutes was always allowed.

NOMENCLATURE

A	Total interfacial area, cm^2
A_{max}	Maximum axis length, cm
A_n	Eigen value in Equation (4.19).
Ao	Initial surface area of an oscillating drop, cm^2.
a	Specific interfacial area, cm^2/cm^3.
a'	Distribution parameter (skewness parameter).
a_c	Fraction of drops in dispersion undergoing circulation on area basis.
a_o	Fraction of drops in dispersion undergoing oscillation on volume basis.
a_o	Initial horizontal radius in Equations (4.26) and (4.28).
a_p	Amplitude in x-axis in Equations (4.26) and (4.28).
a_d	Surface area of drop in Equations (4.5) and (4.6).
b	Vertical radius of spheroid in Equation (4.29).
b_o	Initial vertical radius in Equation (4.27).
ΔC	Concentration driving force, g/cm^3.
ΔC_m	Actual mean concentration driving force, g/cm^2.
C	Solute concentration, g/cm^3.
C*	Equilibrium solute concentration, g/cm^3.
C_R	Constriction factor.
D	Molecular diffusivity, cm^2/s.
D	Column diameter, cm.
D_c	Molecular diffusion of acetone in continuous phase.
D_d	Molecular diffusion of acetone in dispersed phase.
D_E	Effective diffusivity in Equation (4.24), cm^2/s.

D_N	Nozzle inside diameter in Equation (3.1), cm.
Δ_D	Distance between agitator and column wall (D - R)/2, cm.
d	Drop diameter, cm.
d_{32}	Volume - surface, or Sauter mean drop diameter, cm.
d_{max},d_m	Maximum stable drop size, cm.
d_o	Mean drop diameter, cm.
d_{10}, d_{50}, d_{90}	Drop sizes at 10%, 50% and 90% cumulative volume as well as area fraction.
d_{vg}	Geometric mean drop diameter, cm.
d_F	Diameter of detached drop in Equation (3.1).
E_c, E_d	Axial mixing coefficient in continuous and dispersed phases respectively, cm^2/s.
E_m	Extraction efficiency.
e	Eddy diffusivity, cm^2/s.
E	Power input per unit mass.
E	Extract phase.
F	Feed volumetric flowrate.
F	Harkins Brown correction fractor in Equation (3.1).
F_B	Superficial flowrate of interstage mixing per unit cross sectional area of columns, cm/s.
g	Gravitational constant, cm/s^2.
h_c	Column height, cm.
H	Compartment height, cm.
H_E	Effective column height, cm.
H.T.U.	Height of transfer unit, cm.
h	Column height at certain point, cm.
h_m	Height equivalent to the stage $= \frac{H_E}{N_c}$, cm.

K	Overall mass transfer coefficient, cm/s.
K_{exp}	Experimental overall mass transfer coefficient, cm/s.
K_{cal}	Theoretical overall mass transfer coefficient, cm/s.
$(K_{cal})^{I}_{v}$ } $(K_{cal})^{I}_{a}$ }	Theoretical overall mass transfer coefficient calculated using Rose and Kintner (4.30) and Garner et al (4.46) correlations for oscillating drops based on volume and area fractions respectively, cm/s.
$(K_{cal})^{II}_{v}$ } $(K_{cal})^{II}_{a}$ }	Theoretical overall mass transfer coefficient calculated using Angelo et al (4.33) and Garner et al (4.46) correlations for oscillating drops based on volume and area fractions respectively, cm/s.
Ka	Overall volumetric mass transfer coefficient, sec^{-1}.
k_c	Continuous phase mass transfer coefficient, cm/s.
$k_{c.c}$	Continuous phase mass transfer coefficient of circulating drops, cm/s.
$k_{c.o}$	Continuous phase mass transfer coefficient of oscillating drop, cm/s.
k_d	Dispersed phase mass transfer coefficient, cm/s.
$k_{d.c}$	Dispersed phase mass transfer coefficient of circulating drops, cm/s.
$k_{d.o}$	Dispersed phase mass transfer coefficient of oscillating drops, cm/s.
$K_{o.c}$	Overall mass transfer coefficient of circulating drops, cm/s.
$K_{o.o}$	Overall mass transfer coefficient of oscillating drop, cm/s.
K_{df}	Mass transfer coefficient during drop formation, cm/s.
K_1, K_2, K_3, K_4	Geometric factor (constants).
L	Superficial velocity of stripped (feed) phase.
L	Characteristic dimension of turbulence, cm.
L	$\frac{V_d}{V_c}$ ---- ratio of the superficial velocity of dispersed phase to superficial velocity of continuous phase under flooding condition.
m	Equilibrium distribution coefficient.

N	Rotor speed, revolutions per unit time.
N	Rate of mass transfer, g/sec.
N_c	Total number of compartments.
N_p	Power number.
N.T.U.	Number of transfer units.
n	Compartment number or number of drops.
P	Power input, erg/s.
P_c	Fraction of drops in dispersion undergoing circulation on volume basis.
P_o	Fraction of drops in dispersion undergoing oscillation on volume basis.
Q	Volumetric flow rate, cm^3/s.
Q	Volumetric flow rate of dispersed phase through nozzle in Equation (3.1), cm^3/s.
Q_o	Initial solute concentration, in Equation 4.52.
Q_t	Concentration at time t, in Equation 4.52.
R	Raffinate volumetric flow rate, cm^3/s.
R	Rotor disc diameter, cm.
Rr	Phase flow ratio at inversion.
r	Radius of sphere of volume equal to that of a drop, cm.
$r_{s.d.}$	Stable drop radius, cm.
r_o	Initial radius of drop in Equations (4.5) and (4.6).
S	Stator ring opening diameter, cm.
S	Solvent volumetric flow rate, cm^3/s.
S_w	Specific surface, cm.
$\bar{S}_w$	Average specific surface, cm.
t	Time, sec.

t_f	Time of drop formation, sec.
U_N	Dispersed phase average velocity through the nozzle in Equation (3.1), cm/s.
V	Volume of column, cm^3.
V_c, V_d	Superficial velocity in continuous phase and dispersed phase respectively, cm/s.
V_F	Drop volume after break off from the nozzle in Equation (3.1), cm^3.
V_N	Characteristic drop velocity, cm/s (ie. the mean vertical drop velocity at substantially zero flow rates and at rotor speed N).
V_S	Slip velocity of drops cm/s.
V_T	Tip velocity, cm/s.
W	Function of oscillating drop characteristics defined by Equation (4.26).
X	Solute concentration in the dispersed phase g/100g.
X	Dispersed phase hold-up.
X	Length of droplet x-axis in Equation (4.27), cm.
X_F	Feed solute concentration.
X_f	Dispersed phase hold-up at flooding point.
X_i	Dispersed phase hold-up at phase inversion point.
X_o	Fictitious film thickness in Equation (4.27), cm.
X_R	Solute concentration in the raffinate phase (g/100g).
X	Distance.
Y,y	Solute concentration in the continuous phase, (g/100g).
y_E	Solute concentration in the extract phase (g/100g).
Δy_m	Actual mean concentration driving force, g/100g.
y_S	Solute concentration in the solvent (g/100g).
Z	Coalescence coefficient.

Greek Symbols

α	Back flow coefficient.
α	Back mixing correlation factor.
α	Constant in Equation (5.16).
α	Coalescence frequency in Equation (3.39).
Δ	Size increment (cm).
γ	Surface tension, dynes/cm (mNm^{-1})
δ	Uniformity distribution parameter.
ρ	Density, g/cm^3.
ρ_m	Mean density = $\rho_d . x + \rho_c (1 - x)$, g/cm^3.
$\Delta\rho$	Density difference, g/cm^3.
μ	Viscosity, g/cm.sec.
υ	Kinematic viscosity, cm^2/sec.
υ	Cumulative volume of drops, cm^3.
σ	Interfacial tension, dynes/cm.
τ	Dimensionless time.
ψ_1	Function of Schmidt group defined by Equation (5.23).
ψ_2	Function of the physical properties defined by Equation (5.25).
ω	Frequency of oscillation, 1/sec.
π	Constant = 3.1416.
$\varepsilon, \bar{\varepsilon}$	Energy input per unit mass and time (erg/g.sec).

ε	Amplitude of oscillation.
ε_o	Function of amplitude of oscillation defined by Equation (4.34).
λ_n	Eigen value in Equation (4.19).

Subscripts

A	Refers to phase A.
a	Area basis.
act	Actual
C	Continuous phase and/or circulating drop.
C	Column.
cal	Calculated or theoretical.
Crit	Critical
d	Drop and/or dispersed phase.
E	Effective.
E	Extract.
EXP	Experimental.
F	Feed.
f	Flooding condition.
f	Drop formation.
i	Initial.
i	Ith stage.
m	Mean.
max	Maximum.
min	Minimum.
N	Nozzle.
o	Initial.

O	Overall and/or oscillating drop.
obs.	Observed.
R	Raffinate phase.
R	Drop release.
r	Rotating disc.
s	Stagnant drop.
s	Slip.
s.d.	Stable drop.
T	Tip and/or top of the column.
vg	Geometric mean.
VS	Sauter mean. Volume to surface ratio of droplets.
w	Weight.

Superscripts

*	Refers to the equilibrium condition.
–	Mid-sector in average.
I	Refers to Equations (4.30) and (4.46).
II	Refers to Equations (4.33) and (4. 46).

Dimensionless Groups

Fr Froude number $= \dfrac{V_c^2}{gD_c}$

Fr Modified Froude number $= \dfrac{V_d^2}{g\,D_c\,X^2}$

Fr Rotor Foude number = $\frac{N^2 R}{g}$

Ga Galileo number = $\frac{d^3 \rho^2 g}{\mu^2}$

Np Power number = $\frac{P}{N^3 R^5 \rho_m}$

$(P_e)_c$ Peclet number = $\frac{V_c . H}{E_c}$ for continous phase.

$(P_e)_d$ Peclet number = $\frac{V_d . H}{E_d}$ for dispersed phase.

Re Droplet Reynolds number = $\frac{d V_s \rho_c}{\mu_c}$

Re Disc Reynolds number = $\frac{R^2.N.\rho_c}{\mu_c}$

Re Column Reynolds number = $\frac{V_d.H.\rho_c}{\mu_c.x}$

Sc Schmidt number = $\frac{\mu}{\rho.D}$

Sh Sherwood number $= \frac{kd}{D}$

We Droplet Weber number $= \frac{d.V_s^2.\rho_c}{\sigma}$

We Disc Weber number $= \frac{N^2 R^3 \rho_c}{\sigma}$

REFERENCES

(1) Abdul Hamid, A R.
PhD Thesis, University of Aston in Birmingham, UK (1983).

(2) Smith, T E and Bonner, R F.
Ind. Eng. Chem. 42, 896 (1950), Ch.12, TecQuipment Ltd (1980).

(3) Davies, G A.
"Choices of Solvent in Liquid-Liquid Extraction", 2nd Solvent Symposium, UMIST, Manchester (1977).

(4) Oberg, A G and Jones, S C.
Chem. Eng. Sci., 7, 70, 119, (1963).

(5) Hanson, C.
Chem. Eng., 26, 76, (1968).

(6) Reman, G H.
Proceedings, 3rd World Petroleum Congress, The Hague Section 3, 121, (1951).

(7) Brandt, H W, Reissinger, K H and Schroeter, J.
Chem. Eng. Techn. 50, 345, (1978).

(8) Treybal, R E.
"Liquid Extraction", McGraw-Hill, New York, 2nd Edition (1963).

(9) Mumford, C J.
Brit. Chem. Eng. 13, 7, 981, (1968).

(10) Simsons, A J F.
Chem. Eng. Techn. 48, 5, 487, (1976).

(11) Karr, A E and Lo, T C.
Chem. Eng. Prog. 11, 68 (1976).

(12) Misek, T.
Chem. Eng. 68, 58, (1961).

(13) Marek, J, Misek, T and Windmer, F.
Soc. Chem. Eng. Symposium, University of Bradford, UK, October (1967).

(14) Marek, J and Misek, T.
Soc. Chem. Eng. Conf. Solvent Extraction, London, March (1969).

(15) Oldshue, J Y and Rushton, J H.
Chem. Eng. Prog. 48, 297, (1952).

(16) Simonis, H.
Process Eng. 110, Nov. (1972).

(17) Scheibel, E G.
U S Pat. 2, 493, 265, (1950).

(18) Kuhni, A G.
Verfahrens Technik and Apparatebau CH-4123, Aleschwnil-Basel, Schweiz.

(19) Thornton, J D.
Trans, Instn. Chem. Engrs. 35, 316, (1957).

(20) Coggan, G C.
I. Chem. Eng. Symposium Series No. 26 (1967).

(21) Todd, D B.
Chem. Eng., 69, 156, (1962).

(22) Logsdail, D H and Lowes, L.
"Recent Advances in Liquid Extraction", Chapter 5, Pergamon, London, (1971).

(23) Reman, G H and Olney, R B.
Chem. Eng. Prog. 51, 141, (1955).

(24) Kagan, S Z, Trukhanov, V G, Kostin, P A and Kudryavtsev, E N.
Int. Chem. Eng. 4, 473, (1964).

(25) Theyze, U G, Wall, R J, Train, K E and Olney, R B.
Oil Gas J. 59, 70, (1961).

(26) Anon.
Pet. Processes, 10, 230, (1955).

(27) Misek, T and Rozkos, B.
Int. Chem. Eng. 6, 130, (1966).

(28) Brinke, A A and Gericke, J J.
S. African Ind. chemist. 18, 11, 152 (1964).

(29) Reman, G H and Van de Vusse, J G.
Pet. Refiner, 34, 129, (1955).

(30) Reman, G H.
Pet. Refiner, 36, 269, (1957).

(31) Reman, G H and Van de Vusse, J G.
Genie Chemie, 74, 106, (1955).

(32) Cronan, C S.
Chem. Eng. 65, 54, (1958).

(33) Al-Hemiri, A A A.
PhD Thesis, University of Aston in Birmingham, UK, (1973).

(34) Mumford, C J and Jeffreys, G V.
Paper presented to 3rd CHISA Congress, Marianske Lazme, Sept. (1969).

(35) Haynes, L G, Himmelblau, D M and Schechter, R S.
Process Design and Development, 7, 508, (1968).

(36) Jeffreys, G V.
Chem. and Process Eng. 49, 111, (1968).

(37) Morello, V S and Poffenberger, N.
Ind. Eng. Chem. 42, 1021, (1950).

(38) Jeffreys, G V and Ellis, E M R.
CHISA (1962).

(39) Heertjes, P M and de Nie, L H.
"Mass Transfer to Drops", Recent Advances in Liquid-Liquid Extraction, Edited by Hanson, Pergamon Press, NY, (1971).

(40) Harkins, W D and Brown, F E.
J. Am. Chem. Soc., 41, 449, (1919).

(41) Treybal, R E and Hayworth, C B.
Ind. Eng. Chem. 42, 1174, (1950).

(42) Null, H R and Johnson, H F.
A.I.Ch.E.J., 4, 273, (1958).

(43) Meister, B J.
PhD Thesis, Cornell University, NY, (1966).

(44) Scheele, G F and Meister, B J.
A.I.Ch.E. J., 14, 9, (1968).

(45) Groothuis, H and Kramers, H.
Chem. Eng. Sci. 4, 17, (1955).

(46) Dixon, B E and Russell, A A W.
J. Soc. Chem. Ind., London, 69, 284 (1950).

(47) Kolmogoroff, A N.
Doklo Akad, Nauk. SSSR, 66, 825, (1949).

(48) Hinze, J O.
A.I.Ch.E.J., 1, 289, (1955).

(49) Clay, P H.
Nad. Akad. Can. Wetenskapen Proc. Roy. Acad. Sci., Amsterdam, 43, 852, 979, (1940).

(50) Levich, V G.
"Physico Chemical Hydrodynamics", Prentice-Hall, New Jersey, (1962).

(51) Jeffreys, G V and Mumford, C J.
Proc. Int. Solvent Extraction Conf., The Hague, (ISEC), Vol. 1, 667, (1971).

(52) Olney, R B.
A.I.Ch.E.J., 10, 827, (1964).

(53) Dallavalle, J M.
"Micrometrics, the Technology of Fire Particles", 2nd Edition, Pitman Publishing Co., NY (1948).

(54) Mumford, C J and Al-Hemiri, A A A.
Proc. Int. Solvent Ext. Conf., (ISEC), Lyon, Vol. 2, 1591, (1974).

(55) Rod, V.
Brit. Chem. Eng., 11, 68 (1976).

(56) Misek, T.
Coll. Czech. Chem. Eng., 32, 4018 (1976).

(57) Misek, T and Marek J.
Brit. Chem. Eng. 5, 202, (1970).

(58) Thorson, G et al.
Chem. Eng. Sci. 23, 413 (1968).

(59) Chen, H T and Middlemans, S.
A.I.Ch.E. J. 13, 987, (1967).

(60) Sprow, F B.
Chem. Eng. Sci. 22, 435 (1967).

(61) Brown, D E and Pitt, K.
Proc. Chemeca 70, Butterworth, Australia, (1970).

(62) Giles, J G, Hanson, C and Marsland, J.
Proc. Int. Solvent Extraction Conference, The Hague, (ISEC) 74, (1971).

(63) Chartes, R H and Korchinsky, W J.
Trans. Inst. Chem. Eng. 53, 247, (1975).

(64) Korchinsky, W J and Azimzadeh-Khataylo, S.
Chem. Eng. Sci. 31, 871, (1976).

(65) Jeffreys, G V, Al-Aswad, K and Mumford, C J.
Paper presented in the 2nd Symposium on Sep. Sci. and Techn. for Energy App., Galtinburg, Tenn. USA, May (1981).

(66) Misek, T.
Rotating Disc Contactor, Statni Nakladatelstvi Technicke Literatory, Prague, (1964).

(67) Mumford, C J.
PhD Thesis, University of Aston in Birmingham, UK, (1970).

(68) Thornton, J D.
Ind. Chemist., 12, 632 (1963).

(69) Blazej, L et al.
Chem. Zvesti, 32, 341, (1978).

(70) Mugele, R A and Evans H D.
Ind. Chem. 43, 1317, (1951).

(71) Gal-or, B and Hoelscher, H E.
A.I.Ch.E. J. 8, 350 (1962).

(72) Rod, V.
Paper presented at meeting of the European Federation of Chem. Engineers, in Prague, Czechoslovakia, (1970).

(73) Rosin, P and Rammler, E.
J. Inst. of Fuel 7, 29 (1933).

(74) Lawson, G B.
PhD Thesis, University of Manchester (1967).

(75) Davies, J T, Ritchie, J M and Southward, D C.
Trans. Instn. Chem. Eng. 38, 31, (1960).

(76) Strand, C P, Olney, R B and Ackerman, G H.
A.I.Ch.E.J., 8, 252, (1962).

(77) Howarth, W J.
Chem. Eng. Sci. 19, 33, (1966).

(78) Madden, A J and Damarell, G C.
A.I.Ch.E.J., 8, 233, (1962).

(79) Misek, T.
Coll, Czech. Chem. Comm. 29, 2086 (1964).

(80) Jeffreys, G V and Lawson, G B.
Trans. Inst. Chem. Eng. 43, 294, (1965).

(81) Smith, A R, Caswell, J E, Larson, P P and Cavees, S D.
Canad. J. Chem. Eng., Aug. 150 (1963).

(82) Charles, G E and Marson, S G.
J. Colloid Sci. 15, 236 (1960).

(83) Groothuis, H and Zuiderweg, F J.
Chem. Eng. Sci. 12, 288, (1960).

(84) Sherwood, T K et al.
Ind. Eng. Chem., 31, 1144, (1939).

(85) West, F B et al.
Ind. Eng. Chem. 43, 234 (1951) & 44, 625, (1952).

(86) Licht, W and Pansing, W F.
Ind. Eng. Chem. 45, 1885, (1953).

(87) Hines, L A and Maddox R N.
"Mass Transfer Fundamentals and Applications", Prentice-Hall Inc.
Engelwood, New Jersey (1985).

(88) Angelo, J B, Lightfoot, E N and Howard, D W.
A.I.Ch.E.J. 12, 751, (1966).

(89) Sawistowski, H and Goltz, G E.
Trans. Insts. Chem. Eng. 41, 174, (1963).

(90) Heertjes, P M, Holve, W A and Talsma, H.
Chem. Eng. Sci. 3, 122, (1954).

(91) Coulson, J H and Skinner, S J.
Chem. Eng. Sci. 1, 197, (1952).

(92) Heertjes, P M and de Nie, L H.
Chem. Eng. Sci., 21, 755, (1966).

(93) Ilkovic, D.
Coll. Czech. Chem. Comm. 6, 498, (1934).

(94) Skelland, A H P and Minhas, S S.
A.I.Ch.E.J. 17, 1316, (1971).

(95) Popovich, A T, Jervis, R E and Trass, O.
Chem. Eng. Sci. 19, 357, (1964).

(96) Johnson, A I and Hamielec, A I.
A.I.Ch.E.J. 6, 145, (1960).

(97) Rose, P M and Kintner, R C.
A.I.Ch.E.J. 12, 530, (1966).

(98) Licht, W and Conway, J B.
Ind. Eng. Chem. 421, 1151, (1950).

(99) Al-Aswad, K.
PhD Thesis, University of Aston in Birmingham, UK, (1982).

(100) Marsh, B D and Heideger, W J.
Ind. Eng. Chem. Fundamental, 4, 129, (1965).

(101) Newman, A B.
Trans. Am. Inst. Chem. Engrs., 27, 203, (1931).

(102) Vermeulen, T.
Ind. Eng. Chem. 45, 1664, (1953).

(103) Kronig, R and Brink, J C.
Appl. Sci. Research A2, 142, (1960).

(104) Hadamard, C R and Rybezynski, A.
Acad. Sci. Paris, 152, 1735, (1911).

(105) Calderbank, P H and Korchinski, I J O.
Chem. Eng. Sci. 6, 65 (1956).

(106) Handlos, A E and Baron, T.
A.I.Ch.E.J. 3, 127, (1957).

(107) Skelland, A H P and Wellek, R M.
A.I.Ch.E.J. 10, 491, (1964).

(108) Olander, D R.
A.I.Ch.E.J. 12, 1018, (1966).

(109) Linton, M and Sutherland, K L.
Chem. Eng. Sci. 12, 214, (1960).

(110) Sideman, S and Shabtai, H.
Cadan, J. Chem. Eng. 42, 107, (1964).

(111) Griffith, R M.
Chem. Eng. Sci. 12, 198, (1960).

(112) Garner, F H and Suckling, R D.
A.I.Ch.E.J. 4, 114, (1958).

(113) Garner, F H, Jenson, V G and Keey, R B.
T.I.C.E. 37, 197, (1957).

(114) Garner, F H and Tayeban, H.
Am. R. Sco. Esp. Qui. 56B, 479, (1960).

(115) Rowe, P N et al.
Trans. Instn. Chem. Eng. 43, 14, (1965).

(116) Kinard, G E, Mannig, F S and Manning, W P.
Brit. Chem. Eng. 8, 326, (1963).

(117) Boussinesq, J.
C R Acad. Sci. Paris, 156, 983, 1035, 1124, (1913).

(118) Garner, F H, Foord, A and Tayeban, H.
J. Appl. Chem. 9, 315, (1959).

(119) Mekasut, C, Molinier, J and Angelino, H.
Chem. Eng. Sci. 33, 821, (1978).

(122) Yamaguchi, M, Watanabe, S and Katayama, T.
J. Chem. Eng. Japan, 8, 415, (1975).

(121) Yamaguchi, M, Fujimoto and Katayama, T.
J. Chem. Eng. Japan, 8, 361, (1975).

(122) Al-Hassan, T S.
PhD Thesis, University of Aston in Birmingham, UK, (1979).

(123) Hughmark, G A.
Ind. Eng. Chem. Funds. 6, 408, (1967).

(124) Hendrix, C D, Shashikant, B D and Johnson, H F.
A.I.Ch.E.J. 13, 1972, (1967).

(125) Sawistowski, H.
Recent Advances in Liquid-Liquid Extraction. Edited by Hanson, C,
Pergamon Press, NY, (1971).

(126) Arnold, D R.
PhD Thesis, University of Aston in Birmingham, UK, (1974).

(127) Arnold, D R, Mumford, C J and Jeffreys, G V.
Proc. Int. Solvent Ext. Conf. (ISEC), Lyon, 1619, (1974).

(128) McFerrin, A R and Davison, R R.
A.I.Ch.E.J. 17, 1021, (1971).

(129) Heertjes, P M and de Nie, L H.
Chem. Eng. Sci. 26, 697, (1971).

(130) Crank, V.
"Mathematics of Diffusion", Oxford University Press, London (1956).

(131) Schroeder, R R And Kintner, R C.
A.I.Ch.E. 11, 5, (1965).

(132) Bakker, C A P, Van Buytenen, P M and Beek, W J.
Chem. Eng. Sci., 21, 1039, (1966).

(133) Thomson, J.
Phil. Mag. 10(4), 330, (1855).

(134) Marangoni, C.
Annln. Phys. 143, 337 (1871).

(135) Takeuchi, H and Numata, Y.
Ind. Chem. Eng. 17, 468 (1977).

(136) Treybal, R E.
"Mass Transfer Operations", McGraw-Hill, NY (1980).

(137) Pearson, J R A.
J. Fluid Mech., 4, 489 (1958).

(138) Sternling, C V and Scriven, L E.
A.I.Ch.E.J., 5, 514, (1959).

(139) Orell, A and Westwater, J W.
A.I.Ch.E.J., 8, 350, (1953).

(140) Sherwood, T K and Wei, J C.
Ind. Chem. 49, 1030, (1957).

(141) Haydon, D A.
Proc. Roy. Soc. A243, 483, (1958).

(142) Maroudas, N G and Sawistowski, H.
Nature, London, 171, 1155 (1960).

(143) Maroudas, N G and Sawistowski, H.
Chem. Eng. Sci., 19, 919 (1964).

(144) Davies, J T.
"Turbulence Phenomena", Academic Press, New York (1972).

(145) de Nie, L E.
Chem. and Process Eng. 50, 133 (1969).

(146) Kintner, R S.
Adv. Chem. Eng. 4, 51 (1963).

(147) Garner, F H and Hale, A R.
Chem. Eng. Sci., 2, 157 (1953).

(148) Garner, F H and Skelland, A H P.
Ind. Eng. Chem., 48, 51 (1956).

(149) Dunn, I, Lapidus, L and Elgin, J C.
A.I.Ch.E. J., 11, 158 (1965).

(150) Misek, T and Rozkos, B.
Chem. Prum., 15, 450 (1965).

(151) Edge, R M and Grant, C D.
Chem. Eng. Sci., 27, 1709 (1972).

(152) Skelland, A H P and Caenepeel, C L.
A.Ch.E. J., 18, 1154 (1972).

(153) Alden, L.
"Liquid-Liquid Extraction", Elsevier Publishing Company (1959).

(154) Rod, V.
Brit. Chem. Eng. 16, 617, (1971).

(155) Reman, G H.
Pet. Ref., 36, 269 (1967).

(156) Logsdail, D H, Thornton, J D and Pratt, H R C.
Trans. Inst. Chem. Eng., 35, 301, (1957).

(157) Kung, K Y and Beckmann, R B.
A.I.Ch.E. J. 7, 319, (1961).

(158) Vermijs, H J A and Kramers, H.
Chem. Eng. Sci., 3, 55, (1954).

(159) Anon.
Chem. Eng. 9, 58, 60, 68 (1961).

(160) Reman, G H.
Dutch Patent 70, 866 (1952).

(161) Gouroji, I C, Narula, A S and Pai, M.
Brit. Chem. Eng., 5, 67, (1971).

(162) Krishmaiah, N M et al.
Brit. Chem. Eng., 12, 719 (1978).

(163) Sokov, Y F et al.
Tr. Vses. Nouchn. Tekn., Soveshch Protsessy Zhid Kostnoi Elektra Ktsil Khemorbtsii, 2nd Edition, Leningrad, pp. 228 (1966).

(164) Gayler, R, Roberts, M W and Pratt, H R C.
Trans. Instn. Chem. Eng. 31, 57, (1953).

(165) Thornton, J D and Pratt, H R C.
Trans. Instn. Chem. Eng., 31, 289, (1953).

(166) Thornton, J D.
Chem. Eng. Sci., 5, 201, (1956).

(167) Misek, T.
Coll. Czech. Comm. 28, 426, 570, 1613, (1963).

(168) Pratt, H R C.
Ind. Chem. 31, 505, (1955).

(169) Kasatkin, A G, Kagan, S Z and Trankhanov, G V.
Appl. Chem. (USSR), 35, 1903, (1962).

(170) Murakami, A, Misonou, A and Inoue, K.
Int. Chem. Eng. 18, 16, (1978).

(171) Laddha, G S, Degaleesan, T E and Kannappan, R.
Can. J. Chem. Eng. 56, 137, (1978).

(172) Rozkos, B.
Research Rep. 918/69 VUCHZ Praha.

(173) Baird, M H I and Shen, Z J.
Canad. J. Chem. Eng., 62, 218 (1984).

(174) Reman, G H.
Joint Symposium - The Scaling-up of Chem. Plant and Processes, Inst. of Chem. Eng., 26 (1957); and Pet. Ref., 36, 9, 269 (1967).

(175) Reman, G H.
Chem. Eng. Prog. 62, 9, 56, (1966).

(176) Selker, A H and Schleichter, C A.
Can. J. Chem. Eng. 43, 298 (1964).

(177) Lunning, R W and Sawistowski, H.
Solvent Extraction Proc. ISEC Vol II, 873 (1977).

(178) Clarke, S I and Sawistowski, H.
Trans. Inst. Chem. Eng. 56, 1, 50 (1978).

(179) Sarkar, S, Phillips, C R, Mumford, C J and Jeffreys, G V.
Trans. IChemE. Vol. 58, 34 (1980).

(180) McSween, D.
BSc Project Report (University of Aston in Birmingham) UK, (1976).

(181) Osipon, L I.
"Surface Chemistry", Rheinhold Publishing Corp. (1962).

(182) Sege, G and Woodfield, F M.
Chem. Eng. Prog., 50, 396 (1954).

(183) Garner, F H, Ellis, S R M and Hill, J W.
A.I.Ch.E. J., 1, 185 (1955) and Trans. Inst. Chem. Eng. 34, 223 (1956).

(184) Sobolic, R H and Himmelblau, D M.
A.I.Ch.E. J. 6, 619 (1960).

(185) Treybal, R E.
Ind. Eng. Chem., 51, 262 (1960).

(186) Misek, T.
Coll. Czech, Chem. Commun., 29, 1767 (1964).

(187) Mecklenburgh, J C and Hartland, S.
IChemE Symposium Series, 26, 22 (1967).

(188) Stainthorp, F B and Sudall, N.
Trans. Inst. Chem. Engrs. Vol. 42, 198, (1964).

(189) Westerterp, K R and Landsman, P.
Chem. Eng. Sci. 17, 363, (1962).

(190) Teruratsu, M et al.
A.I.Ch.E. J., 12, 508 (1966).

(191) Bruin, T.
Trans. Inst. Chem. Eng. 51, 355, (1973).

(192) Blazej, L, Vajda, M, Bafrncova, S and Havalda, J.
Chem. Zvesti, 32, 328, (1978).

(193) Bibaud, R E and Treybal, R E.
A.I.Ch.E. J., 12, 472, (1966).

(194) Kagan, S Z, Volkova, T S and Aerov, M E.
Chim. Prom. 12, 39, (1961).

(195) Pratt, H R C.
Trans. Instn. Chem. Engrs., 29, 195 (1951).

(196) Geankoplis, C J and Hixon, A N.
Ind. Eng. Chem. 42, 1141, (1950).

(197) Gier, T E and Hougen, J O.
Ind. Eng. Chem. 45, 1362, (1953).

(198) Newman, M L.
Ind. Eng. Chem. 44, 2457, (1952).

(199) Cavers, S D and Ewanchyna, J E.
Can. J. Chem. Eng. 113, (1957).

(200) Nagala, S et al.
Chem. Eng., Tokyo, 21, 784 (1957).

(201) Westerterp, K R and Mayburg, W H.
Chem. Eng. Sci. 17, 373, (1962).

(202) Stemerding, S, Lumb, E C and Lips, J.
Chem. Eng. Techn., 35, 844 (1963).

(203) Misek, T and Rod, V.
"Calculation of Contactors with Longitudinal Mixing", Chapter 7, Recent Advances in Liquid-Liquid Extraction (1971).

(204) Misek, T and Rozkos, B.
Int. Chem. Eng. 6, 130, (1966).

(205) Misek, T.
Paper presented in CHISA II Congress, Marienbad, Czechoslovakia (1965).

(206) Miyauchi, T, Mitsutake, H and Harase, I.
A.I.Ch.E. J. 12, 508, (1966).

(207) Nece, R E and Daily, J W.
Trans. Am. Soc. Mech. Eng. D82, 562, (1960).

(208) Rodger, W A, Trice, V G and Rushton, J H.
Chem. Eng. Prog. 52, 515, (1956).

(209) Pebalk, V L, Shashkova, M N and Baranova, E P.
The Soviet Chemical Industry, 3 (1970).

(210) Elenkov, D and Temniskov, I.
Comptes Rendus Acad. Bulg. Sci. 6, 679, (1974).

(211) Venkataramana, Degaleesan, T E and Laddha, G S.
Can. J. Chem. Eng. Vol. 58, P. 296, (1980).

(212) Murakami, A and Misonou, A.
Intern. Chem. Eng. Vol. 18, 22 (1978).

(213) Marr, R and Moser, F.
Chem. Ing. Tech. 50, 2, 90, (1978).

(214) Zhang, S H, Ni, X D and Su, Y F.
Canad. J. Chem. Eng. Vol. 59, 573 (1981).

(215) Lu, Fan, and Chen.
ISEC, Denver, USA 98,(1983).

(216) Young, E F.
Chem. Eng., 64, 241 (1957).

(217) Miyauchi, T and Vermeulen, T.
Ind. Eng. Chem. Found. 2, 304, (1957).

(218) Sleicher, C A.
A.I.Ch.E. J. 5, 145, (1959).

(219) Hartland, S and Mecklenburgh, J C.
Chem. Eng. Sci. 21, 1209, (1966).

(220) Rod, V.
Brit. Chem. Eng., 9, 300, (1964).

(221) Danckwerts
Chem. Eng. Sci. 2, 1, (1953).

(222) Steiner, L, Laso, M and Hartland, S.
IChemE Symposium Series No.88, 90 (1984).

(223) Khandelwal, A N.
PhD Thesis, University of Aston in Birmingham, UK, (1978).

(224) Marr, R.
Chem. Ing. Techn. 50, 337 (1978).

(225) Wilke, C R and Chang, Pin.
A.I.Ch.E. J., 1, 264 (1955).

(226) Null, A R.
"Phase Equilibrium in Process Design", Wiley Interscience, N Y (1970).

(227) Gasmelseed, G A.
PhD Thesis, University of Aston in Birmingham, UK (1985).

(228) Cochran, W G.
Proc. Cambridge, Phil. Soc. 30, 365, (1934).

(229) Rod, V, Fei Wei-Yang and Hanson, C.
Chem. Eng. Res. Des. Vol. 61, 291 (1983).

(230) Thomas, R and Mumford, C J.
Proc. Int. Solvent Ext. Conf. (ISEC), The Hague, (1971).

(231) Jeffreys, G V and Davies, G A.
"Advances in Liquid-Liquid Extraction", edited by Hanson, C, Pergamon Press, N Y, (1971).

(232) Al-Aswad, K K, Mumford, C J and Jeffreys, G V.
A.I.Ch.E. J., 31, 1488, (1985).

(233) Lamb, H.
"Hydrodynamics", 473, Dover, NY (1945).

(234) Horvath, M, Steiner, L and Hartland, S.
Canad. J. Chem. Eng., 56, 9, (1978).